

Innovation and Discovery in Russian Science and Engineering

Levon R. Mailyan · Sergey A. Stel'makh ·
Evgenii M. Shcherban' ·
Mikhail G. Kholodnyak ·
Alla S. Smolyanichenko ·
Ivan A. Parinov · Alexander V. Cherpakov

Management of Structure Formation and Properties of Cement Concretes

Innovation and Discovery in Russian Science and Engineering

Series Editors

Stavros Syngellakis, Ashurst Lodge, Wessex Inst of Technology, Southampton, Hampshire, UK

Jerome J. Connor, Department of Civil & Environmental Engineering,
Massachusetts Institute of Technology, Cambridge, MA, USA

This Series provides rapid dissemination of the most recent and advanced work in engineering, science, and technology originating within the foremost Russian Institutions, including the new Federal District Universities. It publishes outstanding, high-level pure and applied fields of science and all disciplines of engineering. All volumes in the Series are published in English and available to the international community. Whereas research into scientific problems and engineering challenges within Russia has, historically, developed along different lines than in Europe and North America. It has yielded similarly remarkable achievements utilizing different tools and methodologies than those used in the West. Availability of these contributions in English opens new research perspectives to members of the scientific and engineering community across the world and promotes dialogue at an international level around the important work of the Russian colleagues. The broad range of topics examined in the Series represent highly original research contributions and important technologic best practices developed in Russia and rigorously reviewed by peers across the international scientific community.

More information about this series at <https://link.springer.com/bookseries/15790>

Levon R. Mailyan • Sergey A. Stel'makh •
Evgenii M. Shcherban' • Mikhail G. Kholodnyak •
Alla S. Smolyanichenko • Ivan A. Parinov •
Alexander V. Cherpakov

Management of Structure Formation and Properties of Cement Concretes



Springer

@seismicisolation

Levon R. Mailyan
Don State Technical University
Rostov-on-Don, Russia

Sergey A. Stel'makh
Don State Technical University
Rostov-on-Don, Russia

Evguenii M. Shcherban'
Don State Technical University
Rostov-on-Don, Russia

Mikhail G. Kholodnyak
Don State Technical University
Rostov-on-Don, Russia

Alla S. Smolyanichenko
Don State Technical University
Rostov-on-Don, Russia

Ivan A. Parinov
Mathematics, Mechanics
and Computer Sciences
Southern Federal University
Rostov-on-Don, Russia

Alexander V. Cherpakov
Mathematics, Mechanics
and Computer Sciences
Southern Federal University
Rostov-on-Don, Russia

ISSN 2520-8047

ISSN 2520-8055 (electronic)

Innovation and Discovery in Russian Science and Engineering

ISBN 978-3-031-08918-3

ISBN 978-3-031-08919-0 (eBook)

<https://doi.org/10.1007/978-3-031-08919-0>

© The Editor(s) (if applicable) and The Author(s), under exclusive license to Springer Nature Switzerland AG 2023

This work is subject to copyright. All rights are solely and exclusively licensed by the Publisher, whether the whole or part of the material is concerned, specifically the rights of translation, reprinting, reuse of illustrations, recitation, broadcasting, reproduction on microfilms or in any other physical way, and transmission or information storage and retrieval, electronic adaptation, computer software, or by similar or dissimilar methodology now known or hereafter developed.

The use of general descriptive names, registered names, trademarks, service marks, etc. in this publication does not imply, even in the absence of a specific statement, that such names are exempt from the relevant protective laws and regulations and therefore free for general use.

The publisher, the authors, and the editors are safe to assume that the advice and information in this book are believed to be true and accurate at the date of publication. Neither the publisher nor the authors or the editors give a warranty, expressed or implied, with respect to the material contained herein or for any errors or omissions that may have been made. The publisher remains neutral with regard to jurisdictional claims in published maps and institutional affiliations.

This Springer imprint is published by the registered company Springer Nature Switzerland AG
The registered company address is: Gewerbestrasse 11, 6330 Cham, Switzerland

Preface

Increasing construction volumes requires new technological, structural, and design solutions for reinforced concrete elements. Centrifugation, being an undervalued production technology, leads to functionally gradient concrete structures made by it. These structures vary in their characteristics (density, strength, deformability, etc.) in cross section. In many cases, this should be taken into account in the analysis and design, but such studies are insufficiently conducted in practice. In this regard, when calculating and designing the building constructions with a functionally gradient structure, an unreasonably large margin is usually adopted, which leads to a noticeable increase in the cost of promising building constructions. In the existing Russian State Standards and scientific literature, there are no theoretical and practical methods for calculating centrifuged reinforced concrete structures, taking into account the functional gradient structure and the characteristics of concrete in cross section. Separate data confirm the high efficiency of centrifugal compaction, but the existing calculation methods do not allow us to fully use the advantages of centrifugation due to the lack of accounting for the functional gradient structure.

Moreover, there is not enough research that theoretically combine the use of chemical additives in the composition of the mixing water for further thermal, mechanical, and mechanochemical treatment (activation) of the initial components of concrete. The interpretation of the mechanism of influence of this technology from the standpoint of electromagnetic effects on the forming concrete structure allows a better understanding of the conceptual approaches to obtaining optimal characteristics.

By studying and evaluating the electrical properties of the dispersed phase, it is advisable to use ideas about the active centers of solids. The kinetics and completeness of chemical transformations significantly depend on the type and concentration of active centers in the solid components of concrete (cement, aggregate, filler), especially at the interfaces where these reactions are realized. By adjusting the polarity, charge, and concentration of active centers in the bulk and on the surface of dispersed components using various technological techniques, it is possible to

significantly influence the rheology of concrete mixtures as well as the rate of growth of concrete strength, its permeability, and durability.

The prospects of work in the field of construction materials science and R&D of new-generation materials are determined by (i) involving previously unused types of raw materials and structures, including those obtained on the base of nanotechnology, and industrial waste, and (ii) the use of fundamentally new electrophysical technologies for processing, obtaining, and activating of building materials during manufacture. This book attempts to show the prospects of these approaches both as from the viewpoint of the theoretical explanation of the activation effect mechanism, as the prediction of new ways to improve the efficiency of concrete and reinforced concrete technology.

The book comprises nine chapters organized into two parts. Part I includes the first six chapters and discusses influence of mechanical vibrations on technology of heavy concretes. Part II includes the last three chapters and is devoted to discussion of electrophysical impacts on manufacture of cement, foam, and fiber-foam concretes.

Chapter 1 describes the state of the art and theoretical background for heavy concrete manufactured by using mechanical vibration. Technologies for the manufacture of reinforced concrete products and structures of annular cross section with functionally gradient structure are discussed with a presentation of the features of the functionally gradient structures of centrifuged (CF) concretes. The theoretical basis of calculation methods, accompanied working concepts, goals, and objectives are given.

Chapter 2 is devoted to technology and experimental setup for manufacturing CF and vibro-centrifuged (VCF) concrete elements with functionally gradient structure. The theoretical basis of the formation of the functionally gradient structure of these solids with annular cross-section are present with experimental centrifugation facilities. Their features and calculations of parameters are discussed with a selection of basic concrete compositions of test samples. The resonance method and instrumental approaches to experimental studies of prototypes are developed.

Chapter 3 presents the aggregate and local characteristics of vibrated (V), CF, and VCF concretes. The schedule and methodology of experimental studies are discussed together with the aggregate and local structural characteristics of V, CF, and VCF concretes. In particular, analysis of aggregate density, strength, ultimate deformations, modulus of elasticity, and diagrams of concrete deformation under compression and tension is performed and numerical results are obtained. Moreover, the methods of experimental studies of the local characteristics of the concretes by ultrasonic method are developed and the mechanical characteristics of the layers of functionally gradient cross-section are estimated together with the influence of concrete age on the local characteristics.

Chapter 4 is devoted to the evaluation of the aggregate and local structural properties of V, CF, and VCF concretes. Differences in the integral structural characteristics of V, CF, and VCF concretes depending on the manufacturing technology and age are stated. The main factors of influence are centrifugal and centripetal forces, depending on the distance from the center of rotation and the

angular velocity of rotation. Analytical description of stress-strain diagrams under compression and tension of the concretes as well as their mutual relationships and dependence on age are presented. Local structural characteristics of CF and VCF concretes depending on technological parameters are also studied.

Chapter 5 develops calculation methods of the load-bearing capacity of V, CF, and VCF reinforced concrete columns, taking into account the standard, aggregate, and local characteristics of concrete. The diagram approach to the calculation of the load-bearing capacity of short V, CF, and VCF-columns is presented. Moreover, iterative, approximate, and simplified calculations of the bearing capacity of short centrally compressed reinforced concrete columns are discussed. A schedule and experimental methodology together with the features of manufacturing and testing of prototypes are created and results of numerical experiments are obtained. The comparison of experimental and theoretical results obtained for V, CF, and VCF reinforced concrete columns according to the standard, aggregate, and local approaches to calculation of concrete characteristics is performed with the determination of the load-bearing capacity of these samples.

The methods and approaches to redesign and improvement of CF and VCF reinforced concrete columns, taking into account the technology of their manufacture, are presented in Chap. 6. Technological, structural, and design advantages of the proposed actual structures are discussed, and implementation of the research results in the design practice, building, and regulatory documents is carried out.

Chapter 7 presents the classification of electrophysical methods regulating the properties of cement concretes on the base of known scientific results. Electrothermal impact on concretes and concrete mixtures is treated. The electromagnetic activation of mixing water being one of the directions in the field of improving the technology for preparing concrete mixtures is discussed and experimental results are present. Electrophysical impact on cement slurries and concrete mixtures is studied with classification of corresponding processes and phenomena.

Chapter 8 presents the mechanism of interaction between the magnetic field and mixing water and its influence on concrete strength. The processing of aggregates for concrete is discussed from viewpoint of hardening the contact layers of aggregates in dependence on electric pulse. The features of the processing of cement for the preparation of concretes and mortars are considered. The processing of cement dough in concrete is studied and the mechanism of the influence of the electric field on the hardening of cements is explained in addition to the effects at the molecular and ionic levels. The ultrasonic and acoustic activations of concrete mixtures, similar to electrophysical effects, are also considered.

In Chap. 9, a method is developed for the activation of concrete mixtures in a high-voltage AC field at the stage of mixing, allowing one to obtain concretes with increased physical, mechanical, and operational properties. Electric treatment leads to a decrease in destructive phenomena at early stage of hardening, acceleration of structure formation at the stage of formation of a condensation-crystallization structure, and more intensive growth of plastic strength. A method for regulating the structure formation and properties of foam and fibro-foam concretes activated by low-energy AC impact is proposed and its optimal modes are experimentally

revealed. Then, the optimal modes of low-energy processing of foam and fiber-foam concrete mixtures with AC field are found. The prescription parameters (type, dosage, particle size of the components of concrete mixtures) are identified that have the greatest effect on the structure formation and properties of foam and fiber-foam concretes. Finally, the influence of electrical activation on the change in the porosity of heat-insulating concrete is investigated.

The book, presenting the modern theoretical and experimental problems of heavy concrete elements and constructions with functionally gradient structure, and also foam- and fiber-foam concretes, manufactured by using various mechanical and electromagnetic vibrations, is intended for a wide range of students, engineers, and specialists interested and participating in R&D of the modern problems of building materials and constructions.¹

Rostov-on-Don, Russia
January 2022

Levon R. Mailyan
Sergey A. Stel'makh
Evgenii M. Shcherban'
Mikhail G. Kholodnyak
Alla S. Smolyanichenko
Ivan A. Parinov
Alexander V. Cherpakov

¹Research was financially supported by Southern Federal University, grant No. VnGr-07/2020-04-IM (Ministry of Science and Higher Education of the Russian Federation).

Contents

Part I Heavy Concretes and Mechanical Vibration

1 State-of-the-Art and Theoretical Background	3
1.1 Technologies for the Manufacture of Reinforced Concrete Goods and Structures of Annular Cross-Section with Functionally Gradient Structure	3
1.2 Features of the Functionally Gradient Structure of Centrifuged Concretes	6
1.3 Theoretical Grounds of Calculation Methods for Centrifuged Reinforced Concrete Structures with Annular Cross-Sections	8
1.4 Working Concepts, Goals, and Objectives	13
2 Technology and Experimental Setup for Manufacturing Centrifuged (CF) and Vibro-centrifuged (VCF) Concrete Elements with Functionally Gradient Structure	15
2.1 Theoretical Grounds of the Formation of the Functionally Gradient Structure of Concrete CF- and VCF-Elements of Annular Cross-Section	15
2.2 Experimental Centrifugation Facilities	22
2.2.1 Functional Gradient of Centrifuged Concrete	22
2.2.2 Centrifugation Setups	22
2.3 Combined Unit for Centrifugation and Vibration Centrifugation, Its Features, and Calculations of Parameters	23
2.4 Selection of Basic Concrete Compositions of Test Samples	31
2.5 Resonance Method	33
2.6 Instrumental Methods of Experimental Studies of Prototypes	34
2.7 Conclusions	36

3 Aggregate and Local Characteristics of Vibrated (V), Centrifuged (CF), and Vibro-Centrifuged (VCF) Concretes	37
3.1 Schedule and Methodology of Experimental Studies of the Ultimate Characteristics of Concrete	37
3.1.1 Manufacture Methods	37
3.1.2 Test Method	38
3.2 Aggregate Structural Characteristics of V-, CF-, and VCF-Concretes	45
3.2.1 Results of Studies of the Aggregate Characteristics of Concrete	45
3.2.2 Analysis of Aggregate Density, Strength, Ultimate Deformations, Modulus of Elasticity, and Diagrams of Concrete Deformation Under Compression and Tension	46
3.3 Local Design Characteristics of CF- and VCF-Concretes of Functionally Gradient Cross-Sections	50
3.3.1 Methods of Experimental Studies of the Local Characteristics of Concrete by Ultrasonic Method	51
3.3.2 Analysis of the Results of Studies of the Local Characteristics of Concrete	54
3.4 Conclusions	62
4 Modeling of Aggregate and Local Structural Characteristics of V-, CF-, and VCF-Concretes	67
4.1 Calculation of the Aggregate Characteristics of V-, CF-, and VCF-Concretes	68
4.1.1 Standard and Design Resistances of V-, CF-, and VCF-Concretes	68
4.1.2 Differences in the Aggregate Structural Characteristics of V-, CF-, and VCF-Concretes Depending on the Manufacturing Technology and Age	69
4.1.3 Analytical Description of Stress-Strain Diagrams Under Compression and Tension of V-, CF-, and VCF-Concretes, Their Mutual Relationship, and Dependence on Age	72
4.2 Calculation of Local Structural Characteristics of CF- and VCF-Concrete Depending on Technological Parameters	74
4.3 Conclusions	90
5 Calculation of the Load-Bearing Capacity of V-, CF-, and VCF-Reinforced Concrete Columns, Taking into Account the Standard, Aggregate, and Local Characteristics of Concrete	95
5.1 Standards and Regulatory for Calculating the Load-Bearing Capacity of Short CF- and VCF-Columns, Taking into Account the Standard, Aggregate, and Local Characteristics of Concretes	95

5.2	Diagram Approach to the Calculation of the Load-Bearing Capacity of Short V-, CF-, and VCF-COLUMNS, Taking into Account the Standard, Aggregate, and Local Characteristics of Concretes	97
5.2.1	Iterative Calculation of the Strength of Short Centrally Compressed Reinforced Concrete Columns	97
5.2.2	Approximate Calculation of the Strength of Short Centrally Compressed Reinforced Concrete Columns	103
5.2.3	Simplified Calculation of the Strength of Short Centrally Compressed Reinforced Concrete Columns	103
5.3	Schedule and Methodology of the Experiment	105
5.3.1	Features of Manufacturing and Testing of Prototypes	105
5.3.2	Analysis of the Results of Experimental Studies	106
5.4	Schedule, Methodology, and Results of Numerical Experiments	108
5.5	Comparison of Experimental and Theoretical Results Obtained for V-, CF-, and VCF-Reinforced Concrete Columns According to the Standard, Aggregate, and Local Characteristics of Concretes	110
5.5.1	Determination of the Load-Bearing Capacity of V-, CF-, and VCF-Reinforced Concrete Columns According to the Standard, Aggregate, and Local Characteristics of Concretes	110
5.5.2	Calculation of the Load-Bearing Capacity of V-, CF-, and VCF-Reinforced Concrete Columns by the Proposed Diagram Methods Based on the Standard, Aggregate, and Local Characteristics of Concretes	112
5.6	Conclusions	120
6	Redesign and Improvement of CF- and VCF-Reinforced Concrete Columns, Taking into Account the Technology of Their Manufacture	123
6.1	Technological, Structural, and Design Advantages of the Proposed Actual Structures	123
6.2	Redesign of Actual Reinforced Concrete Column and Calculation of the Load-Bearing Capacity of Such a VCF-Column	124
6.3	Implementation of the Research Results in the Practice of Building and Designing and Regulatory Documents	131
6.4	Conclusions	132

Common Conclusions to Part I**Part II Cement, Foam, Fiber-Foam Concretes
and Electrophysical Impacts**

7 Classification of Electrophysical Methods Regulating the Properties of Cement Concretes	139
7.1 Existing Methods of Electrophysical Impact in Cement Concrete Technology	139
7.1.1 Electrothermal Action on Concretes and Concrete Mixtures	143
7.1.2 Electromagnetic Activation of Concrete Mixture Components	150
7.2 Conclusions	158
8 Electrophysical Effect on Concrete Mixtures and Their Components	159
8.1 Treatment of Mixing Water for Concrete	159
8.2 Processing of Aggregates for Concrete	163
8.3 Processing of Cement for the Preparation of Concretes and Mortars	164
8.4 Processing of Cement Dough for Concrete	166
8.5 Concrete Mixture Treatment	169
8.6 Systematization of Ideas About the Mechanisms of Electrophysical Effects on the Concrete Mixture and Its Components	171
8.7 Conclusions	174
9 Features of Electrophysical Impact on Mortar and Concrete Mixtures	177
9.1 Optimization of the Parameters of Electric Treatment of Concrete Mixtures According to the Criterion of Concrete Strength	177
9.2 Influence of the Composition of the Concrete Mixture on the Efficiency of Electrical Activation	180
9.3 Influence of High-Voltage Electric Field of Corona Discharge on Mineral Components of Concrete	185
9.4 Influence of High-Voltage Electrostatic Field on the Rheological Properties of Mineral Powders	191
9.5 The Idea and Essence of the Activation of Aerated Concrete Mixtures with Low-Power AC Electrophysical Impact	192
9.6 Theoretical Substantiation of the Expediency of Activation of Aerated Concrete Mixtures by Low-Power AC Electrophysical Impact	194

9.7	Characteristics of the Optimal Activation Mode for Foam and Fiber-Foam Concrete by Low-Power Variable Electrophysical Impact	195
9.8	Identifying Rational Modes of Low-Power Electrophysical Impact on Foam and Fiber-Foam Concrete Mixtures and Concretes	202
9.9	Identification of the Optimal Mode of Activation of Foam and Fiber-Foam Concrete by Low-Energy-Consuming Electrophysical Impact	210
9.10	Features of Changes in the Structure Formation and Properties of Foam and Fiber-Foam Concrete Mixtures and Concretes During Their Optimal Manufacture	211
9.11	Conclusions	213
Common Conclusions to Part II		
References	219
Index	233

Part I

Heavy Concretes and Mechanical Vibration

Chapter 1

State-of-the-Art and Theoretical Background



Abstract This chapter presents the state-of-the-art and theoretical background for reinforced concrete products with functionally gradient structure. First, known technologies (in particular, external vibration, roll pressing, centrifugation, vertical vibroforming, etc.) for the manufacture of concrete goods with annular cross-section are discussed. Features of the functionally gradient structure of centrifuged concretes are considered. It is concluded that the directed structure formation of the functionally gradient centrifuged concrete can be performed by sequential layer-by-layer molding or by using the concomitant vibration in the process of centrifuging concrete structures. Then the theoretical grounds of calculation methods for centrifuged reinforced concrete structures with annular cross-sections are discussed. The results of the analysis allow us to state directions for further investigation and describe the research objects and subjects. Moreover, the working hypothesis and objectives of the study are found.

Key words Reinforced concrete · Functionally gradient structure · Annular cross-section

1.1 Technologies for the Manufacture of Reinforced Concrete Goods and Structures of Annular Cross-Section with Functionally Gradient Structure

A large group of reinforced concrete constructions and structures of annular and circular cross-sections are manufactured on specialized setups by using various methods of compaction of a concrete mixture, namely, vibration shaping, vibration hydraulic pressing, roll pressing, centrifugation, etc. [25, 246, 280, 283, 318].

The most effective process at *external vibration* is the use of harmonic oscillations with a frequency of 50 Hz perpendicular to the surface of the concrete structure with a thickness of 4–60 cm. In highly reinforced constructions of complex shape with a wall thickness of 4–8 cm, a frequency of more than 66 Hz is advisable.

Vibration hydraulic pressing is used in the manufacture of pressured reinforced concrete pipes. The molding process consists of two stages. First, the concrete mixture is fed by a helical concrete paver into a mold consisting of an outer casing and an inner core. On the core with two walls, a rubber cover is put on, adjacent to the perforated wall. The outer casing consists of two half-molds for pipes of small diameters, equipped with flanges for interconnection using bolts and calibrated springs [14, 111].

Laying and initial compaction of low-moving concrete mixtures for pipes of small diameter is carried out using suspended pneumatic vibrators MV-64, for pipes of large diameters. By this the vibrating platforms with multicomponent vibrators having a carrying capacity of 20–28 tons are used. In this case, vibration propagates through the outer casing and the inner core [26].

Roll pressing is especially actively applied by McCracken and Besser company (USA), by Siome company (Italy), and by Schlosser-Pfeiffer GmbH (Germany). With this method, the formwork into which the concrete mixture is fed forms the outer surface of the construction. For uniform distribution of concrete in the mold and its compaction, a radially rotating tool is used, which consists of pressing and distributing heads. It performs several functions simultaneously: (i) distribution of concrete, (ii) pressing, and (iii) grouting the walls of the inner surface of construction. The manufacturing process begins with the installation on a vibrating platform of a formwork form with a funnel-forming ring fixed to it. The forming head, located at the end of the long saw shaft, is lowered into the mold, where the concrete mixture is fed. First of all, the socket is molded with simultaneous rotation of the head and vibration of the vibrating table. The simultaneous operation of pressing and vibration allows one to provide the necessary compaction of concrete. The rotation of the shaft head is clockwise, while the rollers rotate counterclockwise at three times greater than the shaft speed. Thus, torsional stresses, arising in freshly formed constructions due to pressing reinforcement into concrete, are eliminated [1, 19, 157, 231, 271].

In practice, *centrifugation* is the most effective and widespread method of forming long concrete structures with an annular cross-section. This method is based on the compaction of a concrete mixture by squeezing out part of the water into a rotating form under the influence of centrifugal forces.

Research carried out in this area by the Prague Physicochemical Institute at the end of the nineteenth century introduced significant contribution in the theory of concrete centrifugation. This theory was further developed in the works of famous Russian scientists: N. N. Abramov, I. N. Akhverdov, S. A. Dmitriev, V. G. Dubinina, N. N. Geniev, B. V. Gusev, A. P. Kudzis, S. P. Leonovich, V. V. Mikhailov, E. E. Mikhelson, A. N. Popov, Yu. Ya. Shtayerman, V. P. Sirotkin, V. I. Soroker, L. A. Volkov, L. A. Zekiev, and A. I. Zvezdov et al. [8–10, 56–58, 60, 83, 129, 134, 171, 217, 218, 241, 243, 267, 281, 299, 301, 321].

There are two known centrifugation methods, namely, sedimentation and filtration. Their main difference consists in the design of the forms. In the first method, the forms with solid walls are used; in the second one, the perforated forms lined from the inside with a cotton filter are applied [318].

The advantages of the centrifuged molding method, used for concrete structures of annular cross-section in comparison with other methods of compacting the concrete mixture, are in a high degree of compaction and reduced water permeability and water absorption of concrete. However, centrifugation requires a relatively high capital investment; in addition, machine parts and molds wear out quickly in the manufacture process.

This centrifuged molding method has become widespread in France (Bonna firm), Italy (Montoro firm), and Australia (Roela firm). This method is usually used in the manufacture of drainage pipes of large diameters and it consists in the distribution and compaction of a concrete mixture with a ratio $W/C = 0.4$ or more due to centrifugal and dynamic forces [323].

Shaping of pipes is carried out on a centrifuge, in split molds, consisting of two half-molds tightened by bolts. A reinforcing frame is installed in the lower half of the mold. Then, the upper half-shape is attached using a pneumatic nutrunner; a socket-former and a sleeve ring are inserted, too. On the form prepared in this way with reinforcement, bandages are put on, with which the form is attached to the centrifuge rollers. Moreover, the mold is pressed by the upper rollers to prevent its ejection during centrifugation. After installing the mold on the centrifuge, the machine is started and the concrete mixture at an initial speed of 5–6 m/s is supplied with simultaneous vibration during a whole filling process. Further, centrifugation begins with a speed of 26–28 m/s. Upon completion of the seal, the squeezed sludge is drained from the pipe, tilting the pipes with a special hydraulic lift. The freshly formed pipe is then fed to the place for removing the bandages and tilting in a vertical position into the chambers of heat and moisture treatment [116].

To obtain a higher quality inner surface of the pipe, the Zublin firm (Germany) [322] uses the technology of *vertical vibroforming* in production. The mold prepared for the pipe is placed on the work table and rotated under the press head. The head is lowered into the mold. With the help of a conveyor belt, concrete is fed from the bunker. The socket is sealed with vibrators. The main pipe is manufactured using a pressing head. The exact length of the pipe is achieved by compacting the concrete under a press. The mold with the freshly formed pipe is removed from the working position and at the same time the mold for the new pipe is installed under the pressing head [44, 305].

By using the method of centrifugation on three-stage technology, the Bohnna company manufactures pipes from 0.3 to 2 m with an inner metallic cylinder, designed for pressures up to 1.5 MPa. Their distinctive feature is the length of 7 m. In Great Britain, its subsidiary company (Stanton Bonna) manufactures reinforced concrete pipes with a steel cylinder with a diameter of 0.25 to 4 m [290].

1.2 Features of the Functionally Gradient Structure of Centrifuged Concretes

The physical foundations of the functionally gradient structure of centrifuged concretes are described in detail in the works of R. U. Akhmedov, I. N. Akhverdov, S. T. Androsov, V. M. Batashev, G. S. Burlakov, E. E. Mikhelson, G. V. Nesvetaev, V. I. Ovsyankin, B. G. Pashkovsky, V. P. Petrov, V. I. Podolsky, E. Yu. Romanenko, V. L. Shchutsky, Yu. Ya. Stayerman, R. Suval, and G. A. Tkachenko [8–10, 24, 57, 58, 120, 206, 212, 223, 226, 227, 247–249, 281]. The essence of the functionally gradient structure formation lies in the fact that, first, when the mold rotates at low speed, the material is evenly distributed over the annular section. Then, with an increase in the speed of rotation, under the influence of centrifugal pressure, part of the water is squeezed out of the cement paste mixing together with highly dispersed fractions. There is a convergence of larger aggregate particles, which achieves the highest degree of compaction of the concrete mixture.

For the first time, the mechanism of aggregate drift during centrifugal compaction of concrete was studied by Yu. Ya. Stayerman. Considering the aggregate grains, suspended in the cement dough, he established the effect of the hydrodynamic pressure on the aggregate particles and showed the quantitative nature of the distribution of aggregates and cement dough over the cross-section of the concrete structure.

Later, I. N. Akhverdov showed that the magnitude of the compression pressure depends on the geometric dimensions of the molded concrete structure and the speed of mold rotation. The compression pressure varies across the wall thickness of the concrete structure unevenly: from a minimum on the inner surface to a maximum on the outer surface. It affects the uniqueness of the process of pressing the liquid phase out of the compacted concrete mixture. The characteristic unevenness of the cement dough distribution over the thickness of the molded concrete structure is accompanied by the formation of directed radial filtration channels, the cross-section and number of which increase from the outer to the inner surface. This leads to a very high porosity of the inner slurry layer of the concrete ring.

With an appropriate compression pressure, an increase in the consumption of cement, the thickness of the wall of the concrete structure, and the water content of the concrete mixture t_c , water separation will continue. However, strong dehydration of the concrete mixture predetermines a decrease in strength.

One of the decisive factors affecting the strength and uniformity of centrifuged concrete is the normal consistency of the cement dough. R. U. Akhmedov found that its change from 24% up to 28% increases the centrifugation time by 1.3 times. An increase (over optimal) in cement consumption also does not lead to corresponding increase in the strength of centrifuged concrete. B. G. Pashkovsky found that an increase in cement consumption over 500 kg/m^3 doubles the heat shrinkage stress. In his research, the possibility of improving the quality of centrifuged concrete was proved by regulating the properties of the materials used.

In the researches of other authors, it is shown that, using a mixture of aggregate grains with different average densities, it is possible to achieve their uniform and desirable distribution over the cross-section of the concrete structure at appropriate centrifugation speeds. It is caused by the uneven distribution of these components over the cross-section of a concrete element that has a significant effect on the fluctuation of its physical and mechanical properties [6, 46, 47, 54, 98, 262, 304, 306].

When studying the strength of centrifuged concrete, a significant difference was found in the physical and mechanical properties of concrete in the outer and inner layers of the ring. The results obtained not only confirmed the difference in the physical and mechanical properties of individual layers of concrete of centrifuged samples, but also revealed their significant difference from the similar properties of vibrated concrete [43, 72, 73, 81, 117, 119, 178, 185, 186, 213, 214, 294].

V. M. Batashev and S. T. Androsov have devoted their research to the study of the deformative properties of centrifuged concretes (modulus of elasticity, parametric points of microcracking, creep, and shrinkage). The strength properties of centrifuged concretes significantly depend on the scale factor. Therefore, for their objective assessment, it is desirable that the prototypes be prepared under conditions as close as possible to the conditions of forming real structures. The deformative properties of centrifuged concrete differ significantly in the thickness of the annular cross-section wall, namely, the inner layers have higher compressibility and shrinkage. The variety of properties also depends on the age of the samples, namely, the deformations of concrete of an early age are equal to 50–100%, and they become 20–40% after 50–60 days [87, 153].

In experimental studies of the samples of centrifuged concrete with annular cross-section, performed by A. P. Kudzis, the measured shrinkage deformations, as well as for vibrated concretes of medium grades, amounted to 0.13–0.23%. According to V. M. Batashev, shrinkage deformations change from 0.20% to 0.23%. The deformations of free shrinkage on outer and inner surfaces differ significantly from each other and are equal to 0.65% on the inner surface and 0.15% on the outer one. A large spread of experimental data was also recorded in determining the creep deformations. On the inner layers, they were 1.5 times greater than on the outer. When testing samples of annular cross-section, the measured creep strains on the inner and outer walls turned out to be approximately equal.

During the operation of centrifuged concrete structures, constantly changing stresses and strains appear in them, due to the action of uneven temperature and humidity fields that arise in the concrete structure [65, 133, 187–191].

V. I. Podolsky established that in a closed ring of a centrifuged reinforced concrete support, there are two types of forced deformations, which determine:

- (i) Internal deformations arising in the element regardless of its static scheme due to the curvilinear distribution of moisture content over the cross-section
- (ii) Forced deformations that appear in a closed ring due to the restriction of the freedom of strain either along the entire contour or along its part

During cyclic moistening and drying, significant shrinkage strains develop in the product, contributing to cracking [95, 183, 196].

The resistance of centrifuged concrete to periodic freezing and thawing also has its own characteristics associated with its inhomogeneous or functionally gradient structure.

It can be considered that the directed structure formation of the functionally gradient centrifuged concrete can be carried out by such technological methods as sequential layer-by-layer molding or the use of concomitant vibration in the process of centrifuging concrete structures [89, 181, 184, 261, 291].

1.3 Theoretical Grounds of Calculation Methods for Centrifuged Reinforced Concrete Structures with Annular Cross-Sections

At present, the field of research of reinforced concrete constructions of annular cross-section with a functionally gradient structure, subjected to various force effects, the calculations of which cannot be reduced to conventional methods due to a more complex picture of their stress-strain state, is expanding and deepening. The works of A. G. Aivazov, G. A. Aksomitas, G. I. Berdichevsky, L. R. Mailyan, G. P. Pastushkov, T. M. Pezold, I. M. Schubert, and V. L. Shchutsky et al. [7, 13, 15, 28, 88, 93, 107–109, 112, 136, 138–148, 151, 198, 230, 247–249, 252, 253] are devoted to the theoretical foundations of the existing methods for calculating centrifuged reinforced concrete structures of circular cross-sections.

As an example, the results of such studies on the calculation of reinforced concrete structures of the annular cross-section, subjected to various types of stress-strain state, are indicated in [22, 27, 30, 43, 51, 84, 85, 122, 130, 132, 179, 180, 192, 194, 204, 207, 222, 240].

The closest analogue of the calculation of centrifuged concrete structures of annular cross-section is the research carried out by G. A. Aksomitas [13] for short centrifuged columns of annular cross-section with longitudinal reinforcement of class At-V under short-term compression.

The longitudinal force under axial loading of reinforced elements is determined as

$$N = (\sigma_{b,s} + \epsilon_s \mu_s E_s) A_b, \quad (1.1)$$

where $\sigma_{b,s} = f(\epsilon_{b,s})$ are the stresses in reinforced concrete, $\epsilon_s = \epsilon_{b,s}$ is the strain of longitudinal reinforcement, μ_s is the coefficient of longitudinal reinforcement, E_s is the modulus of elasticity of longitudinal high-strength reinforcement, and A_b is the concrete cross-section area in the compressed zone.

From the condition:

$$dN/d\epsilon_{b,s} = (d\sigma_{b,s}/d\epsilon_{b,s})A_b + \mu_s E_s A_b = 0 \quad (1.2)$$

at the moment, when the element reaches the bearing capacity N_{\max} , the tangent modulus of strain of reinforced concrete, $E_{b,s}$, is defined as

$$E_{b,s} = d\sigma_{b,s}/d\epsilon_{b,s} = -\mu_s E_s. \quad (1.3)$$

Then at N_{\max} , a stress in reinforced concrete $\sigma_{b,s} < R_{b,s}$ (where $R_{b,s}$ is the design resistance of concrete to axial compression), that is, the coefficient of using the strength of concrete, is determined as

$$\gamma_b = \sigma_{b,s}/R_{b,s} < 1. \quad (1.4)$$

As shown in [13], the deformation of the outer layer of reinforced concrete, $\epsilon_{b,s,2}$, corresponding to the force N_{\max} , cannot be equal to the deformation of the inner layer of reinforced concrete, $\epsilon_{b,s,1}$, at which the shear modulus of concrete deformation $E_{b,s} = 0$ and the stress $\sigma_{b,s} = R_{b,s}$. This indicates that the degree of utilization of the compressive strength of the reinforcement bars depends on the strain of the reinforced concrete: $\epsilon_{b,s,2} > \epsilon_{b,s,1}$.

In calculations, this can be estimated by a coefficient characterizing the degree of use of the compressibility of concrete in a reinforced concrete element according to the formula:

$$\beta_b = \epsilon_{b,s,2}/\epsilon_{b,s,1}. \quad (1.5)$$

If the analytical expression of the dependence $\sigma_b - \epsilon_b$ is known, then the coefficients can be calculated using the expression:

$$\gamma_b(\epsilon_b) = \frac{\sigma_b(\epsilon_b)}{R_b} = \frac{\theta_b \eta_b - \eta_b^2}{1 + (\theta_b - 2)\eta_b}, \quad (1.6)$$

where $\eta_b = \epsilon_b/\epsilon_{b,1}$ is the ratio of the longitudinal deformations of concrete (where ϵ_b , $\epsilon_{b,1}$ are the concrete deformation at uniform axial compression inside the concrete and at the inner surface of the inner layer, respectively):

$$\theta_b = \epsilon_{b,1} E_{b,0}/R_b, \quad (1.7)$$

where θ_b is the coefficient characterizing the elastic-plastic properties of concrete and $E_{b,0}\theta_b = \epsilon_{b,1}E_{b,0}/R_b$, R_b are the modulus of elasticity of concrete at compression and tension, and design resistance of concrete to axial compression, respectively ($\theta_b = 1.56$ at compression of high-strength concretes, $\theta_b = 2.0$ at compression of medium-strength concrete).

Presumably, under short-term compression of reinforced concrete elements with longitudinal high-strength reinforcement, formula (1.7) well describes the nature of concrete deformation.

Then, taking into account the characteristics of reinforced concrete $\varepsilon_{b,s,1}$, $R_{b,s}$, $E_{b,s,0}$, it turns out:

$$\theta_{b,s} = \varepsilon_{b,s,1} E_{b,s,0} / R_{b,s}, \quad (1.8)$$

where $E_{b,s,0}$ is the modulus of elasticity of reinforced concrete in compression and tension, $\theta_{b,s}$ is the coefficient characterizing the elastic-plastic properties of reinforced concrete, and

$$\gamma_b(\varepsilon_{b,s}) = (\theta_{b,s} \eta_{b,s} - \eta_{b,s}^2) / [1 + (\theta_{b,s} - 2) \eta_{b,s}], \quad (1.9)$$

where $\eta_{b,s}$ is the ratio of the longitudinal deformations of reinforced concrete.

Hence, the tangential modulus of concrete strain is defined as

$$E_{b,s} = \frac{R_{b,s} [\theta_{b,s} - 2\eta_{b,s} - \eta_{b,s}(\theta_{b,s} - 2)]}{\varepsilon_{b,s,1} [1 + 2(\theta_{b,s} - 2)\eta_{b,s}^2 + (\theta_{b,s} - 2)^2 \eta_{b,s}^2]}. \quad (1.10)$$

It is necessary to compare the right parts of Eqs. (1.9) and (1.10), knowing that under the force N_{\max} for the reinforced element, the coefficient $\eta_{b,s} = \beta_b$. Then the coefficient of using the compressibility of concrete β_b is defined as

$$\beta_b = \left(-1 + \sqrt{\frac{\mu_s \varepsilon_{b,s,1} E_s / (\theta_{b,s} R_{b,s}) + 1}{1 / (\theta_{b,s}^2 - 2\theta_{b,s}) - \mu_s \varepsilon_{b,s,1} E_s / (\theta_{b,s} R_{b,s})}} + 1 \right) / (\theta_{b,s} - 2). \quad (1.11)$$

The strength factor of concrete is:

$$\gamma_b = (\theta_{b,s} \beta_b - \beta_b^2) / [1 + (\theta_{b,s} - 2) \beta_b]. \quad (1.12)$$

For a particular case (at $\theta_{b,s} = 2$), the following coefficients are calculated as

$$\beta = 1 + 0.5 \mu_s \varepsilon_{b,s,1} E_s / R_{b,s}, \quad (1.13)$$

$$\gamma_b = 1 - (0.5 \mu_s \varepsilon_{b,s,1} E_s / R_{b,s})^2. \quad (1.14)$$

The degree of positive influence of concrete work on the descending section of the compression diagram on the bearing capacity of a reinforced concrete element is characterized by the ratio of longitudinal forces:

$$N_{\max}/N_1 = (\gamma_b R_{b,s} + \beta_b \mu_s \varepsilon_{b,s,1} E_s) / (R_{b,s} + \mu_s \varepsilon_{b,s,1} E_s) \quad (1.15)$$

where N_1 is the force applied to the concrete element.

To determine the design compressive resistance of reinforced concrete columns of annular cross-section in the absence of their longitudinal reinforcement, G. A. Aksomitas proposed the following formula [13]:

$$N_{b,\max} = R_b A_b \alpha_b, \quad (1.16)$$

where α_b is the relative area of the compressed zone of concrete.

For practical application, it was proposed to determine the relative area of the compressed concrete zone using a simplified formula:

$$\alpha_b = 1 - 0.85 e_0 / r_m \quad (1.17)$$

The mechanical characteristics of compressed concrete and their variability practically do not affect the value of the coefficient χ_b . Then these factors also practically do not affect the value of the relative area.

At present, the strength of the annular sections of the columns is calculated in accordance with the Russian Building Regulations 63.13330, taking into account the ratio of the inner and outer radii of annular cross-section: $r_1/r_2 \geq 0.5$ and the reinforcement uniformly distributed around the circumference (seven longitudinal bars). The calculation is carried out depending on the relative area of the compressed zone of concrete (Fig. 1.1):

$$\xi_{cir} = \frac{N + R_s A_{s,tot}}{R_b A + (R_{sc} + 1.7 R_s) A_{s,tot}} \quad (1.18)$$

where ξ_{cir} is the relative area of the compressed zone of concrete, R_s is the design tensile strength of reinforcement, R_b is the resistance of concrete to axial

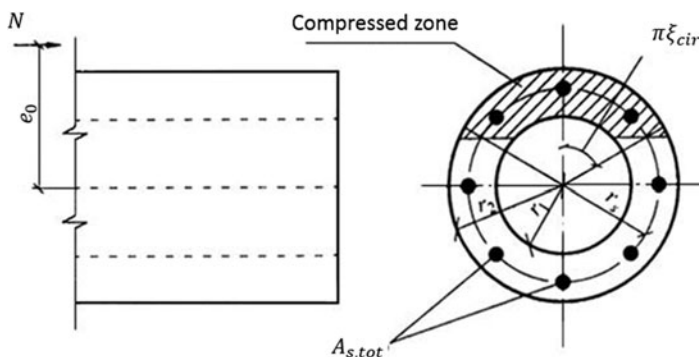


Fig. 1.1 Calculation scheme for the annular section of compressed element

compression, R_{SC} is the design compressive strength of reinforcement, A is the concrete cross-sectional area, and $A_{s,tot}$ is the cross-sectional area of all longitudinal reinforcement.

(i) At $\xi_{cir} \leq 0.15$, based on the condition for the bending moment M :

$$M \leq (R_b A r_m + R_{sc} A_{s,tot} r_s) \frac{\sin \pi \xi_{cir1}}{\pi} + 0.295 R_s A_{s,tot} r_s, \quad (1.19)$$

where

$$\xi_{cir1} = \frac{N + 0.75 R_s A_{s,tot}}{R_b A + R_{sc} A_{s,tot}}. \quad (1.20)$$

(ii) At $0.15 < \xi_{cir} < 0.6$, based on the condition for the bending moment M :

$$M \leq (R_b A r_m + R_{sc} A_{s,tot} r_s) \frac{\sin \pi \xi_{cir}}{\pi} + R_s A_{s,tot} r_s (1 - 1.7 \xi_{cir}) \times (0.2 + 1.3 \xi_{cir}). \quad (1.21)$$

(iii) At $\xi_{cir} \geq 0.6$, based on the condition for the bending moment M :

$$M \leq (R_b A r_m + R_{sc} A_{s,tot} r_s) \frac{\sin \pi \xi_{cir2}}{\pi}, \quad (1.22)$$

where

$$\xi_{cir2} = \frac{N}{R_b A + R_{sc} A_{s,tot}}. \quad (1.23)$$

In formulae (1.18), (1.19), (1.20) and (1.21), $A_{s,tot}$ is the cross-section square of the entire longitudinal reinforcement and

$$r_m = \frac{r_1 + r_2}{2} \quad (1.24)$$

is the radius of the circle passing through the centers of gravity of the longitudinal reinforcement bars and the moment M is determined taking into account the influence of the deflection of the concrete element.

1.4 Working Concepts, Goals, and Objectives

The performed analysis of existing studies made it possible to draw the following conclusions:

- (i) It is obvious that centrifugation of predominantly compressed concrete elements is the most promising technology for creating constructions with a functionally gradient structure that is made of the same material, but with different cross-sectional characteristics that are quite different from each other.
- (ii) In the long run, variatropy itself should be assessed as a positive phenomenon that has a positive effect on the characteristics of materials, provided it is regulated in the desired goals and directions.
- (iii) From the first two conclusions it follows that for certain building constructions, it is advisable to enhance variatropy by technological methods. With this aim, it is necessary to improve the centrifugation technology chosen as the base one and to determine its optimal parameters.
- (iv) It is necessary to introduce into the calculation of constructions made of functionally gradient concrete different (or local) characteristics of concrete, improving the existing standards and creating new calculation methods.
- (v) It is advisable to check all above concepts not only with physical experiments in laboratory conditions, supplementing them with a numerical experiment with significantly expanded boundaries of variation of the factors under study, but also in manufacture conditions, redesigning and improving real building constructions.

The results of the analysis and directions for further research are presented below.

The research objects are centrifuged and vibro-centrifuged concretes of functionally gradient structure and their compressed elements.

The research subjects are (i) the technologies for producing concretes of functionally gradient structure, (ii) structural characteristics of functionally gradient concretes, and (iii) account of the functional gradient in the calculation and design of compressed reinforced concrete elements from the concretes.

The working hypothesis of the research is the improvement of (i) the *manufacturing technology* due to the transition to vibro-centrifugation, (ii) the *design solutions* due to the manufacture of vibro-centrifuged compressed reinforced concrete elements, and (iii) their *calculation and design* taking into account the variation and characteristics of concrete differing in cross-section and, as a whole, the use of previously hidden reserves.

The objectives of the study are (i) to improve the manufacturing technology and the method of obtaining concretes of functionally gradient structure and their vibro-centrifuged constructions with concrete characteristics differing in cross-section, and (ii) to develop recommendations for the computational assessment of the characteristics of concrete and the operation of structures.

The research objectives are:

- (i) To analyze the technologies for manufacturing concretes of functionally gradient structure and constructions of their annular cross-section
- (ii) To study the physics of the processes occurring when obtaining the functionally gradient structure of vibro-centrifuged concrete goods
- (iii) To identify and evaluate the influence of technological factors on the properties of centrifuged and vibro-centrifuged concretes and to state optimal combinations of their values
- (iv) To investigate aggregate (the same in section) and local (differing in section) design characteristics of centrifuged and vibro-centrifuged concretes of functionally gradient cross-sections
- (v) To propose theoretical recommendations for the calculation of the design characteristics of centrifuged and vibro-centrifuged concretes, depending on technological factors and age
- (vi) To develop methods for calculating centrifuged and vibro-centrifuged reinforced concrete columns, taking into account the functionally gradient concrete
- (vii) To identify and evaluate previously disregarded hidden strength reserves of centrifuged reinforced concrete columns

Chapter 2

Technology and Experimental Setup for Manufacturing Centrifuged (CF) and Vibro-centrifuged (VCF) Concrete Elements with Functionally Gradient Structure



Abstract In this chapter, the theoretical substantiation and physical essence of obtaining the functionally gradient structure of centrifuged and vibro-centrifuged concrete elements of annular cross-section are formulated. Then, analysis of existing devices for centrifugation is presented together with an original experimental device, developed for centrifugation and vibro-centrifugation of concrete. It allows one to choose initial materials for the research of concrete samples and basic compositions of centrifuged and vibro-centrifuged concrete elements of annular cross-section with a functional gradient structure. The resonance method, used for study column concrete structures, based on measuring and calculating the amplitudes and spectral characteristics of construction, and the damping decrement of small vibrations are discussed. Finally, the methods and instrumental apparatus are selected for test investigations of the considered concrete structures.

Key words Centrifuged · Vibro-centrifuged concrete elements · Resonance method · Spectral characteristics · Damping

2.1 Theoretical Grounds of the Formation of the Functionally Gradient Structure of Concrete CF- and VCF-Elements of Annular Cross-Section

First, a qualitative picture of the change in the characteristics of the concrete cross-section during centrifugation is considered [8–10, 206].

The forces developing during centrifugation give the particles of the mixture an acceleration that is directly proportional to the mass of the particles, the square of the angular velocity, and the distance from the axis of rotation.

The study of the scheme for applying forces to a unit of mass during centrifugation made it possible to draw the following conclusion: so that the particles of the mixture, raised during the rotation of the mold to the uppermost position, do not break away from its walls and do not fall, it is necessary that the force of gravity of

the particle mg and the centrifugal force are balanced (Fig. 2.1). Centrifugal force acts on a particle of concrete mix according to the dependence:

$$P_n = m\omega^2 \delta = \frac{P_p \omega^2 \delta}{g}, \quad (2.1)$$

$$P_p = mg, \quad (2.2)$$

where m is the mass of a concrete mixture particle; ω is the angular velocity of the particle; δ is the radius of rotation of the center of gravity of the particle, m ; P_p is the particle weight; and g is the acceleration of free fall.

The force P acting on a particle of the concrete mixture is determined as the sum of P_n and P_p (see Fig. 2.2):

Fig. 2.1 Sectional element of the sample wall

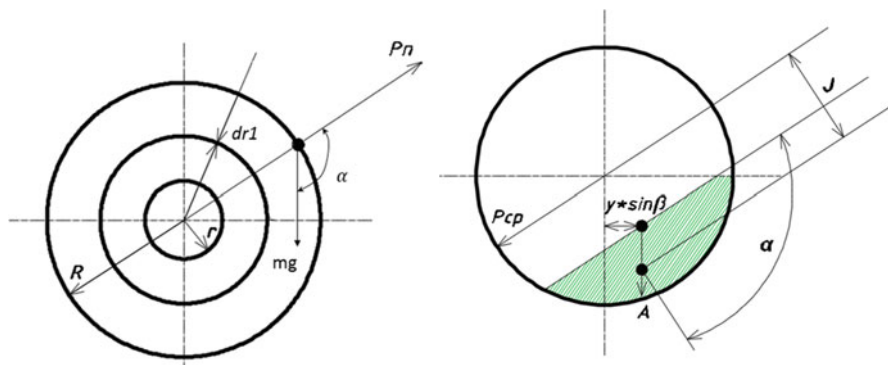
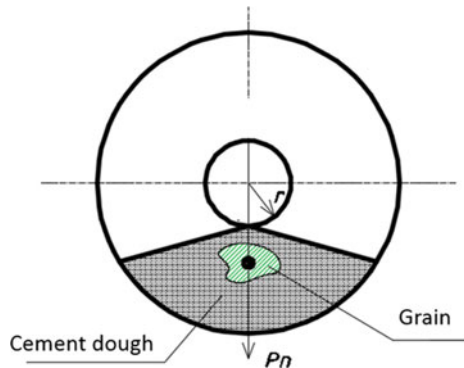


Fig. 2.2 Scheme for calculating the force acting on a concrete particle

$$P = P_n + P_p = \sqrt{(m\omega^2\delta)^2 + (mg)^2 + 2m\omega^2\delta mg \cos\alpha} \quad (2.3)$$

When the particle is in the top position, that is, at $\alpha = 0$, $\cos\alpha = 1$.

Then $P_1 = \sqrt{m^2(\delta\omega^2 + g)^2} = m\omega^2\delta + mg$, that is, $P_n = P_p$.

When the particle is in the down position, that is, at $\alpha = 180^\circ$, $\cos\alpha = -1$.

Then

$$P_2 = \sqrt{m^2(\delta\omega^2 - g)^2} = m\omega^2\delta - mg \quad (2.4)$$

The average force P_a acting on a particle will be:

$$P_a = \frac{P_1 + P_2}{2} = \frac{(m\omega^2\delta + mg) + (m\omega^2\delta - mg)}{2} = m\omega^2\delta. \quad (2.5)$$

The critical angular velocity ω_c of the mold is determined, which is necessary to keep the particle of the concrete mixture in the upper position as

$$\omega_c = \sqrt{\frac{g}{\delta}} \approx \frac{3.14}{\sqrt{\delta}} \quad (2.6)$$

or the number of revolutions per second, n_c :

$$n_c = \frac{1}{2\sqrt{\delta}}. \quad (2.7)$$

The angular velocity during the distribution of the concrete mixture should have a necessary minimum value in order to prevent the stratification of the concrete into its constituent parts due to the different masses of the particles. Taking into account the properties of the concrete mixture, the necessary minimum value of the angular velocity ω_{\min} should be greater than the critical value in $k = 1.4 \div 1.5$ times:

$$\omega_{\min} = k\omega_c = \frac{(1.4 \div 1.5)3.14}{\sqrt{\delta}} = \frac{4.4 \div 4.7}{\sqrt{\delta}} \quad (2.8)$$

or

$$n_{\min} = kn_c = \frac{1.4 \div 1.5}{2\sqrt{\delta}} = \frac{0.7 \div 0.75}{\sqrt{\delta}}. \quad (2.9)$$

During the period of compaction of the concrete mixture, the angular velocity of the mold, ω_a , is determined in [10] as

$$\omega_a = \sqrt{\frac{3P_n g R}{Y_{sw}(R^3 - \delta^3)}} \approx 5.4 \sqrt{\frac{P_n R}{Y_{sw}(R^3 - \delta^3)}}, \quad (2.10)$$

where R is the radius of the outer annular element, δ is the inner radius of the annular element, and Y_{sw} is the specific weight of concrete mixture.

Or the number of revolutions is:

$$n_r \approx 0.86 \sqrt{\frac{P_n R}{Y_{sw}(R^3 - \delta^3)}}. \quad (2.11)$$

To check the physical model of the movement of the components of the concrete mixture and the formation of the structure during centrifugation in a laboratory centrifuge, samples of annular cross-section with basic dimensions of $0.300 \times 0.165 \text{ m}^2$ (height \times outer diameter) and a wall thickness of 0.05 m were manufactured. Then, the samples were cut with a diamond disk into half rings and segments, which were ground from the ends.

As can be seen from Fig. 2.3, when compacting by centrifugation, the concrete mixture is divided into zones according to the grain sizes. A coarse-grained aggregate with greater mass moves to the outer surface of the product, and with lesser mass, accordingly, closer to the inner surface. The speed of separation of particles is the faster, the denser, and larger the aggregate and the higher the rotation speed of the mold. A large dense aggregate reaches the outer surface of the product during several full mold revolutions (for 1–1.5 s) that is still being distributed; at the same time, the small dense aggregate attains this position only after 200–205 s.

It is this difference in the drift velocity of particles of different sizes that determines the specific (functionally gradient) structure of freshly formed

Zones of the centrifuged product:	Zones of vibro-centrifuged product:
I – coarse-grained aggregate;	I – coarse-grained aggregate;
II – ordinary aggregate;	II – ordinary aggregate ate;
III – fine-grained aggregate;	III – fine-grained dense aggregate;
IV – cement stone;	IV – fine-grained loose aggregate;
V – cement slurry	V – small amount of cement slurry

Fig. 2.3 Scheme of dividing the concrete mixture into zones during centrifugation and vibro-centrifugation

centrifuged concrete. Its outer layer is formed, in the main, by a coarse-grained aggregate with a layer of cement paste. As it approaches the inner surface, the content of fine-grained aggregate particles and cement dough gradually increases. The control of this process when obtaining a three-layer vibro-centrifuged concrete structure can be carried out under the condition that the coarse-grained aggregate must be monodisperse.

As a result, the functional gradient of concrete density is expressed not only by the heterogeneity of the structure of the cement stone but also by the features of the distribution of aggregate grains over the wall thickness of the concrete structure. Then the acting centrifugal force, proportional to the mass of the rotating solid, will affect the formation of layers in the process of compaction during vibration centrifugation.

To confirm the above, a calculation is carried out based on the action of centrifugal force on the grain of a dense (granite) aggregate.

Let r_{mg} be the mean grain radius of the coarse-grained aggregate and ρ_{mg} be the average density of the aggregate grains (granite-2690). Then the centrifugal force, F_{cf} , can be expressed in the form (perfect sphere assumed) [10]:

$$F_{cf} = \frac{4\pi}{3g} r_{mg}^3 \rho_{mg} l \omega^2, \quad (2.12)$$

where r_{mg} , ρ_{mg} are the mean grain radius and the density of the coarse-grained aggregate and l is the distance from the rotation center to the center of the grain and

$$\omega = \frac{\pi n}{0} \quad (2.13)$$

where ω is the angular speed of rotation at the number of revolutions for concrete compaction $n = 2179$ rpm for the sample with $D = 0.165$ m.

The results of calculations on the action of centrifugal force are presented in Table 2.1.

From expression (2.12) it follows that the effect of centrifugal force (Fig. 2.4) is the more significant, the larger the mean radius and average density of the grains (Fig. 2.5).

Table 2.1 Results of calculations on the action of centrifugal force

Mean grain radius of coarse-grained aggregate, m	Distance from the center of rotation to the center of the grain aggregate, m	Centrifugal force acting on the mean grain of coarse-grained aggregate, N dense (granite)
0.0025	0.08	0.075
0.005	0.0775	0.58
0.01	0.0725	4.35
0.015	0.0675	13.7
0.02	0.0625	30.0

Fig. 2.4 Scheme for determining the distance from the center of rotation to the center of the grain with the outer diameter of the centrifuged concrete structure $D = 165$ mm

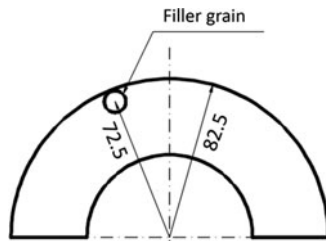
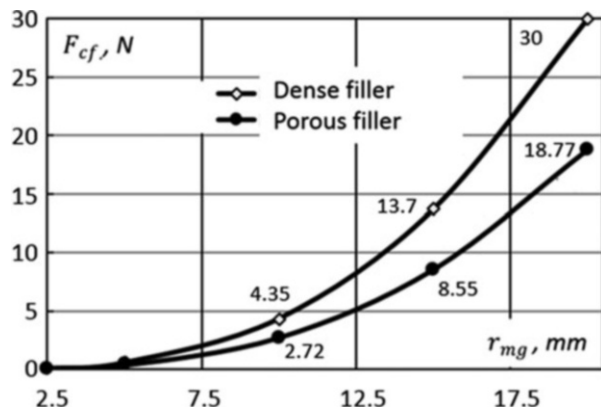


Fig. 2.5 Change in centrifugal force (F_{cf}) vs. the mean grain radius of the coarse-grained aggregate (r_{mg})



In accordance with this, the distribution of grains of denser and more porous aggregates over the section of the concrete structure also changes, forming a multilayer (approximately three-layer) annular cross-section with a functionally gradient structure. This variation will affect the strength of vibro-centrifuged concrete in comparison with that which would be with a non-uniform distribution of grains of dense aggregate, consisting of a mixture of grains with 0.005–0.02 m over the entire section of the element.

To obtain a quantitative picture, a surface sounding technique is suitable. A certain volume ABCD with a wall thickness h is allocated from a cylindrical element of a tubular section (Fig. 2.6) and the change in its average density of the concrete mixture along the thickness and length of the concrete structure is determined. At the same time, according to the known data, the wall thickness is recommended to be taken as 1/10 of the tube diameter. Therefore, for the presented sample with an inner diameter of 0.165 m, the wall thickness of the concrete structure is assumed to be 0.0165 m. The physical and mechanical properties of the molded samples of the vibrated and centrifuged concrete structures are presented in Table 2.2, and the overall dimensions should correspond to those shown in Fig. 2.6.

The sounding results for centrifuged concrete samples are presented in Table 2.3.

Based on the results of sounding the samples of centrifuged concrete structures, the following conclusions can be drawn:

Fig. 2.6 Layout of points for surface sounding

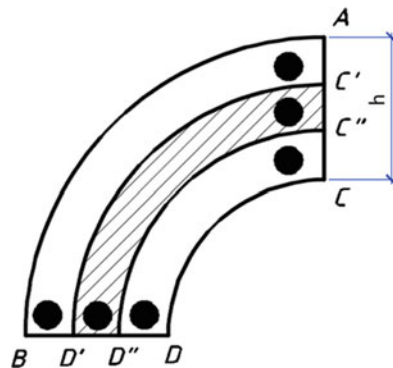


Table 2.2 Physical and mechanical properties of four test concrete samples

No.	Mass, kg	Volume, m ³	Average density, kg/m ³	Compressive strength, MPa	
				Vibrated concrete	Centrifuged concrete
1	5.837	2308×10^{-6}	2528	29.1	39.8
2	5.871		2543	29.2	40.0
3	5.903		2557	30.0	41.0
4	5.789		2508	28.1	38.4

Table 2.3 Sounding results four test concrete samples

No.	Wave velocities, m/s			Compressive strength, MPa		
	Outer	Middle	Inner	Outer	Middle	Inner
1	4940	4891	4741	44.2	42.9	39.4
2	5110	4921	4632	44.4	43.2	37.8
3	5120	4938	4852	45.2	44.1	41.5
4	4890	4861	4684	43.0	42.1	38.3

- (i) *Density of the centrifuged product.* The closer to the outer layer, the higher the ultrasound propagation speed and, respectively, the denser the concrete. The closer to the inner layer, the lesser the ultrasound propagation speed and the lesser the density of concrete.
- (ii) *Crushed stone fractions in the composition of concrete.* Most dense and strength concrete frame is obtained with one fraction of 0.005–0.01 m. It is due to the greater homogeneity of the structure of the concrete mixture. At the same time, the functional gradient of concrete properties is minimal (the difference in strength between the outer and inner layers is equal to 8.2%). For a mixture of two fractions of 0.005–0.01 m and 0.01–0.02 m, the functional gradient takes an intermediate position (the difference in strength between the outer and inner layers is equal to 11.5%). For one fraction of 0.01–0.02 m, the functional gradient is maximum (the difference in strength between the outer and inner layers is 15%).

Thus, it is obvious that the concrete structure of the wall of centrifuged and vibro-centrifuged concrete is not uniform in thickness, but *functionally gradient*, that is, it has differences in properties, which can be quite significant and in certain cases it should be taken into account in calculations.

2.2 Experimental Centrifugation Facilities

2.2.1 Functional Gradient of Centrifuged Concrete

It is known that in the process of compaction by centrifugation, the composition of concrete changes significantly. So, about 20–45% of water is squeezed out of the concrete mixture, depending on the compaction force. A positive factor is that after centrifugation, the rest of the water combines together with some cement additives and particles of lightweight contaminants in the mixture with a sludge.

At the same time, a contamination remains in concrete, compacted in any other way. It significantly impairs the concrete structural properties. Thus, the strength can be significantly increased by centrifugation, compared to vibration.

As noted above, centrifuged concrete is characterized by a substantially inhomogeneous structure and texture over the thickness of the annular cross-section wall. The heavy components of the concrete mixture are concentrated at the outer surface of the element, where the concrete has a higher strength, and the lighter components are shifted to the center of rotation. Thus, concrete is obtained with different physical and mechanical characteristics within the same structure. This phenomenon is called *functionally gradient*.

Compressible centrifuged elements (columns), due to the greater strength of concrete and greater stiffness in bending, can be made with a smaller cross-section, that is, lighter [113]. Therefore, the cost of centrifuged structures on average is 30–40% less than vibrated structures for the same purpose.

The main shortcoming of the centrifuged molding of constructions is the separation of sludge and non-uniform distribution of components over the thickness of the concrete cross-section. The resulting filtration channels increase the permeability of the concrete. Here a lot depends on the design of centrifuging devices [66, 169].

2.2.2 Centrifugation Setups

Roller centrifuges are relatively simple in design, but their noise level is significantly higher than the standards. Their shortcomings are as follows: (i) significant metal consumption of forms due to the need to install tires, (ii) an increase in the total labor intensity of manufacture, (iii) frequent repairs due to the transfer of rotation due to friction forces on the tires from rollers, and (iv) replacement of worn-out parts, which is laborious and expensive.

The advantages of the roller centrifuges are as follows: (i) the possibility of manufacturing large-diameter pipes, (ii) loading a mixture into the mold while rotating in large doses, and (iii) convenient drainage of sludge after centrifugation.

Centrifuged columns are usually made from mobile concrete mixtures with a grade of M1 workability (the draft of the concrete mixture cone is 2–3 cm). During the manufacturing process, due to the influence of centrifugal forces, excess water is squeezed out, which flows out of the mold in the form of sludge, and freshly formed concrete has sufficient strength for transporting molds with the concrete to the steaming chambers [6, 217, 218, 281, 319].

It could be assumed that in order to improve the quality of the compaction of mixture, it is advisable to combine centrifugation with vibration. Then this mode can be called *vibro-centrifugation*. By using it, the initial water content in the cement gel can be reduced to $W/C = 0.24$, and compaction will occur without sludge delamination due to the redistribution of the liquid phase and other factors.

It should be noted that during vibro-centrifugation, a more uniform distribution of aggregate grains is achieved, and cement consumption can be reduced additionally by about 30% compared to filtration centrifugation of a viscoplastic concrete mixture [10].

By vibro-centrifugation, it is possible to form structures of an annular cross-section from a concrete mixture at a W/C ratio close to 0.28. In this case, vibration can also be considered as a mean of liquefying the concrete mixture at the stages of its distribution and compaction under the action of centrifugal force.

To create rotary motion, centrifuges driven by DC electric motors with variable speeds are usually used. This provides two modes of operation: (i) the distribution of the concrete mixture and (ii) its compaction [60, 198, 206, 223, 226].

2.3 Combined Unit for Centrifugation and Vibration Centrifugation, Its Features, and Calculations of Parameters

For studying the centrifuged and vibro-centrifuged concretes, the authors developed and applied a universal experimental setup, namely, an experimental laboratory centrifuge TsSRL-1 with a DC electric motor with thyristor power supply. This ensured smooth speed switching by changing the rotational speed of the electric motor shaft [107, 148, 269, 273]. The schematic diagram of the TsSRL-1 experimental centrifuge is shown in Fig. 2.7.

The experimental laboratory roller centrifuge TsSRL-1 (Fig. 2.7) consists of a frame on which two roller supports are mounted with lower support rollers. The drive includes a multi-speed electric motor with smooth stroke control. A general view of a laboratory centrifuge is shown in Fig. 2.8, and support rollers are presented in Fig. 2.9.

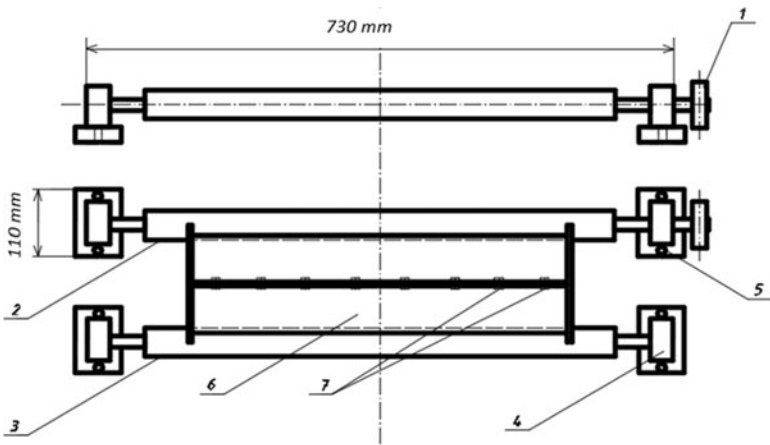


Fig. 2.7 Scheme of an experimental laboratory centrifuge TsSRL-1: 1 centrifuge drive pulley, 2 leading support roller, 3 driven support roller, 4 stop of the shaft of the support clutch with a ball bearing, 5 fasteners of the stop to the bed (bolt M12), 6 form, and 7 connection of the halves of the mold (bolt M8)



Fig. 2.8 General view of laboratory device TsSRL-1 to manufacture centrifuged and vibro-centrifuged prototypes

The support rollers are supportive and, depending on the shape diameter, can be adjusted in width.

To prevent the shape from jumping off and the occurrence of bending deformations, some of the roller supports are manufactured in the form of lunettes with rollers that encircle the shape (a total of four rollers: two upper rollers located under angle of 60° and two lower ones disposed under angle of 120°). These rollers have folding brackets, which are closed after the mold is installed.

The originality of the design of the proposed centrifuge TsSRL-1 is defined by the original solution for the implementation of high-frequency vibration of the concrete mixture in addition to centrifugation. This is achieved by applying a serrated surface to the drive and driven roller of the centrifuge. The distance between the teeth is

Fig. 2.9 Support rollers for laboratory centrifuge TsSRL-1

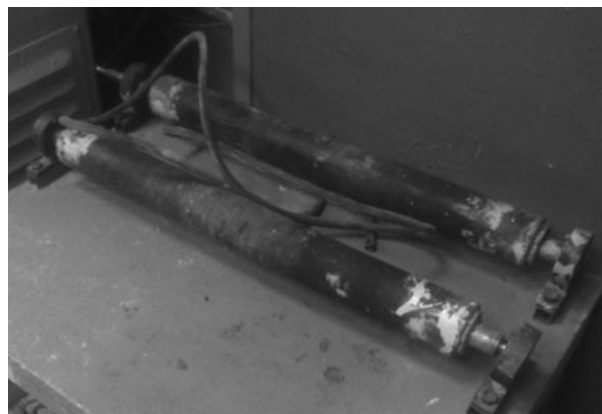


Fig. 2.10 Prefabricated metal molds for laboratory centrifuge TsSRL-1 with a diameter of 0.165 m



chosen in such a way that the vibration of the rotated form generated by them could be regulated; in particular, at a given maximum number of revolutions, it would provide more than 10,000 beats per minute and an amplitude of oscillations of about 1×10^{-4} m.

The order of forming the product is as follows: the concrete mixture is loaded into the assembled and installed on the roller form, after which the electric motor is switched on at the first speed. The mode of distribution of concrete in the mold is switched on; after finishing the regime, it is changed to the mode of compacting of concrete. As a side rigging for the centrifuge, two types of metal molds were used, namely, with a diameter of 0.168 and 0.205 m and a length of 0.3 m (see Fig. 2.10).

Common view of test centrifuged samples is shown in Fig. 2.11.

Modeling the main stages of molding by using device TsSRL-1 made it possible to adjust such parameters as the number of mold revolutions and the compaction time. As a whole, the generalized molding modes for centrifuged products [8, 9, 60] are presented in Fig. 2.12. Several main sections can be distinguished, which are characterized by rotation speeds and time.

Fig. 2.11 Common view of test centrifuged samples

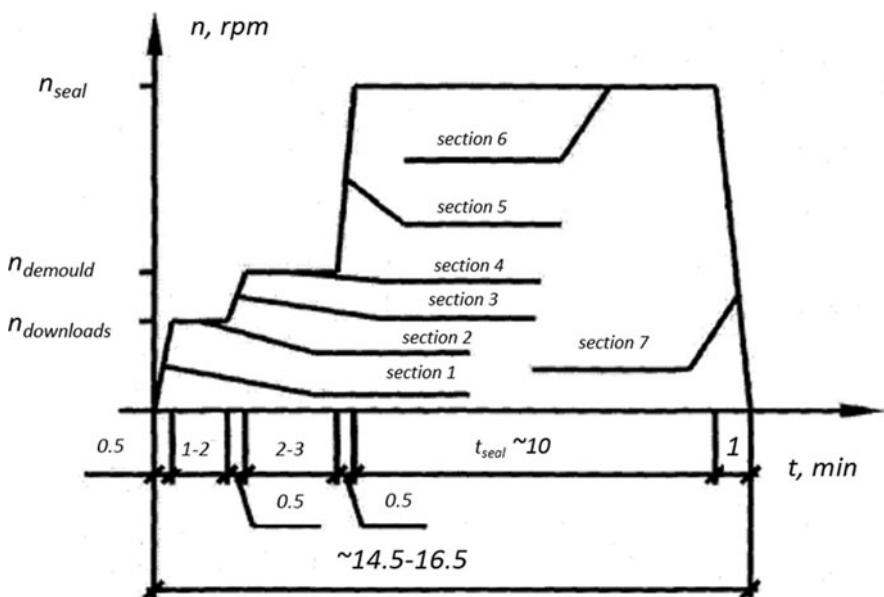
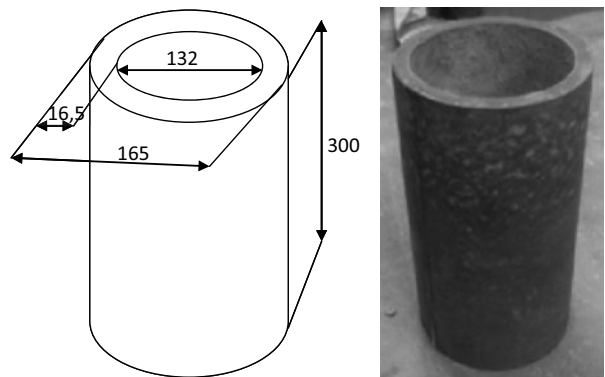


Fig. 2.12 Generalized modes of concrete mixture molding when centrifuging concrete structures of annular cross-section. The following sections are shown: 1 mold acceleration up to loading speed, 2 mold rotation, 3 mold acceleration up to distribution speed, 4 mold rotation at distribution speed, 5 mold acceleration up to compaction speed 6 centrifugation, and 7 smooth speed reduction

Section 2.1 is characterized by the acceleration of the mold from zero to the loading speed, and Sect. 2.2 is characterized by the subsequent rotation of the mold at this speed. The number of revolutions of the mold by loading the concrete mixture into the mold in the case of belt centrifuges is recommended to be determined by the formula [60, 321]:

$$n_{\text{load}} = 370 \sqrt{\frac{(R^2 - r^2)}{(R^3 - r^3)}}, \quad (2.14)$$

where R , r are the external and internal radii of the tube, respectively.

By molding concrete structures, the number of revolutions of the form when loading usually ranges from 80 to 150; at the same time, the larger the diameter of the mold, the lower the number of revolutions.

E. E. Mikhelson proposed to determine the number of revolutions based on the assumption that the value of the centrifugal force, created by the rotation of the concrete mass, is 3.5–3.7 times greater than the weight P of the concrete structure. This dependence was determined at W/C = 0.45–0.5 and cement grade 400–500 according to the formula [171]:

$$n_{\text{load}} = 700 \sqrt{\frac{(R^2 - r^2)}{(R^3 - r^3)}}. \quad (2.15)$$

The number of revolutions when loading the concrete mixture into the mold is presented in Table 2.4 and Fig. 2.13.

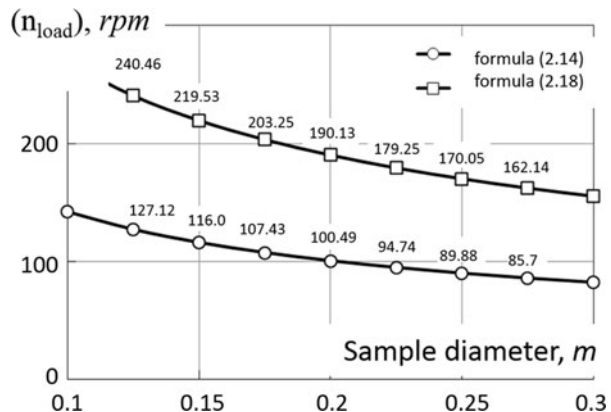
In Sect. 2.3, there is a smooth acceleration of the mold from the number of revolutions for loading speed to the number of revolutions for distribution speed. In Sect. 2.4, further rotation of the mold takes place at the distribution speed.

A. N. Popov proposed to determine the number of revolutions of molds during distribution as [217, 218]:

Table 2.4 Number of revolutions when loading the concrete mixture into mold

Sample diameter (D), m	Sample wall thickness ($D/10$), m	Sample inner radius (r), m	Sample outer radius (R), m	Number of revolutions during loading (n_{load}), rpm	
				Formula (2.14)	Formula (2.15)
0.100	0.0100	0.04	0.0500	142.1	268.87
0.125	0.0125	0.05	0.0625	127.1	240.46
0.150	0.0150	0.06	0.0750	116.0	219.53
0.175	0.0175	0.07	0.0875	107.4	203.25
0.200	0.0200	0.08	0.1000	100.5	190.13
0.225	0.0225	0.09	0.1125	94.7	179.25
0.250	0.0250	0.10	0.1250	89.9	170.05
0.275	0.0275	0.11	0.1375	85.7	162.14
0.300	0.0300	0.12	0.1500	82.0	155.24

Fig. 2.13 Dependence of the change in the number of revolutions on the diameter of the sample when loading the concrete mixture into the mold



$$n_{\text{dis}} = 30K \frac{\sqrt{g/r_1}}{p} = \frac{45}{\sqrt{r_1}}, \quad (2.16)$$

where $K = 1.4\text{--}1.45$ is the practical safety factor taking into account the vibration of the concrete mixture, r_1 is the inner radius of a reinforced concrete tube, g is the acceleration of free fall, and p is the pressure in the concrete mixture.

In accordance with the research of L. A. Volkov [299], in order to prevent the concrete mixture from collapsing and the shear of lubricant, the spreading stage should last from 50 to 100 s at a speed of 100 to 350 rpm, depending on the diameter. In this case, the concrete mixture receives a preliminary compaction under the influence of compression pressure, approximately equal to 0.005–0.01 MPa. Therefore, in [299], a formula is proposed that takes into account the viscosity of a concrete mixture, similar to formula (2.16):

$$n_{\text{dis}} = \frac{42}{\sqrt{r_1}} \div \frac{54}{\sqrt{r_1}}. \quad (2.17)$$

B. V. Gusev and A. I. Zvezdov [321] proposed to calculate the number of revolutions of the mold for the uniform distribution of the concrete mixture during centrifugation by using the formula of I. N. Akhverdov [8, 9]:

$$n_{\text{dis}} = 3268 \sqrt{\frac{R}{(R^3 - r^3)}}. \quad (2.18)$$

For calculating the number of revolutions of the mold, the numerical coefficient can be increased to 60, which is consistent with the experimental data of L. A. Volkov [299]. Thus, taking adjustment into account, formula (2.21) takes the form:

$$n_{\text{dis}} = \frac{60}{\sqrt{r_1}}. \quad (2.19)$$

In practice, the distribution speeds of the molds are taken in the range from 120 to 300 rpm, depending on the diameter of the mold. The number of revolutions when distributing the concrete mixture in the mold is presented in Table 2.5 and Fig. 2.14.

After loading and distributing the mixture into the mold, the most important stage in terms of the quality of centrifuged concrete structure begins, namely, the stage of compaction. In Sect. 2.5, there is an increase in the acceleration of the mold from the number of revolutions when distributing the concrete mixture to its compaction number. In Sect. 2.6, there is mold rotation at maximum speed during the estimated time of centrifugation. Here, the final compaction of the centrifuged concrete structure takes place at maximum compression pressure.

The main parameters of centrifugation at the final stage are two quantities, namely, the number of revolutions of molds during compaction and the duration (time) of centrifugation.

I. N. Akhverdov [8, 9] assumes the optimal pressure to be the one at which the concrete is stabilized on its porosity, defined as the ratio of the sample surface to its volume, and the optimal compaction time is taken to be the one at which its mass stabilizes.

When calculating the number of revolutions of the mold during compaction, the formula of V. N. Sizov was used, as close as possible to practical results [315]:

$$n_{\text{com}} = 10375 \sqrt{\frac{r_2 p}{(r_2^3 - r_1^3)}}, \quad (2.20)$$

where r_1 and r_2 are the inner and outer radii of the tubular structure and $p = 0.145$ MPa is the pressure on the concrete mixture.

Table 2.5 Number of revolutions when distributing concrete mixture

Sample diameter, (D), m	Sample wall thickness ($D/10$), m	Sample inner radius (r), m	Sample outer radius (R), m	Number of revolutions during distributing (n_{dis}), rpm	
				Formula (2.18)	Formula (2.19)
0.100	0.0100	0.04	0.0500	225.0	300.0
0.125	0.0125	0.05	0.0625	201.3	268.3
0.150	0.0150	0.06	0.0750	183.7	244.9
0.175	0.0175	0.07	0.0875	170.0	226.8
0.200	0.0200	0.08	0.1000	159.1	212.1
0.225	0.0225	0.09	0.1125	150.0	200.0
0.250	0.0250	0.10	0.1250	142.3	189.7
0.275	0.0275	0.11	0.1375	135.7	180.9
0.300	0.0300	0.12	0.1500	129.9	173.2

Fig. 2.14 Dependence of the change in the number of revolutions on the sample diameter when distributing concrete mixture into the mold

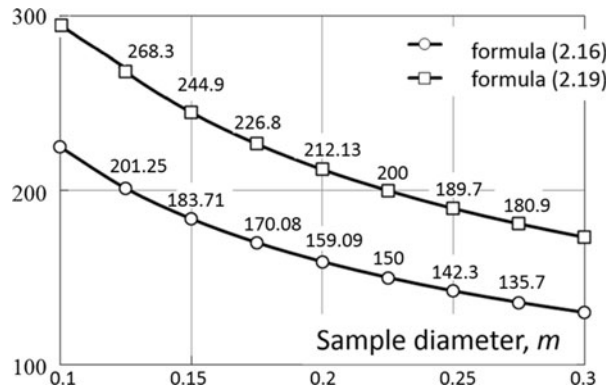


Table 2.6 Number of revolutions when compacting the concrete mixture in the mold

Sample diameter, (D), m	Sample wall thickness (D/10), m	Sample inner radius (r_1), m	Sample outer radius (r_2), m	Number of revolutions during compaction (n_{com}), rpm	
				$p = 0.07 \text{ MPa}$	$p = 0.145 \text{ MPa}$
0.100	0.0100	0.04	0.0500	2485.2	3576.77
0.125	0.0125	0.05	0.0625	1988.2	2861.35
0.150	0.0150	0.06	0.0750	1656.8	2384.55
0.175	0.0175	0.07	0.0875	1420.1	2043.81
0.200	0.0200	0.08	0.1000	1242.59	1788.39
0.225	0.0225	0.09	0.1125	1104.5	1589.68
0.250	0.0250	0.10	0.1250	994.07	1430.72
0.275	0.0275	0.11	0.1375	903.7	1300.64
0.300	0.0300	0.12	0.1500	828.4	1192.26

The number of revolutions when compacting the concrete mixture in the mold is presented in Table 2.6 and Fig. 2.15.

Based on the calculation formulae, the required number of mold revolutions was calculated in the main sections in the process of vibro-centrifugation of products of an annular cross-section on a laboratory device TsSRL-1 at various compression pressures. The calculation results are summarized in Table 2.7.

Thus, in this section, the existing centrifugation setups are analyzed, the original combined experimental setup for centrifugation and vibro-centrifugation is presented, its parameters are calculated, and test studies are carried out that confirm the correctness of the calculation assumptions and postulates.

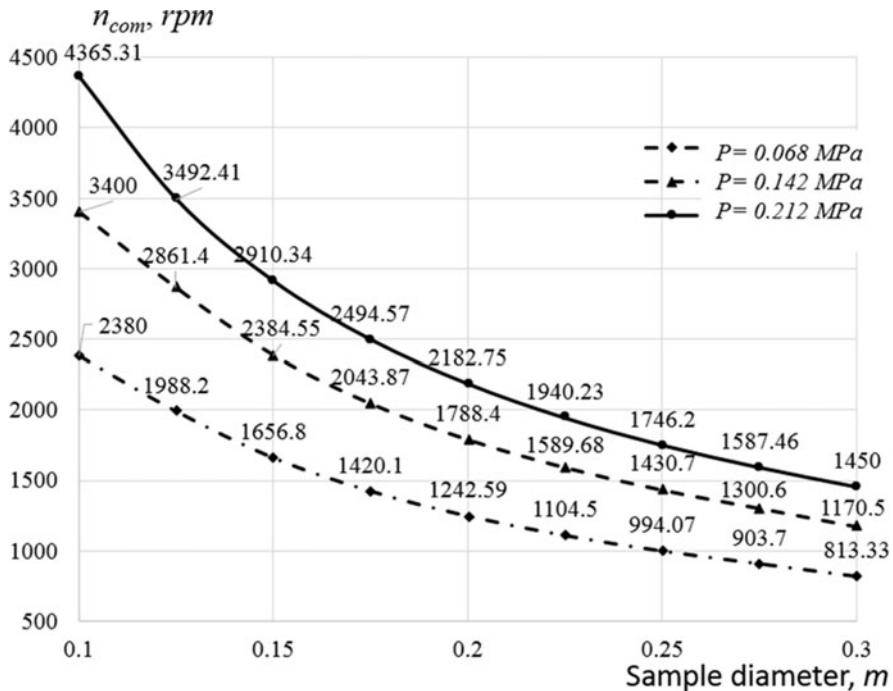


Fig. 2.15 Dependence of the change in the number of revolutions from the sample diameter during compaction

Table 2.7 Results of calculating the molding parameters on the experimental laboratory device TsSRL-1

Sample diameter, (D), m	Sample wall thickness ($D/10$), m	The number of revolutions in the sections				Actual pressure on concrete mixture, p , MPa	
		n_{load}	n_{dis}	n_{com} at pressure p , MPa			
				0.07	0.145		
2.05	0.205	145	185	1214	1748	0.104	
1.65	0.165	160	205	1514	2179	0.216	

2.4 Selection of Basic Concrete Compositions of Test Samples

After analysis of scientific data for research, the following were accepted as aggregates:

- (i) Crushed stone granite of the JSC “Pavlovsk Nerud” with a fraction of 0.005–0.02 m.
- (ii) Quartz sand of the Grushevskoye deposit (size modulus of sand $M_k = 2.0$).

Table 2.8 Physical properties of coarse-grained aggregate

Material	Fraction, m	Specific surface, m^2/kg	Bulk density, kg/m^3	True (average) density, kg/m^3	Void, %	Total water absorption
Crushed stone granite	0.0025–0.02	0.42	1460	2700 (2690)	0.457	0.41
	0.010–0.02	0.27	1430		0.468	0.40
	0.005–0.01	0.54	1510		0.438	0.42
	0.0025–0.005	0.94	1590		0.408	0.45

Table 2.9 Physical and mechanical indicators of crushed granite of fraction 0.005–0.02 m (JSC “Pavlovsk Nerud”)

Name of indicators	Actual indicators	Requirements of Russian GOST 8267
Content of dusty and clay particles, % by weight	0.66	<1
Clay content in lumps, % by weight	—	0.25
The content of lamellar (flaky) grains and needle forms, %	37.0	From more than 35 to 50 for group No. 5
Crushing capacity, % by weight	10.6	To 12 including for brand Dr1400

Table 2.10 Physical properties of fine-grained aggregate

Fraction, m	Particular residue, %	Specific surface, m^2/kg	Bulk density, kg/m^3	True density, kg/m^3	Void, %	Total water absorption
0.0025–0.005	2.41	8.89	1259.4	2600	0.515	1.914
0.00125–0.0025	2.95					2.07
0.00063–0.00125	7.3					2.3
0.000315–0.00063	50.4					3.46
0.00014–0.000315	30.19					6.0
<0.00014	4.24					12.0

The physical properties of coarse-grained aggregate are presented in Tables 2.8 and 2.9, and the properties of fine-grained aggregate are shown in Table 2.10. Portland cement was used as a binder, the physical and mechanical properties of which are presented in Table 2.11.

As a result of calculated selection, the compositions of concrete mixtures (see Table 2.12) were determined. The optimization of concrete compositions and the choice of the type of components for them were carried out using the method of mathematical planning of the full factorial experiment (FFE). Statistical analysis and processing of the obtained results were carried out by using “MathCAD.”

Table 2.11 Physical and mechanical properties of cement

Name	Specific surface, m ² /kg	Normal density, %	Setting time, hours-min		Activity, MPa	
			Beginning	End	R _{bend}	R _{comp}
Portland cement	365	25.5	1–05	3–15	5.9	51.5

Table 2.12 Compositions of concrete mixtures

No.	Fraction of coarse filler, m	Material consumption per 1 m ³				Cone dis-placement, m	Average density of concrete mixture, kg/m ³
		Crushed stone	Sand	Cement	Water		
1	0.005–0.02	1203	696	416	181	0.038	2496
2	0.01–0.02	1173	717	426	185	0.040	2501
3	0.005–0.01	1274	658	398	175	0.035	2505
4	0.0025–0.005	1332	615	371	165	0.031	2483

All accepted concrete compositions were used in test experimental studies in order to work out the parameters of the proposed experimental combined device for centrifugation and vibro-centrifugation. For the main experimental studies, the results of which are given further, the selected composition of concrete No. 1 from Table 2.12 was used.

Then some experimental methods and devices for the study of building materials and constructions will be presented.

2.5 Resonance Method

The resonance method, used for study column concrete structures, is based on measuring and calculating the amplitudes and spectral characteristics of construction and also the damping decrement of small vibrations. The longitudinal, bending, and torsional oscillations of simple rod structure can be considered as ideal ones [11, 23, 49, 52, 55, 197, 250, 303]. The method consists of the following stages:

- The vibration amplitudes are measured at several points of the structure at its stationary oscillations with obtainment of dynamic images of the construction vibrations in the form of output characteristics.
- The data of the vibration patterns are processed by using the analytical Fourier transform and the vibration resonances are selected.
- The application of inverse methods for restoring properties based on analytical dependences, for example, by applying the Bernoulli beam theory, allows calculating the elastic modulus E , shear modulus G , and Poisson's ratio ν of the considered construction.

For example, for a simple beam structure with a length l at a certain spectrum of natural bending frequencies ω_n , the modulus of elasticity E can be determined as

$$E = \omega_n^2 \left(\frac{l}{\pi n} \right)^4 \frac{\rho F}{J}, \quad (2.21)$$

where ρ is the mass density, F is the cross-sectional area of the beam, J is the moment of inertia of the cross-section, $n = 1, 2, \dots$ is the number of the vibration mode, and $\omega_n = 2\pi f_n$, where f_n is the oscillation frequency. In the presence of natural frequencies of longitudinal vibrations, the modulus of elasticity E can be determined as

$$E = \omega_n^2 \frac{\rho}{\pi^2 n^2}. \quad (2.22)$$

The spectrum ω_n of transverse vibrations of an elastic beam with a thickness h is expressed as follows:

(i) For asymmetric oscillations:

$$\omega_n = \frac{2\pi n V_L}{h}, n = 1, 2 \dots \quad (2.23)$$

(ii) For symmetric oscillations:

$$\omega_n = \frac{(2n - 1)\pi V_L}{h}, n = 1, 2 \dots \quad (2.24)$$

where V_L is the speed of the longitudinal wave.

By using indirect analysis, the dependences of material properties, defectiveness, and stiffness of individual nodes on the amplitudes $E \sim f(A)$ and frequencies $E \sim f(\omega_n)$ can be obtained on the basis of analytical functional characteristics of regression analysis [50, 123, 219, 220]. The analytical and numerical methods of the theory of vibrations make it possible to study the vibrations of elastic bodies of a more complex shape [12, 48, 79, 216, 263–265].

2.6 Instrumental Methods of Experimental Studies of Prototypes

During the development of the experimental combined device for centrifugation and vibro-centrifugation with the choice of parameters of the studied concrete samples, most interest was directed to the characteristics of concrete density and porosity (both general in cross-section and in its separate layers).

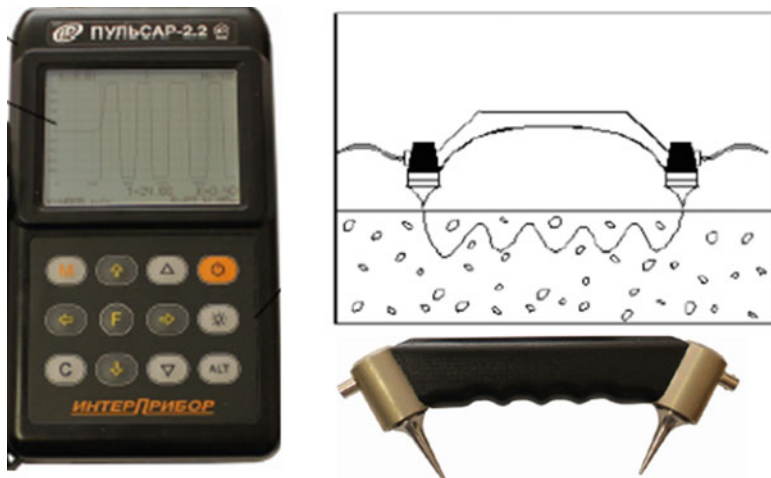


Fig. 2.16 Common view of the device and its disposition at sounding the surface

Table 2.13 Technical characteristics of device “Pulsar 2.2”

No.	Characteristic	Units	Value
1	Measurement range of ultrasonic propagation velocity	m/s	1000–10,000
2	Measurement range of ultrasonic propagation time	mks	10–100
3	Measurement base for sounding the surface	mm	120 ± 1
4	Power consumption, no more	W	0.7
5	Device mass with complete set, no more	kg	1.5
6	Overall dimensions (length × width × height)	mm	
	Of electronic unit		$205 \times 115 \times 35$
	Of the sensor of sounding the surface		$250 \times 50 \times 100$
	Of the sensor of through sounding		$\varnothing 36 \times 62$

The characteristics of the integral porosity of concrete (the average radius $\bar{\lambda}_2$ and uniformity of the distribution of pores α in concrete) were determined in accordance with the graph-analytical method of M. I. Brusser [39] based on the study of the kinetics of water absorption. Surface sounding of centrifuged concrete samples was carried out using a meter of time and velocity of propagation of ultrasound “Pulsar-2.2.” It was designed to assess the strength, density, and modulus of elasticity and also defectoscopy of building materials in terms of time, velocity of propagation, and the shape of ultrasonic impulses. The general view of the device and its disposition during sounding are shown in Fig. 2.16. The technical characteristics of the device are presented in Table 2.13.

Moreover, another experimental approach can be used for estimating the properties of material structure based on measuring the sound speed in concrete structures [150, 266]. The adopted instrumental research methods of concrete prototypes and the used instruments and equipment made it possible to assess the picture of the real functionally gradient structure and make sure that the accepted direction of research was correct.

2.7 Conclusions

1. The theoretical substantiation and physical essence of obtaining the functionally gradient structure of centrifuged and vibro-centrifuged concrete elements of annular cross-section are formulated. The qualitative and quantitative picture of the density functional gradient of the layers of annular cross-section during centrifugation and vibro-centrifugation at different ratios of concrete aggregate fractions is presented.
2. The analysis of existing devices for centrifugation has been carried out; an original combined experimental device has been developed, which allowed performing both centrifugation and vibro-centrifugation; the calculation of its parameters has been carried out; and test experimental studies have been performed, which have confirmed the correctness of the design conception and postulates.
3. The choice of initial materials for concrete research has been made, and the basic compositions of centrifuged and vibro-centrifuged concrete elements of annular cross-section with a variotropic structure have been determined.
4. The resonance method, used for the study of column concrete structures, based on measuring and calculating the amplitudes and spectral characteristics of construction, and also the damping decrement of small vibrations is discussed in necessary details.
5. Methods and instrumental apparatus were selected for experimental studies of centrifuged and vibro-centrifuged concrete structures of annular cross-section, which made it possible to assess the picture of the real functional gradient structure and make sure that the accepted direction of research was correct.

Chapter 3

Aggregate and Local Characteristics of Vibrated (V), Centrifuged (CF), and Vibro-Centrifuged (VCF) Concretes



Abstract This chapter presents the original test method for researching the functionally gradient cross-sections of vibrated, centrifuged, and vibro-centrifuged concretes in order to determine their aggregate (general) and local (differing in layers) strength and strain properties with deformation diagrams. It is proved that by using vibro-centrifugation it becomes possible to obtain concretes with improved structure and higher characteristics compared with centrifugation and vibration procedures. A three-layer model of the functionally gradient structure of centrifuged and vibro-centrifuged concrete has been experimentally confirmed. Differentiation of the characteristics of layers of functionally gradient concrete is obtained: the concrete of the outer layers has the highest strength, modulus of elasticity, and the least deformability; the concrete of the inner layers demonstrates the lowest strength, modulus of elasticity, and the highest deformability; the concrete of the middle layers shows average characteristics. The corresponding deformation diagrams are also differentiated by layers.

Key words Aggregate · Local properties; Vibrated · Centrifuged · Vibro-centrifuged concretes; Deformation diagram

3.1 Schedule and Methodology of Experimental Studies of the Ultimate Characteristics of Concrete

3.1.1 Manufacture Methods

As a whole, nine experimental vibrated, centrifuged, and vibro-centrifuged samples of annular cross-section were manufactured and tested (see Fig. 3.1) with an outer diameter $D = 450$ mm, an inner diameter of hole $d = 150$ mm, and a total height $H = 1200$ mm.

For their manufacture, the equipment and techniques described in Chap. 2 were used. In the experiments, the manufacturing technology was varied and the next manufacturing technologies were adopted in the sample codes: vibration (V), centrifugation (C), and vibro-centrifugation (VC).

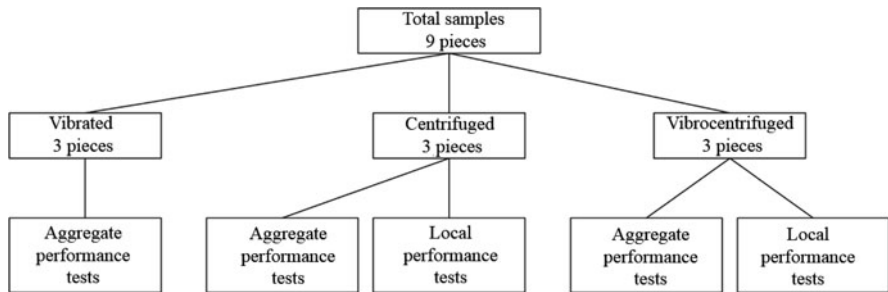


Fig. 3.1 Schedule of experimental studies of the aggregate and local characteristics of vibrated, centrifuged, and vibro-centrifuged prototypes

The problem of assessing the influence of manufacturing technology (vibration, centrifugation, vibro-centrifugation) on the aggregate (general, averaged over cross-section) and local (differing in the layers of the cross-section) characteristics of concrete was investigated [90–92, 94, 96, 97, 101]:

- (i) Density ρ .
- (ii) Axial compression strength (cubic, $R_{b,cub}$, and prismatic, R_b).
- (iii) Limiting strains during axial compression, ε_b .
- (iv) Axial tensile, R_{bt} , and flexural tensile strength, $R_{btb,i}$
- (v) Limiting strains during axial tension, ε_{bt}
- (vi) Elastic modulus (in compression, E_b , and tension E_{bt})
- (vii) Diagram “stress-strain ($\sigma_b - \varepsilon_b$)” in compression
- (viii) Diagram “stress-strain ($\sigma_{bt} - \varepsilon_{bt}$)” in tension

3.1.2 Test Method

The test method had distinctive features, namely, each manufactured prototype basic sample was used in several types of tests. One basic sample was tested at the age of 7, 28, and 180 days.

The *first type of tests* was carried out to study the integral (common, cross-section averaged) characteristics of concrete. With this purpose, three conditional quadrants A, B, C were selected from the total annular section (see Fig. 3.2), from which the small-sized samples (see Figs. 3.3 and 3.5) were cut for subsequent testing of the integral characteristics at axial compression, axial tension, and tension in bending.

For axial compression and tension tests, in both cases four cubes with dimensions of $15 \times 15 \times 15 \text{ cm}^3$ were cut out from quadrant A for axial compression tests (levels 1–4 of quadrant A in height) and 1 prism with sizes of $15 \times 15 \times 60 \text{ cm}^3$ for bending tests (level 5 of quadrant A in height).

Then, two prisms with dimensions of $15 \times 15 \times 60 \text{ cm}^3$ were cut out from quadrant B for axial compression tests (levels 1 and 2 of quadrant B in height).

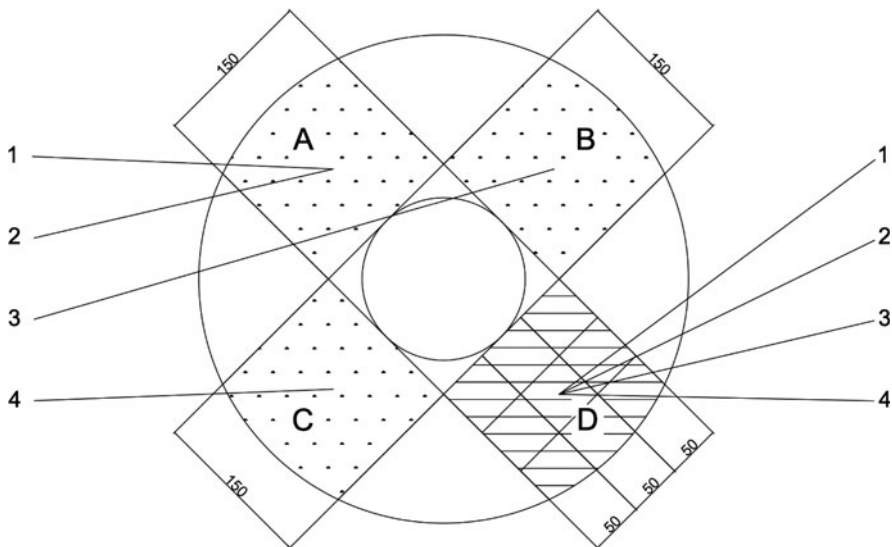


Fig. 3.2 Scheme of obtaining small-sized test concrete samples from quadrants A–D of full-size annular specimens (in plan)

Finally, two prisms with dimensions of $15 \times 15 \times 60 \text{ cm}^3$ were also cut out from quadrant C for axial tension tests (levels 1 and 2 of quadrant C in height).

As a result of testing the cubes for axial compression, we obtained the values of $R_{b,cub}$; as a result of testing the prisms for axial compression, we found the values of R_b , ϵ_{bR} , R_{bt} , ϵ_{btR} , $E_b = E_{bt}$ and the deformation diagram " $\sigma_b - \epsilon_b$ "; as a result of testing the prisms for axial tension, we determined the values of R_{bt} and the deformation diagram " $\sigma_{bt} - \epsilon_{bt}$ "; and as a result of testing the prisms for bending, we calculated the values of R_{btb} .

The *second type of tests* was carried out to study the local (differing over the cross-section) characteristics of concrete. With this purpose, fourth quadrant D was considered in general cross-section of the base sample (see Fig. 3.2).

The entire cross-section of the quadrant D was conventionally divided into three layers of 5 cm each (external, middle, and internal; see Figs. 3.4 and 3.6), and the characteristics of each layer were determined separately.

For axial compression and tensile tests, the following samples were cut out from quadrant D of the same basic sample along the entire length: (i) nine cubes with dimensions of $5 \times 5 \times 5 \text{ cm}^3$ (a level 1 of quadrant D) for tests on axial compression, (ii) nine prisms with dimensions of $5 \times 5 \times 20 \text{ cm}^3$ (a level 2 of quadrant D) for tests on tensile bending, (iii) nine prisms with dimensions of $5 \times 5 \times 20 \text{ cm}^3$ (a level 3 of quadrant D) for tests on axial compression, and (iv) nine prisms with dimensions of $5 \times 5 \times 20 \text{ cm}^3$ (a level 4 of quadrant D) for tests on axial tension.

As a result of testing the cubes for axial compression, we obtained the values of $R_{b,cub,i}$; as a result of testing prisms for axial compression, we found the values of $R_{b,i}$, $\epsilon_{bR,i}$, $R_{bt,i}$, $\epsilon_{btR,i}$, $E_{b,I} = E_{bt,i}$, and the deformation diagrams " $\sigma_{b,i} - \epsilon_{b,i}$ "; and as a

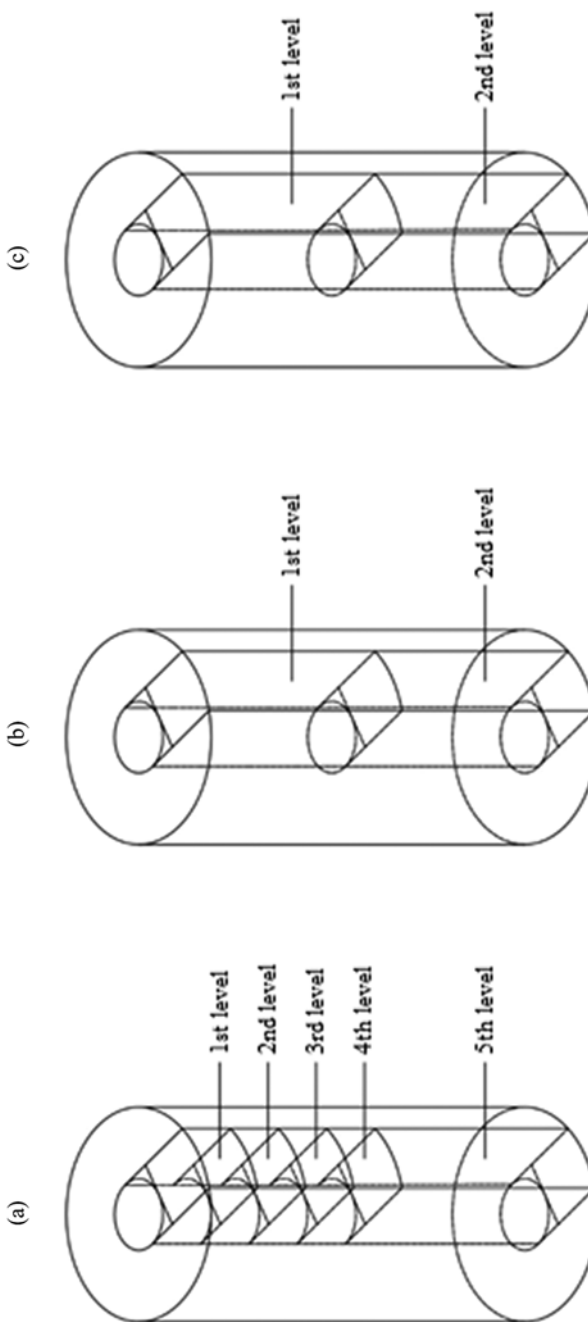


Fig. 3.3 Scheme of obtaining small-sized concrete samples from quadrants A, B, and C in height from experimental full-size samples of annular cross-section for testing the aggregate characteristics. (a) quadrant A, (b) quadrant B, and (c) quadrant C

Fig. 3.4 Scheme of obtaining small-sized concrete samples from quadrant D in height of experimental full-size samples with annular cross-section for testing the local characteristics

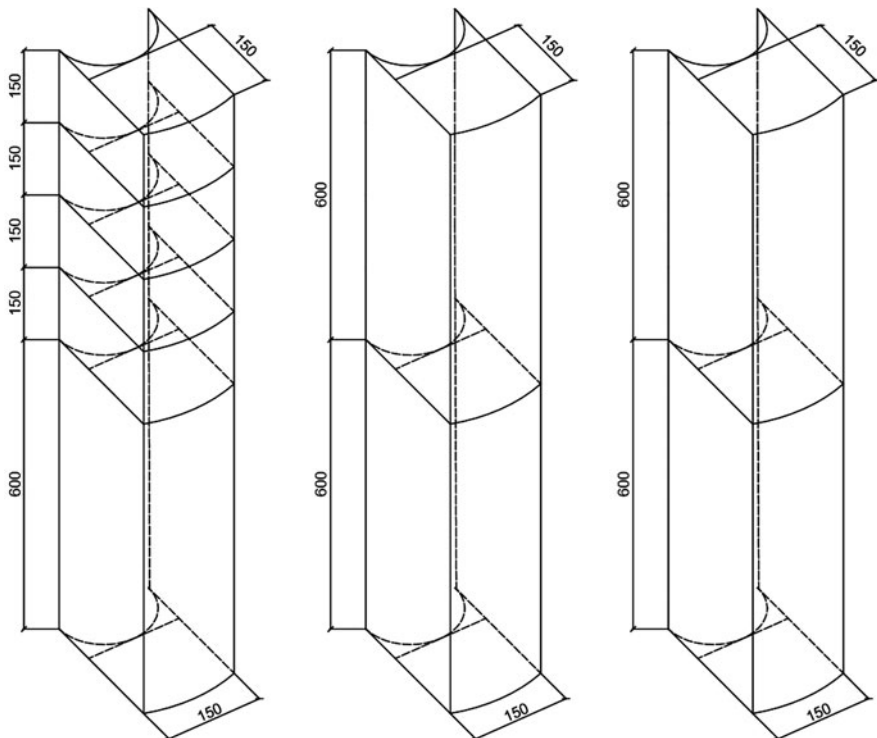
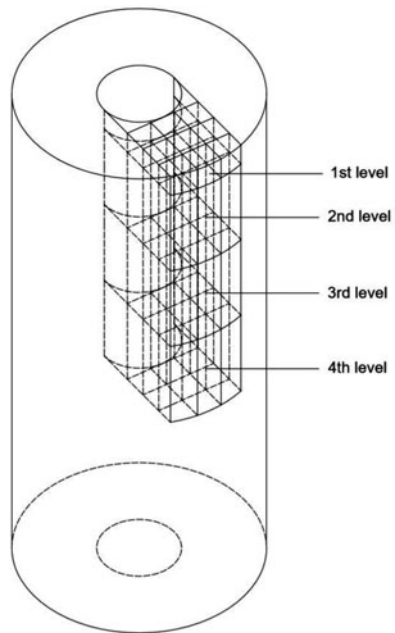
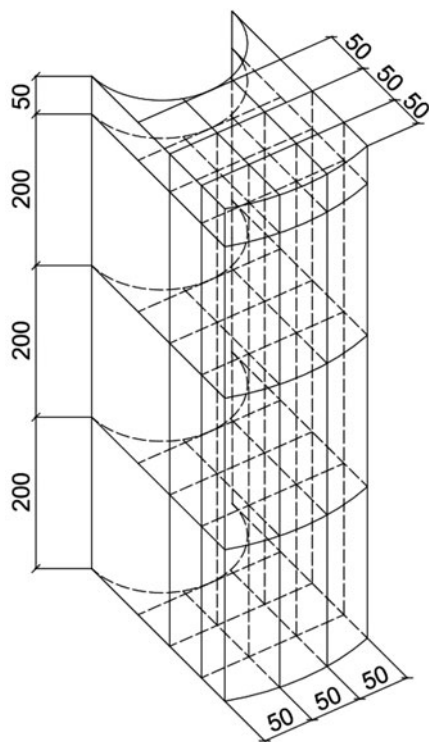


Fig. 3.5 Small-sized concrete samples, obtained from quadrants A, B, and C of experimental full-size samples with annular cross-section, for testing the aggregate characteristics

Fig. 3.6 Small-sized concrete samples, obtained from quadrant D of experimental full-size samples with annular cross-section, for testing the local characteristics



result of testing the prisms for axial tension, we determined values of $R_{bt,i}$ and deformation diagrams “ $\sigma_{bt,i} - \varepsilon_{bt,I}$ ”; and as a result of testing the prisms for bending tension, we calculated the values of $R_{btb,i}$.

We especially note that only basic centrifuged and vibro-centrifuged samples were tested for aggregate and local characteristics, while vibrated base samples were tested only for aggregate characteristics (see Figs. 3.1 and 3.7).

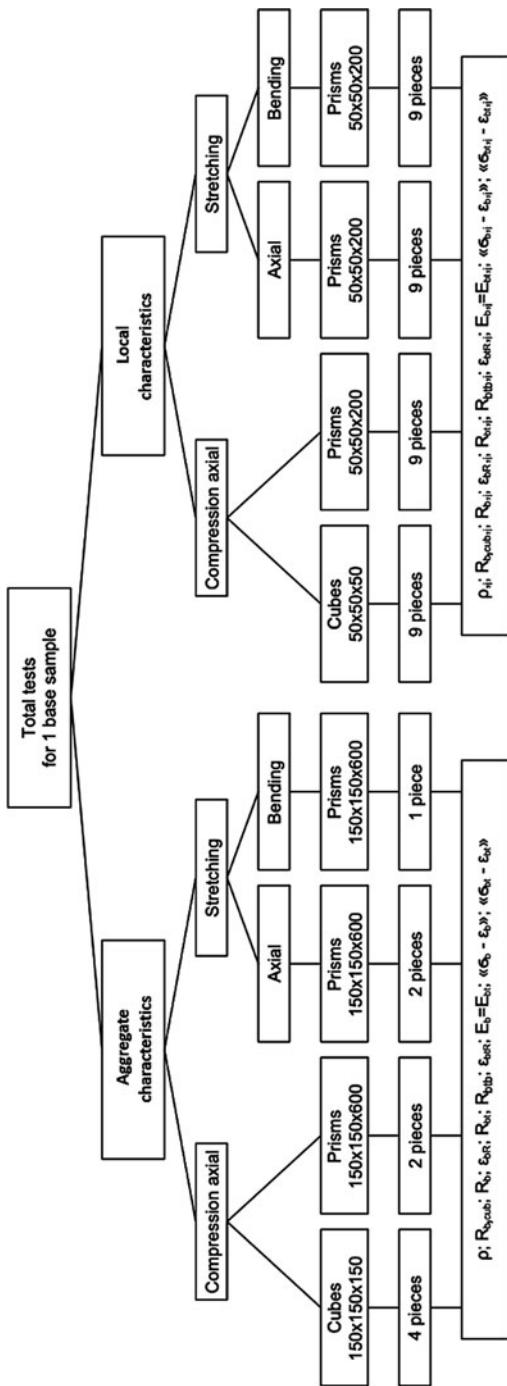
All samples were tested at the age of 7, 28, and 180 days in accordance with Russian GOST 10180. To correctly compare the results of samples with different sizes, a scale factor was taken into account.

Experimental cubes were tested for axial compression at a constant loading rate.

The testing of the prisms on axial compression was carried out on a test press IPS-1. The testing of the prisms on axial tension was carried out by using a special setup into a test press IPS-1.

For the study of *aggregate characteristics* (see designations on the left): 1 four cubes with an edge of 150 mm for axial compression, $R_{b,cub}$ (levels 1–4 of quadrant A in height); 2 one prism with sizes of $150 \times 150 \times 600 \text{ mm}^3$ for tension in bending, R_{btb} (level 5 of quadrant A in height); 3 two prisms with sizes of $150 \times 150 \times 600 \text{ mm}^3$ for axial compression, R_b (levels 1–2 of quadrant B in height); 4 two prisms with sizes of $150 \times 150 \times 600 \text{ mm}^3$ for axial tension, R_{bt} (levels 1–2 of quadrant C in height).

Fig. 3.7 Schedule of experimental researching small-sized concrete samples, obtained from experimental base sample of annular cross-section by vibrating (left part), centrifuging, and vibrocentrifugation (left and right parts)



For the study of *local characteristics* (see designations on the right): 1 nine cubes with an edge of 50 mm for axial compression $R_{b, \text{cub}, i}$ (level 1 of quadrant D in height); 2 nine prisms with sizes of $50 \times 50 \times 200 \text{ mm}^3$ for tension in bending, $R_{b\text{tb}, i}$ (level 2 of quadrant D in height); 3 nine prisms with sizes of $50 \times 50 \times 200 \text{ mm}^3$ for axial compression, $R_{b, i}$ (level 3 of quadrant D in height); 4 nine prisms with sizes of $50 \times 50 \times 200 \text{ mm}^3$ for axial tension, $R_{bt, i}$ (level 4 of quadrant D in height).

Measurements of the deformations of the test concrete prisms were carried out with a chain of strain gauges with a base of 50 mm and dial indicators with a graduation value of 0.001 mm.

The experimental prisms were tested for axial compression and axial tension at a constant rate of deformation in order to obtain not only the strength and deformation characteristics of concrete but also its full deformation diagrams “ $\sigma - \varepsilon$ ” with descending branches.

With this purpose, high-precision measuring equipment has been used in experiments. It allowed one to obtain not only ultimate tensile strength, strain limit, and elasticity modulus but their full deformation diagram “stress-strain” under compression and tension.

When tested at the same loading rate, the stepwise loading steps were approximately 0.1 times of the ultimate strength R of concrete, while when tested with a constant deformation rate, the strains of the prisms increased stepwise by 0.1 times of the ultimate value of concrete deformations ε_R (see Fig. 3.8).

In the last test mode, the load first increased, up to reaching a maximum, and then began to decrease with a continued increase in deformations. Thus, during the tests, a descending branch of the “stress-strain” diagram of concrete was recorded. In our studies, it had a fairly stable outline up to approximately $\sigma = 0.8R$ both under compression and under tension, and then acquired an unstable character.

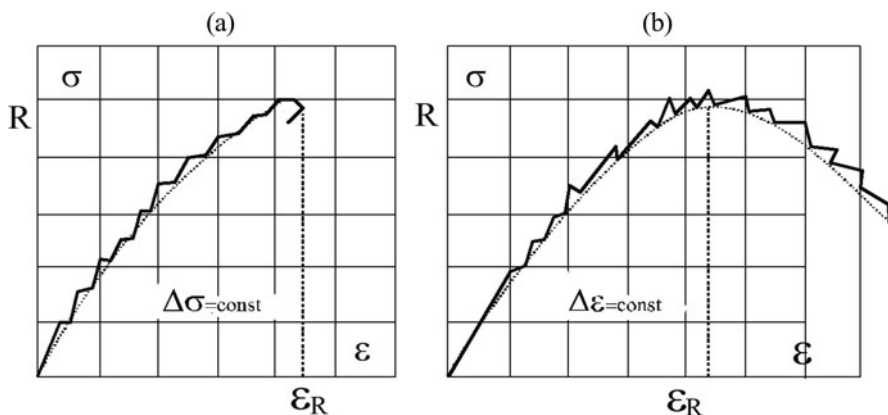


Fig. 3.8 Test modes for small-sized prototypes: (a) in stages, with a constant loading rate, and (b) in stages, with a constant deformation rate

Overall, the studies varied:

- (i) Manufacturing technology—vibration, centrifugation, vibro-centrifugation.
- (ii) Type of stress-strain state, namely, axial compression and axial tension.
- (iii) Type of samples, namely, cubes $5 \times 5 \times 5 \text{ cm}^3$ and $15 \times 15 \times 15 \text{ cm}^3$, prisms $5 \times 5 \times 20 \text{ cm}^3$ and $15 \times 15 \times 60 \text{ cm}^3$.
- (iv) Test mode with a constant loading rate and with a constant deformation rate.
- (v) Concrete age, namely, 7, 28, and 180 days.

The schedule of experimental studies of aggregate and local design characteristics of vibrated, centrifuged, and vibro-centrifuged prototypes is shown in Fig. 3.1.

3.2 Aggregate Structural Characteristics of V-, CF-, and VCF-Concretes

3.2.1 Results of Studies of the Aggregate Characteristics of Concrete

When analyzing the obtained experimental results, we estimated the influence of manufacturing technology. The results of experimental studies of the averaged aggregate characteristics of the test concrete samples are shown in Figs. 3.9, 3.10, 3.11, 3.12, 3.13, 3.14, 3.15, 3.16 and 3.17 and Table 3.1.

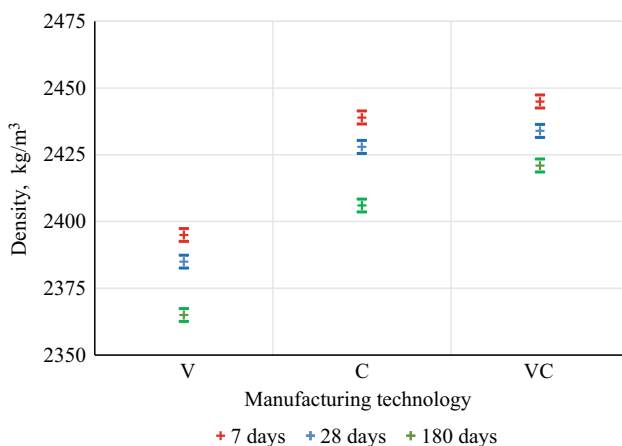


Fig. 3.9 Dependence of concrete density on manufacturing technology

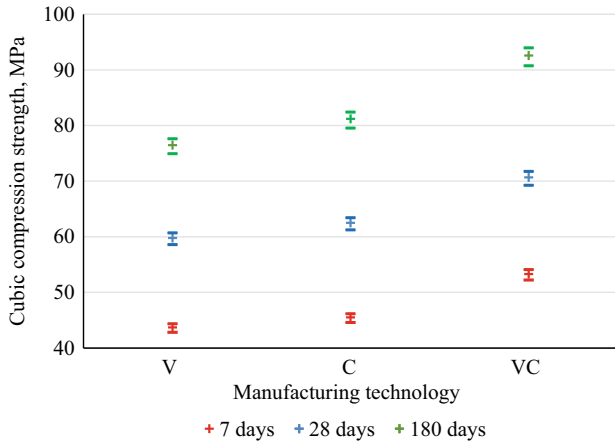


Fig. 3.10 Dependence of the cubic compression strength of concrete on the manufacturing technology

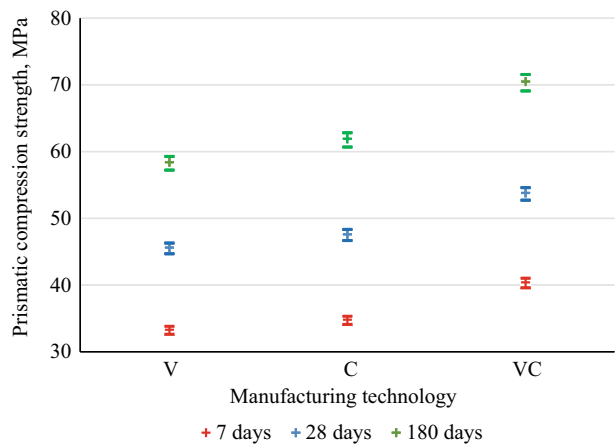


Fig. 3.11 Dependence of the prismatic strength of concrete at axial compression on the manufacturing technology

3.2.2 Analysis of Aggregate Density, Strength, Ultimate Deformations, Modulus of Elasticity, and Diagrams of Concrete Deformation Under Compression and Tension

Analysis of the obtained experimental results, shown in Table 3.1 and Figs. 3.9, 3.10, 3.11, 3.12, 3.13, 3.14, 3.15, 3.16 and 3.17, allowed us to draw the following conclusions.

Fig. 3.12 Dependence of the tension strength of concrete in bending on the manufacturing technology

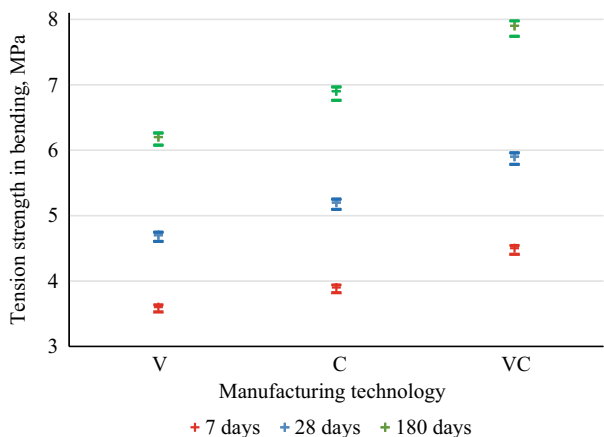
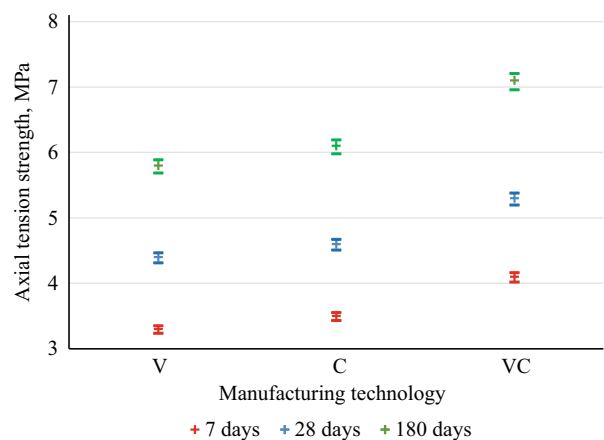


Fig. 3.13 Dependence of axial tension strength of concrete on the manufacturing technology



The *density* (Table 3.1 and Fig. 3.9) did not depend much on the technology of concrete manufacture for all concrete ages (within 2%); therefore, the technology can be ignored when calculating the density.

The *compressive and tensile strength* of vibro-centrifuged concretes at any age was noticeably higher compared to centrifuged and vibrated concretes. This applied to cubic and prismatic compressive strength (up to 22.0%; see Table 3.1 and Figs. 3.10 and 3.11) and axial tension and flexural tensile strength (up to 26.6%; see Table 3.1 and Figs. 3.12 and 3.13). The excess of the compressive and tensile strength of vibro-centrifuged concretes in comparison with vibrated and centrifuged concretes grows with increasing age of concrete and is approximately within the same ranges for all ages of concrete (from 7 to 180 days). It is explained by the ordering of the ongoing hydration processes in the cement stone during all this period.

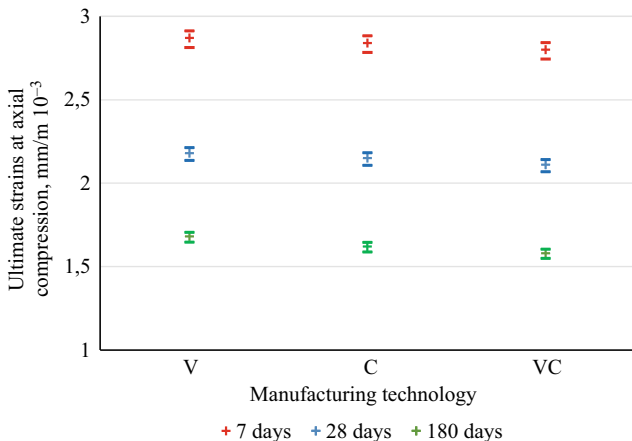


Fig. 3.14 Dependence of the ultimate strains of concrete at axial compression on the manufacturing technology

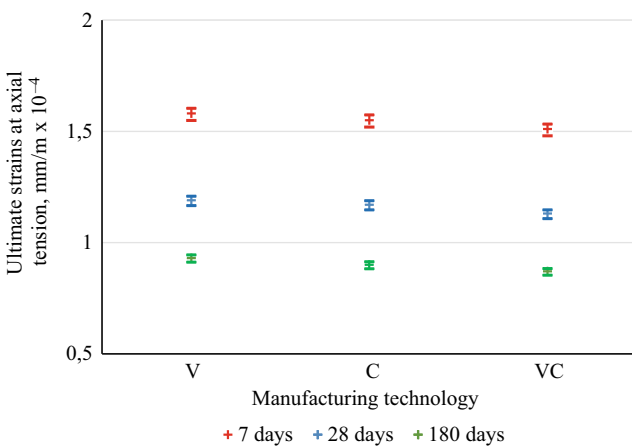


Fig. 3.15 Dependence of the ultimate strains of concrete at axial tension on the manufacturing technology

The *ultimate deformations under axial compression and tension* (corresponding to the maximum strength of concrete) showed the opposite picture, namely, in vibro-centrifuged concretes, compared with centrifuged and vibrated concretes, these strains decreased for all concrete ages, although these decreases were generally insignificant and were within 6% (see Table 3.1 and Figs. 3.13 and 3.14). It should be noted that all limiting deformations (both during axial compression and axial tension) in vibro-centrifuged concretes, in comparison with centrifuged and vibrated ones, turned out to be less at any concrete age.

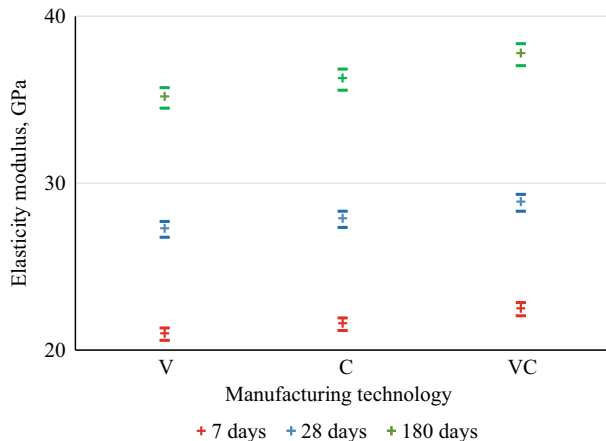


Fig. 3.16 Dependence of the modulus of elasticity of concrete on the manufacturing technology

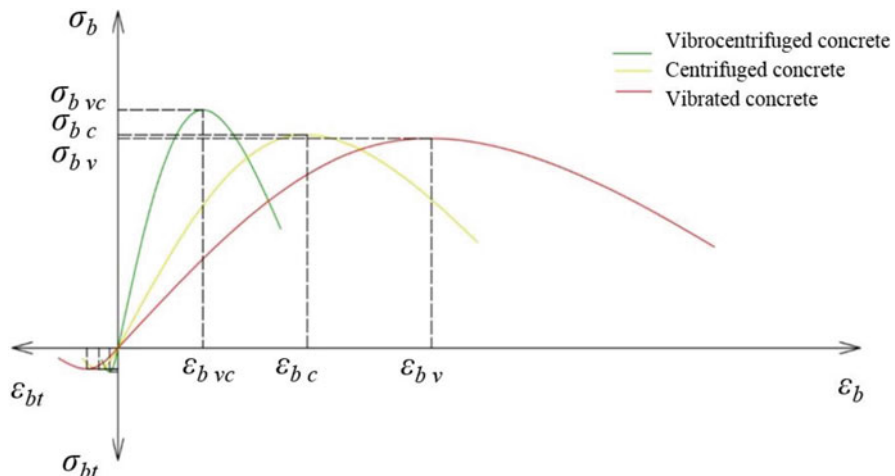


Fig. 3.17 Principal dependences of the “ $\sigma - \epsilon$ ” diagrams of concrete on the technology of their manufacture

The *modulus of elasticity* in compression E_b and tension E_{bt} in vibro-centrifuged concretes in comparison with centrifuged and vibrated concretes at all times of hardening was up to 7.4% higher and approximately equal to each other (see Table 3.1 and Fig. 3.16). Increasing the initial modulus of elasticity under compression and tension was explained by strength increase with a simultaneous decrease in the strain limit of vibro-centrifuged concretes compared with centrifuged and vibrated ones, which displaces up and to the left the maximum in the diagram “stress-strain.”

Table 3.1 Results of experimental studies: averaged integral characteristics of vibrated (V), centrifuged (C), and vibro-centrifuged (VC) test concrete samples

Characteristics of concrete	Manufacturing technology			Deviations, %		
	V	C	VC	$\Delta_1 = \frac{C-V}{V} \times 100\%$	$\Delta_2 = \frac{VC-V}{V} \times 100\%$	$\Delta_3 = \frac{VC-C}{C} \times 100\%$
Density, kg/m ³	2395/ 2385/ 2365	2439/ 2428/ 2406	2445/ 2434/ 2421	1.8	2.1	0.2
Compressive strength, MPa:	43.7/ 59.8/ (i) Cubic (ii) Prismatic	45.5/ 62.5/ 81.2 34.8/ 47.6/ 61.9	53.3/ 70.7/ 92.6 40.4/ 53.8/ 70.5	4.2/4.5/ 6.1 4.5/4.4/ 6.0	22.0/18.2/ 21.0 21.0/18.0/ 20.7	17.1/13.1/ 14.0 16.0/13.0/ 13.9
Tensile strength, MPa:	3.6/4.7/ 6.2 (i) By bending (ii) Axial	3.9/5.2/ 6.9 3.5/4.6/ 6.1	4.5/5.9/ 7.9 4.1/5.3/ 7.1	7.0/10.6/ 11.3 6.0/4.4/ 5.2	24.0/25.5/ 26.6 24.0/20.5/ 22.4	16.0/13.5/ 13.8 16.9/15.2/ 16.4
Limiting deformations At axial compression, mm/m × 10 ⁻³	2.87/ 2.18/ 1.68	2.84/ 2.15/ 1.62	2.80/ 2.11/ 1.58	1.1/1.4/ 3.6	2.44/3.3/ 5.9	1.4/1.9/2.5
Limiting deformations At axial tension, mm/m × 10 ⁻⁴	1.58/ 1.19/ 0.93	1.55/ 1.17/ 0.90	1.51/ 1.13/ 0.87	1.9/1.7/ 3.2	4.4/5.3/6.4	2.6/3.4/3.3
Elastic modulus, GPa	21/27.3/ 35.2	21.6/ 27.9/ 36.3	22.5/ 28.9/ 37.8	2.9/2.2/ 3.1	7.1/5.9/7.4	4.2/3.6/4.1

Note: The values of characteristics corresponding to the age of 7, 28, and 180 days are indicated through a fraction

The diagrams of “stress-strain” under compression and tension in vibro-centrifuged concretes in comparison with centrifuged and vibrated ones at all concrete ages were characterized by the following features:

- (i) The maximum shifts up and to the left (strength increases, and ultimate deformations decrease).
- (ii) The initial modulus of elasticity increases.

3.3 Local Design Characteristics of CF- and VCF-Concretes of Functionally Gradient Cross-Sections

As shown above, during centrifugation and vibro-centrifugation of concrete elements with a sufficiently thick wall, the centrifugal and centripetal forces acting on the outer, middle, and inner layers of the cross-section differ greatly. It leads to a

significant difference in the structure and characteristics of these layers of the element, which in some cases must be taken into account in calculations.

Therefore, after identifying the influence of manufacturing technology (vibration, centrifugation, vibro-centrifugation) on concrete integral (common) characteristics, we investigate a functionally gradient concrete structure of prototypes with annular cross-section and local design characteristics of concrete layers.

The previously obtained aggregate results for all three technologies gave the cross-section-averaged characteristics of the concrete prototypes as a whole. Therefore, the characteristics of each of the three conditional separate layers (outer, middle, and inner) of the prototypes with annular cross-sections were also studied. These characteristics differed from each other due to centrifugation and vibro-centrifugation.

Note that vibrated samples were not investigated for local design characteristics due to the absence of functionally gradient cross-section in them.

3.3.1 Methods of Experimental Studies of the Local Characteristics of Concrete by Ultrasonic Method

So, with the exception of vibrated prototypes, the centrifuged and vibro-centrifuged samples were functionally gradient in their cross-section, that is, they were a combination of conditional layers of one element, the properties and characteristics of which differed from each other due to the manufacturing technology.

The schedule and methodology for experimental studies of the local design characteristics of concrete were described in detail in Sect. 3.3.1.

However, in order to obtain more detailed data, the following instrumental approach was additionally applied.

To reveal the change in the properties of the samples by layers, we additionally applied ultrasonic sounding with the device Pulsar 2.2. This method is described in Chap. 2. Based on the obtained results, it was concluded that this method can be used for centrifuged and vibro-centrifuged samples of a functionally gradient structure.

With this purpose, three prisms with dimensions of $1200 \times 150 \times 50 \text{ mm}^3$ (see Fig. 3.18) were conditionally distinguished in the wall of each sample. The device sensors were attached according to the diagram in Fig. 3.18 on all three layers (inner, middle, and outer) of the functionally gradient structure across the thickness of cross-section wall.

The described studies were carried out for all centrifuged and vibro-centrifuged concrete samples. Let us show in Table 3.2 the qualitative and quantitative picture of the distribution of density and strength of centrifuged and vibro-centrifuged concrete.

From Table 3.2 it can be seen that, confirming the theoretical calculations, the outer layer of the structure, on which the maximum centrifugal force acts, has the

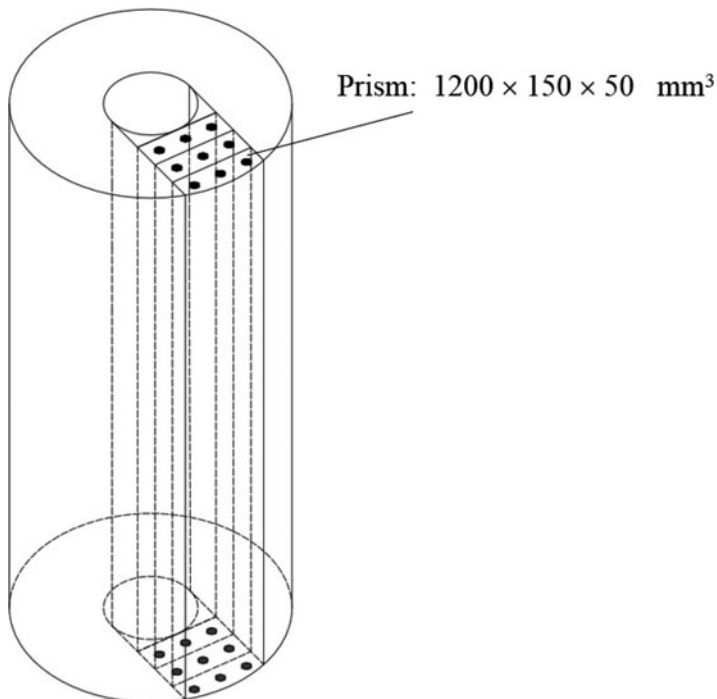


Fig. 3.18 Places of disposition of the sensors of ultrasonic device

Table 3.2 Results of sounding the layers of prototypes

Characteristic	Technology							
	Centrifugation			Vibro-centrifugation				
	Layer	External	Middle	Interior	Layer	External	Middle	Interior
Ultrasound speed, m/s		4432	4054	3785		4710	4561	4110
Density, kg/m ³		2495	2403	2316		2544	2492	2396
Compression strength, MPa		43.4	35.5	32.2		68.2	65.1	41.6
Elastic modulus, GPa		34.3	27.8	24.8		38.8	35.2	28.5

greatest strength both for centrifuged and vibro-centrifuged samples and the inner layer has the least strength.

However, for centrifuged concrete, the plot of changes in strength by layers (from outer to inner) takes the form of a descending curve (Fig. 3.19) with a bulge down.

For vibro-centrifuged concrete, the plot of changes in strength by layers (from outer to inner) also takes the form of a descending curve (Fig. 3.20), but with a bulge upward.

In other words, for centrifuged concrete, the middle layer shows an intermediate strength between the outer and inner layers, but less than the arithmetic average

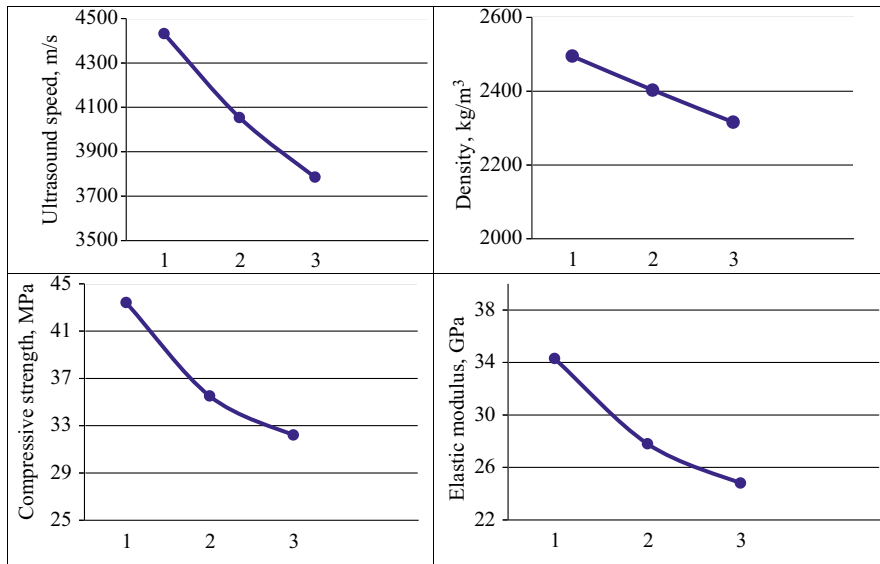


Fig. 3.19 Plots of the distribution of ultrasound speed, density, strength, and elastic modulus by layers during centrifugation: 1 outer layer; 2 middle layer; 3 inner layer

between the strength values of the outer and inner layers. At the same time, for vibro-centrifuged concrete, the middle layer also shows an intermediate strength between the outer and inner layers, but greater than the arithmetic average between the strength values of the outer and inner layers. It leads to the reverse change in the convexity of the strength curve by layers (see Figs. 3.19 and 3.20).

Thus, the substantiation of the three-layer functionally gradient structure of the computational model of vibro-centrifuged and centrifuged concrete has been confirmed experimentally.

Theoretically, deformations of concrete layers, as well as their moduli of elasticity, underwent similar changes. The concrete of outer layer must have the highest modulus of elasticity. At the same time, the concrete of inner layer, on the contrary, must have the minimum value of the modulus of elasticity. The modulus of elasticity of the middle layer will have an intermediate value between them, somewhat less for centrifuged concrete and more for vibro-centrifuged concrete.

For deformations, the picture will be reversed.

Accordingly, these results also lead to differences in the diagrams “ $\sigma - \varepsilon$ ” of various concrete layers, which will be described in more detail further. Experimentally, we shall identify all these changes and confirm them in experiments, the results of which are given below.

So, the above results also confirm the functionally gradient structure of concrete and the validity of the three-layer structure of the calculation model of centrifuged or

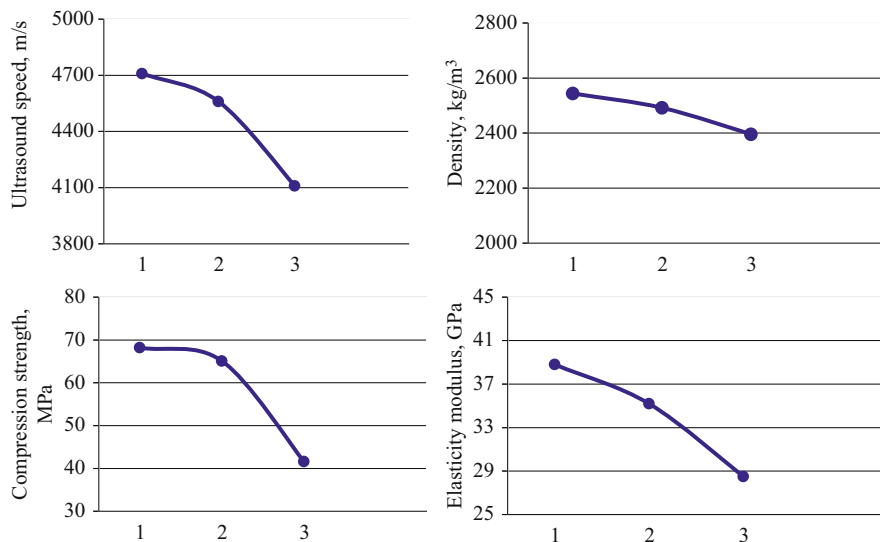


Fig. 3.20 Plots of the distribution of ultrasound speed, density, strength, and elastic modulus by layers for vibro-centrifuged concrete: 1 outer layer; 2 middle layer; 3 inner layer

vibro-centrifuged concrete in constructions, which must be taken into account in the calculations.

3.3.2 Analysis of the Results of Studies of the Local Characteristics of Concrete

Compressive and Tensile Strength of the Layers of Functionally Gradient Cross-Section

The values of compressive and tensile strength of various concrete layers, into which the functionally gradient cross-section was conventionally divided (internal, middle, and external with 5 cm thickness each), were compared with each other both for different layers and for different manufacture technologies of concrete.

The analysis of the experimental results of the study of strength (see Table 3.3) and the deviations obtained (see Table 3.4), for clarity, presented also in Figs. 3.21 (under compression) and 3.22 (under tension) led to the following conclusions.

It should be noted that the compressive strength of concrete (both cubic and prismatic) showed the same qualitative picture; therefore, in the future, we shall analyze the change in compressive strength as a whole. The same is true for tensile strengths (both axial and bending), which also gives us reason to analyze the change in tensile strength as a whole.

Table 3.3 Results of experimental studies for local characteristics of the functionally gradient cross-section layers of centrifuged and vibro-centrifuged concrete samples

Characteristics of concrete	Manufacturing technology					
	Centrifugation			Vibro-centrifugation		
	Layer	Layer	Layer	External VC _I	Middle VC _{II}	Interior VC _{III}
External C _I	Middle C _{II}	Interior C _{III}	External VC _I	Middle VC _{II}	Interior VC _{III}	
Density, kg/m ³	2342/ 2335/ 2319	2443/ 2432/ 2411	2502/ 2495/ 2470	2350/ 2344/ 2329	2466/ 2455/ 2436	2515/ 2502/ 2477
Compressive strength, MPa: (i) Cubic (ii) Prismatic	40.9/ 51.1/66.5 31.5/38/ 8/51.3	49.3/ 61.6/80.1 38.2/ 47.1/62.2	60.1/ 75.1/98.5 46.2/ 57.5/76.5	38.6/ 51.3/67.6 29.2/ 39.2/51.2	52.9/ 70.3/92.3 40.1/ 53.6/70.1	59.2/ 78.7/ 104.3 45.1/ 60.0/ 79.2
Tensile strength, MPa: (i) By bending (ii) Axial	3.5/4.3/ 5.7 3.2/3.9/ 5.1	4.2/5.2/ 6.8 3.7/4.5/ 5.9	5.2/6.4/ 8.3 4.4/5.5/ 7.2	3.4/4.4/ 5.9 3.0/3.9/ 5.3	4.6/6.0/ 8.1 4.2/5.4/ 7.2	5.2/6.8/ 9.1 4.7/6.1/ 8.1
Limiting deformations At axial compression, mm/m × 10 ⁻³	3.40/ 2.64/2.10	2.80/ 2.15/1.72	2.35/ 1.82/1.45	3.10/ 2.40/1.80	2.80/ 2.12/1.61	2.00/ 1.54/ 1.17
Limiting deformations At axial tension, Mm/m × 10 ⁻⁴	1.97/ 1.48/1.35	1.60/ 1.20/1.05	1.38/ 1.04/0.90	1.64/ 1.30/1.00	1.49/ 1.14/0.90	1.10/ 0.83/ 0.65
Elastic modulus, GPa	19.6/ 23.9/31.3	22.5/ 27.8/36.4	27.2/ 33.9/44.8	16.8/ 21.6/28.0	22.8/ 29.2/38.2	25.7/ 33.0/ 43.1

Note: The values of characteristics corresponding to the concrete age of 7, 28, and 180 days are indicated through a fraction

So, let us first analyze the functional gradient by layers. In centrifuged concretes, the excess of the compressive strength of the middle layer in comparison with the strength of the inner layer (taken by us as the starting point, since the influence of the manufacturing technology on its characteristics is minimal) ranged from 20.5% to 21.4%. To an even greater degree, an excess of the compressive strength of the outer layer was observed in comparison with the strength of the middle layer, namely, from 20.9% to 23.0%, not to mention the excess of the compressive strength of the outer layer over the strength of the inner layer, namely, from 46.7% to 49.1% (see Fig. 3.21).

In vibro-centrifuged concrete, the picture was approximately the same.

The excess of the compressive strength of the middle layer in comparison with the inner layer ranged from 36.5% to 37.3%. Slightly less was the excess of the strength of the outer layer in comparison with the strength of the middle layer, namely, from 11.9% to 13.0%. The excess of the compressive strength of the outer layer over the inner layer was from 53.1% to 54.7%.

Table 3.4 Deviations for local characteristics of the functionally gradient cross-section layers of centrifuged and vibro-centrifuged concrete samples

Characteristics of concrete	Deviations, %								
	C			VC			VC-C		
	Layer		Layer			Layer			
	Δ_1	Δ_2	Δ_3	Δ_4	Δ_5	Δ_6	Δ_7	Δ_8	Δ_9
Density, kg/m ³	4.3/	2.4/	6.8/	4.9/	2.0/	7.0/	0.3/	0.9/	0.5/
	4.2/	2.6/	6.9/	4.7/	1.9/	6.7/	0.4/	0.9/	0.3/
	4.0	2.4	6.5	4.6	1.7	6.4	0.4	1.0	0.3
Compressive strength, MPa:	20.5/	21.9/	46.9/	37.0/	11.9/	53.4/	5.6/	7.3/	1.5/
	20.5/	21.9/	47.0/	37.0/	11.9/	53.4/	0.4/	14.1/	4.8/
(i) Cubic	20.5	23.0	48.1	36.5	13.0	54.3	1.7	15.2	5.9
(ii) Prismatic	21.3/	20.9/	46.7/	37.3/	12.5/	54.5/	7.3/	5.0/	2.4/
	21.4/	22.1/	48.2/	36.7/	11.9/	53.1/	1.0/	13.8/	4.3/
	21.2	23.0	49.1	36.9	13.0	54.7	0.2	12.7	3.5
Tensile strength, MPa:	20.0/	23.8/	48.6/	35.3/	13.0/	52.9/	2.9/	9.5/	0.0/
	20.9/	23.1/	48.8/	36.4/	13.3/	54.5/	2.3/	15.4/	6.2/
(i) By bending	19.3	22.1	45.6	37.3	12.3	54.2	3.5	19.1	9.6
(ii) Axial	15.6/	18.9/	37.5/	40.0/	11.9/	56.7/	6.3/	13.5/	6.8/
	15.4/	22.2/	41.0/	38.5/	13.0/	56.4/	0.0/	20.0/	10.9/
	15.7	22.0	41.2	35.8	12.5	52.8	3.9	22.0	12.5
Limiting deformations At axial compression, mm/m × 10 ⁻³	17.65/	16.07/	30.88/	9.68/	28.57/	35.48/	8.82/	0.00/	14.89/
	18.56/	15.35/	31.06/	11.67/	27.36/	35.83/	9.09/	1.40/	15.38/
	18.10	15.70	30.95	10.56	27.33	35.00	14.29	6.40	19.31
Limiting deformations At axial tension, Mm/m × 10 ⁻⁴	18.78/	13.75/	29.95/	9.15/	26.17/	32.93/	16.75/	6.88/	20.29/
	18.92/	13.33/	29.73/	12.31/	27.19/	36.15/	12.16/	5.00/	20.19/
	22.22	14.29	33.33	10.00	27.78	35.00	25.93	14.29	27.78
Elastic modulus, GPa	14.8/	20.9/	38.8/	35.7/	12.7/	53.0/	14.3/	1.3/	5.5/
	16.3/	21.9/	41.8/	35.2/	13.0/	52.8/	9.6/	5.0/	2.7/
	16.3	23.1	43.1	36.4	12.8	53.9	10.5	4.9	3.8

Note: The values of characteristics corresponding to the concrete age of 7, 28, and 180 days are indicated through a fraction

$$\Delta_1 = \frac{C_{II} - C_I}{C_I} \times 100\%; \quad \Delta_2 = \frac{C_{III} - C_{II}}{C_{II}} \times 100\%; \quad \Delta_3 = \frac{C_{III} - C_I}{C_I} \times 100\%; \quad \Delta_4 = \frac{VC_{II} - VC_I}{VC_I} \times 100\%; \quad \Delta_5 = \frac{VC_{III} - VC_{II}}{VC_{II}} \times 100\%; \quad \Delta_6 = \frac{VC_{III} - VC_I}{VC_I} \times 100\%; \quad \Delta_7 = \frac{VC_I - C_I}{C_I} \times 100\%; \quad \Delta_8 = \frac{VC_{II} - C_{II}}{C_{II}} \times 100\%; \quad \Delta_9 = \frac{VC_{III} - C_{III}}{C_{III}} \times 100\%$$

So, for vibro-centrifuged samples, the picture of the distribution of the compressive strength of concrete layers was approximately the same as for centrifuged concrete. However, it was qualitatively expressed a little differently, namely, if the strength dependence for the layers of a functionally gradient centrifuged cross-section was a curve with a slight downward bulge, then for a functionally gradient vibro-centrifuged cross-section, it was a curve with a slight upward bulge.

The same picture was observed for tensile strength.

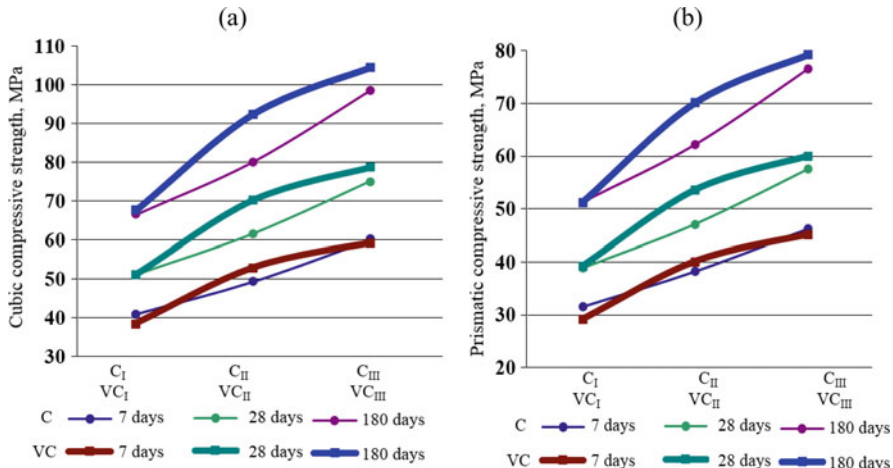


Fig. 3.21 Compressive strength centrifuged (C) and vibro-centrifuged (VC) concretes: (a) cubic and (b) prism

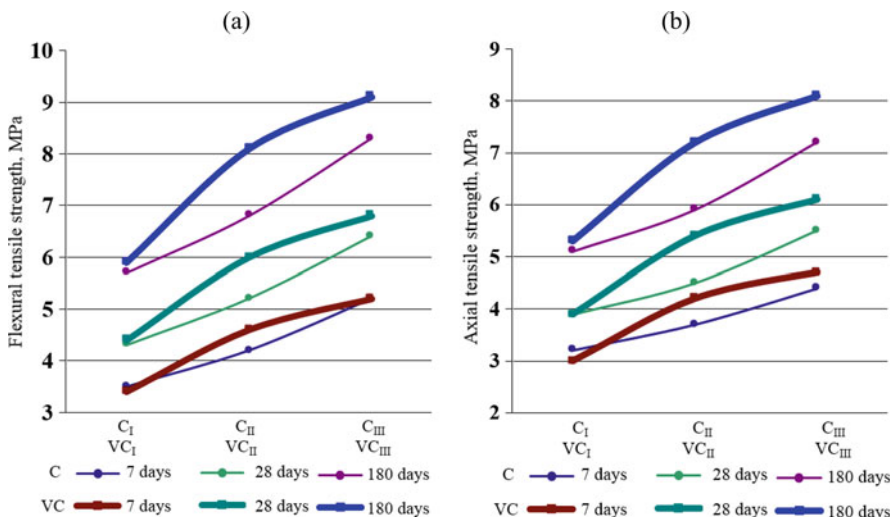


Fig. 3.22 Tensile strength centrifuged (C) and vibro-centrifuged (VC) concretes: (a) when bending and (b) axial

Here, for centrifuged concretes, the tensile strength of the outer layer, both axial and by bending, exceeded the similar characteristics of the middle layer by 18.9% and 23.8%, respectively. The quantitative increase in the axial tensile and tensile strength during bending of the middle layer of the centrifuged functionally gradient cross-section relative to the inner layer turned out to be equal to 15.7% and 20.9%, respectively (see Fig. 3.22).

In respect to vibro-centrifuged concretes, with the distribution of tensile strength of both types, the tendency of a slight increase in the values of the characteristics of the middle layer remained. The outer layer of vibro-centrifuged concrete also had an increase in strength compared to the outer layer of centrifuged concrete, while the inner layer demonstrated approximately the same low value of strength compared to other layers of the cross-section. The difference in the values of tensile strength for axial and bending cases between the outer and middle layers was 12.5% and 13.3%; between the middle and inner layers, it was 40.0% and 37.3%; and between the outer and inner layers, it turned out to be 52.8% and 54.5% (see Fig. 3.22).

The above analysis has shown it is obvious that by calculating constructions, the functionally gradient cross-sections and the resulting strength characteristics of concrete should be taken into account in the calculations.

Changes in the Ultimate Deformations Under Compression and Tension in the Layers of the Functionally Gradient Cross-Section

After analyzing the strength differential characteristics of centrifuged and vibro-centrifuged concretes, let us now estimate the effect of the functionally gradient cross-sections on the deformations of individual concrete layers under compression and tension. The results of experimental studies have confirmed our assumption regarding the variability of the deformability of individual layers of concrete with a functionally gradient structure (see Figs. 3.23 and 3.24). It has been established that the concrete of the outer layer undergoes the smallest ultimate deformations, both under compression and under tension. At the same time, the concrete of the inner layer, on the contrary, has the maximum deformability, while the middle layer occupies an intermediate position between them in terms of deformations, somewhat more during centrifugation and less during vibro-centrifugation.

It should be noted that all these results must lead to differences in the diagrams “ $\sigma - \varepsilon$ ” of different concrete layers.

Features of the Change in the Elastic Modulus for the Layers of Functionally Gradient Cross-Section

After analyzing the deformability of individual layers of concrete with a functionally gradient structure, let us study the change in their modulus of elasticity. As we assumed above, the greatest modulus of elasticity was found in the concrete of the outer layer and in the concrete of the inner layer; on the contrary, this characteristic was minimal. At the same time, the modulus of elasticity of the middle layer took an intermediate position between them in magnitude, somewhat less for centrifuged concrete and more for vibro-centrifuged concrete. The foregoing refers to the moduli of elasticity both in compression and in tension, which practically did not differ from each other (Fig. 3.25).

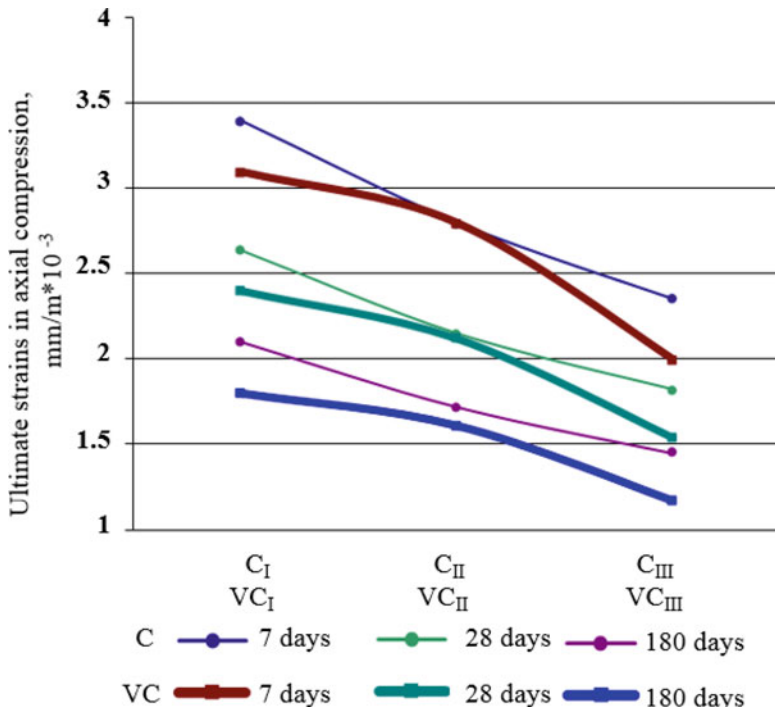


Fig. 3.23 Change in ultimate deformations in compression by layers of functionally gradient cross-section of centrifuged (C) and vibro-centrifuged (VC) concretes

Transformation of Deformation Diagrams for the Various Layers of Functionally Gradient Cross-Section

For centrifuged and vibro-centrifuged concrete, three experimental diagrams were built for the inner, middle, and outer layers. They differed among themselves in accordance with the differences in strength and deformation characteristics described above (Fig. 3.26).

As a whole, in the case of centrifuged concretes, the diagram “ $\sigma - \varepsilon$ ” for the inner layer was lowest and shallowest, which had the lowest strength, the highest ultimate deformations, and a lower modulus of elasticity, characterized by the lifting capacity of the diagram. For the outer layer, which, on the contrary, has the highest strength, the lowest ultimate deformations, and a large elastic modulus, the diagram “ $\sigma - \varepsilon$ ” is characterized by a shift of the maximum up and to the left with greater sharpness and lift in the ascending part and a sharper decline in the descending part of the diagram. The deformation diagram of the middle layer occupies an intermediate position between the diagrams of the inner and outer layers, but closer to the inner layer, differing nevertheless from both of them.

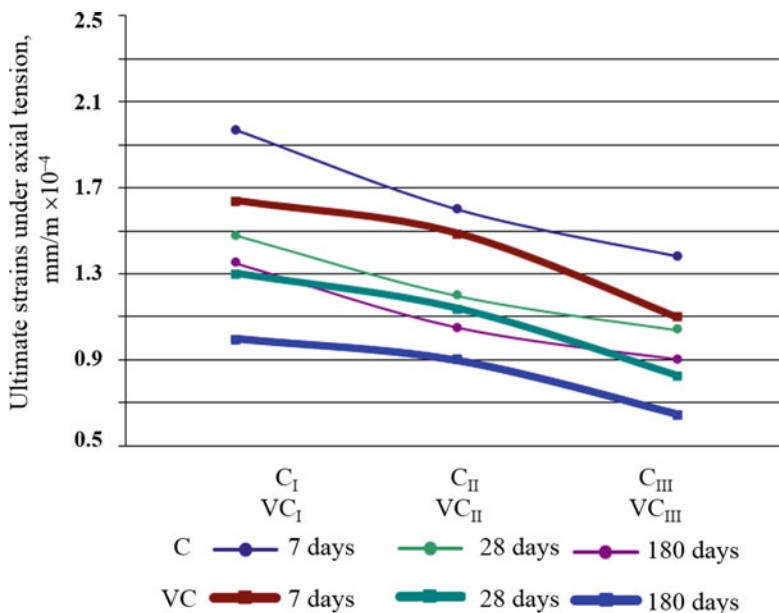


Fig. 3.24 Change in ultimate tensile deformations by layers of functionally gradient cross-section for centrifuged (C) and vibro-centrifuged (VC) concretes

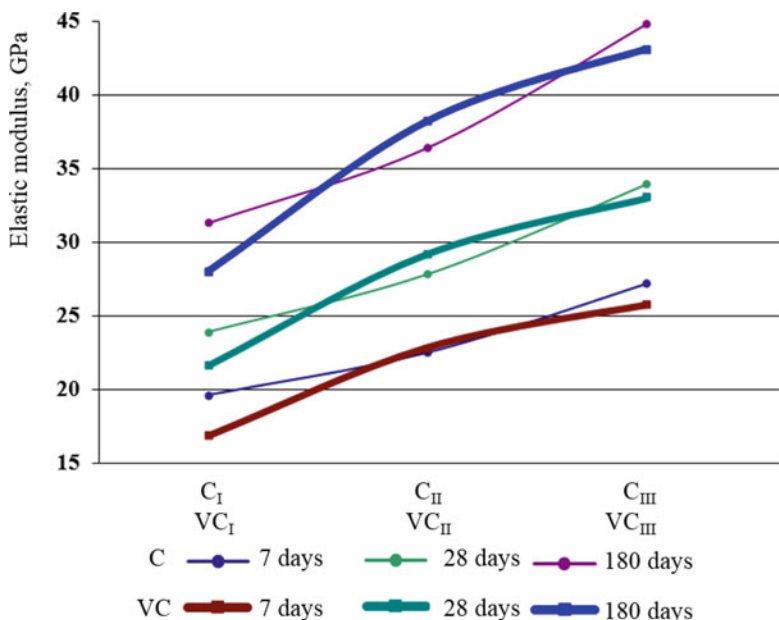


Fig. 3.25 Change in the modulus of elasticity over the layers of the functionally gradient cross-section of centrifuged (C) and vibro-centrifuged (VC) concretes

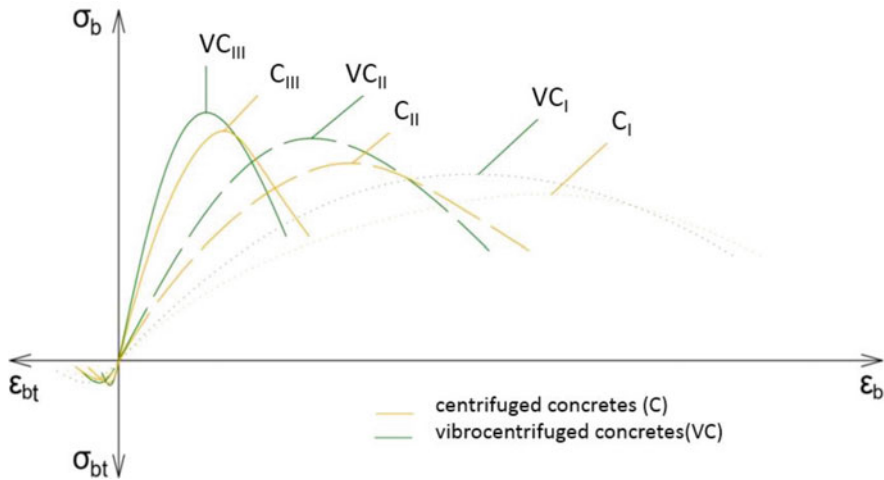


Fig. 3.26 Transformation of diagrams “ $\sigma - \varepsilon$ ” for individual layers of the functionally gradient cross-sections of centrifuged and vibro-centrifuged concretes

For vibro-centrifuged concretes, the deformation diagrams and their differences in layers show approximately the same picture as for centrifuged concretes. It should only be noted here that the difference in the diagrams of the inner and outer layers is even more striking, and the diagram of the middle layer is closer to the diagram of the outer layer than to the diagram of the inner layer.

Figure 3.26 shows the diagrams “ $\sigma - \varepsilon$,” built according to our experimental data.

Analysis of the experimental data revealed the following results:

- (i) The diagrams of both centrifuged and vibro-centrifuged concretes differ significantly in their layers, confirming the functional gradient of the concrete structure.
- (ii) For all the diagrams, both centrifuged and vibro-centrifuged concretes, the deformation diagrams for the outer concrete layer are the highest in strength (along the ordinate axis), and the deformation diagrams for the inner concrete layer are the smallest.
- (iii) For all the diagrams of both centrifuged and vibro-centrifuged concretes, the largest diagrams in terms of deformability (along the abscissa axis) are, on the contrary, the diagrams for the inner concrete layer, and the smallest diagrams are the deformation diagrams for the outer concrete layer.
- (iv) The deformation diagrams for the outer concrete layer had the highest lift (i.e., the elastic modulus) and the deformation diagrams for the inner concrete layer had the lowest elastic modulus.
- (v) In both centrifuged and vibro-centrifuged concretes, the deformation diagrams for the middle layer of concrete have intermediate indicators, approaching in centrifuged concretes to the arithmetic mean values, and in vibro-centrifuged

concretes to the indicators of the deformation diagram for the outer concrete layer.

Influence of Age on the Differential Characteristics of the Concrete Layers of Functionally Gradient Cross-Section

In Points 3.3.2.2, 3.3.2.3 and 3.3.2.4 above, we analyzed the change in strength and deformation characteristics for layers of functionally gradient cross-sections of centrifuged and vibro-centrifuged concrete at the age of 28 days.

However, in our experimental studies, the same characteristics were studied in other characteristic ages, namely, 7 and 180 days.

Based on the results of the analysis as a whole, it can be noted that the functional gradient of centrifuged and vibro-centrifuged concrete manifests itself immediately and does not depend on age. In other words, the qualitative picture of the change in the strength and deformative characteristics over the layers of functionally gradient cross-sections at the age of 28 days, and at the ages of 7 and 180 days, remains unchanged.

In respect to the quantitative picture, it naturally changes somewhat in accordance with the age and concrete strength gain (Fig. 3.27).

At the age of 7 days, the values of compressive and tensile strength were equal to 73–81% of their values at 28 days. Limiting deformations corresponding to them, on the contrary, were higher up to 21–29%. The elastic moduli were also lower 13–17%.

At the age of 180 days, the values of compressive and tensile strength increase up to 11–13%, the limiting deformations corresponding to them decrease to 9–12%, respectively, and the elastic modulus also increases to 15%, although all these changes, in general, are not so significant.

Accordingly, the diagrams “ $\sigma - \varepsilon$ ” at the age of 7 and 180 days are also somewhat transformed in comparison with the diagrams at 28 days (see Fig. 3.28), namely, their rise, flatness, and shift of the maximum point of the diagrams change.

As a whole, summing up the analysis of the functionally gradient and local characteristics of concrete of both centrifuged and vibro-centrifuged structures, it is obvious that in many cases they must be taken into account in the calculations.

3.4 Conclusions

1. An original method of experimental research of the functionally gradient cross-sections of vibrated, centrifuged, and vibro-centrifuged concretes is proposed to determine their aggregate (general) and local (differing in layers) strength and deformation characteristics and deformation diagrams.

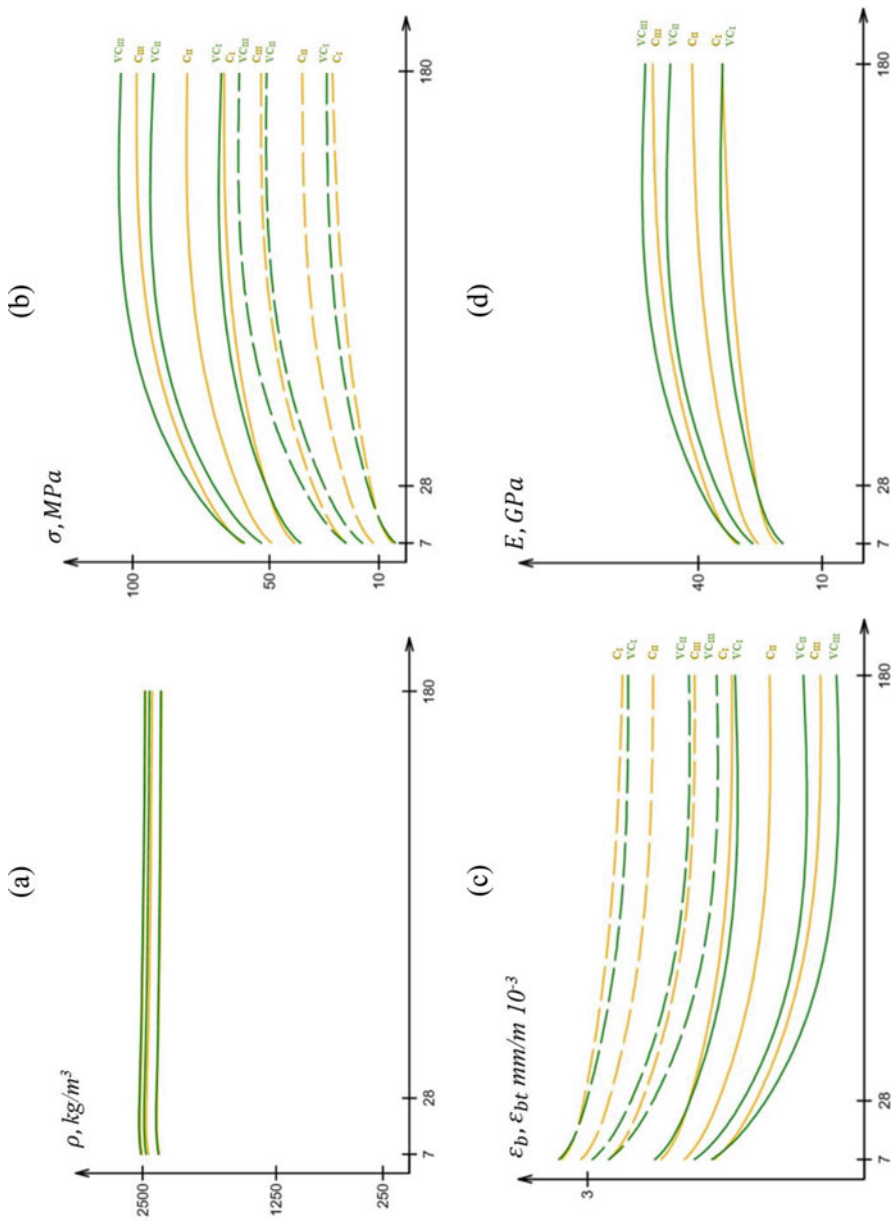


Fig. 3.27 General view of the quantitative picture of the change in the characteristics of functionally gradient cross-sections of centrifuged and vibrocentrifuged concretes depending on age: (a) density, (b) strength, (c) ultimate deformations in compression and tension, and (d) elastic modulus

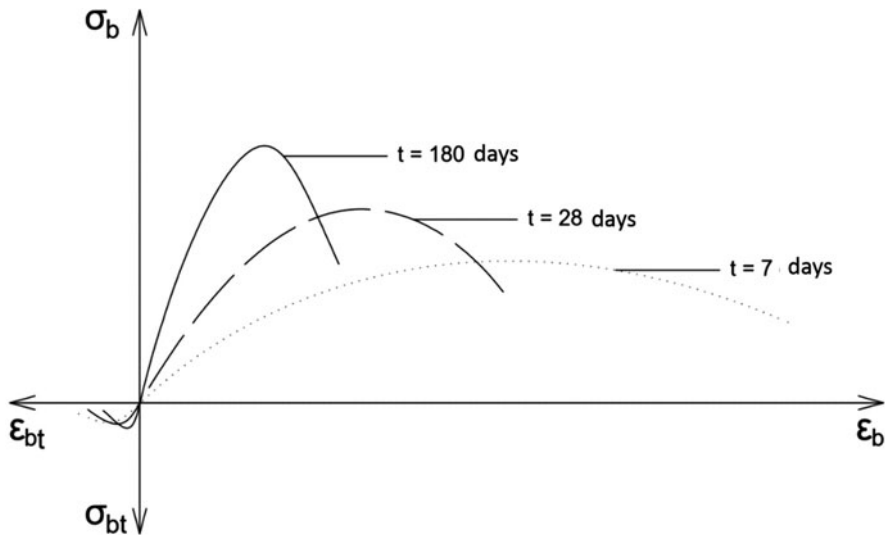


Fig. 3.28 Fundamental changes in deformation diagrams during compression and tension at different ages of concrete

2. Experimental studies of the integral characteristics of vibrated, centrifuged, and vibro-centrifuged concretes at the age of 7, 28, and 180 days under compression and tension revealed:
 - (i) The characteristics of concretes are higher with vibro-centrifugation than with centrifugation and vibration, and with centrifugation it is better than with vibration.
 - (ii) Compressive and tensile strength increases at all ages up to 20–22%.
 - (iii) Ultimate deformations during axial compression and axial tension decrease—down to 6–8%.
 - (iv) The modulus of elasticity under axial compression and axial tension increases (by 5–10%).
3. A change in the integral diagrams “ $\sigma - \epsilon$ ” under compression and tension of vibro-centrifuged concretes in comparison with vibrated and centrifuged concretes was revealed:
 - (i) The maximum shifts up and to the left.
 - (ii) The ascent angle at the origin increases.
 - (iii) The rise of the diagram in the ascending branch increases.
4. It has been proved that by using vibro-centrifugation it becomes possible to obtain concretes with improved structure and higher characteristics than by using centrifugation and vibration.
5. Experimental studies of the local characteristics of centrifuged and vibro-centrifuged concretes at the age of 7, 28, and 180 days under compression and

tension revealed that the outer layer of concrete has the best characteristics during centrifugation and vibro-centrifugation, while the inner layer has the worst.

6. The substantiation of the three-layer model of the functionally gradient structure of centrifuged and vibro-centrifuged concrete has been experimentally confirmed. Differentiation of the characteristics of layers of functionally gradient concrete is obtained: the concrete of the outer layers has the highest strength and modulus of elasticity and the least deformability; the concrete of the inner layers demonstrates the lowest strength, modulus of elasticity, and the highest deformability; the concrete of the middle layers has average characteristics.
7. The deformation diagrams of centrifuged and vibro-centrifuged concretes are also differentiated by layers, confirming the functionally gradient structure of such concretes. Among them, the deformation diagrams for the outer concrete layer are the highest in strength, the deformation diagrams for the inner concrete layer have the lowest strength, and the middle concrete layer has average indicators.

Chapter 4

Modeling of Aggregate and Local Structural Characteristics of V-, CF-, and VCF-Concretes



Abstract The values of standard and design resistances for limiting states, ultimate deformations, and initial moduli of elasticity in compression and tension of three considered types of concretes are based on the results of statistical processing of test data. The differences in the aggregate design characteristics of the types of concretes are revealed, depending on the manufacturing technology and age of concrete. It is experimentally and theoretically shown that different concrete layers during centrifugation and vibro-centrifugation are affected by centrifugal and centripetal forces, depending on the distance from the center of rotation and the angular velocity of rotation. To assess the local characteristics of the concretes, universal calculation dependencies are proposed, in which the characteristics of concrete (strength, ultimate deformations, and moduli of elasticity in compression and tension) are used as functions, and the distances from the center and angular speed of rotation are used as arguments.

Key words Limiting states · Statistical processing · Centrifugal force · Centripetal force · Rotation

For practical application of the obtained vibrated, centrifuged, and vibro-centrifuged heavy concretes and building constructions, it is necessary to be able to calculate their main structural characteristics.

In Chap. 3, we established changes in the aggregate and local design characteristics of vibrated, centrifuged, and vibro-centrifuged concretes, depending on various factors.

In this chapter, we are developing empirical relations for the calculation of these characteristics.

4.1 Calculation of the Aggregate Characteristics of V-, CF-, and VCF-Concretes

4.1.1 Standard and Design Resistances of V-, CF-, and VCF-Concretes

It is necessary, first of all, to develop recommendations for the calculation of the standard and design resistances of vibrated, centrifuged, and vibro-centrifuged heavy concretes for the possibility of calculating the limit states of groups I and II according to the Russian Building Regulations.

This requires certain statistics based on a large amount of experimental data. With this purpose, we have analyzed the results of numerous test studies of samples made of vibrated, centrifuged, and vibro-centrifuged concretes [3, 59, 86, 154–156, 172, 174–177].

Based on the results of statistical processing of test data, we determined the standard resistances to compression and tension of vibrated, centrifuged, and vibro-centrifuged concretes with a reliability of 0.95. Their values, which are at the same time the design resistances $R_{b,ser}$ and $R_{bt,ser}$ for the limiting states of the second group for the investigated vibrated, centrifuged, and vibro-centrifuged concretes, are given in Table 4.1.

The design resistances of vibrated, centrifuged, and vibro-centrifuged concretes for the limiting states R_b and R_{bt} of the first group were obtained as ratios of the standard compressive strength and tensile strength to the corresponding reliability factors for concrete in compression ($\gamma_b = 1.3$) and tension ($\gamma_{bt} = 1.5$).

It is also necessary to take into account the deformation characteristics of vibrated, centrifuged, and vibro-centrifuged concretes by their calculating and designing elements [228, 229, 232, 234–236, 293, 307, 313].

With short-term loading of vibrated concrete, their relative ultimate compressibility can be taken equal to 200×10^{-5} and the relative ultimate tensile strength as 25×10^{-5} .

With short-term loading of centrifuged and vibro-centrifuged concretes, the limiting relative values of compression should be taken equal to 180×10^{-5} and 160×10^{-5} and the limiting relative values of tension should be taken equal to

Table 4.1 Recommended values from Russian Building Regulations and design characteristics of vibrated, centrifuged, and vibro-centrifuged concrete of class B40

Resistance type	Standard and design characteristics of vibrated/centrifuged/vibro-centrifuged concretes, MPa		
	Standard R_{bn} , R_{bm} or calculated $R_{b,ser}$, $R_{bt,ser}$ resistances of II group	Calculated resistances R_b , R_{bt} of I group	Initial moduli of elasticity $E_{b(bt)} \times 10^3$
Axial compression	45/47/51	35/36/39	22/23/25
Axial tension	4.5/5/5.5	1.5/3.3/3.7	22/23/25

23×10^{-5} and 20×10^{-5} , respectively. In other words, the ultimate values of compression and tension of centrifuged and vibro-centrifuged concretes are reduced by about 10–20% compared to vibrated concretes, which led to an increase in the initial modulus of elasticity.

4.1.2 Differences in the Aggregate Structural Characteristics of V-, CF-, and VCF-Concretes Depending on the Manufacturing Technology and Age

Differences in the Aggregate Characteristics of Concretes Depending on the Manufacturing Technology

Let us first give the relative values of the strength and deformation characteristics of vibrated, centrifuged, and vibro-centrifuged concretes at a base age of 28 days in Table 4.2. Here the characteristics of vibrated concrete are taken as a unit, and the values of the characteristics of centrifuged and vibro-centrifuged concretes are given in the form correction factors to the characteristics of the vibrated concrete.

Then the proposals for the computational assessment of the aggregate design characteristics of centrifuged and vibro-centrifuged concretes, depending on the manufacturing technology, will consist in the use of coefficients introduced to each of the strength and deformative characteristics: $K_{Rb,28}R_b$; $K_{ebR,28}\epsilon_{bR}$; $K_{Eb,28}E_b$ in compression, and $K_{Rbt,28}R_{bt}$; $K_{ebtR,28}\epsilon_{btR}$; $K_{EBt,28}E_{bt}$ under tension, where $K_{i,28}$ are correction factors equal to the ratio of a particular structural characteristic to its base value for vibrated concrete, which is taken as its value at the age of 28 days.

Thus, to obtain the strength and deformation characteristics of centrifuged and vibro-centrifuged concrete at 28 days of age, it will be enough to simply multiply their values for vibrated concrete by the values of the correction factors given in Table 4.2.

Table 4.2 Relative values of the characteristics of vibrated, centrifuged, and vibro-centrifuged concretes at the age of 28 days

Design characteristics	Values of correction factors at the age of 28 days, normalized at values relative to vibrated		
	Concrete type		
	Vibrated	Centrifuged	Vibro-centrifuged
R_b	1.00	1.14	1.28
ϵ_b	1.00	0.89	0.81
R_{bt}	1.00	1.08	1.18
ϵ_{bt}	1.00	0.94	0.85
$E_b = E_{bt}$	1.00	1.18	1.32

Determination of the Aggregate Characteristics of Vibrated, Centrifuged, and Vibro-centrifuged Concretes Depending on Age

The calculation assessment of the aggregate design characteristics of vibrated, centrifuged, and vibro-centrifuged concretes, depending on the age of concrete, is proposed to be performed according to analytical dependencies to determine the coefficients $K_{i,t}$, introduced to each of the strength and deformative characteristics: $K_{Rb,t}R_b$; $K_{ebR,t}\epsilon_{bR}$; $K_{Eb,t}E_b$ in compression and $K_{Rbt,t}R_{bt}$; $K_{ebtR,t}\epsilon_{btR}$; $K_{Ebt,t}E_{bt}$ in tension, where $K_{i,t}$ are coefficients equal to the ratio of one or another structural characteristic to its basic value, which is taken as its value at the concrete age of 28 days.

For a single function $f_{i,t}(t)$ in formula (4.1), for the sake of uniformity, we take the dependence of M. Sargin, recommended by the EKB-FIP for describing the deformation diagrams of concrete [233, 320]. Coefficients $K_{i,t}$ are determined in the form:

$$K_{i,t} = f_{i,t}(t/28),$$

$$K_{i,t} = \frac{K_0\left(\frac{t}{28}\right) - \left(\frac{t}{28}\right)^2}{1 + (K_0 - 2)\left(\frac{t}{28}\right)}, \quad (4.1)$$

where $f_{i,t}$ are the corresponding functions of the same type and t is the age of concrete in relation to the basic value (28 days).

This formula can be modified for a more flexible description of the parameters of the function $f_{i,t}(t/28)$ in the form:

$$K_{i,t} = \frac{a\left(\frac{t}{28}\right) - c\left(\frac{t}{28}\right)^2}{1 + (a - b)\left(\frac{t}{28}\right)}. \quad (4.2)$$

Here the arguments $K_{i,t}$ are the ratios of the desired values of the current characteristic of concrete at the age of t to its values at the age of 28 days; K_0 , a , b , c are control parameters for each characteristic. That is, to take into account the effect of age on the change in the strength and deformative characteristics of vibrated, centrifuged, and vibro-centrifuged concretes, it is proposed to multiply the values of their characteristics at the age of 28 days by the corresponding parameters $K_{i,t}$. The values of the last parameters were determined by statistical processing of the results, obtained for all characteristics of concrete at any age.

The analysis made it possible to determine and systematize the values of $K_{i,t}$ and obtain dependencies of the type (4.2) for all structural characteristics of the investigated concretes, bringing them down for reference ages in Table 4.3.

Thus, the general aggregate characteristics of vibrated, centrifuged, and vibro-centrifuged concretes can be determined by the expressions: $K_{Rb,28}K_{Rb,t}R_b$; $K_{ebR,28}K_{ebR,t}\epsilon_{bR}$; $K_{Eb,28}K_{Eb,t}E_b$ with compression and $K_{Rbt,28}K_{Rbt,t}R_{bt}$; $K_{ebtR,28}K_{ebtR,t}\epsilon_{btR}$; $K_{Ebt,28}K_{Ebt,t}E_{bt}$ in tension.

Table 4.3 Values of parameters a , b , c of dependence (4.2) for determining the design characteristics of vibrated, centrifuged, and vibro-centrifuged concretes depending on age

Characteristics of concrete	Age, days	Manufacturing technology			a , b , c control parameters			
		V	C	VC	V	C	VC	
Density, kg/m ³	7	2395	2439	2445	<i>a</i>	-2280132	-2149314	-1866517
	28	2385	2428	2434	<i>b</i>	-2279176	-2148429	-1865750
	180	2365	2406	2421	<i>c</i>	-3149	-3207	-1458
Compressive strength, MPa								
(i) Cubic	7	43.7	45.5	53.3	<i>a</i>	514.353	532.98	512.11
	28	59.8	62.5	70.7	<i>b</i>	506.495	525.17	506.85
	180	76.5	81.2	92.6	<i>c</i>	-15.349	-17.72	73.76
(ii) Prismatic	7	33.3	34.8	40.4	<i>a</i>	391.2934	413.3209	527.5655
	28	45.6	47.6	53.8	<i>b</i>	383.4546	405.3431	518.3809
	180	58.4	61.9	70.5	<i>c</i>	-11.7565	-14.0204	-20.3643
Tensile strength, MPa								
(i) By bending	7	3.6	3.9	4.5	<i>a</i>	50.8948	51.0598	63.1485
	28	4.7	5.2	5.9	<i>b</i>	40.6078	41.8310	52.9546
	180	6.2	6.9	7.9	<i>c</i>	-2.1543	-2.1299	-2.8952
(ii) Axial	7	3.3	3.5	4.1	<i>a</i>	43.0431	48.3541	61.0173
	28	4.4	4.6	5.3	<i>b</i>	33.8693	38.3901	49.9586
	180	5.8	6.1	7.1	<i>c</i>	-1.7215	-2.0807	-2.8940
Limiting deformations at axial compression, mm/m ($\times 10^{-3}$)	7	2.87	2.84	2.8	<i>a</i>	-30.5276	-30.1075	-29.1606
	28	2.18	2.15	2.11	<i>b</i>	-15.9768	-15.6002	-14.8403
	180	1.68	1.62	1.58	<i>c</i>	-0.9868	-1.0667	-1.0547
Limiting deformations at axial tension, mm/m ($\times 10^{-4}$)	7	1.58	1.55	1.51	<i>a</i>	-16.0475	-16.0367	-15.0249
	28	1.19	1.17	1.13	<i>b</i>	-1.9671	-1.7742	-1.1543
	180	0.93	0.9	0.87	<i>c</i>	-0.4818	-0.5196	-0.4811
Elastic modulus, GPa	7	26.1	27	28.5	<i>a</i>	269.6841	259.9814	263.7882
	28	37.4	39.9	42.9	<i>b</i>	263.2833	254.2862	258.4681
	180	48.1	52.3	56.8	<i>c</i>	-7.1051	-7.1577	-7.3474

The analysis showed good convergence of the developed theoretical recommendations with our experimental results.

4.1.3 Analytical Description of Stress-Strain Diagrams Under Compression and Tension of V-, CF-, and VCF-Concretes, Their Mutual Relationship, and Dependence on Age

As it has been noted in Point 4.1.2.2, one of the most convenient and common dependencies for describing the diagrams of concrete deformation under compression and tension is the function proposed by P. Sargin and recommended by EKB-FIP for calculating reinforced concrete constructions [233, 320]:

$$\frac{\sigma}{R} = \frac{K \left(\frac{\varepsilon}{\varepsilon_R} \right) - \left(\frac{\varepsilon}{\varepsilon_R} \right)^2}{1 + (K - 2) \left(\frac{\varepsilon}{\varepsilon_R} \right)} \quad (4.3)$$

where R and ε_R are the maximum strength and the corresponding compressive or tensile deformations and $K = \varepsilon_R E / R$ is a numerical parameter equal to the ratio of the initial E (tangent) elastic modulus to the limiting (secant) elastic modulus R/ε_R at the moment of reaching the maximum of function (4.3) with coordinates R and ε_R .

The relationship between the deformation diagrams “ $\sigma - \varepsilon$ ” of concrete in compression and tension is usually most simply reflected in the EKB-FIP recommendations, in which the equality of the initial moduli of elasticity in compression and tension is assumed ($E_b = E_{bt}$), that is, tangents to the diagrams “ $\sigma_b - \varepsilon_b$ ” and “ $\sigma_{bt} - \varepsilon_{bt}$ ” at the origin of coordinates and the same parameter value is recommended for compression and tension:

$$K_b = \frac{\varepsilon_b R E_b}{R_b} = \frac{\varepsilon_{bt} R E_{bt}}{R_{bt}} = K_{bt}, \quad (4.4)$$

that is, secants at the maximum points of the diagrams “ $\sigma_b - \varepsilon_b$ ” and “ $\sigma_{bt} - \varepsilon_{bt}$ ” and the same function “ $\sigma - \varepsilon$ ” are given in compression and tension by formula (4.4).

Thus, the compression and tension diagrams are assumed to be similar (Fig. 4.1).

The analysis showed that the assumption about the similarity of the diagrams of concrete deformation under compression and tension can be attributed not only to vibrated concrete, but also to extend it to centrifuged and vibro-centrifuged concrete.

The analysis also revealed additional facts about the effect of the age of concrete on the relationship between changes in the diagrams “ $\sigma - \varepsilon$ ” during compression and tension of vibrated, centrifuged, and vibro-centrifuged concretes.

First, it was found that the coordinates of the maxima of the diagrams “ $\sigma_b - \varepsilon_b$ ” and “ $\sigma_{bt} - \varepsilon_{bt}$ ” at any age dispose under compression and tension on one straight line passing through the origin of the plot coordinates, and this is observed for all concretes, namely, vibrated, centrifuged, and vibro-centrifuged ones.

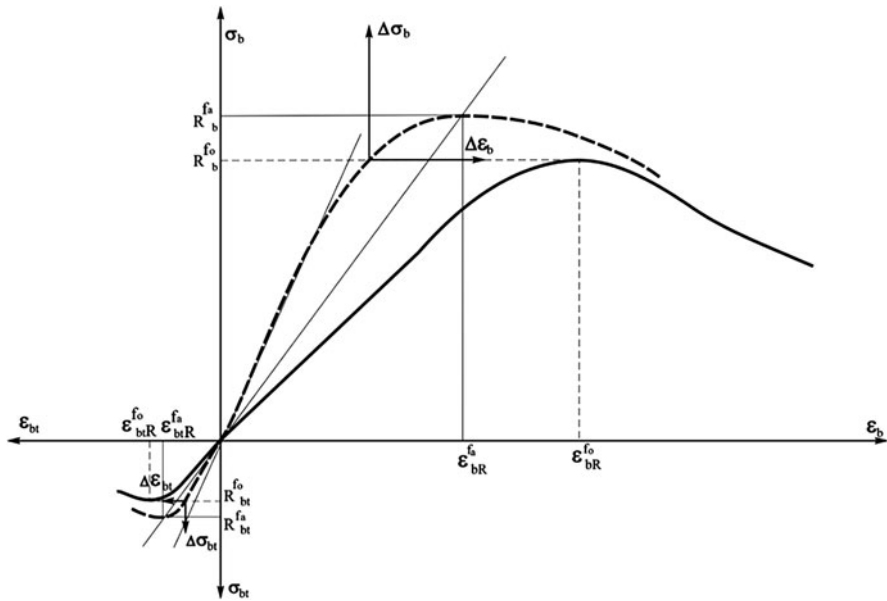


Fig. 4.1 Similarity of deformation diagrams and their increments for vibrated, centrifuged, and vibro-centrifuged concretes at compression and tension in any age

That is, for vibrated, centrifuged, and vibro-centrifuged concretes at any age, the similarity of the diagrams “ $\sigma_b - \varepsilon_b$ ” and “ $\sigma_{bt} - \varepsilon_{bt}$ ” under compression and tension was also revealed.

Second, it has been experimentally proved that the similarity of the diagrams “ $\sigma_b - \varepsilon_b$ ” and “ $\sigma_{bt} - \varepsilon_{bt}$ ” in compression and in tension takes place even for the increments of these diagrams in the plot with the origin at the points with coordinates R_b, ε_{bR} at compression and $R_{bt}, \varepsilon_{btR}$ at tension of vibrated, centrifuged, and vibro-centrifuged concretes at any age.

Thus, we have proved the similarity of the diagrams “ $\sigma_b - \varepsilon_b$ ” and “ $\sigma_{bt} - \varepsilon_{bt}$ ” in compression and in tension: (i) not only for vibrated but also for centrifuged and vibro-centrifuged concretes, (ii) not only at the age of 28 days but also at any other age, and (iii) both for diagrams in absolute terms and in their increments after reaching the maximum strength of concretes.

Note that in studies of vibrated, centrifuged, and vibro-centrifuged concretes for the uniformity of the calculated dependences, we applied the same functions (4.2) and (4.3) with three purposes:

- (i) To assess changes in strength and deformation characteristics during compression and tension
- (ii) To describe deformation diagrams and their increments under compression and tension

- (iii) To assess the effect of concrete age on changes in strength and deformation characteristics and also deformation diagrams and their increments under compression and tension

As a whole, to determine the calculated strength and deformation characteristics and deformation diagrams of vibrated, centrifuged, and vibro-centrifuged concretes at any age, the following algorithm is proposed.

At the *first stage*, the changes in the strength and deformation characteristics of centrifuged and vibro-centrifuged, in comparison with vibrated concretes at the age of 28 days, are determined: $K_{Rb,28}R_b$; $K_{ebR,28}\varepsilon_{bR}$; $K_{Eb,28}E_b$ in compression and $K_{Rbt,28}R_{bt}$; $K_{ebtR,28}\varepsilon_{btR}$; $K_{Ebt,28}E_{bt}$ in tension, according to dependence (4.2) and Table 4.2.

At the *second stage*, the effect of concrete age on the strength and deformation characteristics of vibrated, centrifuged, and vibro-centrifuged concretes is assessed with the parameters: $K_{Rb,t}K_{Rb,28}R_b$; $K_{ebR,t}K_{ebR,28}\varepsilon_{bR}$; $K_{Eb,t}K_{Eb,28}E_b$ in compression and $K_{Rbt,t}K_{Rbt,28}R_{bt}$; $K_{ebtR,t}K_{ebtR,28}\varepsilon_{btR}$; $K_{Ebt,t}K_{Ebt,28}E_{bt}$ in tension, according to Table 4.3.

At the *third stage*, an analytical description of the diagrams “ $\sigma - \varepsilon$ ” of vibrated, centrifuged, and vibro-centrifuged concretes under compression and tension at different concrete ages is performed, according to function (4.3) with the help of substitution, respectively: $K_{Rb,t}K_{Rb,28}R_b$; $K_{ebR,t}K_{ebR,28}\varepsilon_{bR}$; $K_{Eb,t}K_{Eb,28}E_b$ in compression and $K_{Rbt,t}K_{Rbt,28}R_{bt}$; $K_{ebtR,t}K_{ebtR,28}\varepsilon_{btR}$; $K_{Ebt,t}K_{Ebt,28}E_{bt}$ in tension, according to Table 4.3.

The analysis showed good convergence of experimental and calculated results.

4.2 Calculation of Local Structural Characteristics of CF- and VCF-Concrete Depending on Technological Parameters

As we showed in Chap. 3, during centrifugation and vibro-centrifugation, different forces act on different layers of concrete with annular or circular cross-sections. It ultimately leads to significantly different characteristics of concrete layers, first of all, density, as well as strength, deformability, and elasticity modulus.

The main factors that should be taken into account in this case and included in the future in the calculation dependencies as arguments will be centrifugal and centripetal forces.

Therefore, in the universal calculation dependencies, taking into account the change in the structural characteristics of concrete, as functions, it is expedient to accept the structural characteristics of concrete or their increments (i.e., in absolute or relative terms). At the same time, as arguments, the forces of inertia at rotation should be included for consideration, which are, in turn, by functions of the distance from the center of rotation and the angular velocity of rotation.

After solution of this task, we will obtain design dependencies for differentiated ones accounting for changes in all the characteristics of concrete necessary for calculation. It will allow us to introduce into the calculation of construction parameters the strength and deformation characteristics of concrete that differ in cross-section, more accurately and fully using the available reserves of the bearing capacity of the elements.

It is known [8–10, 206] that the centrifugation of concrete is based on the ability of the concrete mixture to compact inside a rotating mold under the action of centrifugal forces proportional to the mass of particles, the square of the angular velocity, and the distance from the axis of rotation:

$$F_{cf} = \frac{4}{3g} \pi r_{ca}^3 \rho_{ca} l \omega^2 \quad (4.5)$$

where l is the distance from the center of rotation to the center of the grain aggregate and ω is the angular velocity of rotation:

$$\omega = \frac{\pi n}{30} \quad (4.6)$$

The effect of centrifugal force on a grain of coarse-grained aggregate (Fig. 4.2) is the more it is significant, the larger the radius r_{ca}^3 and density ρ_{ca} of particles. In this regard, coarse grains move to the outer layer of the product, and fine grains displace to the inner layer.

We also propose to take into account another, more general formula for calculating the centrifugal force, in which $F_{cf} = f(\omega, l)$ [149]:

$$F_{cf} = |m| \omega^2 l, \quad (4.7)$$

where m is the mass of the rotating body, ω is the angular velocity of rotation, and l is the distance from the center of rotation to the center of the grain.

Due to, the centrifuged concrete differs from vibrated concrete by a significantly greater heterogeneity of the distribution of coarse-grained aggregate grains over the cross-section of the concrete structure, which leads to a difference in the characteristics of different layers, that is, the functionally gradient cross-section arises.

This relates even more to vibro-centrifuged concrete, in which the functional gradient is manifested even more strongly. In these elements, the concentration of coarse-grained aggregate grains and, accordingly, strength, in the outer layers is even higher.

All this clearly demonstrates the need to take into account differences in the strength and deformability of concrete layers of the functionally gradient cross-sections in calculations.

To confirm this, we shall perform a calculation based on the action of centrifugal force on a grain, for example, a dense (granite) aggregate. Substituting all the initial data in (4.5), we obtain the centrifugal force acting on the granite grain (Table 4.4).

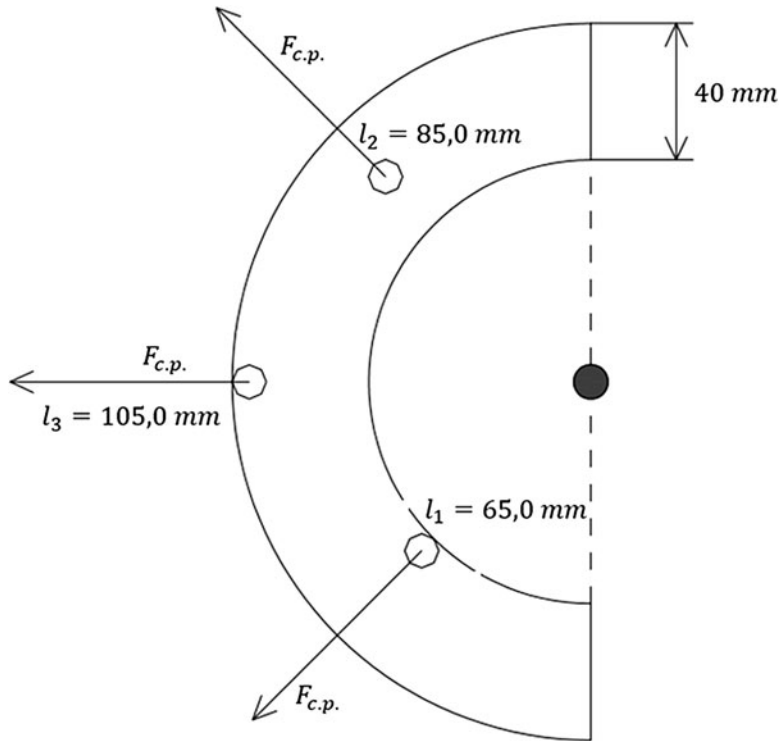


Fig. 4.2 Scheme of the action of centrifugal forces on grains of coarse-grained aggregate along the wall thickness of the centrifuged concrete structure

Table 4.4 Basic parameters of the acting centrifugal force

Grain radius of coarse-grained aggregate, m	Distance from the center of rotation to the center of the grain, m	Angular velocity, rad/s	Mold rotation speed during compaction, rpm	Pressure on concrete mix, MPa	Centrifugal force acting on granite grain of coarse-grained aggregate, N
0.01	0.105	84	800	0.7	316.5×10^{-6}
		157	1500	2.16	1105.6×10^{-6}

We use the method of mathematical planning of experiment, and we take the full factorial experiment (FFE). Based on our recommendations [142, 147], we shall take the time of centrifugation of the concrete mixture equal to 4.2 min. The values of the variation factors and their physical meaning are presented in Table 4.5.

The following parameters were taken as the response function:

- (i) $Y_1 (X_1, X_2)$ is the axial compression strength.
- (ii) $Y_2 (X_1, X_2)$ is the axial tensile strength.
- (iii) $Y_3 (X_1, X_2)$ is the ultimate deformations at axial compression.

Table 4.5 Factors of variation in FFE

Factor code	Physical meaning of factor	Units	Variation range	Factor levels		
				-1	0	+1
X_1	Distance from center of rotation to center of grain	m	± 0.05	0.10	0.15	0.20
X_2	Angular velocity	rad/s	± 36	84	120	156

Table 4.6 Calculation coefficients of regression equations for the inner layer of centrifuged prototypes

Output parameter of equation	Coefficients of equations					
	B_0	B_1	B_2	B_3	B_4	B_5
Y_1 Axial compressive strength, MPa	23.25	0.877	—	—	—	0.345
			1.446	1.618	1.047	
Y_2 Axial tensile strength, MPa	3.852	0.767	—	—	—	0.189
			0.204	0.892	0.311	
Y_3 Ultimate deformations at axial compression, mm/m	3.247	—	0.027	—	0.006	—
		1.245		0.417		0.032
Y_4 Ultimate deformations at axial tension, mm/m	2.679	—	—	—	-0.34	—
		0.788	0.215	0.509		0.056
Y_5 Elastic modulus, MPa	21.32	4.86	—	0.299	1.168	-0.38
			0.639			

(iv) $Y_4 (X_1, X_2)$ is the ultimate deformations at axial tension.

(v) $Y_5 (X_1, X_2)$ is the elastic modulus.

According to the results of the study, the basic regression equations were obtained by the least squares method, presented in the form of polynomials of the second degree:

$$Y (X_1, X_2) = B_0 + B_1 X_1 + B_2 X_2 + B_3 X_1 X_2 + B_4 X_1^2 + B_5 X_2^2 \quad (4.8)$$

Statistical analysis of the obtained regression equations was assessed according to three criteria: homogeneity of variances, significance of coefficients, and adequacy, which was verified using Fisher's criterion. The plan of the experiment and the results of the optimization parameters were adopted according to the test results obtained by us in Chap. 3. The significance of the coefficients in equations was established by the calculated value of the Student's t -test. The values of the obtained coefficients are given in Tables 4.6, 4.7, 4.8, 4.9, 4.10 and 4.11.

Statistical data processing was carried out using the software Mathcad, which made it possible to obtain 30 regression equations in the form of polynomials of the second degree for centrifuged and vibro-centrifuged concrete:

Table 4.7 Calculation coefficients of regression equations for the middle layer of centrifuged prototypes

Output parameter of equation	Coefficients of equations					
	B_0	B_1	B_2	B_3	B_4	B_5
Y_6 Axial compressive strength, MPa	27.54	1.147	-1.226	-1.394	-0.899	0.675
Y_7 Axial tensile strength, MPa	4.356	1.024	-0.051	-0.567	-0.181	-0.137
Y_8 Ultimate deformations at axial compression, mm/m	4.341	-1.031	7.29×10^{-3}	-0.203	0.038	0.01
Y_9 Ultimate deformations at axial tension, mm/m	3.021	-0.532	-0.015	-0.353	-0.01	0.001
Y_{10} Elastic modulus, MPa	26.507	5.67	-0.442	0.572	1.314	-0.05

Table 4.8 Calculation coefficients of regression equations for the outer layer of centrifuged prototypes

Output parameter of equation	Coefficients of equations					
	B_0	B_1	B_2	B_3	B_4	B_5
Y_{11} Axial compressive strength, MPa	35.89	3.166	1.287	0.812	-0.015	1.781
Y_{12} Axial tensile strength, MPa	6.184	1.867	-0.83	-0.336	0.452	-0.06
Y_{13} Ultimate deformations at axial compression, mm/m	5.310	0.543	1.456	1.002	0.569	0.59
Y_{14} Ultimate deformations at axial tension, mm/m	2.886	1.592	-0.273	0.987	0.256	0.043
Y_{15} Elastic modulus, MPa	29.111	6.49	1.65	-0.399	1.678	0.68

Table 4.9 Calculation coefficients of regression equations for the inner layer of vibro-centrifuged prototypes

Output parameter of equation	Coefficients of equations					
	B_0	B_1	B_2	B_3	B_4	B_5
Y_{16} Axial compressive strength, MPa	32.31	8.774	-0.450	0.67	0.308	0.809
Y_{17} Axial tensile strength, MPa	3.882	0.459	-0.043	-0.49	1.282	1.511
Y_{18} Ultimate deformations at axial compression, mm/m	3.214	-1.412	0.037	-0.82	-1.07	0.086
Y_{19} Ultimate deformations at axial tension, mm/m	1.95	-0.825	0.007	1.16	0.778	0.534
Y_{20} Elastic modulus, MPa	31.11	7.626	-0.117	-1.12	-5.134	-1.223

Table 4.10 Calculation coefficients of regression equations for the middle layer of vibro-centrifuged prototypes

Output parameter of equation	Coefficients of equations					
	B_0	B_1	B_2	B_3	B_4	B_5
Y_{21} Axial compressive strength, MPa	38.467	10.506	-0.231	0.7	0.558	-0.05
Y_{22} Axial tensile strength, MPa	5.089	0.768	-0.02	-0.35	-0.04	0.046
Y_{23} Ultimate deformations at axial compression, mm/m	3.983	-1.202	0.075	-0.14	0.041	0.005
Y_{24} Ultimate deformations at axial tension, mm/m	2.48	-0.637	0.017	-0.052	-0.029	0.083
Y_{25} Elastic modulus, MPa	38.129	9.321	-0.51	0.089	-3.713	0.638

Table 4.11 Calculation coefficients of regression equations for the outer layer of vibro-centrifuged prototypes

Output parameter of equation	Coefficients of equations					
	B_0	B_1	B_2	B_3	B_4	B_5
Y_{26} Axial compressive strength, MPa	48.45	13.77	0.65	1.44	2.014	0.45
Y_{27} Axial tensile strength, MPa	8.132	1.56	1.09	0.321	0.563	0.12
Y_{28} Ultimate deformations at axial compression, mm/m	5.451	0.85	1.345	0.47	1.047	0.06
Y_{29} Ultimate deformations at axial tension, mm/m	5.98	1.12	-0.003	-0.008	0.844	0.141
Y_{30} Elastic modulus, GPa	43.18	14.23	1.231	1.157	-0.09	1.98

Centrifuged (CF) Concrete(i) *Inner layer (CF_I):*

$$Y_1 (X_1, X_2) = 23.25 + 0.877X_1 - 1.446X_2 - 1.618X_1X_2 - 1.047X_1^2 + 0.345X_2^2;$$

$$Y_2 (X_1, X_2) = 3.852 + 0.767X_1 - 0.204X_2 - 0.892X_1X_2 - 0.311X_1^2 - 0.189X_2^2;$$

$$Y_3 (X_1, X_2) = 3.247 - 1.245X_1 + 0.027X_2 - 0.417X_1X_2 + 0.006X_1^2 - 0.032X_2^2;$$

$$Y_4 (X_1, X_2) = 2.679 - 0.788X_1 - 0.215X_2 - 0.509X_1X_2 - 0.34X_1^2 - 0.056X_2^2;$$

$$Y_5 (X_1, X_2) = 21.32 + 4.86X_1 - 0.639X_2 + 0.299X_1X_2 + 1.168X_1^2 - 0.38X_2^2.$$

(ii) *Middle layer (CF_{II}):*

$$Y_6 (X_1, X_2) = 27.54 + 1.147X_1 - 1.226X_2 - 1.394X_1X_2 - 0.899X_1^2 + 0.675X_2^2;$$

$$Y_7 (X_1, X_2) = 4.356 + 1.024X_1 - 0.051X_2 - 0.567X_1X_2 - 0.181X_1^2 - 0.137X_2^2;$$

$$Y_8 (X_1, X_2) = 4.341 - 1.031X_1 + 7.29 \times 10^{-3}X_2 - 0.203X_1X_2 + 0.038X_1^2 + 0.01X_2^2;$$

$$Y_9 (X_1, X_2) = 3.021 - 0.532X_1 - 0.015X_2 - 0.353X_1X_2 - 0.01X_1^2 + 0.001X_2^2;$$

$$Y_{10} (X_1, X_2) = 26.507 + 5.67X_1 - 0.442X_2 + 0.572X_1X_2 + 1.314X_1^2 - 0.05X_2^2.$$

(iii) *Outer layer (CF_{III})*:

$$Y_{11} (X_1, X_2) = 35.89 + 3.166X_1 + 1.287X_2 + 0.812X_1X_2 - 0.015X_1^2 + 1.781X_2^2;$$

$$Y_{12} (X_1, X_2) = 6.184 + 1.867X_1 - 0.83X_2 - 0.336X_1X_2 + 0.452X_1^2 - 0.06X_2^2;$$

$$Y_{13} (X_1, X_2) = 5.31 - 0.543X_1 + 1.456X_2 + 1.002X_1X_2 + 0.569X_1^2 + 0.59X_2^2;$$

$$Y_{14} (X_1, X_2) = 2.886 + 1.592X_1 - 0.273X_2 + 0.987X_1X_2 + 0.256X_1^2 + 0.043X_2^2;$$

$$Y_{15} (X_1, X_2) = 29.111 + 6.49X_1 + 1.65X_2 - 0.399X_1X_2 + 1.678X_1^2 + 0.68X_2^2.$$

Vibro-centrifuged (VCF) Concrete

(iv) *Inner layer (VCF_I)*:

$$Y_{16} (X_1, X_2) = 32.31 + 8.774X_1 - 0.450X_2 + 0.67X_1X_2 + 0.308X_1^2 + 0.809X_2^2;$$

$$Y_{17} (X_1, X_2) = 3.882 + 0.459X_1 - 0.043X_2 - 0.49X_1X_2 + 1.282X_1^2 + 1.511X_2^2;$$

$$Y_{18} (X_1, X_2) = 3.214 - 1.412X_1 + 0.037X_2 - 0.82X_1X_2 - 1.07X_1^2 + 0.086X_2^2;$$

$$Y_{19} (X_1, X_2) = 1.95 - 0.825X_1 + 0.007X_2 + 1.16X_1X_2 + 0.778X_1^2 + 0.534X_2^2;$$

$$Y_{20} (X_1, X_2) = 31.11 + 7.626X_1 - 0.117X_2 - 1.12X_1X_2 - 5.134X_1^2 - 1.223X_2^2.$$

(v) *Middle layer (VCF_{II})*:

$$Y_{21} (X_1, X_2) = 38.467 + 10.506X_1 - 0.231X_2 + 0.7X_1X_2 + 0.558X_1^2 - 0.05X_2^2;$$

$$Y_{22} (X_1, X_2) = 5.089 + 0.768X_1 - 0.02X_2 - 0.35X_1X_2 - 0.04X_1^2 + 0.046X_2^2;$$

$$Y_{23} (X_1, X_2) = 3.983 - 1.202X_1 + 0.075X_2 - 0.14X_1X_2 + 0.041X_1^2 + 0.005X_2^2;$$

$$Y_{24} (X_1, X_2) = 2.48 - 0.637X_1 + 0.017X_2 - 0.052X_1X_2 - 0.029X_1^2 + 0.083X_2^2;$$

$$Y_{25} (X_1, X_2) = 38.129 + 9.321X_1 - 0.51X_2 + 0.089X_1X_2 - 3.713X_1^2 + 0.638X_2^2.$$

(vi) *Outer layer (VC_{III}):*

$$\begin{aligned}
 Y_{26} (X_1, X_2) &= 48.45 + 13.77X_1 + 0.65X_2 + 1.44X_1X_2 + 2.014X_1^2 + \\
 &\quad 0.45X_2^2; \\
 Y_{27} (X_1, X_2) &= 8.132 + 1.56X_1 + 1.09X_2 + 0.321X_1X_2 + 0.563X_1^2 \\
 &\quad + 0.12X_2^2; \\
 Y_{28} (X_1, X_2) &= 5.451 + 0.85X_1 + 1.345X_2 + 0.47X_1X_2 + 1.047X_1^2 \\
 &\quad + 0.06X_2^2; \\
 Y_{29} (X_1, X_2) &= 5.98 + 1.12X_1 - 0.003X_2 - 0.008X_1X_2 + 0.844X_1^2 \\
 &\quad + 0.141X_2^2; \\
 Y_{30} (X_1, X_2) &= 43.18 + 14.23X_1 + 1.231X_2 + 1.157X_1X_2 - 0.09X_1^2 \\
 &\quad + 1.98X_2^2.
 \end{aligned}$$

Our proposed calculation equations are summarized in Table 4.12.

Graphical interpretations of mathematical dependencies (for different layers of centrifuged and vibro-centrifuged concrete) are presented in Figs. 4.3, 4.4, 4.5, 4.6, 4.7, 4.8, 4.9, 4.10, 4.11, 4.12, 4.13, 4.14, 4.15, 4.16, 4.17, 4.18, 4.19 and 4.20.

We now interpret and transform the regression equations obtained into calculation equations for determining the local characteristics of layers of the functionally gradient cross-sections of centrifuged and vibro-centrifuged concretes.

Our proposed calculation equations are summarized in Table 4.12.

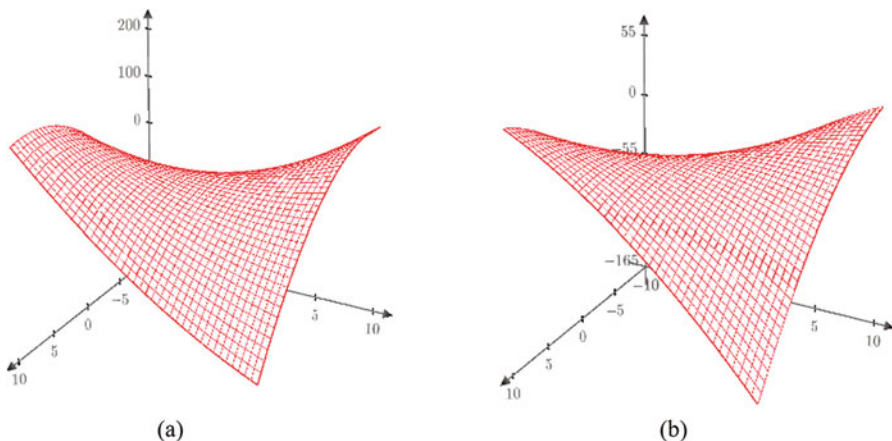


Fig. 4.3 Graphical interpretation of the dependences of: (a) compressive strength and (b) tensile strength for the inner layer of the functionally gradient cross-section of centrifuged concrete vs. the distance from the center of rotation to the center of the grain and the angular velocity

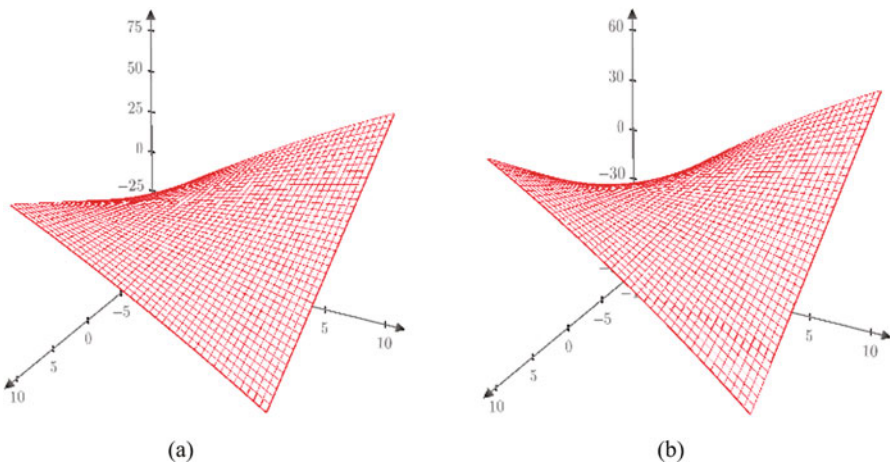
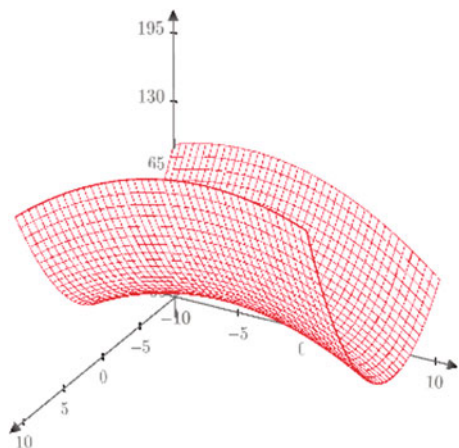


Fig. 4.4 Graphical interpretation of the dependence of: (a) ultimate deformations in compression and (b) tension for the inner layer of the functionally gradient cross-section of centrifuged concrete vs. the distance from the center of rotation to the center of the grain and the angular velocity

Fig. 4.5 Graphical interpretation of the dependence of the elastic modulus for the inner layer of the functionally gradient cross-section of centrifuged concrete vs. the distance from the center of rotation to the center of the grain and the angular velocity



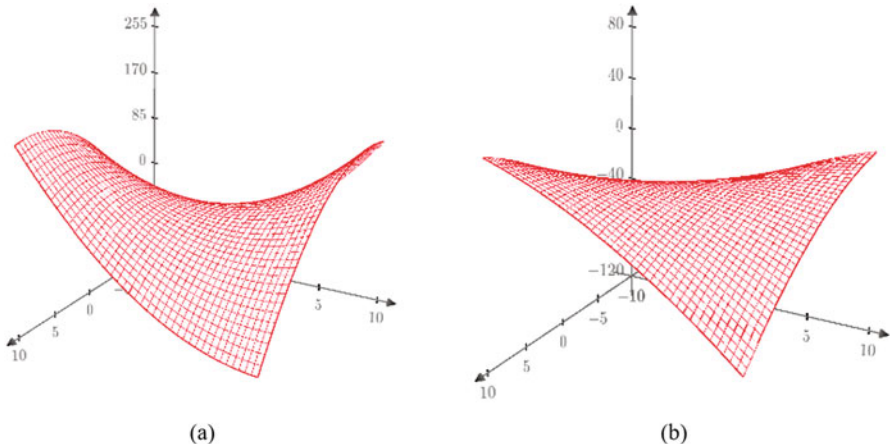


Fig. 4.6 Graphical interpretation of the dependences of: (a) compressive strength and (b) tensile strength for the middle layer of the functionally gradient cross-section of centrifuged concrete vs. the distance from the center of rotation to the center of the grain and the angular velocity

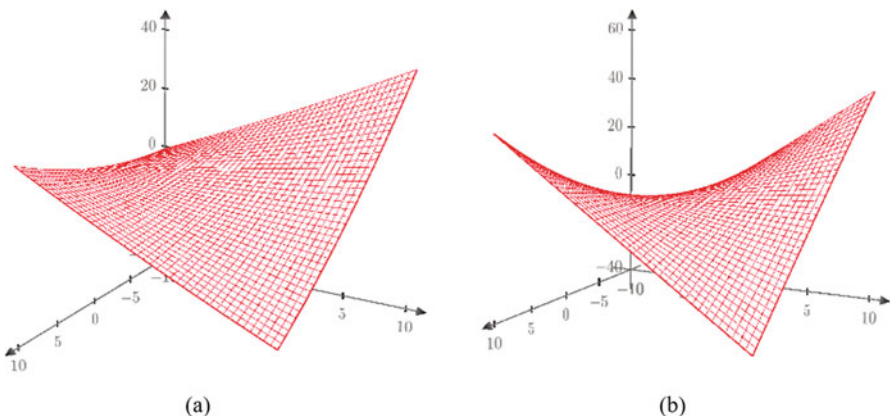


Fig. 4.7 Graphical interpretation of the dependence of: (a) ultimate deformations in compression and (b) tension for the middle layer of the functionally gradient cross-section of centrifuged concrete vs. the distance from the center of rotation to the center of the grain and the angular velocity

Fig. 4.8 Graphical interpretation of the dependence of the elastic modulus of the middle layer of the functionally gradient cross-section of centrifuged concrete vs. the distance from the center of rotation to the center of the grain and the angular velocity

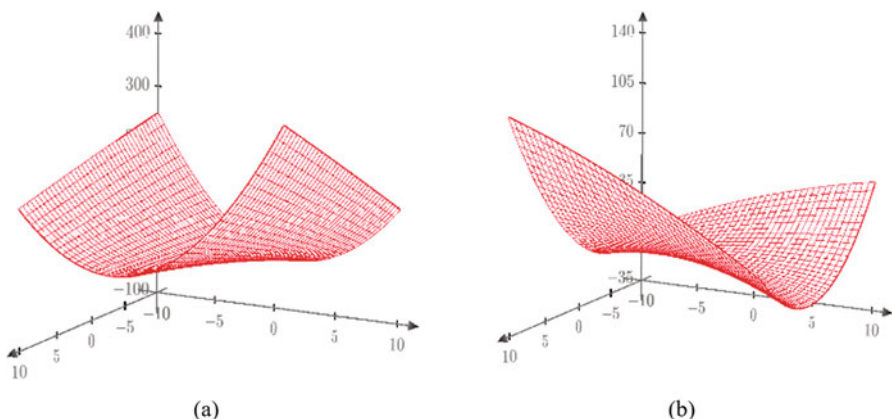
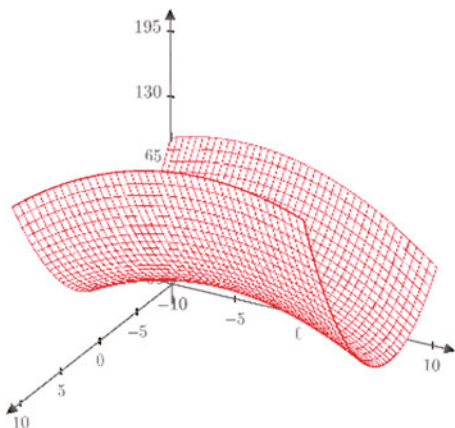


Fig. 4.9 Graphical interpretation of the dependence of: (a) compressive strength and (b) tensile strength for outer layer of the functionally gradient cross-section of centrifuged concrete vs. the distance from the center of rotation to the center of the grain and the angular velocity

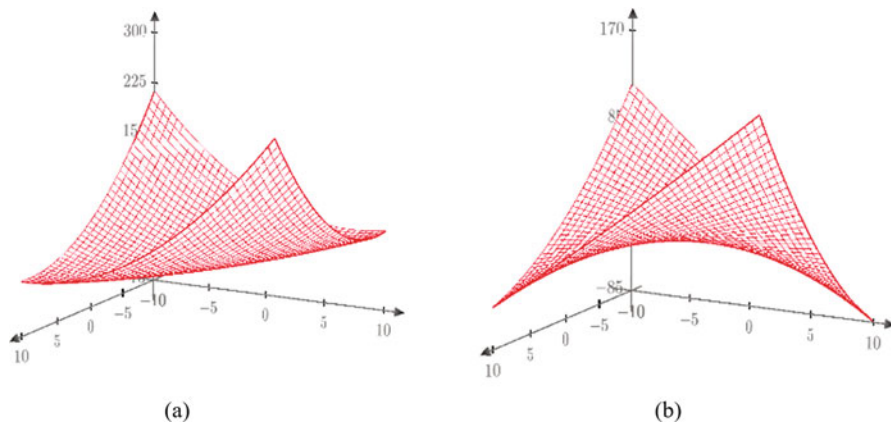
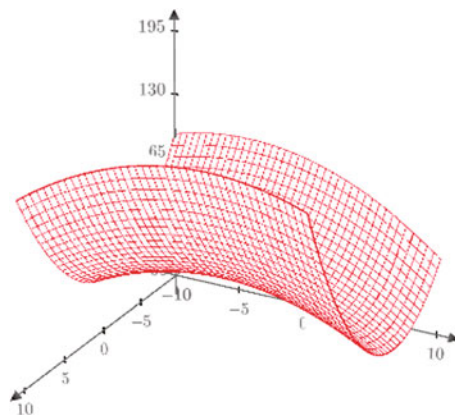


Fig. 4.10 Graphical interpretation of the dependence of: (a) ultimate deformations in compression and (b) tension for the outer layer of the functionally gradient cross-section of centrifuged concrete vs. the distance from the center of rotation to the center of the grain and the angular velocity

Fig. 4.11 Graphical interpretation of the dependence of the elastic modulus for the outer layer of the functionally gradient cross-section of centrifuged concrete vs. the distance from the center of rotation to the center of the grain and the angular velocity



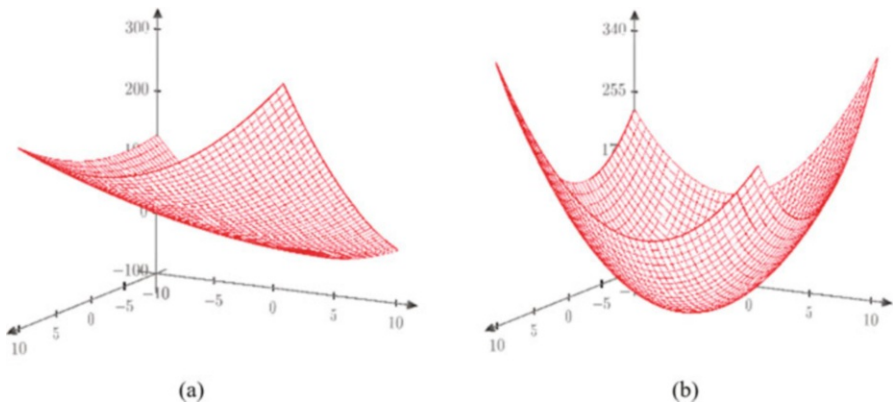


Fig. 4.12 Graphical interpretation of the dependence of: (a) compressive strength and (b) tensile strength for the inner layer of the functionally gradient cross-section of vibro-centrifuged concrete vs. the distance from the center of rotation to the center of the grain and the angular velocity

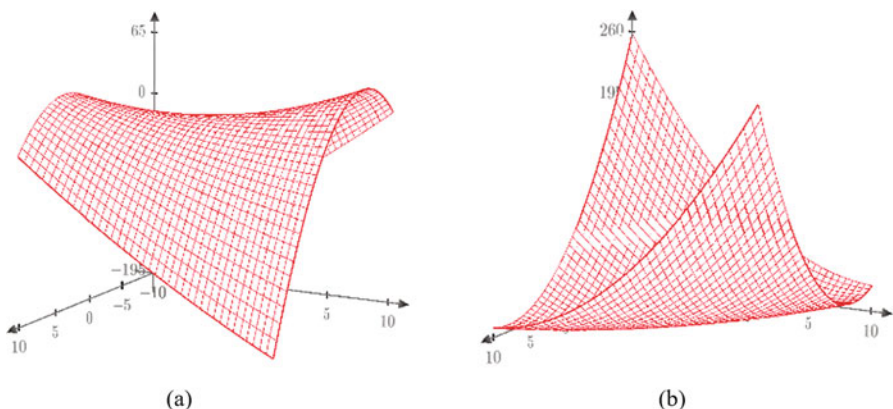


Fig. 4.13 Graphical interpretation of the dependence of ultimate deformations: (a) in compression and (b) tension for the inner layer of the functionally gradient cross-section of vibro-centrifuged concrete vs. the distance from the center of rotation to the center of the grain and the angular velocity

Fig. 4.14 Graphical interpretation of the dependence of the elastic modulus for the inner layer of the functionally gradient cross-section of vibro-centrifuged concrete vs. the distance from the center of rotation to the center of the grain and the angular velocity

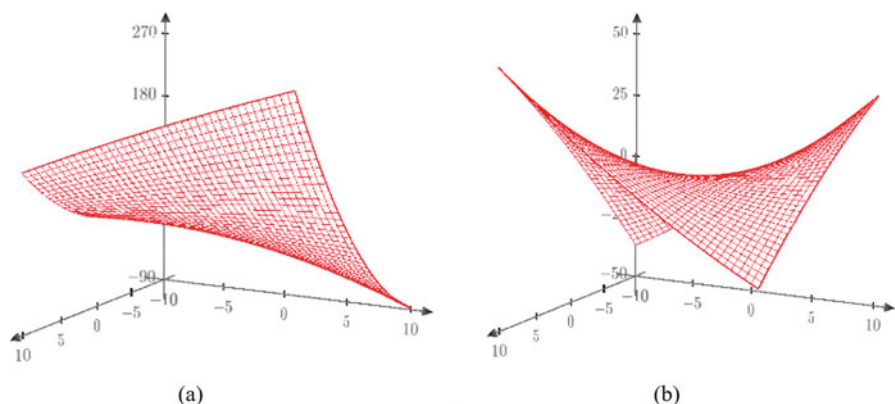
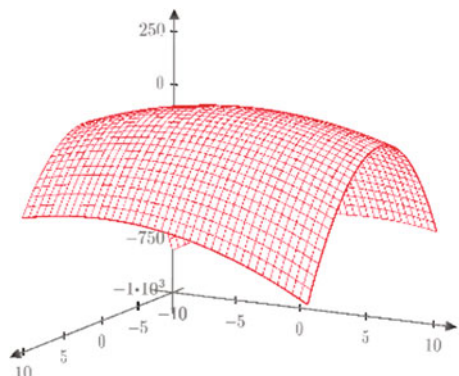


Fig. 4.15 Graphical interpretation of the dependence of: (a) compressive strength and (b) tensile strength for the middle layer of the functionally gradient cross-section of vibro-centrifuged concrete vs. the distance from the center of rotation to the center of the grain and the angular velocity

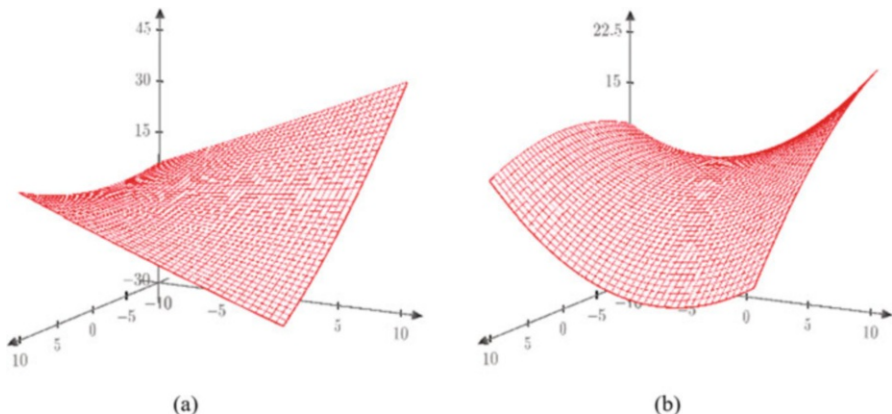
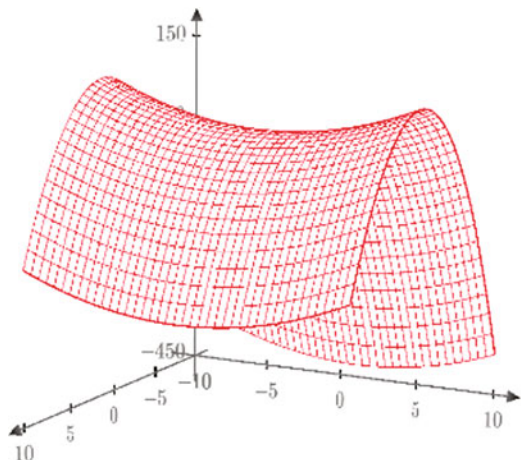


Fig. 4.16 Graphical interpretation of the dependence of ultimate deformations: (a) in compression and (b) tension for the middle layer of the functionally gradient cross-section of vibro-centrifuged concrete vs. the distance from the center of rotation to the center of the grain and the angular velocity

Fig. 4.17 Graphical interpretation of the dependence of the elastic modulus for the middle layer of the functionally gradient cross-section of vibro-centrifuged concrete vs. the distance from the center of rotation to the center of the grain and the angular velocity



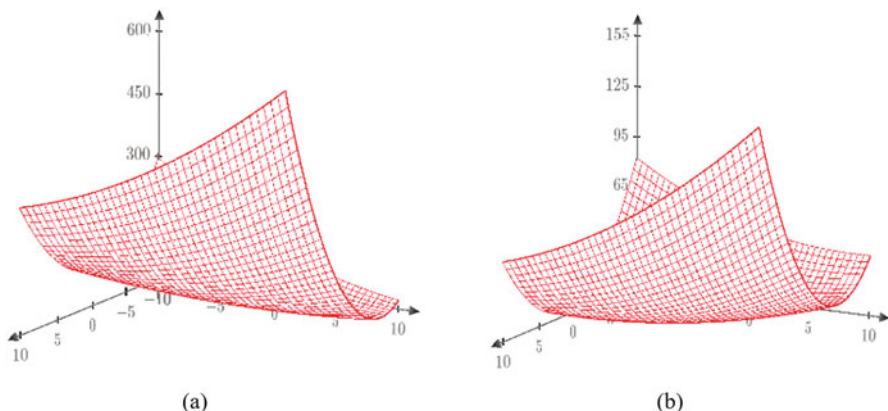


Fig. 4.18 Graphical interpretation of the dependence of: (a) compressive strength and (b) tensile strength for the outer layer of the functionally gradient cross-section of vibro-centrifuged concrete vs. the distance from the center of rotation to the center of the grain and the angular velocity

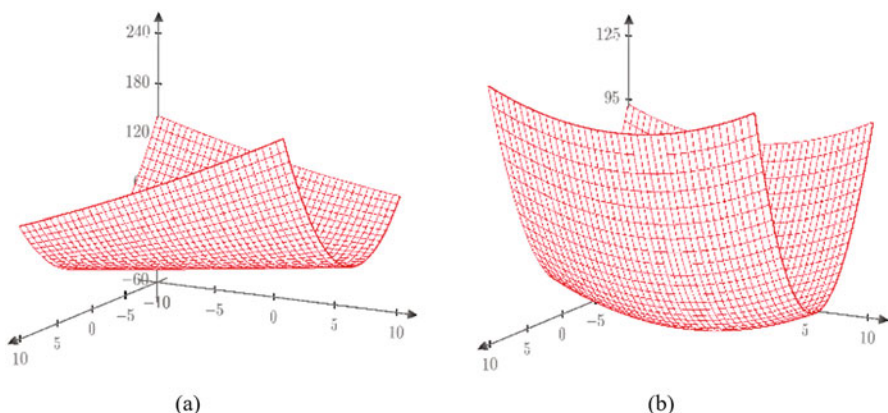
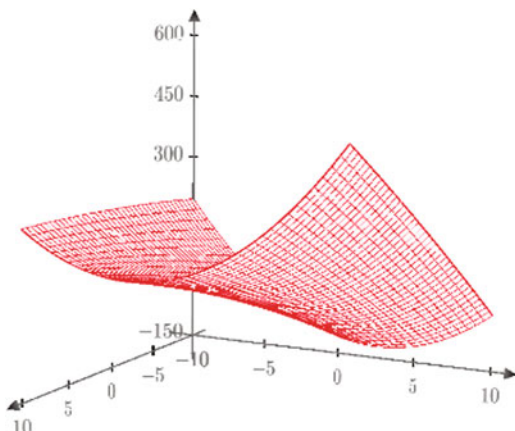


Fig. 4.19 Graphical interpretation of the dependence of ultimate deformations: (a) in compression and (b) tension for the outer layer of the functionally gradient cross-section of vibro-centrifuged concrete vs. the distance from the center of rotation to the center of the grain and the angular velocity

Fig. 4.20 Graphical interpretation of the dependence of the elastic modulus for the outer layer of the functionally gradient cross-section of vibro-centrifuged concrete vs. the distance from the center of rotation to the center of the grain and the angular velocity



4.3 Conclusions

1. The values of standard and design resistances for limiting states of I and II groups, ultimate deformations, and initial moduli of elasticity in compression and tension of vibrated, centrifuged, and vibro-centrifuged concretes are recommended based on the results of statistical processing of experimental data with a reliability of 0.95.
2. The differences in the aggregate design characteristics of vibrated, centrifuged, and vibro-centrifuged concretes are revealed, depending on the manufacturing technology and age of concrete.
3. The proposals are given for the calculated determination of the aggregate characteristics of centrifuged and vibro-centrifuged concretes at the age of 28 days based on the introduction of correction factors to the corresponding characteristics of vibrated concrete.
4. To determine the aggregate characteristics of vibrated, centrifuged, and vibro-centrifuged concretes, depending on age, dependences are proposed, the values of the coefficients of which are determined by statistical methods.
5. Experimental and analytical diagrams of deformation in compression and tension of vibrated, centrifuged, and vibro-centrifuged concretes at any age are obtained, their similarity is proved, and recommendations for their construction are given.
6. It is experimentally shown and theoretically substantiated that different concrete layers during centrifugation and vibro-centrifugation are affected by inertial forces differing in magnitude, leading to variation in cross-sections and differentiation of strength and deformation characteristics of its layers.
7. It was revealed that the main factors of influence are centrifugal and centripetal forces, depending on the distance from the center of rotation and the angular velocity of rotation.

Table 4.12 Calculation equations for determining the local characteristics of layers of the functionally gradient cross-sections of centrifuged and vibrocentrifuged concretes

Characteristics of concrete	Concrete type		Equation type
	Centrifuged	Vibro-centrifuged	
		Equation type	
Inner layer			
Axial compressive strength, MPa	$R_b = 23.25 + 0.877 l - 1.446 \omega - 1.618 l\omega - 1.047 l^2 + 0.345 \omega^2$	$R_b = 32.31 + 8.774 l - 0.450 \omega + 0.67 l\omega + 0.308 l^2 + 0.809 \omega^2$	
Axial tensile strength, MPa	$R_{bt} = 3.852 + 0.767 l - 0.204 \omega - 0.892 l\omega - 0.311 l^2 - 0.189 \omega^2$	$R_{bt} = 3.882 + 0.459 l - 0.043 \omega - 0.49 l\omega + 1.282 l^2 + 1.511 \omega^2$	
Limiting deformations at axial compression, mm/m	$\varepsilon_{bR} = 3.247 - 1.245 l + 0.027 \omega - 0.417 l\omega + 0.006 l^2 - 0.032 \omega^2$	$\varepsilon_{bR} = 3.214 - 1.412 l + 0.037 \omega - 0.82 l\omega - 1.07 l^2 + 0.086 \omega^2$	
Limiting deformations at axial tension, mm/m	$\varepsilon_{btR} = 2.679 - 0.788 l - 0.215 \omega - 0.509 l\omega - 0.34 l^2 - 0.056 \omega^2$	$\varepsilon_{btR} = 1.95 - 0.825 l + 0.007 \omega + 1.16 l\omega + 0.778 l^2 + 0.534 \omega^2$	
Elastic modulus, MPa	$E_b = E_{bt} = 21.32 + 4.86 l - 0.639 \omega + 0.299 l\omega + 1.168 l^2 - 0.38 \omega^2$	$E_b = E_{bt} = 31.11 + 7.626 l - 0.117 \omega - 1.12 l\omega - 5.134 l^2 - 1.223 \omega^2$	
Middle layer			
Axial compressive strength, MPa	$R_b = 27.54 + 1.147 l - 1.226 \omega - 1.394 l\omega - 0.899 l^2 + 0.675 \omega^2$	$R_b = 38.467 + 10.506 l - 0.231 \omega + 0.7 l\omega + 0.558 l^2 - 0.05 \omega^2$	
Axial tensile strength, MPa	$R_{bt} = 4.356 + 1.024 l - 0.051 \omega - 0.567 l\omega - 0.181 l^2 - 0.137 \omega^2$	$R_{bt} = 5.089 + 0.768 l - 0.02 \omega - 0.35 l\omega - 0.04 l^2 + 0.046 \omega^2$	
Limiting deformations at axial compression, mm/m	$\varepsilon_{bR} = 4.341 - 1.031 l + 7.29 \times 10^{-3} \omega - 0.203 l\omega + 0.038 l^2 + 0.01 \omega^2$	$\varepsilon_{bR} = 3.983 - 1.202 l + 0.075 \omega - 0.14 l\omega + 0.041 l^2 + 0.005 \omega^2$	
Limiting deformations at axial tension, mm/m	$\varepsilon_{btR} = 3.021 - 0.532 l - 0.015 \omega - 0.353 l\omega - 0.01 l^2 + 0.001 \omega^2$	$\varepsilon_{btR} = 2.48 - 0.637 l + 0.017 \omega - 0.052 l\omega - 0.029 l^2 + 0.083 \omega^2$	
Elastic modulus, MPa	$E_b = E_{bt} = 26.507 + 5.67 l - 0.442 \omega + 0.572 l\omega + 1.314 l^2 - 0.05 \omega^2$	$E_b = E_{bt} = 38.129 + 9.321 l - 0.51 \omega + 0.089 l\omega - 3.713 l^2 + 0.638 \omega^2$	

(continued)

Table 4.12 (continued)

Characteristics of concrete	Concrete type		Equation type
	Centrifuged	Vibro-centrifuged	
Outer layer			
Axial compressive strength, MPa	$R_b = 35.89 + 3.166 l + 1.287 \omega + 0.812 l\omega - 0.015 l^2 + 1.781 \omega^2$	$R_b = 48.45 + 13.77 l + 0.65 \omega + 1.44 l\omega + 2.014 l^2 + 0.45 \omega^2$	
Axial tensile strength, MPa	$R_{bt} = 6.184 + 1.867 l - 0.83 \omega - 0.336 l\omega + 0.452 l^2 - 0.06 \omega^2$	$R_{bt} = 8.132 + 1.56 l + 1.09 \omega + 0.321 l\omega + 0.563 l^2 + 0.12 \omega^2$	
Limiting deformations at axial compression, mm/m	$\varepsilon_{bR} = 5.31 - 0.543 l + 1.456 \omega + 1.002 l\omega + 0.569 l^2 + 0.59 \omega^2$	$\varepsilon_{bR} = 5.451 + 0.85 l + 1.345 \omega + 0.47 l\omega + 1.047 l^2 + 0.06 \omega^2$	
Limiting deformations at axial tension, mm/m	$\varepsilon_{btR} = 2.886 + 1.592 l - 0.273 \omega + 0.987 l\omega + 0.256 l^2 + 0.043 \omega^2$	$\varepsilon_{btR} = 5.98 + 1.12 l - 0.003 \omega - 0.008 l\omega + 0.844 l^2 + 0.141 \omega^2$	
Elastic modulus, MPa	$E_b = E_{bt} = 29.111 + 6.49 l + 1.65 \omega - 0.399 l\omega + 1.678 l^2 + 0.68 \omega^2$	$E_b = E_{bt} = 43.18 + 14.23 l + 1.231 \omega + 1.157 l\omega - 0.09 l^2 + 1.98 \omega^2$	

8. To assess the local characteristics of concrete during centrifugation and vibro-centrifugation, universal calculation dependencies are proposed, in which the characteristics of concrete, namely, strength, ultimate deformations, and moduli of elasticity in compression and tension (or their increments in absolute or relative terms), are used as functions, and the distances from the center and angular speeds of rotation are used as arguments.
9. The developed analytical dependencies for determining the differentiated strength and deformation characteristics of centrifuged and vibro-centrifuged concretes make it possible to enter into calculation the characteristics of concrete differing in cross-section and more fully use the reserves of the bearing capacity of building constructions.

Chapter 5

Calculation of the Load-Bearing Capacity of V-, CF-, and VCF-Reinforced Concrete Columns, Taking into Account the Standard, Aggregate, and Local Characteristics of Concrete



Abstract In this chapter, an improvement of the standard approach to the calculation of the strength of centrifuged and vibro-centrifuged reinforced concrete columns is proposed. It uses the calculation of aggregate (averaged over the cross-section) or local (differing in the layers of the section) characteristics of concrete. Based on the diagram approach, iterative, approximate, and simplified methods of calculating the bearing capacity of reinforced concrete vibrated, centrifuged, and vibro-centrifuged columns are developed. Calculation of the strength of short centrally compressed vibrated, centrifuged, and vibro-centrifuged columns according to the improved standard approach gave the best results using the local characteristics of concrete. For centrifuged and vibro-centrifuged columns, the diagram approach in any setting (iterative, approximate, and simplified methods) gives better results, when using the local characteristics of concrete than when using the aggregate ones.

Key words Standard approach · Aggregate · Local characteristics · Short centrally compressed columns

5.1 Standards and Regulatory for Calculating the Load-Bearing Capacity of Short CF- and VCF-Columns, Taking into Account the Standard, Aggregate, and Local Characteristics of Concretes

According to the standard approach [182, 193, 199, 200, 202, 279, 282, 285, 287], the bearing capacity of centrally compressed (or compressed with a small eccentricity) elements is achieved with a rectangular stress diagram in compressed concrete with an ordinate equal to R_b . By using the standard characteristics of concrete, it is determined as follows:

- (i) For *concrete elements*—the product of the ultimate strength (calculation resistance) of concrete in compression on the area of compressed concrete:

$$N = R_b A_b \quad (5.1)$$

- (ii) For *reinforced concrete elements*—the sum of the products of the ultimate strength (design resistance) of concrete in compression on the area of compressed concrete and the calculation resistance of reinforcement in compression on the cross-sectional area of reinforcement:

$$N = R_b A_b + R_{sc} A_s \quad (5.2)$$

However, in the centrifuged or vibro-centrifuged compressed concrete and reinforced concrete elements, in comparison with vibrated ones, the ultimate strength of concrete increases and in general form it is already $R_{b, red} = K_{Rb} R_b$, which leads to a modification of formulae (5.1) and (5.2).

Thus, when using the aggregate characteristics, formulae (5.1) and (5.2) for concrete and reinforced concrete elements take the form:

$$N = R_{b,red} A_b, \quad (5.3)$$

$$N = R_{b,red} A_b + R_{sc} A_s, \quad (5.4)$$

where the strength of concrete for centrifuged or vibro-centrifuged compressed elements at any age is.

$$R_{b,red} = K_{Rb,28} K_{Rb,Rb} R_b.$$

When using the aggregate characteristics of concrete in the standard approach, only the compressive strength (design resistance) of concrete changes, while the area of compressed concrete remains unchanged.

If, in the standard approach, differential characteristics of concrete are used, then formulae (5.1) and (5.2) for concrete and reinforced concrete elements take the form:

$$N = \sum R_{b,red,i} A_{bi}, \quad (5.5)$$

$$N = \sum R_{b,red,i} A_{bi} + R_{sc} A_s, \quad (5.6)$$

that is, they will now include not only differing values of ultimate strength (calculation resistances) of concrete in compression for individual layers, $R_{b, red, i}$, but also the areas of these layers of compressed concrete A_{bi} .

There is no doubt that formulae (5.5) and (5.6) should most accurately describe the bearing capacity of compressed concrete and reinforced concrete elements, but this must be confirmed by experimental and calculated studies, which were carried out.

5.2 Diagram Approach to the Calculation of the Load-Bearing Capacity of Short V-, CF-, and VCF-Columns, Taking into Account the Standard, Aggregate, and Local Characteristics of Concretes

In the diagram approach, in contrast to the standard one, individual strength and deformation characteristics of concrete are not used, but its complete stress-strain diagrams with descending branches. Calculation of reinforced concrete compressed members based on the deformation diagrams of concrete and reinforcement accurately describes the actual work of the elements.

The standard approach determines the bearing capacity, deformability, and crack resistance discretely on the basis of completely different prerequisites at different stages of the element operation. At the same time, the diagram approach allows determining the bearing capacity, deformability, and crack resistance integrally on the basis of iterative calculation. By this, the iterative calculation is carried out from the beginning of work to the exhaustion of the bearing capacity on the basis of the same prerequisites.

Strictly speaking, the division in this point of approaches into standard and diagram is rather arbitrary, since the diagram approach is also recommended in some cases by the standards. However, according to the established practice, they are nevertheless separated for the convenience of orientation.

5.2.1 Iterative Calculation of the Strength of Short Centrally Compressed Reinforced Concrete Columns

The calculation equations for the diagram approach are as follows:

- (i) For concrete elements:

$$N = N_b = \int_0^h \sigma(\varepsilon) A_b dx, \quad (5.7)$$

- (ii) For reinforced concrete elements:

$$N = N_b + N_s = \int_0^h \sigma(\varepsilon) A_b dx + \sigma_{sc} A_s. \quad (5.8)$$

In iterative calculation according to the general characteristics (standard or integral) of concrete for the entire cross-section, the deformation diagrams “ $\sigma_b - \varepsilon_b$ ”

with two groups of characteristics: R_b ; ε_{bR} ; E_b and K_{Rb} , $28R_b$; K_{ebR} , $28\varepsilon_{bR}K_{Eb}$, $28E_b$ are used in compression, respectively.

Direct integration of Eqs. (5.7)–(5.8) is replaced by the final summation over the sections:

(i) For concrete elements:

$$N = N_b = \sum \int_0^h \sigma(\varepsilon) A_b dx; \quad (5.9)$$

(ii) For reinforced concrete elements:

$$N = N_b + N_s = \sum \int_0^h \sigma(\varepsilon) A_b dx + \sigma_{sc} A_s. \quad (5.10)$$

Note again that Eqs. (5.9) and (5.10) are used when calculating the strength according to the common standard for the entire cross-section or integral characteristics of concrete, that is, vibrated and, with some simplification of the calculation, centrifuged and vibro-centrifuged columns.

The iterative strength calculation for concrete local characteristics, differing in cross-section of centrifuged and vibro-centrifuged columns, will be based on other equations:

(i) For concrete elements:

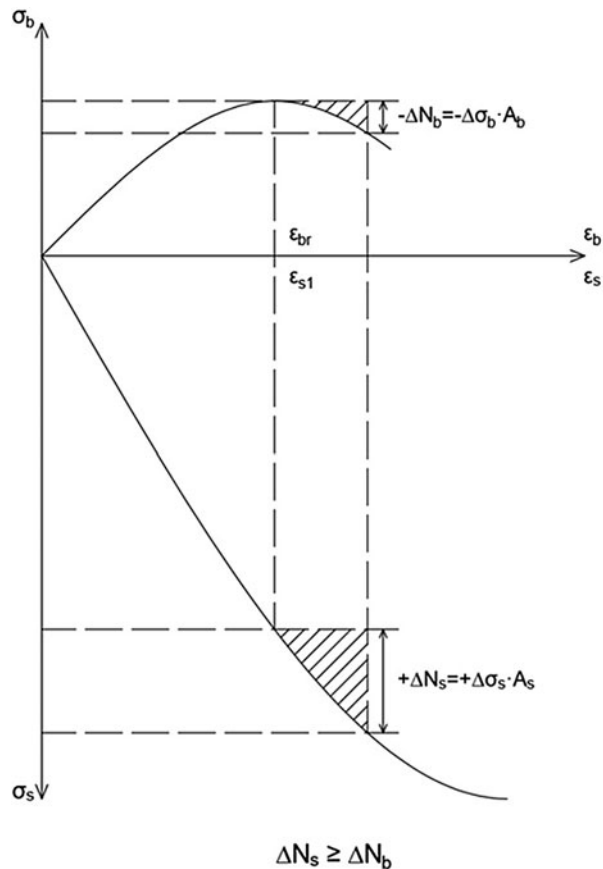
$$N = N_b = \int_0^h \int_{\omega_1}^{\omega_2} \int_d^D \sigma(\varepsilon) A_{bi} dx d\omega dl; \quad (5.11)$$

(ii) For reinforced concrete elements:

$$N = N_b + N_s = \int_0^h \int_{\omega_1}^{\omega_2} \int_d^D \sigma(\varepsilon) A_{bi} dx d\omega dl + \sigma_{sc} A_s. \quad (5.12)$$

In the iterative approach, the calculation at each iteration is carried out according to concrete deformations ε_b , specified with a certain step. The equations of projections are written for elements of concrete (5.9) and reinforced concrete (5.10) for calculation according to the standard or aggregate characteristics of concrete. For

Fig. 5.1 Compensation of force reduction in concrete increase in force in reinforcement at the diagram approach



calculations according to the local characteristics of concrete, Eq. (5.11) for concrete elements and Eq. (5.12) for reinforced concrete elements are used.

A feature of the iterative calculation is that, in contrast to the standard one, it allows one to assess the bearing capacity of compressed elements not only in the critical but also in the supercritical stage. In this stage, it accounts of in calculation the often situation, in which the reduction of stresses in concrete takes place already on the descending branch of the diagram. It is compensated and even overlapped by an increase in stresses in the reinforcement (Fig. 5.1):

$$\Delta N_s \geq \Delta N_b \quad (5.13)$$

Note that this, of course, must be a high-strength reinforcement with a diagram without a yield area, but in the case of a conventional reinforcement with a diagram with a yield area, the bearing capacity of the element will be exhausted when the maximum concrete strength is reached.

The initial data for the iterative calculation are:

- (i) Analytical diagrams of deformation “ $\sigma - \varepsilon$ ” of concrete and high-strength reinforcement.
- (ii) The shape and dimensions of the cross-section of the element.
- (iii) Areas of concrete and reinforcement.

As the main design prerequisite, the condition of compatibility of deformations of compressed concrete and reinforcement at all stages of work, including the super-critical one, is taken:

$$\varepsilon_b = \varepsilon_s = \varepsilon \quad (5.14)$$

The longitudinal force perceived by the cross-section at all stages of work is determined by the expression:

$$N = N_b + N_s = \sigma_b(\varepsilon_b)A_b + \sigma_s(\varepsilon_s)A_s \quad (5.15)$$

or, taking into account (5.14):

$$N = N_b + N_s = \sigma_b(\varepsilon)A_b + \sigma_s(\varepsilon)A_s \quad (5.16)$$

The bearing capacity, determined by the maximum longitudinal force perceived by the cross-section, will be characterized by the maximum of the function “longitudinal force N – longitudinal deformation ε ,” that is:

$$\frac{dN}{d\varepsilon} = 0. \quad (5.17)$$

It is possible to determine from Eq. (5.17) the longitudinal deformations of concrete and reinforcement $\varepsilon = \varepsilon_b = \varepsilon_s$, according to which, after substituting ε in (5.16), the maximum longitudinal force N , that is, the bearing capacity, is determined.

Analytical deformation diagrams “ $\sigma - \varepsilon$ ” of concrete and reinforcement were constructed on the base of EKB-FIP formula (4.3) with substitution therein our recommendations to determine the strength and deformability of concrete characteristics and strength deformation characteristics of high-strength reinforcement, identified in our experiments (see Sect. 5.3).

The calculation was carried out as follows.

A certain value of concrete deformation $\varepsilon_b = \varepsilon$ was set in the area close to the maximum of the diagram “ $\sigma_b - \varepsilon_b$,” respectively; the deformations of the reinforcement were also taken to be equal to $\varepsilon_s = \varepsilon$.

The stresses in concrete and reinforcement were calculated according to their analytical diagrams “ $\sigma - \varepsilon$ ” according to formula (4.3).

The forces N_b and N_s , perceived by concrete and reinforcement, and the total bearing capacity of the cross-section were determined:

$$N = N_b + N_s.$$

Next, a new value of concrete deformation $\varepsilon_b = \varepsilon + \Delta\varepsilon$ was set and the described calculation was repeated again. Several iterations were carried out in this way until the value of N reached its maximum and began to decrease.

The maximum value of N corresponded to the bearing capacity of the reinforced concrete column.

But further additional explanations should be made related to the value of the longitudinal deformations of concrete ε_{cr} , at which the maximum value of N was reached, that is, the bearing capacity was exhausted.

In *vibrated reinforced concrete columns*, in which all layers of concrete had the same strength and deformability characteristics, the longitudinal deformations of concrete ε_{cr} , when the bearing capacity of the columns is exhausted in the general case, could be equal to or greater than the ultimate deformations of concrete ε_{bR} , corresponding to the maximum concrete strength R_b . Therefore, the stresses in the concrete of the entire cross-section when the non-existent capacity of the columns is exhausted could be less than or equal to R_b .

In the first case (<), this occurred with weak reinforcement of the columns, the increase in forces in the reinforcement of which could not be compensated for the decrease in the force in concrete after reaching the maximum of its deformation diagram $R_b; \varepsilon_{bR}$.

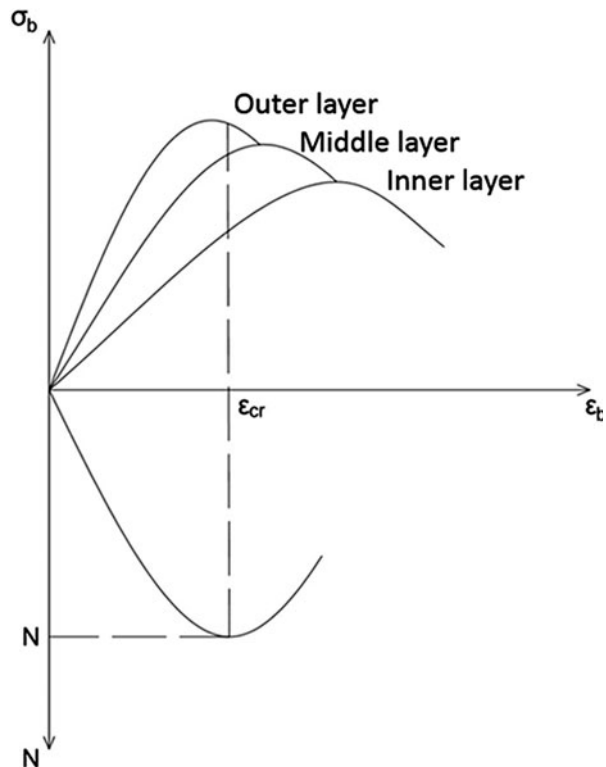
In the second case (=), this occurred with a strong or over-reinforcement of the columns, the increase in forces in the reinforcement of which not only compensated but also overlapped the decrease in the force in concrete after reaching the maximum of its deformation diagram $R_b; \varepsilon_{bR}$. This, in general, increased the bearing capacity of the columns and depleted it when the concrete was deformed already on the descending branch of its diagram (Fig. 5.1).

In centrifuged and vibro-centrifuged reinforced concrete columns, in which all layers of concrete had unequal characteristics of strength and deformability, the longitudinal deformations of concrete ε_{cr} , when the bearing capacity of the columns was exhausted in the general case for all layers, were also the same. However, they could be less, equal, or more than ultimate deformations of concrete ε_{cr} , of a concrete layer, corresponding to the maximum strength of their concrete R_{bi} .

This time, it is due not only to the degree of reinforcement of the columns but also to the difference in the strength and deformation characteristics of concrete layers, each of which, when the bearing capacity of the column is exhausted, can deform both on the ascending and descending branches of its deformation diagram.

So, a situation is quite possible in which the exhaustion of the bearing capacity of the column with the same deformations ε_{cr} for all layers of its concrete occurs when the inner layer is still in the ascending direction, the middle layer is at the maximum,

Fig. 5.2 Deformations and stresses in conditional concrete layers, when the bearing capacity of column with functionally gradient cross-section is exhausted



and the outer layer is already at the descending branch of their deformation diagrams “ $\sigma_b - \varepsilon_b$ ” (see Fig. 5.2).

In this regard, the calculation equations with a single term for concrete of vibrated columns are transformed into equations with three (according to the number of conditional layers) terms for concrete of centrifuged and vibro-centrifuged columns.

Accordingly, the picture of the distribution of forces in the concrete layers and in the reinforcement when the bearing capacity of the columns is exhausted is greatly complicated.

Now it is possible here that even with a weak reinforcement of the columns, a decrease in the force in the concrete of the inner layer after reaching the maximum of its deformation diagram can be compensated not by an increase in the force in the reinforcement but by an increase in the force in the outer layer or even immediately in the outer and middle layers, especially for vibro-centrifuged columns.

Thus, functionally gradient cross-sections of building constructions have a significantly greater ability to redistribute stresses and efforts than conventional ones.

5.2.2 Approximate Calculation of the Strength of Short Centrally Compressed Reinforced Concrete Columns

Analysis of the results of a physical and numerical experiment, which will be described in more detail in Points 5.3 and 5.4, allows one to reveal that the exhaustion of the bearing capacity of compressed reinforced concrete columns occurs at deformations ε_{cr} , which are in the range of $0.85\text{--}1.15\varepsilon_{bR}$.

In this regard, to reduce the number of computational iterations and the possibility of performing them manually, the following *approximate method* can be proposed.

To calculate the bearing capacity of compressed reinforced concrete columns, vibrated, centrifuged, and vibro-centrifuged, it is proposed to carry out the calculation in just three iterations. In this case, the deformations ε_{cr} at each iteration can be taken equal to 0.9, 1, and 1.1 ε_{bR} , taking the value of ε_{bR} in centrifuged and vibro-centrifuged columns equal to ε_{bR} of the middle layer.

Moreover, taking into account the high strength of the A600 reinforcement operating in the column, when its bearing capacity is exhausted practically in the elastic stage, it is possible to take its operation diagram in the form of Hooke's law:

$$\sigma_s = E_s \varepsilon_s \quad (5.18)$$

With this in mind, the calculation equation for determining the bearing capacity will be written in the form:

$$N = N_b + N_s = \sigma_b(\varepsilon_{cr})A_b + \varepsilon_{cr}E_s A_s. \quad (5.19)$$

Based on the results of the approximate calculation, the bearing capacity of the column is determined by the choice of the maximum or by simple interpolation between the obtained three values.

5.2.3 Simplified Calculation of the Strength of Short Centrally Compressed Reinforced Concrete Columns

For the following simplification of calculation, two simplified methods are proposed [152].

In the first method, the premise is again used, that is, taking into account the high strength of the A600 reinforcement operating in the column, when its bearing capacity is exhausted almost in the elastic stage, it is possible to take its work diagram in the form of Hooke's law (5.18).

Equation (5.16) after substitution of (4.3) and (5.18) into it and its subsequent differentiation takes the following form:

$$ae^2 + be + c = 0 \quad (5.20)$$

where parameters a , b , c are defined as [152]:

$$\begin{aligned} a &= E_b^2(K - 2)[\mu\alpha K(K - 2) - 1]; \\ b &= -2E_b K R_b [\mu\alpha K(K - 2) - 1]; \\ c &= K^3 R_b^2 (1 + \mu\alpha). \end{aligned} \quad (5.21)$$

where $\mu = A_s/A_b$ is the relative reinforcement of the element and $\alpha = E_s/E_b$ is the ratio of the moduli of elasticity of reinforcement and concrete.

Equation (5.20) gives the value of the ultimate deformations at which the maximum longitudinal force is achieved.

Thus, the proposed approach is implemented in the first simplified way.

The *second method* of the simplified calculation is based on some assumptions simplifying the calculation.

So, the exhaustion of the bearing capacity of short reinforced concrete vibrated columns occurs, when the longitudinal deformations ε_{cr} are equal to the ultimate deformations ε_{bR} , which corresponds to the stresses in the concrete of the entire section R_b and the stresses in the reinforcement $\sigma_s = E_s \varepsilon_{bR}$.

This allows one to express their calculated bearing capacity in the form:

$$N = N_b + N_s = R_b A_b + E_s \varepsilon_{bR} A_s \quad (5.22)$$

Exhaustion of the bearing capacity of short reinforced concrete centrifuged and vibro-centrifuged columns will be assumed to occur, when longitudinal deformations ε_{cr} , equal to the ultimate deformations ε_{bR} of the middle layer, are reached.

Then (i) for concrete of the middle layer, a deformation $\varepsilon_{b, mid} = \varepsilon_{bR, mid}$ and stress $\sigma_{b, mid} = R_{bmid}$; (ii) for concrete of the inner layer a deformation $\varepsilon_{b, in} = \varepsilon_{bR, in}$, $\varepsilon_{b, in} < \varepsilon_{bR, in}$ and stress $\sigma_{b, in} < R_{bin}$, and (iii) for concrete of the outer layer $\varepsilon_{b, out} = \varepsilon_{bR, out} > \varepsilon_{bR, out}$ and stress $\sigma_{b, out} < R_{bout}$ at stress in the reinforcement $\sigma_s = E_s \varepsilon_{bR, mid}$.

In other words, in a simplified formulation, it is assumed that the depletion of the bearing capacity of the columns occurs, when the middle layer is deformed at the maximum of its diagram “ $\sigma_{b, mid} - \varepsilon_{b, mid}$,” the inner layer is deformed on the ascending branch of its diagram “ $\sigma_{b, in} - \varepsilon_{b, in}$,” and the deformation of the outer layer is on the descending branch of its diagram “ $\sigma_{b, out} - \varepsilon_{b, out}$.”

Then the calculation equation for determining the strength is:

$$\begin{aligned} N &= N_{b,in} + N_{b,mid} + N_{b,out} + N_s \\ &= \sigma_{b,in}(\varepsilon_{bR,mid}) A_{b,in} + R_{b,mid} A_{b,mid} + \sigma_{b,out}(\varepsilon_{bR,mid}) A_{b,out} + E_s \varepsilon_{bR,mid} A_s \end{aligned} \quad (5.23)$$

Thus, the proposed approach is implemented in the second simplified way.

In general, the conclusion is that, within the framework of the diagram approach, iterative approximations and simplified calculations of the bearing capacity of short reinforced concrete vibrated, centrifuged, and vibro-centrifuged columns are proposed.

5.3 Schedule and Methodology of the Experiment

5.3.1 *Features of Manufacturing and Testing of Prototypes*

The research schedule included the manufacture and testing of nine experimental concrete and reinforced concrete annular cross-section columns, of which:

- (i) Three columns were made using vibration technology.
- (ii) Three columns were made using centrifugation technology.
- (iii) Three columns were made using vibro-centrifugation technology.

The dimensions of the experimental columns were taken as follows: a height of 1.2 m; an outer diameter of the cross-section is 0.45 m; an internal diameter of the cross-section is 0.30 m.

The concrete of the test columns was an ordinary heavy class B30, and rod reinforcement included six bars with $\varnothing 10$ A400 and six bars with $\varnothing 10$ A600.

Thus, in each technology, 1 column without reinforcement, 1 column with $6\varnothing 10$ A400 reinforcement, and 1 column with $6\varnothing 10$ A600 reinforcement were manufactured and tested.

The compositions of concrete, equipment, modes, and technologies for the manufacture and hardening of the test columns were taken in accordance with the recommendations developed in Chaps. 2 and 3.

Experimental columns were tested for short-term central compression at the age of 30–35 days from the date of manufacture. Experimental columns were tested on a press IPG-500.

The load on the columns was applied step by step in 10–12 stages, with the same increments of longitudinal deformations, which allowed one to follow the work of the columns with an increase in the load to the maximum, and then, with its decrease, on the descending branch until destruction.

After each stage of loading, the element was held for 10 min. At each stage, the readings of the devices were taken twice: immediately after increasing the load and after holding before the next stages of loading.

Deformations of concrete and reinforcement were measured with strain gauges with a base of 0.05 m and 0.02 m, respectively. The experiments used strain gauge and oscilloscope equipment.

To determine the actual strength and deformation characteristics of concrete, simultaneously with the testing of each experimental column, the standard samples, namely, cubes and prisms, were tested.

5.3.2 Analysis of the Results of Experimental Studies

Based on the results of the experimental studies, the bearing capacity and deformability of the prototypes were analyzed, as well as their influence on the manufacturing technology and the availability and class of reinforcement.

The results are shown in Table 5.1 and Figs. 5.3, 5.4, 5.5 and 5.6.

In our analysis, the indicators of vibrated columns were taken as the starting points of reference, and all deviations in the text are given precisely by comparing them.

Table 5.1 Strength of test columns according to experimental results

Column code (in Russian)	Manufacturing technology	Reinforcement	Bearing capacity, kN	Deformability, m
B0	Vibration	—	1810	2.2×10^{-3}
B4	Vibration	6Ø10 A400	1946	1.7×10^{-3}
B6	Vibration	6Ø10 A600	2048	1.6×10^{-3}
Ц0	Centrifugation	—	2155	2.0×10^{-3}
Ц4	Centrifugation	6Ø10 A400	2211	1.5×10^{-3}
Ц6	Centrifugation	6Ø10 A600	2301	1.4×10^{-3}
ВЦ0	Vibro-centrifugation	—	2342	1.7×10^{-3}
ВЦ4	Vibro-centrifugation	6Ø10 A400	2484	1.5×10^{-3}
ВЦ6	Vibro-centrifugation	6Ø10 A600	2557	1.2×10^{-3}

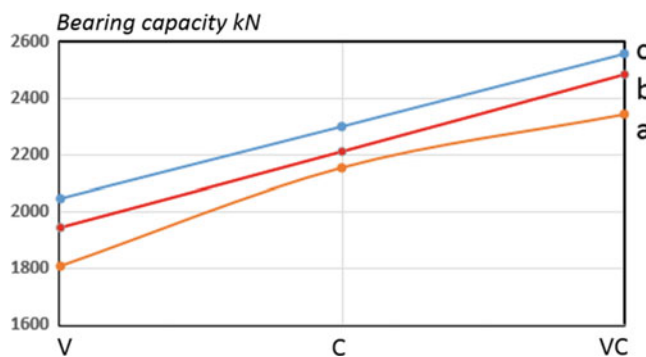


Fig. 5.3 Dependence of the bearing capacity of the columns on the manufacturing technology: a unreinforced, b with A400 reinforcement, and c with A600 reinforcement

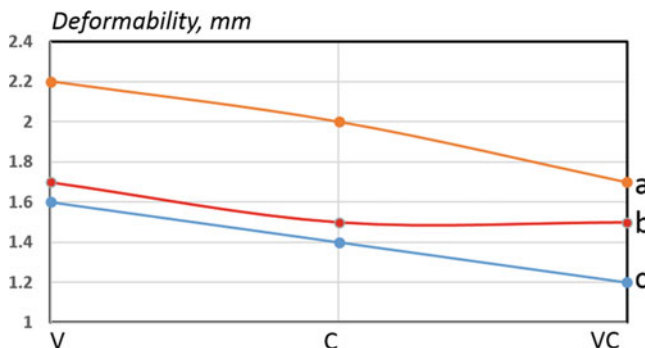


Fig. 5.4 Dependence of column deformations on manufacturing technology: a unreinforced, b with A400 reinforcement, and c with A600 reinforcement

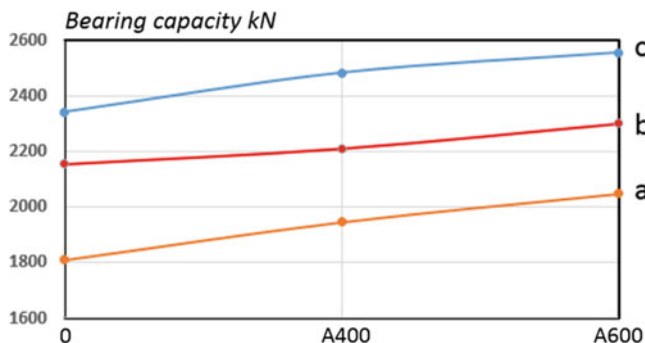


Fig. 5.5 Dependence of the bearing capacity of the columns on the reinforcement: (a) vibrated, (b) centrifuged, and (c) vibro-centrifuged

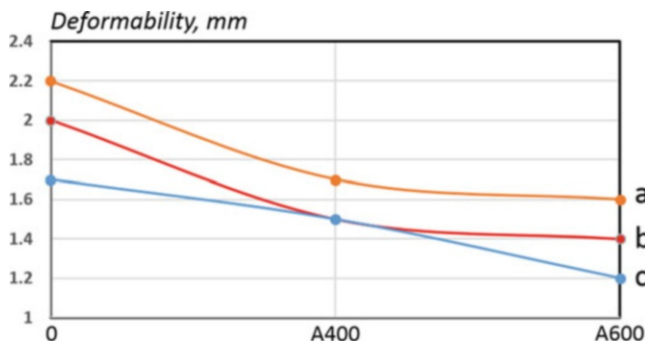


Fig. 5.6 Dependence of column deformations on reinforcement: (a) vibrated, (b) centrifuged, and (c) vibro-centrifuged

Load-Bearing Capacity

The influence of manufacturing technology on the bearing capacity of the columns was greatest for vibro-centrifuged columns (by 29.4% for unreinforced ones, 27.6% for reinforced A400, and 24.9% for reinforced A600) and slightly less for centrifuged columns (by 19.1% for unreinforced, 13.6% for reinforced A400, and 12.4% for reinforced A600) in comparison with vibrated columns.

The Influence of the Class of Reinforcement

This influence on the bearing capacity of the columns increases with an increase in the class of reinforcement. So, in vibrated columns with A400 and A600 class reinforcements, it increased by 7.5% and 13.1%, respectively, compared to unreinforced ones. It has the same figures in centrifuged and vibro-centrifuged columns: 2.6% and 6.8%, 6.1%, and 9.2%, respectively.

Deformability

Approximately the same picture was observed when analyzing the influence of manufacturing and reinforcement technology.

In this case, the influence of manufacturing technology on deformability defined the deformations of the columns compared to similarly reinforced vibrated ones which were always less in all variants as in centrifuged ones (by 9.1% for unreinforced, 1.2% for reinforced A400, and 12.5% for reinforced A600) and vibro-centrifuged ones (by 22.7% for unreinforced, 11.8% for reinforced A400, 25.0% for reinforced A600).

The influence of the class of reinforcement was expressed in a decrease in deformability with an increase in the class of reinforcement used. So, in vibrated columns with reinforcement of A400 and A600 classes, deformations decreased by 22.7% and 27.3%, respectively, compared with unreinforced ones. It has the same figures in centrifuged and vibro-centrifuged columns: 25.0% and 30.0%, and 11.8% and 29.4%, respectively (Table 5.1, Figs. 5.3, 5.4, 5.5 and 5.6).

5.4 Schedule, Methodology, and Results of Numerical Experiments

To expand the scope of using our recommendations, a numerical experiment was also carried out, connected with the calculation of conditional reinforced concrete columns with an expanded variation of the reinforcement of elements.

The schedule of numerical experiments included the study of the influence of the same variable factors on the bearing capacity and deformation of the columns as in the physical experiment, but with significantly extended ranges of variation.

So, if in a physical experiment the reinforcement was as follows:

- (i) The reinforcement class with the reinforcements A400 and A600.
- (ii) The value of reinforcements is $6\varnothing 10$.

Then in the numerical experiment, the variation limits were extended:

- (i) The reinforcement class with the addition of reinforcements A500 and A800.
- (ii) The value of reinforcements with the addition of the reinforcements of $6\varnothing 14$ and $6\varnothing 18$.

Analysis of the results of the numerical experiment showed that the tendencies revealed in the course of the physical experiment have been significantly enhanced, both by increasing the number of reinforcements and by increasing its class, namely:

- (i) With weak reinforcement, the bearing capacity of short centrally compressed reinforced concrete columns is determined by the achievement of the maximum value of $R_b; \varepsilon_{bR}$ on the diagram of concrete " $\sigma_b - \varepsilon_b$," since the increase in the force in the reinforcement does not overlap the decrease in the force in the concrete on the descending branch of deformation.
- (ii) With strong reinforcement, the bearing capacity of short centrally compressed reinforced concrete columns is exhausted after reaching the maximum $R_b; \varepsilon_{bR}$ on the diagram " $\sigma_b - \varepsilon_b$ " of concrete and the increase in reinforcement force, overlapping the decrease in force in concrete on the descending branch of deformation.
- (iii) When reinforcing, the bearing capacity of short centrally compressed reinforced concrete columns can exceed its value up to 10% at the moment of attaining the maximum on the " $\sigma_b - \varepsilon_b$ " diagram of concrete.

In other words, the greater the force applied to the reinforcement of vibrated, centrifuged, and vibro-centrifuged compressed elements, the more the effect of redistribution of forces between concrete and reinforcement in the supercritical stage is manifested, when the force in concrete begins to decrease, and it compensates and blocks successfully the increase in force in the reinforcement. Especially, this effect is enhanced in centrifuged and vibro-centrifuged columns, although it is also present in vibrated ones.

Summarizing the analysis of the results of the physical and numerical experiments performed, it can be noted that:

- (i) The depletion of the bearing capacity of the centrally compressed columns actually occurs during deformations of concrete on the descending branch of its diagram " $\sigma_b - \varepsilon_b$ " and during deformations of high-strength reinforcement practically in the elastic stage $\varepsilon_s < \varepsilon_{0.2}$.
- (ii) An increase in the force perceived by high-strength reinforcement, after concrete reaches its maximum strength, can overlap the decrease in the force

perceived by concrete on the descending deformation branch and even lead to an increase in the total bearing capacity of a reinforced concrete element by up to 10%.

5.5 Comparison of Experimental and Theoretical Results Obtained for V-, CF-, and VCF-Reinforced Concrete Columns According to the Standard, Aggregate, and Local Characteristics of Concretes

5.5.1 *Determination of the Load-Bearing Capacity of V-, CF-, and VCF-Reinforced Concrete Columns According to the Standard, Aggregate, and Local Characteristics of Concretes*

The bearing capacity is calculated according to the Russian State Standards for the aggregate characteristics of concrete:

- (i) Cross-sectional area: $A = \pi(r_2^2 - r_1^2) = 3.14(0.45^2 - 0.30^2) = 0.35325\text{m}^2$;
- (ii) Strength (MPa), according to Chap. 3.

Further, the bearing capacity of the columns is calculated according to the Russian State Standards for the local characteristics of concrete, taking into account the developed recommendations set out in Chap. 4. The calculation was carried out taking into account the strength and areas of each of the conditional layers of the section (internal, middle, and external):

- (i) *Area of layers.*

internal:

$$A_{internal} = \pi(r_2^2 - r_1^2) = 3.14(0.35^2 - 0.30^2) = 0.10205 \text{ m}^2;$$

average:

$$A_{average} = \pi(r_2^2 - r_1^2) = 3.14(0.40^2 - 0.35^2) = 0.11775 \text{ m}^2;$$

external:

$$A_{external} = \pi(r_2^2 - r_1^2) = 3.14(0.45^2 - 0.40^2) = 0.133415 \text{ m}^2.$$

- (ii) Layer strength (MPa), according to Chap. 3.

Let us summarize the obtained data in Table 5.2.

Table 5.2 Values of bearing capacity of columns obtained by different calculation methods

Column code (in Russian)	Test value, kN	Calculated values						Diagram approach, according to Iterative, according to the characteristics of concrete						Simplified, according to the characteristics of concrete					
		Standard approach, according to concrete characteristics			Russian standard			Aggregate Local			Russian standard			Aggregate Local			Russian standard		
		Russian standard	Aggregate	Local	Russian standard	Aggregate	Local	Russian standard	Aggregate	Local	Russian standard	Aggregate	Local	Russian standard	Aggregate	Local	Russian standard	Aggregate	Local
V0	1810	1341	1553	—	1605	1625	—	1481	1569	—	1443	1462	—	1462	1462	—	1462	1462	—
V4	1946	1417	1679	—	1736	1753	—	1602	1714	—	1563	1580	—	1580	1580	—	1580	1580	—
V6	2048	1554	1802	—	1841	1851	—	1700	1810	—	1659	1679	—	1679	1679	—	1679	1679	—
C0	2155	1616	1883	1974	1952	1974	2024	1797	1933	1987	1754	1774	1774	1774	1774	1774	1774	1774	1774
C4	2211	1621	1939	2039	2010	2030	2114	1851	1985	2052	1813	1837	1837	1837	1837	1837	1837	1837	1837
C6	2301	1733	2062	2151	2099	2126	2207	1931	2071	2163	1901	1921	1921	1921	1921	1921	1921	1921	1921
VC0	2342	1740	2089	2157	2127	2173	2253	2019	2112	2209	1949	2045	2045	2045	2045	2045	2045	2045	2045
VC4	2484	1893	2248	2305	2278	2308	2409	2174	2278	2372	2082	2201	2201	2201	2201	2201	2201	2201	2201
VC6	2557	1823	2322	2404	2363	2391	2496	2245	2358	2452	2158	2271	2271	2271	2271	2271	2271	2271	2271

5.5.2 *Calculation of the Load-Bearing Capacity of V-, CF-, and VCF-Reinforced Concrete Columns by the Proposed Diagram Methods Based on the Standard, Aggregate, and Local Characteristics of Concretes*

Further, the bearing capacity of vibrated, centrifuged, and vibro-centrifuged reinforced concrete columns is determined by diagrammatic methods according to the standard, aggregate, and local characteristics of concrete following formulae 5.9–5.22. The calculated data on the bearing capacity are summarized in Table 5.2 and for deformations in Table 5.4. Deviations in the values of the bearing capacity and deformation of the columns, obtained by various calculation methods from the experimental value, are determined and given in Tables 5.3 and 5.5 and, for clarity, are presented graphically in Figs. 5.7, 5.8, 5.9 and 5.10.

The analysis of the results obtained allowed one to make the following conclusions.

The calculated values of the strength of similar columns, differing only in the manufacturing technology (vibrated, centrifuged, and vibro-centrifuged), determined according to the standard approach using the Russian standard, aggregate, and local characteristics of concrete, and their experimental strength and deformability, significantly differ from each other.

The deviations of the experimental strengths of the columns from the Russian standards, calculated according to the methodology using the Russian standard characteristics of concretes for vibrated, centrifuged, and vibro-centrifuged columns, reached 20.1%, 24.7%, and 28.7%, respectively.

The same deviations in the strengths of the test columns using the aggregate characteristics of concrete turned out to be equal for vibrated, centrifuged, and vibro-centrifuged columns attained 8.0%, 10.4%, and 11.2%, respectively.

The deviations of the strength values of the experimental columns using the local characteristics of concrete were 4.3% for centrifuged columns and 6.1% for vibro-centrifuged columns.

Thus, the calculation of the strength of short centrally compressed reinforced concrete columns according to the standard method gave the best results using the local characteristics of concrete, differing in cross-section of elements.

The calculation according to the *diagram approach* according to the iterative, approximate and simplified methods gave even more indicative results (see Tables 5.2 and 5.3 and Fig. 5.7).

The deviations reached only 2.4%, not to mention the sum of the squares of the deviations, which is many times less than when calculated by the method of standards.

Two important points should be noted here:

- (i) All the proposed methods, even the simplified approach, showed a significantly better convergence with the experimental data than the calculation by the Russian standards.

Table 5.4 Column deformability values obtained by various calculation methods

Column code (in Russian)	Test value, mm	Deformability, mm		Calculated values			Diagram approach, according to Iterative, according to the characteristics of concrete			Approximate, according to the characteristics of concrete			Simplified, according to the characteristics of concrete		
		Standard approach, according to concrete characteristics		Russian standard			Aggregate Local			Russian standard			Aggregate Local		
		Russian standard	Aggregate Local	Russian standard	Aggregate Local	Russian standard	Aggregate Local	Russian standard	Aggregate Local	Russian standard	Aggregate Local	Russian standard	Aggregate Local	Russian standard	Aggregate Local
V0	2.2	2.7	2.5	—	2.4	2.4	—	2.6	2.5	—	2.6	2.6	—	—	—
V4	1.7	2.1	1.9	—	1.9	1.9	—	2.0	1.9	—	2.0	2.0	—	—	—
V6	1.6	2.0	1.8	—	1.7	1.7	—	1.9	1.8	—	1.9	1.8	—	—	—
C0	2.0	2.5	2.2	2.1	2.2	2.2	2.1	2.3	2.2	2.1	2.4	2.3	2.1	2.1	2.1
C4	1.5	1.9	1.7	1.6	1.6	1.6	1.6	1.7	1.7	1.6	1.8	1.7	1.6	1.6	1.6
C6	1.4	1.8	1.5	1.5	1.5	1.5	1.5	1.6	1.5	1.5	1.6	1.6	1.6	1.5	1.5
VC0	1.7	2.2	1.9	1.9	1.8	1.8	1.8	1.9	1.9	1.8	2.0	1.9	1.8	1.8	1.8
VC4	1.5	1.9	1.6	1.6	1.6	1.6	1.5	1.7	1.6	1.6	1.7	1.7	1.6	1.6	1.6
VC6	1.2	1.6	1.3	1.2	1.3	1.3	1.2	1.4	1.3	1.3	1.4	1.4	1.2	1.2	1.2

Table 5.3 Deviations in the values of the bearing capacity of the columns, obtained by various calculation methods from the experimental values

Column code (in Russian)	Deviations of the calculated values from the experimental ones, %						Simplified, according to the characteristics of concrete					
	Diagram approach, according to Iterative, according to the characteristics of concrete			Approximate, according to the characteristics of concrete								
	Russian standard	Aggregate	Local	Russian standard	Aggregate	Local						
V0	25.9	14.2	—	11.3	10.2	—	18.2	13.3	—	20.3	19.2	—
V4	27.2	13.7	—	10.8	9.9	—	17.7	11.9	—	19.7	18.8	—
V6	24.1	12.0	—	10.1	9.6	—	17.0	11.6	—	19.0	18.0	—
C0	25.0	12.6	8.4	9.4	8.4	5.6	16.6	10.3	7.8	18.6	17.7	7.7
C4	26.7	12.3	7.8	9.1	8.2	4.4	16.3	10.2	7.2	18.0	16.9	7.2
C6	24.7	10.4	6.5	8.8	7.6	4.1	16.1	10.0	6.0	17.4	16.5	6.1
VC0	25.7	10.8	7.9	9.2	7.2	3.8	13.8	9.8	5.7	16.8	12.7	6.8
VC4	23.8	9.5	7.2	8.3	7.1	3.0	12.5	8.3	4.5	16.2	11.4	5.8
VC6	28.7	9.2	6.0	7.6	6.5	2.4	12.2	7.8	4.1	15.6	11.2	5.2
$\sum \Delta^2$	5990.1	1243.1	323.9	806.2	634.3	96.7	2229.5	989.0	218.2	2921.9	2333.9	255.3

Table 5.5 Deviations in the values of the deformability of the columns obtained by various calculation methods from the experimental values

Column code (in Russian)	Deviations of the calculated values from the experimental ones, %					Simplified, according to the characteristics of concrete			
	Diagram approach, according to the characteristics of concrete			Approximate, according to the characteristics of concrete		Russian standard			
	Russian standard	Aggregate	Local	Russian standard	Aggregate	Local	Russian standard	Aggregate	Local
V0	23.2	13.5	—	10.2	9.7	—	18.0	12.8	—
V4	25.5	12.8	—	9.8	9.5	—	17.7	12.4	—
V6	22.8	12.5	—	9.3	9.1	—	17.5	12.0	—
C0	23.7	11.7	6.8	8.4	8.4	5.0	15.2	11.2	6.2
C4	25.2	11.5	6.2	8.2	8.0	4.1	15.1	10.6	5.8
C6	26.9	10.1	6.1	7.9	7.8	3.7	14.1	10.1	5.0
VC0	29.2	9.8	7.0	8.4	7.1	3.2	13.6	9.6	4.7
VC4	25.8	9.2	6.7	8.2	7.0	3.0	13.5	8.8	4.6
VC6	30.1	8.6	6.0	7.4	6.8	2.5	12.7	7.4	4.3
$\sum \Delta^2$	6053.0	1128.1	251.8	679.3	608.2	81.0	2129.9	1025.8	158.8
								2662.0	2133.1
									92.7

Fig. 5.7 Graphical representation of the experimental and theoretical values of the bearing capacity of the columns, calculated by various methods 0 test; 1–3 standard approach (1, 2, 3—according to the Russian standard, aggregate, and local characteristics of concrete); 4–6 diagram approach, iterative method (4, 5, 6—according to the Russian standard, aggregate, and local characteristics of concrete); 7–9 diagram approach, approximate method (7, 8, 9—according to the Russian standard, aggregate, and local characteristics of concrete); 10–12 diagram approach, simplified method (10, 11, 12—according to the Russian standard, aggregate, and local characteristics of concrete)

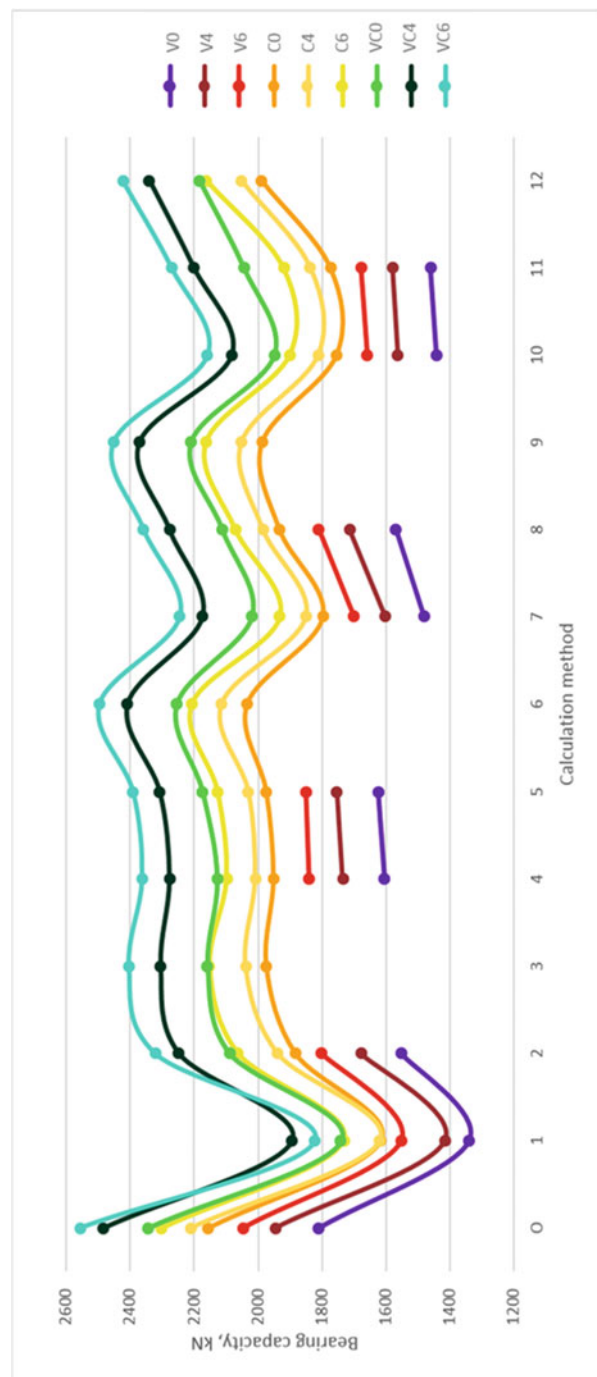
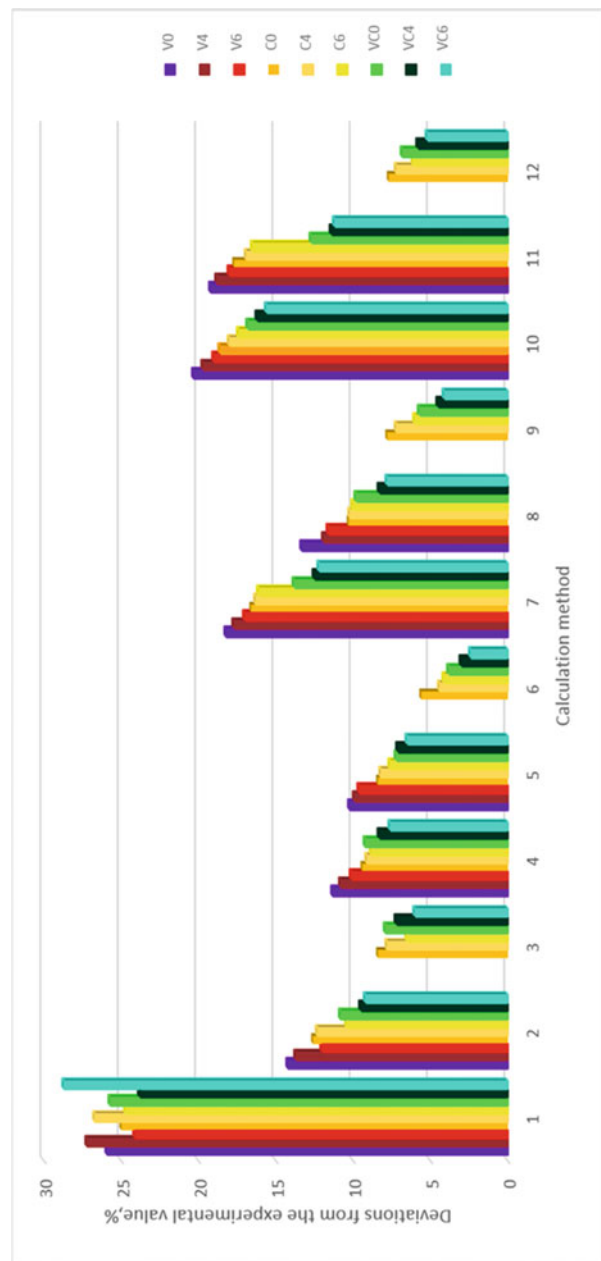


Fig. 5.8 Graphical representation of deviations from the experimental results of the theoretical values of the bearing capacity of the columns, calculated by various methods: 0 by experience; 1–3 standard approach (1, 2, 3—according to the Russian standard, aggregate, and local characteristics of concrete); 4–6 diagram approach, iterative method (4, 5, 6—according to the Russian standard, aggregate, and local characteristics of concrete); 7–9 diagram approach, approximate method (7, 8, 9—according to the Russian standard, aggregate, and local characteristics of concrete); 10–12 diagram approach, simplified method (10, 11, 12—according to the Russian standard, aggregate, and local characteristics of concrete)



- (ii) For centrifuged and vibro-centrifuged columns, the diagram approach in any implementation method gives better results when using the local characteristics of concrete than when using the aggregate characteristics of concrete.

Fig. 5.9 Graphical presentation of experimental results and theoretical values of column deformability, calculated by various methods: 0 by experience; 1–3 standard approach (1, 2, 3—according to the Russian standard, aggregate, and local characteristics of concrete); 4–6 diagram approach, iterative method (4, 5, 6—according to the Russian standard, aggregate, and local characteristics of concrete); 7–9 diagram approach, approximate method (7, 8, 9—according to the Russian standard, aggregate, and local characteristics of concrete); 10–12 diagram approach, simplified method (10, 11, 12—according to the Russian standard, aggregate, and local characteristics of concrete)

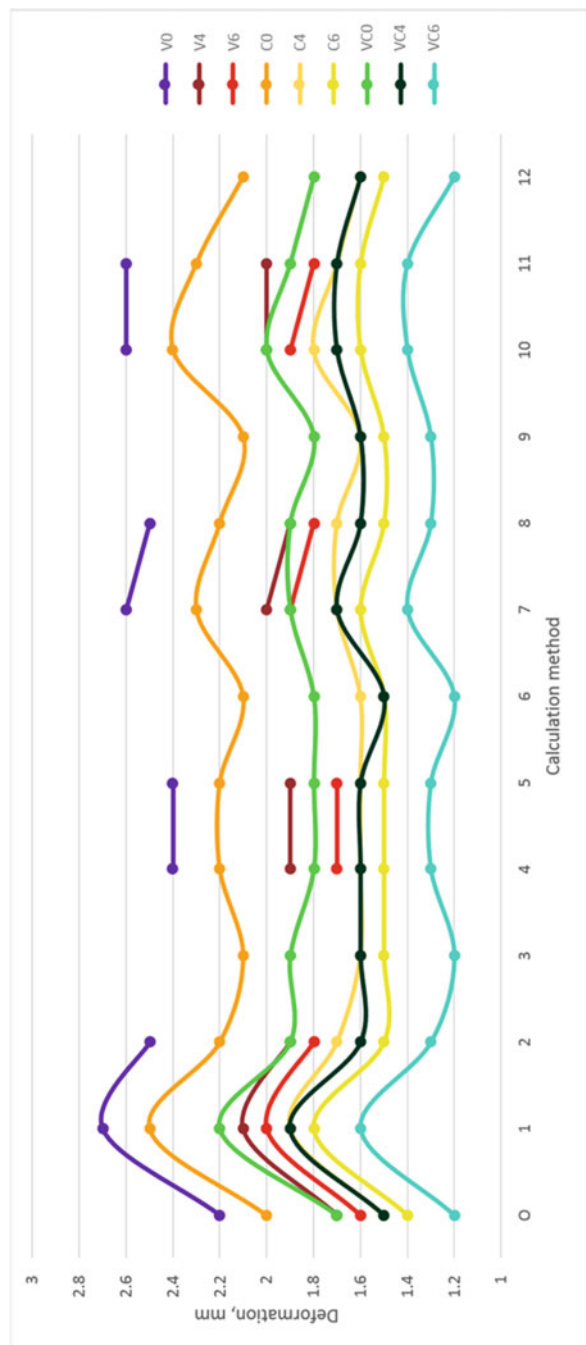
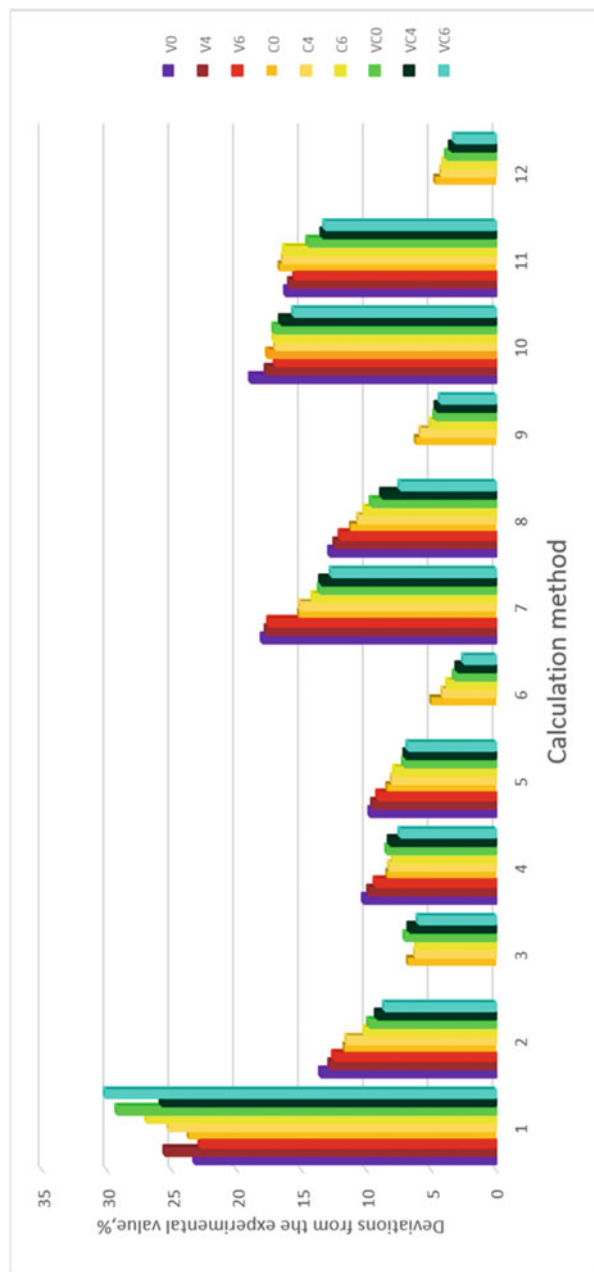


Fig. 5.10 Graphical Representation of Deviations from the Experimental Results of the Theoretical Values of the Deformability of Columns, Calculated by Various Methods: 0 by Experience; 1–3 Standard Approach (1, 2, 3—According to the Russian Standard, Aggregate, and Local Characteristics of Concrete); 4–6 Diagram Approach, Iterative Method (4, 5, 6—According to the Russian Standard, Aggregate, and Local Characteristics of Concrete); 7–9 Diagram Approach, Approximate Method (7, 8, 9—According to the Russian Standard, Aggregate, and Local Characteristics of Concrete); 10–12 Diagram Approach, Simplified Method (10, 11, 12—According to the Russian Standard, Aggregate, and Local Characteristics of Concrete) Potential Capabilities of CF- and VCF-Reinforced Concrete Columns



It should be noted that all the same pointed features of deviations of the calculated values from the experimental results were also characteristic for the deformations of the columns, as well as for their bearing capacities (see Tables 5.4 and 5.5 and Fig. 5.8).

That is, taking into account in the calculations a greater differentiation of the characteristics of concrete leads to a more accurate calculation for both groups of limiting states, sometimes very significant.

As a result, hidden, previously unaccounted for, safety margins of short reinforced concrete columns of functionally gradient design, including real industrial columns, manufactured by centrifugation and vibro-centrifugation methods in the factory, were analytically identified and determined.

The proposed analytical method for calculating the strength of short centrally compressed reinforced concrete columns, based on the material deformation diagrams in iterative, approximate, and simplified formulations satisfactorily estimates the bearing capacity of vibrated, centrifuged, and vibro-centrifuged columns.

5.6 Conclusions

1. An improvement of the standard approach to the calculation of the strength of centrifuged and vibro-centrifuged reinforced concrete columns is proposed, which consists in using the calculation of aggregate (averaged over the cross-section) or local (differing in the layers of the section) characteristics of concrete.
2. Within the framework of the diagram approach, iterative, approximate, and simplified methods of calculating the bearing capacity of reinforced concrete vibrated, centrifuged, and vibro-centrifuged columns are proposed.
3. Experimental and numerical studies of the operation of reinforced concrete vibrated, centrifuged, and vibro-centrifuged columns were carried out, which revealed that:
 - (i) The depletion of the bearing capacity of vibrated columns occurs during deformations of concrete on the descending branch of the diagram " $\sigma_b - \varepsilon_b$ "; the depletion of the bearing capacity of centrifuged and vibro-centrifuged columns occurs during deformations of individual conditional concrete layers on the ascending branch of the diagram " $\sigma_b - \varepsilon_b$ " and some individual concrete layers on the descending branch of its diagram " $\sigma_b - \varepsilon_b$ "; at the same time, the deformations of high-strength reinforcement are practically in the elastic stage $\varepsilon_s < \varepsilon_{0.2}$.
 - (ii) An increase in the force perceived by high-strength reinforcement, after the concrete reaches the cross-section or its individual layers of maximum strength, can overlap the decrease in the force perceived by the concrete on the descending deformation branch and lead to an increase in the total bearing capacity of the reinforced concrete element up to 10%.

4. Calculation of the strength of short centrally compressed vibrated, centrifuged, and vibro-centrifuged columns according to the improved standard approach gave the best results using the local characteristics of concrete, differing in cross-section.
5. Calculation according to the diagram approach in all settings by iterative, approximate, and simplified methods showed significantly better convergence with experimental data than calculation according to the method of standards.
6. For centrifuged and vibro-centrifuged columns, the diagram approach in any setting (iterative, approximate, and simplified methods) gives better results, when using the local characteristics of concrete than when using the aggregate ones and, even more so, the Russian standard characteristics of concrete.

Chapter 6

Redesign and Improvement of CF- and VCF-Reinforced Concrete Columns, Taking into Account the Technology of Their Manufacture



Abstract In this chapter, the previously hidden strength reserves of industrial columns of functionally gradient structure are revealed and determined. The advantages of vibro-centrifuged reinforced concrete columns are defined and formulated in comparison with centrifuged ones. As an example, the centrifuged serial standard reinforced concrete column was redesigned and improved for the vibro-centrifuged column, the bearing capacity of which turned out to be 35% higher. It is shown that the research results could be implemented in practical building and designing by using the developed recommendations, based on (i) various combinations of vibration and centrifugation modes in the manufacture production of centrifuged and vibro-centrifuged columns, (ii) redesigned and improved centrifuged and vibro-centrifuged columns, and (iii) a pilot batch of developed centrifuged and vibro-centrifuged columns, introduced during the building of a real object, namely, a column of a transport overpass.

Key words Vibro-centrifuged reinforced concrete · Centrifuged standard reinforced concrete column · Practical recommendations

6.1 Technological, Structural, and Design Advantages of the Proposed Actual Structures

The main advantages of the set of technologies, structures, and calculation methods we offer are:

- (i) The technological aspect is expressed in the use of vibro-centrifugation.
- (ii) The calculation aspect is expressed in the aggregate and local consideration of changes in the characteristics of concrete due to functional gradient features after centrifugation and vibro-centrifugation.

As a result, all this together leads to:

- (i) Redistribution of concrete characteristics in cross-sections due to functional gradient features after centrifugation and vibro-centrifugation.

- (ii) Due to this, there is a possibility of reducing the longitudinal reinforcement.
- (iii) As a result, an increased standard load on centrifuged and vibro-centrifuged compressed elements or reduced size of their sections is possible.

For this purpose, after our laboratory studies, we will check the stated suggestions on experimental industrial samples in order to redesign and improve real columns.

6.2 Redesign of Actual Reinforced Concrete Column and Calculation of the Load-Bearing Capacity of Such a VCF-Column

For further redesign, a standard centrifuged reinforced concrete column was adopted, being a typical serial one, manufactured in accordance with the Russian GOST No. 23444 "Reinforced concrete centrifuged racks of annular cross-sections for industrial buildings and engineering structures. Technical Conditions." Their characteristics are presented in Table 6.1.

The column reinforcement scheme is shown in Fig. 6.1.

The size of the binding of the reinforcement frames with a diameter of the longitudinal reinforcement $d < 0.016$ m is 0.040 m.

The reinforcement frame of the column and its main dimensions are shown in Fig. 6.2 and Table 6.2.

Calculations are made in accordance with the Russian Building Regulations 63.13330.2018.

The initial data for calculating the bearing capacity of a typical serial column are given in Table 6.3.

Because the outer diameter is $D_{cir} = 0.300$ m and the wall thickness is $B = 0.050$ m, the inner diameter is $D_{in} = D_{cir} - 2B = 0.300 - 0.100 = 0.200$ m.

We accept the cross-section coefficients of the corresponding elements: $n_y = 1.0$, $n_h = 1.19$. The estimated length of rack (column) $L_1 = 4.8$ m.

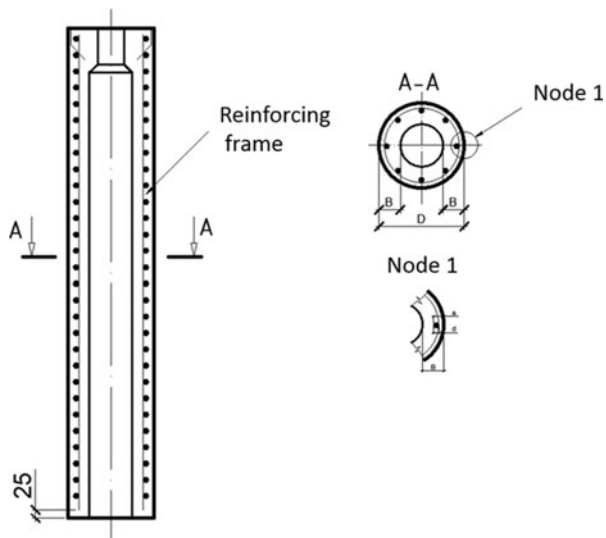
Let us design the column for the standard load according to building regulations.

First, find the total force from all loads. The torque M , taking into account the influence of the deflection of the element, is found as

Table 6.1 Column characteristics according to Russian GOST No. 23444

Rack brand	Main dimensions, m			Consumption of materials		Rack weight, tnf
	Diameter	Length	Wall thickness	Concrete, m ³	Steel, kgf	
C5.48.10-K1	0.300	4.8	0.050	0.41	51	1.0

Fig. 6.1 Scheme of column reinforcement (the pointed sizes in mm)



$$M = M_V + M_h = 20 + 15 = 35 \text{ kN} \cdot \text{m}, \quad (6.1)$$

where M_V is the torque from vertical load and M_h is the torque from wind load.

The total longitudinal compressive force within the cross-section of the element N is found as

$$N = N_V + N_h = 200 + 50 = 250 \text{ kN}, \quad (6.2)$$

where N_V is the longitudinal force from vertical load and N_h is the longitudinal force from wind load.

The initial eccentricity is found as

$$e_0 = \frac{M}{N} = \frac{35}{250} = 0.14 \text{ m} \quad (6.3)$$

The stiffness of element is:

$$r_m = r_s = \frac{r_1 + r_2}{2} = \frac{0.15 + 0.1}{2} = 0.125 \text{ m}, \quad (6.4)$$

where r_m is the mid-circle radius of the column and r_s is the radius of a circle passing through the centers of gravity of longitudinal reinforcement bars.

Then, we find M_l and M_{l1} are the resulting moments relative to the center of the most stretched or least compressed (with a fully compressed cross-section) of the bar from the action of the total load and from the action of constant and long-term loads, respectively:

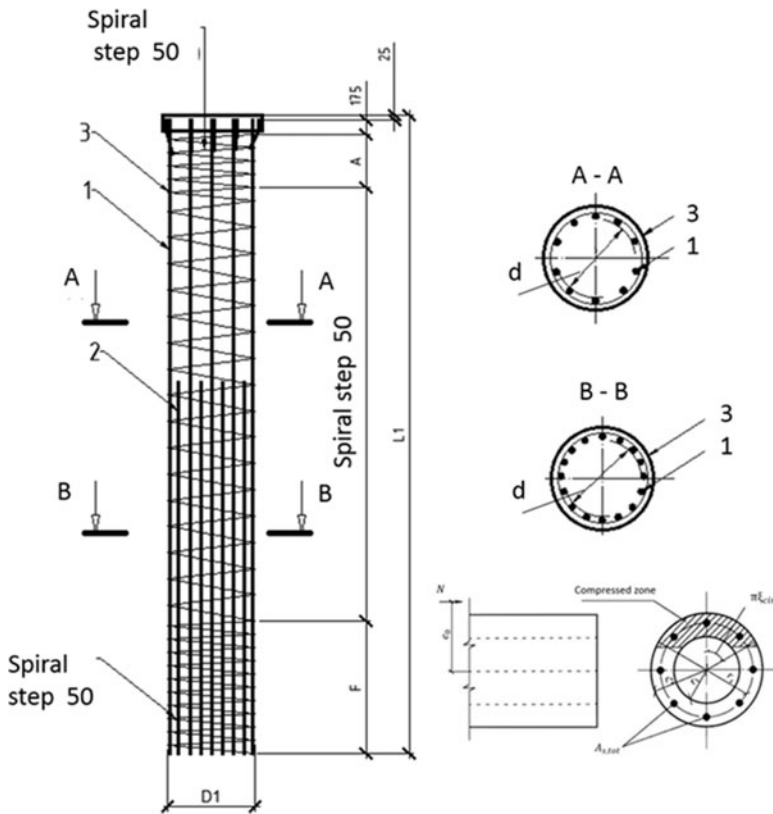


Fig. 6.2 Reinforcing frame of the column (the pointed sizes in mm)

Table 6.2 Main dimensions of the reinforcing frame

Frame dimensions, m		Number of rods
A, m	F, m	
0.400	1.550	10

$$M_l = M + N r_s = 35 + 250 \cdot 0.125 = 66.25 \text{ kN} \cdot \text{m},$$

$$M_{l1} = M_V + N_V r_s = 20 + 200 \cdot 0.125 = 45 \text{ kN} \cdot \text{m}, \quad (6.5)$$

where r_s is the radius of the circle passing through the centers of gravity of the rods of the longitudinal reinforcement.

Taking into account the influence of the load duration, a coefficient φ_1 is found as

Table 6.3 Initial data for calculating the bearing capacity of typical serial column

Parameter		Value
Outer diameter	D_{cir} , m	0.300
Wall thickness	B , m	0.050
Length of rack (column)	L_1 , m	4.800
External radius	r_1 , m	0.15
Inner radius	r_2 , m	0.1
Concrete class		B40
Initial modulus of elasticity of concrete in compression and tension	E_b , GPa	36
Design resistance of concrete to axial compression	R_b , MPa	29
Longitudinal reinforcement		A400
Design tensile strength of reinforcement	R_s , MPa	355
Design compressive strength of reinforcement	R_{sc} , MPa	355
Initial modulus of elasticity of reinforcement	E_s , GPa	200
Number of reinforcing bars		10
Reinforcement diameter	d , m	0.020
Cross-sectional area of all longitudinal reinforcement	$A_{s,tot}$, m^2	3.140×10^{-3}
Longitudinal force from vertical loads	N_V , kN	200
Torque due to vertical loads	M_V , kN·m	20
Longitudinal force from wind loads	N_h , kN	50
Torque due to wind loads	M_h , kN·m	15

$$\varphi_1 = 1 + \frac{M_{l1}}{M_l} = 1 + \frac{45}{66.25} = 1.68. \quad (6.6)$$

Then the condition for the cross-section parameter is checked:

$$\frac{e_0}{D_{cir}} = \frac{0.140}{0.300} = 0.47 > 0.15. \quad (6.7)$$

We accept the relative value of the eccentricity of the longitudinal force b_e as

$$b_e = \frac{e_0}{D_{cir}} = 0.47. \quad (6.8)$$

Let us calculate the moment of inertia of the concrete cross-sect. I :

$$I = \frac{\pi(D_{cir}^4 - D_{in}^4)}{64} = \frac{3.14 \cdot (0.300^4 - 0.200^4)}{64} = 319 \times 10^{-6} \text{ m}^4. \quad (6.9)$$

Then we calculate the moment of inertia I_s of the concrete cross-section relative to the reinforcing frame as

$$I_s = \frac{A_{s,tot}r_s^2}{2} = \frac{3140 \cdot 10^{-6} \cdot 0.125^2}{2} = 2.45 \times 10^{-5} \text{ m}^4. \quad (6.10)$$

The stiffness D of the element is calculated as

$$D = \frac{0.15}{\varphi_1(0.3 + b_e)} E_b I + 0.7 E_s I_s;$$

$$\begin{aligned} D &= \frac{0.15}{1.68 \cdot (0.3 + 0.47)} 36 \cdot 10^9 \cdot 319 \cdot 10^{-6} + 0.7 \cdot 2 \cdot 10^{11} \cdot 2.45 \cdot 10^{-5} \\ &= 4762 \text{ kN} \cdot \text{m}^2 \end{aligned} \quad (6.11)$$

Then, the critical Euler force N_{sb} is calculated as

$$N_{sb} = \frac{\pi^2 D}{L_1^2} = \frac{3.14^2 \cdot 4762}{4.8^2} = 2039 \text{ kN} \quad (6.12)$$

and coefficient η_n is found as

$$\eta_n = \frac{1}{1 - \frac{N}{N_{sb}}} = \frac{1}{1 - \frac{250}{2039}} = 1.1397. \quad (6.13)$$

The moment taking into account the deflection is equal to:

$$M = M_V + M_h \eta_n = 20 + 15 \cdot 1.1397 = 37.1 \text{ kN} \cdot \text{m}. \quad (6.14)$$

The cross-sectional area is equal to:

$$A = \pi(r_1^2 - r_2^2) = 3.14 \cdot (0.150^2 - 0.100^2) = 39.25 \cdot 10^{-3} \text{ m}^2 \quad (6.15)$$

Then, we calculate the relative area of the compressed zone of the concrete cross-section ζ_{cir} :

$$\begin{aligned} \zeta_{cir} &= \frac{N + R_s A_{s,tot}}{R_b A + 2.7 R_s A_{s,tot}} \\ \zeta_{cir} &= \frac{250 \cdot 10^3 + 355 \cdot 10^6 \cdot 3.140 \cdot 10^{-3}}{29 \cdot 10^6 \cdot 39.25 \cdot 10^{-3} + 2.7 \cdot 355 \cdot 10^6 \cdot 3.140 \cdot 10^{-3}} = 0.329. \end{aligned} \quad (6.16)$$

Since $0.15 < \zeta_{cir} (0.329) < 0.6$, we check the strength condition of the cross-section.

According to the Russian Building Regulations No. 63.13330.2018, the maximum load is determined as.

$$M \leq (R_b A r_m + R_{sc} A_{s,tot} r_s) \frac{\sin(\pi \zeta_{cir})}{\pi} + R_s A_{s,tot} r_s (1 - 1.7 \zeta_{cir}) (0.2 + 1.3 \zeta_{cir})$$

$$\begin{aligned} M &= (29 \cdot 10^6 \cdot 39.25 \cdot 10^{-3} \cdot 0.125 + 355 \cdot 10^6 \cdot 3.140 \cdot 10^{-3} \cdot 0.125) \frac{\sin(\pi 0.329)}{\pi} \\ &\quad + 355 \cdot 10^6 \cdot 3.140 \cdot 10^{-3} \cdot 0.125 \cdot (1 - 1.7 \cdot 0.329) \cdot (0.2 + 1.3 \cdot 0.329) \\ &= 115.5 \text{ kN} \cdot \text{m} \end{aligned}$$

$$115.5 \text{ kN} \cdot \text{m} > M = 37.1 \text{ kN} \cdot \text{m}. \quad (6.17)$$

Thus, the strength of the cross-section is ensured.

Now we will redesign a standard centrifuged reinforced concrete column, taking into account our data and results obtained and developed during the study.

The initial data are the same and shown in Table 6.3.

The total force from all loads is (based on formulae 6.1–6.3):

$$M = 35 \text{ kN} \cdot \text{m}; N = 250 \text{ kN}; e_0 = 0.14 \text{ m}.$$

The stiffness of element is (based on formula 6.4):

$$r_s = r_m = \frac{0.150 + 0.100}{2} = 0.125 \text{ m}.$$

Then, we find M_l and M_{l1} are the resulting moments (based on formula 6.5):

$$M_l = 35 + 250 \cdot 0.125 = 66.25 \text{ kN} \cdot \text{m};$$

$$M_{l1} = 20 + 200 \cdot 0.125 = 45 \text{ kN} \cdot \text{m}.$$

Coefficient φ_1 (based on formula 6.6) is found as

$$\varphi_1 = 1 + \frac{45}{66.25} = 1.68.$$

Then we check the condition for the cross-section parameter:

$$\frac{e_0}{D_{cir}} = \frac{0.140}{0.300} = 0.47 > 0.15.$$

We accept:

$$b_e = \frac{e_0}{D_{cir}} = 0.47.$$

Let us calculate the moments of inertia of the concrete cross-section (based on formula 6.9) and the moment of inertia I_s of the concrete cross-section relative to the reinforcing frame (based on formula 6.10):

$$I = \frac{3.14 \cdot (0.300^4 - 0.200^4)}{64} = 319 \times 10^{-6} \text{ m}^4$$

$$I_s = \frac{3140 \cdot 10^{-6} \cdot 0.125^2}{2} = 2.45 \times 10^{-5} \text{ m}^4.$$

Taking into account the new initial modulus of elasticity of concrete $E_b = 43 \text{ GPa}$ in compression and tension, a stiffness D (by formula (6.11)) is defined as

$$\begin{aligned} D &= \frac{0.15}{1.68 \cdot (0.3 + 0.47)} 43 \cdot 10^9 \cdot 319 \cdot 10^{-6} + 0.7 \cdot 2 \cdot 10^{11} \cdot 2.45 \cdot 10^{-5} \\ &= 5026 \text{ kN} \cdot \text{m}^2. \end{aligned}$$

Then, we calculate the critical Euler force N_{sb} (based on formula 6.12):

$$N_{sb} = \frac{3.14^2 \cdot 5026}{4.8^2} = 2150 \text{ kN}.$$

We calculate coefficient η_n as

$$\eta_n = \frac{1}{1 - \frac{250}{2150}} = 1.13.$$

The moment of inertia taking into account the deflection (based on formula 6.14) is equal to:

$$M = 20 + 15 \cdot 1.13 = 36.95 \text{ kN} \cdot \text{m}.$$

The cross-sectional area (based on formula 6.15) is equal to:

$$A = 3.14 \cdot (0.150^2 - 0.100^2) = 39.25 \times 10^{-3} \text{ m}^2.$$

The new design resistance of concrete is taken equal to $R_b = 59 \text{ MPa}$. The relative area of the compressed zone (based on formula 6.16) is:

$$\zeta_{cir} = \frac{250 \cdot 10^3 + 355 \cdot 10^6 \cdot 3.140 \cdot 10^{-3}}{59 \cdot 10^6 \cdot 39.25 \cdot 10^{-3} + 2.7 \cdot 355 \cdot 10^6 \cdot 3.140 \cdot 10^{-3}} = 0.26.$$

Since $0.15 < \zeta_{cir}$ (0.26) < 0.6 , we check the strength of the section from the condition:

$$\begin{aligned} M &= (59 \cdot 10^6 \cdot 39.25 \cdot 10^{-3} \cdot 0.125 + 355 \cdot 10^6 \cdot 3.140 \cdot 10^{-3} \cdot 0.125) \\ &\quad \times \frac{\sin(\pi \cdot 0.329)}{\pi} + \\ &+ 355 \cdot 10^6 \cdot 3.140 \cdot 10^{-3} \cdot 0.125 \cdot (1 - 1.7 \cdot 0.329)(0.2 + 1.3 \cdot 0.329) = \\ &= 115.5 \text{ kN} \cdot \text{m}. \end{aligned}$$

$$155.8 \text{ kN} \cdot \text{m} > M = 36.95 \text{ kN} \cdot \text{m}.$$

Thus, the bearing capacity of the redesigned vibro-centrifuged reinforced concrete column was 35% greater than that of a typical series column.

To work on the same standard load, it is even possible to reduce the percentage of reinforcement and obtain the same structural parameters of the column as in the standard column without changing its parameters.

6.3 Implementation of the Research Results in the Practice of Building and Designing and Regulatory Documents

The implementation of the results of the work was carried out in two directions: (i) in practical building and designing and (ii) regulatory documents.

Implementation in practical building was carried out through the development and implementation of the proposed centrifuged and vibro-centrifuged columns at the JSC RZZhBK plant, Rostov-on-Don, Russia, in 2018.

A pilot batch of the developed centrifuged and vibro-centrifuged columns was introduced during the construction of a real object, namely, a column of a transport overpass in Rostov-on-Don.

Implementation in practical designing was carried out by using the developed designing recommendations for different combinations of vibration and centrifugation modes in the manufacture of centrifuged and vibro-centrifuged columns at the JSC RZZhBK plant.

The developed recommendations for various combinations of vibration and centrifugation modes and the proposed improved centrifuged and vibro-centrifuged columns were introduced at the JSC RZZhBK plant, Rostov-on-Don.

Implementation in regulatory documents was carried out by developing an enterprise standard at the ZAO RZZhBK plant, Rostov-on-Don.

The standard of enterprise “Columns of reinforced concrete centrifuged and vibro-centrifuged with annular cross-section” was published (JSC “RZZhBK,” Rostov-on-Don, Russia, 2018).

6.4 Conclusions

1. The previously hidden strength reserves of industrial columns of functionally gradient structure have been revealed and determined. The columns have been produced by centrifugation and vibro-centrifugation methods. The advantages of vibro-centrifuged reinforced concrete columns are determined and formulated in comparison with centrifuged ones.
2. The centrifuged serial standard reinforced concrete column was redesigned and improved for the vibro-centrifuged column, the bearing capacity of which turned out to be 35% higher. To work on the same standard load, the percentage of reinforcement is reduced and the same design indicators of the column are obtained as for the standard one.
3. The research results have been implemented in practical building and designing by using the developed recommendations, based on (i) different combinations of vibration and centrifugation modes in the manufacture production of centrifuged and vibro-centrifuged columns, (ii) redesigned and improved centrifuged and vibro-centrifuged columns, and (iii) a pilot batch of developed centrifuged and vibro-centrifuged columns, introduced during the building of a real object, namely, a column of a transport overpass.
4. The results have been introduced into the regulatory document of the standard of the enterprise JSC RZZhBK, Rostov-on-Don, “Columns of reinforced concrete centrifuged and vibro-centrifuged with annular cross-section.”

Common Conclusions to Part I

1. The theoretical substantiation and physical essence of the functionally gradient structure of centrifuged and vibro-centrifuged concrete elements with annular cross-section have been formulated. The qualitative and quantitative picture of the density variation of the layers of the annular cross-section during centrifugation and vibro-centrifugation has been presented.
2. An original combined experimental setup has been developed, allowing one to perform both centrifugation and vibro-centrifugation; its parameters have been tested. It has confirmed the correctness of the premises and postulates.
3. An original method of experimental research of the functionally gradient cross-sections of centrifuged and vibro-centrifuged concretes is proposed to determine their aggregate (generalized over the cross-section) and local (differing in layers) strength and deformation characteristics and also deformation diagrams.
4. Experimental studies of the aggregate characteristics of concretes at the age of 7, 28, and 180 days under compression and tension proved that the characteristics of concretes at centrifugation are higher than at vibration; at vibro-centrifugation they are higher than during centrifugation and vibration:
 - (i) Compressive and tensile strength increases up to 20–22% at all ages.
 - (ii) Ultimate deformations during axial compression and tension decrease up to 6–8%.
 - (iii) The modulus of elasticity during axial compression and tension increases by 5–10%.
 - (iv) In the diagrams “stress-strain” during compression and tension, the maximum shifts up and to the left, the ascent angle increases at the beginning of the coordinates, and the lift in the ascending branch increases.
5. Experimental studies of the local characteristics of centrifuged and vibro-centrifuged concretes at the age of 7, 28, and 180 days under compression and tension have confirmed the substantiation of the three-layer model of their functionally gradient structure. Local characteristics of the layers of functionally gradient concrete is obtained: the concrete of the outer layers has the highest strength, modulus of elasticity, and the least deformability; the lowest strength, modulus of elasticity, and the highest deformability correspond to the concrete of the inner layers; the concrete of the middle layers has average characteristics; deformation diagrams also differ, respectively.
6. The values of standard and design resistances are recommended for limiting states of I and II groups, and ultimate deformations and initial moduli of elasticity in compression and tension of vibrated, centrifuged, and vibro-

- centrifuged concretes are based on the results of statistical data processing with a reliability of 0.95.
7. Proposals are given for the calculated determination of the aggregate characteristics of centrifuged and vibro-centrifuged concretes at the age of 28 days on the basis of the introduction of correction factors to the corresponding characteristics of vibrated concrete.
 8. To determine the aggregate characteristics of vibrated, centrifuged, and vibro-centrifuged concretes, depending on age, dependences are proposed, the values of the coefficients of which are determined by statistical methods. Analytical diagrams of deformation in compression and tension of concrete at any age are proposed, their similarity is proved, and recommendations for their creation are given.
 9. It has been experimentally and theoretically proved that different concrete layers during centrifugation and vibro-centrifugation are affected by inertial forces differing in magnitude, leading to functionally gradient cross-sections and localization of strength and deformation characteristics of its layers. It was revealed that the main factors of influence are centrifugal and centripetal forces, depending on the distance from the center of rotation and the angular velocity of rotation. To assess the local characteristics of concrete during centrifugation and vibro-centrifugation, universal design dependencies are proposed. In these dependencies, the characteristics of concrete, namely, strength, ultimate deformations, and modulus of elasticity in compression and tension (or their increments in absolute or relative parameters), are functions, and the distance from the center and the angular speed of rotation are arguments.
 10. An improved standard approach to calculating the strength of centrifuged and vibro-centrifuged reinforced concrete columns is proposed, which consists in using of the calculation of aggregate (averaged over the cross-section) or local (differing in the layers of the cross-section) characteristics of concrete.
 11. Within the framework of the diagram approach, iterative, approximate, and simplified methods of calculating the bearing capacity of reinforced concrete vibrated, centrifuged, and vibro-centrifuged columns are proposed.
 12. Experimental and numerical studies of the operation of reinforced concrete vibrated, centrifuged, and vibro-centrifuged columns were carried out, which revealed that:
 - (i) The depletion of the bearing capacity of vibrated columns occurs during deformations of the concrete of the cross-section on the descending branch of the diagram “ $\sigma_b - \epsilon_b$ ”; for centrifuged and vibro-centrifuged columns, it occurs during deformations of individual conditional concrete layers on the ascending branch, and for certain layers, on the descending branch of its diagram “ $\sigma_b - \epsilon_b$,” while the deformations of the high-strength reinforcement are practically in the elastic stage $\epsilon_s < \epsilon_0.2$.
 - (ii) The increase in force in high-strength reinforcement after the concrete of the cross-section or its individual layers reach maximum strength can overlap the decrease in the force in concrete on the descending deformation branch;

it leads to an increase in the total bearing capacity of the reinforced concrete element up to 10%.

13. Calculation of the strength of short centrally compressed vibrated, centrifuged, and vibro-centrifuged columns according to the improved standard approach gave the best results using the local characteristics of concrete, differing in cross-section. Calculation according to the diagram approach in all settings (iterative, approximate, and simplified) showed significantly better convergence with experimental data than calculation according to the method of the Russian Building Regulations. For centrifuged and vibro-centrifuged columns, the diagram approach in any setting (iterative, approximate, and simplified) gives better results when using the local characteristics of concrete than when using the aggregate ones and, even more so, the standard characteristics of concrete.
14. The previously unaccounted for hidden strength reserves of industrial columns of functionally gradient structure, manufactured by centrifugation and vibro-centrifugation, have been identified and determined. The advantages of vibro-centrifuged reinforced concrete columns in comparison with centrifuged ones are determined and formulated.
15. The centrifuged serial standard reinforced concrete column was redesigned and improved for a vibro-centrifuged one, the bearing capacity of which turned out to be 35% higher. To work on the same standard load, the percentage of reinforcement is reduced and the same design indicators of the column are obtained as for the standard one.
16. The research results have been implemented in practical building and designing, in the regulatory document, and in the educational process in three universities of the Southern and North-Caucasus Federal Districts.
17. The developed recommendations and dependencies for determining the local characteristics of centrifuged and vibro-centrifuged concretes make it possible to enter into the calculation the characteristics of concrete differing in cross-section and more fully use the reserves of the bearing capacity of building structures.

Part II

**Cement, Foam, Fiber-Foam Concretes
and Electrophysical Impacts**

Chapter 7

Classification of Electrophysical Methods Regulating the Properties of Cement Concretes



Abstract This chapter presents the classification of electrophysical methods, regulating the properties of cement concretes. Then existing methods of electrophysical (in particular, electrothermal) impact in cement concrete technology are discussed. The electromagnetic activation of mixing water being one of the directions in the field of improving the technology for preparing concrete mixtures is considered and experimental results are presented. The electrophysical impact on concrete aggregates is treated, too. In this case, the surface is activated by a pulsed discharge, and the specific granulometric composition of the aggregate is provided. The electrophysical effect on cement slurries and concrete mixtures is studied with classification of corresponding processes and phenomena. By this, the polarization and electrization of concrete mixtures in an external high-voltage electric field in the process of vibration compaction change their rheological properties and create an activated nonequilibrium state of the system improving physical and mechanical properties of the final concrete structure.

Keywords Electrophysical methods · Electromagnetic activation · Mixing water · Cement slurries · Polarization · Electrization

7.1 Existing Methods of Electrophysical Impact in Cement Concrete Technology

Electrophysical methods are one of the most effective, but still far from fully studied influences on the processes occurring at the interfaces in concrete. These include the next operations: (i) processing in AC and DC magnetic fields, (ii) application of an external electric field, (iii) exposure to a high-frequency electric field, (iv) discharge-pulse activation, (v) ultrasonic activation, and (vi) acoustic activation.

The analysis of literary sources and the experience of using electrophysical methods for activating hardening processes [1, 2, 4, 5, 10, 16–18, 20, 21, 29, 31–37, 40–42, 53, 61–64, 67–71, 74–78, 80, 82, 90–92, 94, 96, 110, 114, 115, 295–298, 300, 312, 314] revealed a significant variety of these methods both in relation to technical means and parameters of their implementation and in relation to the objects

Table 7.1 Classification of electrophysical methods used in concrete technology

Research object, concrete mixture components	Supposed mechanisms and results of exposure
Water	(i) Processing in AC and DC magnetic fields (ii) Treatment with DC (iii) Processing by high-voltage electric discharge
Placeholders	Aggregate processing by high-voltage spark discharge (electric pulse technology)
Cement	(i) Electric polarization by microcurrents (ii) High-voltage unipolar electric polarization (iii) Combination of low- and high-voltage corona activation
Cement dough (aqueous dispersion of binder)	(i) Processing in a magnetic field (ii) Combination of magnetic treatment with mechanical activation
Concrete mixture	(i) Processing in AC and DC magnetic fields (ii) Application of external electric field (iii) Simultaneous superposition of magnetic and electric fields (iv) Application of high-frequency electric field (v) Discharge-pulse activation (vi) Ultrasonic activation (vii) Combination of ultrasonic activation with compression pressure

for which they are used. The systematization of these data is presented in Table 7.1. For the sake of brevity, Table 7.1 presents a classification related only to the technology of cement concretes, as the most typical representatives.

Treatment of aqueous dispersions of binders in a magnetic field [195] leads to an increase in the strength of cement stone up to 50% due to an increase in the number of crystallization centers and strengthening of bonds in contacts as a result of dipole-dipole and dipole-ion interactions and convergence of particles due to orientation in a magnetic field. At the same time, it is important to choose the right moment for processing the cement dough.

In [239], it is recommended to act with an AC magnetic field on pasty dispersions due to the difficulty in the development of the coagulation structure. As a result, the formation of a denser initial stone structure occurs. At the same time, it is advisable to perform the activation with a DC magnetic field immediately after the start of setting. Due to the orienting effect of a DC magnetic field on the dipoles of the molecules of the liquid phase, the processes of thermal diffusion slow down. As a result, the concentration of interparticle contacts increases (the strength in the first day of hardening increases to 40%).

An external electric field, like a magnetic one, affects in heterogeneous systems the kinetics of adsorption and dissolution, the structure of water, sedimentation processes, as well as the conditions for the formation and growth of crystals [159, 161, 224, 225]. Moreover, it was established in [159] that the electric field not only changes the structure of dispersed systems but also affects the phase composition of the cement hardening products, namely, an increase in the degree

of condensation of gel-like calcium hydrosilicates, an increase in the conversion of alite, and the finely dispersed nature and stability of crystalline hydrates $\text{Ca}(\text{OH})_2$ and ettringite.

In the mechanism of the influence of the electric field on the hardening of cement systems, one should also take into account such a phenomenon as the removal of moisture from the surface of the cement dough [159, 193, 215]. At the beginning of the action of an electric field under the action of electrophoresis, the packing of particles in the cement dough is compacted. As a result, free moisture appears on the surface of the sample. As a result of the processes of moisture evaporation under the action of the field and the gradual structuring of water, which intensifies with an increase in the electric field strength, after the induction period, migration capillaries are formed in the cement dough. It decreases the physical and mechanical properties of the cement stone. Therefore, to obtain the maximum effect from exposure to an electric field, it is necessary to take into account both the constructive and the destructive nature of polarization.

It is noted in [20, 229] that prolonged exposure to a high-frequency electric field on the cement slurry does not increase the final strength (and may even lead to its loss), but only accelerates the growth of the strength of the samples.

Another viewpoint on this matter is given in the study of A. I. Biryukov and A. N. Plugin [33]. According to them, as a result of exposure to a high-frequency electric field, the structure of the cement stone improves and its strength increases. At the same time, the hydration processes are influenced by a change in the thickness of the electric double layer (DEL) on the surface of the particles of the initial substance and its hydration products, the deformation of the DEL, and the occurrence of diffusion flows within and outside the DEL. As a result of these processes, the kinetics of hardening processes changes and the hydration of the binder intensifies.

From the analysis [20, 33, 159, 161, 195, 239], it follows that the electrophysical treatment of cement-water dispersions with magnetic and electric fields is expedient to carry out at the first stage of structure formation, when a coagulation structure is formed. At this moment, the destruction of the adsorption layer or the shielding shell of hydrates occurs. At the later stages of hardening, the considered external influences have a negative effect on the strength of concrete due to the destruction of the forming crystallization structure.

Many studies are devoted to ultrasonic [18, 128] and acoustic [168] effects on concrete mix. When exposed to ultrasound on the cement paste, the cement stone is compacted due to the appearance of radiation (compression) pressure arising from standing waves; acceleration of the process of dissolution of solid particles takes place by breaking the adsorption and diffuse layers by standing waves [18]. Moreover, ultrasonic vibration is accompanied by a dispersing effect due to the cavitation process, which causes the formation of many microcracks in the crystals, facilitating the destruction and dissolution of the substance. The degree of hydration also increases due to the displacement of the gas phase from the surface of the cement particles.

The shortcoming of this effect is the shallow penetration and rapid attenuation of ultrasonic vibrations in the cement paste, which complicates the use of this method on a production scale [18].

I. N. Akhverdov [10] talks about the possibility of combining ultrasonic vibrations and compression pressure. In this case, water is displaced from diffuse shells, and water shells of minimum thickness remain on the surface of the cement particles. Such a combined action of the filtration process and gravitational forces makes it possible to compact not only the cement dough but also the concrete mixture.

According to [168], the best effect is achieved with acoustic activation of the concrete mixture, and not its mortar part or cement dough. This is due to the removal of dust particles from the surface of the filler, as well as adsorbed and trapped gases from microcracks. The result of these processes is an increase in the adhesion of the aggregate to the cement stone.

Foam concrete is a type of concrete, so it can also be exposed to electrophysical methods, while obtaining quite effective results. In particular, the work of A. A. Malodushev [154] notes the positive effect of electric heating of the foam concrete mixture on the rate of strength gain of the foam concrete. At the same time, on the first day of hardening, an increase in the strength of foam concrete is observed up to 90% of the branded one. It allows one to obtain the finished material in the conditions of the building site.

In the work of N. V. Maltsev [155], much attention is paid to the effect of DC field on the physical and mechanical characteristics of foam concrete. It is noted that as a result of the impact of the field on the freshly laid foam concrete mixture for 2 h, the processes of hydration and aggregation are intensified, the slump of the foam concrete mixture is reduced by 3–5 times, and the strength of the foam concrete is increased by 20–30%. The study also provides the results of the influence of a high-frequency AC applied to the mixture for 2 h on the processes of structure formation and the strength of the finished foam concrete. An increase in the mutual adhesion of all solid components of the dispersed mixture and an increase in the strength of foam concrete by 40–50% were recorded. At the same time, it was theoretically and experimentally established that the influence is effective at frequencies of the electric field close to the frequencies of natural oscillations of charged particles of the binder [155].

Foam concrete mixtures at the molding stage are complex multiphase systems consisting of solid, liquid, and gaseous phases. The main task of research in obtaining a sufficiently strong and porous material is the creation of a homogeneous cellular structure and the formation of interpore partitions with high physical and mechanical characteristics.

Based on a thorough analysis and synthesis of theoretical and experimental studies, it can be concluded that in the technology of foam concrete, an electrophysical method of influencing the foam concrete mixture during its formation can be effective. At the same time, acceleration of the chemical interaction between the components of the foam concrete mixture, an increase in the viscosity of the medium, and the formation of a denser and stronger frame built from the material of interporous partitions are expected [155, 156].

Modern science attaches great importance to the study and improvement of relevant and progressive building materials, which undoubtedly include the whole variety of cement concretes.

Concrete is a unique material due to its diversity and the possibility of its application in any area of building. Concretes are among the most widely used in the building industry due to their reliability and durability. It is also a very economical material, because most of its volume falls on the fraction of aggregates of various types, which can also be industrial waste, which makes the use of concrete even more expedient. Their constructive and thermal insulation properties are of greatest importance [121, 175–177].

The role of electrical technologies in the concrete industry is growing every year. Many researchers attempt to identify, consider, and explain the physicochemical processes that occur during electrical action on various types of cement concretes as detailed as possible.

An analysis of scientific and technical literature in this direction shows the variety of scientific works carried out.

The studies of B. A. Krylov, E. L. Leus (electric heating) [126, 135, 170], A. N. Plugin (high-frequency currents) [208–211], V. I. Vereshchagin (activation of dispersed materials in a corona discharge), L. A. Yutkin, A. I. Berezhny, A. I. Kudyakov (activation of mixtures by electric impulses) [128], etc. have been devoted to electric methods of influence in the concrete technologies.

The carried out analysis allows one to systematize at present the methods of electrophysical action on concretes.

7.1.1 *Electrothermal Action on Concretes and Concrete Mixtures*

In Russia, due to climatic conditions, one of the most effective and frequently used methods is the electric heat treatment of concrete [174].

For the first time, electric heating of concrete using electrodes was described by Brund and Bolin in 1931. They found that this type of treatment not only protects concrete from low temperatures, but also accelerates its hardening. In the USSR, in 1932, large research institutes and laboratories began to engage in research in the field of electric heating of concrete. Namely, in the USSR, the theory was developed and electric heating into the practice of construction was introduced.

Electric heating of concrete mixtures, induction heating (in an electromagnetic field), and contact and convection heating of structures using electric heating devices [18, 135, 160] are widely used. A detailed description of these methods is given in Table 7.2.

When preheating the concrete mixture, the temperature could be increased to the required level for any period of time. Electric heating devices supply heat to the

Table 7.2 Methods of electrical heat treatment of concrete and application areas

Name	Principle and application	Methods and modes of electrical heat treatment
1. Electric heating (i) Electrode	Heating monolithic concrete structures by passing current through the entire thickness of concrete (columns, floors, partitions)	Slow rise in temperature; rods, strings, and strips of sheet steel are used as electrodes, sewn onto the inner surface of the formwork
(ii) Peripheral	Heating peripheral zones of the concrete of massive and medium massive constructions	Maintaining the temperature in the peripheral layers 5–10 °C lower or at the same temperature as the inside; the electrodes are fixed to the formwork or special boards
(iii) Using reinforcement as electrodes	Heating structures reinforced with separate, unconnected rods	The temperature of the concrete near the reinforcement should not exceed 90 °C
2. Heating of concrete in electromagnetic field	Heating linear structures with reinforcement uniformly distributed over the cross-section (columns, tubes, silos)	The temperature at the contact of the reinforcement or mold with concrete should not exceed 90 °C
3. Electric heating (i) Using high-temperature infrared heaters	Heating by applying heat directly to concrete or formwork	Heating is carried out with protection of non-decked surfaces from moisture loss
(ii) Using low-temperature heaters	Heating by electric heaters installed in the formwork or in heating mats and blankets	Heat loss to the environment must be prevented
4. Electric heating (i) Preliminary electric heating of the concrete mixture	Warming up the mixture outside the mold. The mixture is stacked and compacted while hot	The required strength is achieved by thermos curing or additional heating
(ii) The same, with repeated vibration in the molds	The mixture is placed in mold, compacted, then reheated and vibrated again	The same

concrete surface from the sources of converting electricity into heat. Heat is transferred to the inner layers of the structure by convection or radiation.

In an electromagnetic field, concrete heating is carried out by the transfer of heat from the steel elements of the formwork, reinforcement, and embedded parts heated by eddy currents.

The principle of using electric current to heat concrete is based on the Joule-Lenz law:

$$Q = 3600I^2RT \quad (7.1)$$

where Q is the amount of heat released during the passage of current, I is the current strength, R is the electric resistance of heated concrete, and T is the time of passage of the current.

Of all the components of concrete, only water dramatically lowers its electric resistance, due to which freshly laid concrete is a conductor that heats up when an electric current passes through it. In this regard, when electrically heating concrete, it is necessary to strive to maintain a sufficient amount of moisture in it [135].

However, the heating of the concrete mixture and the course of electrode processes lead to a significant consumption of electricity [18].

The existence of various methods of electrical heat treatment allows in each specific case (for various designs and conditions of their manufacture) one to choose the most effective and economical one [160].

Extensive scientific research in this area was carried out by such Russian and foreign schools as Bauman Moscow State Technical University (G. A. Nikolaev), National Research University, "MEI" (V. I. Krutov), National Research Institute of Reinforced Concrete (S. A. Mironov, B. A. Krylov, A. V. Lagoida), Stoletov Vladimir State University (A. S. Arbeniev), Tomsk State Architector-Building University (A. I. Gnyrya), Saint-Petersburg State Architector-Building University (A. A. Malodushev), University of Rhode Island (A. Schenck), and University of Massachusetts (R. Feynman). The processing parameters recommended by them cover a wide range of electric voltage and current values: 30–70 V and 80–500 A [36, 135, 182, 317].

The work of I. A. Fizdel "Heating of monolithic joints of reinforced concrete structures in winter" emphasizes that the quality of monolithic joints and nodes in structures can have a decisive effect on the strength and durability of buildings. The author claims that high-quality embedding and accelerated hardening are achieved by electric heating. During the construction process in the winter, after the installation of partitions and flooring, all embedded parts and joints were cleared of ice and snow. In hard-to-reach places, this was done by thermal thawing. The concrete was heated using electric heating devices equipped with heating elements of the Lianozovsky Electromechanical Plant (Moscow). The length of such a heating element was 0.8 m, its power was 1 kW, and the voltage was 36–65 V. The heating elements were mounted in special casings made of sheet steel 4 mm thick. In each casing with a length from 1.5 to 2.5 m, 2–4 heating elements were attached. They were attached to the joints and insulated from above with heat-shielding slag wool mats. Depending on the temperature and windiness of the weather, the duration of heating the structures varied from 2 to 6 h.

Another method of electric heating of concrete, considered in this work, is the manufacture of a box, inside of which, in a layer of sand, heating elements with a power of 4 kW are located in one row. It is proposed to warm up for 4 days at $T = 60\text{--}70^\circ\text{C}$. Heating of joints in the basement parts of buildings, according to the author, should be done through lateral inflows of concrete with rod or floating electrodes. Electric heating in columns should be carried out through rod electrodes or nails in wooden formwork.

S. A. Mironov in his work "Hardening and the technology of winter concrete" describes the essence of the thermos method with preliminary electric heating of concrete mixtures. This method is widely used in the construction of monolithic structures. The author notes the efficiency of the thermos method in comparison with

conventional methods of heat treatment. The high initial temperature of the concrete (60–80 °C) and the insulation of the formwork with effective insulating materials significantly increase the cooling time. This allows one to provide a set of the required strength during cooling at any outside air temperatures. For electric heating, a bunker with a capacity of 0.7–1.5 m³ with built-in electrodes made of sheet steel with a thickness of 4–5 mm is used. The electrodes are secured with dielectric spacers. The electrodes have special leads for connecting current-carrying wires. The voltage during warming up is 220–380 V. At the same time, it is imperative to observe safety precautions. Electricity consumption per 1 m³ depends on the outside temperature. For example, in the regions of the Far North, the consumption ranges from 80 to 100 kW·h. After the mixture has been heated to a predetermined temperature, the voltage is turned off and the bunker is transported to the place of laying using a crane.

S. A. Mironov emphasizes that, in connection with significant heat losses from the surface of the formwork in the Far North, electrode peripheral heating should be used. The expediency of using the thermos method with preliminary electric heating of concrete mixtures at a temperature from –30 °C to –40 °C and a wind speed of up to 10 m/s is noted. In some cases, the use of the thermos method is successfully combined with the use of antifreeze additives—hardening accelerators. The research of the National Research Institute of Reinforced Concrete (Moscow) on the introduction of a method for preliminary electric heating of concrete mixtures in areas of permafrost has shown the possibility of using the method throughout the year.

V. D. Kopylov in his work “The effect of electric heating on the properties of concrete” describes studies of deformations and moisture loss in heavy and light concrete in the process of electric heating and reveals their influence on the conductive properties, strength, and frost resistance of the material, carried out at the Research Institute of Reinforced Concrete of the USSR State Construction Committee under the leadership of S. A. Mironov and B. A. Krylov.

Portland cements of the Bryansk, Mikhailovsky, and Voskresensky plants were used as binders. Limestone crushed stone (a grain size of 5–20 mm) and river sand (up to 5 mm) were used as aggregates for heavy concrete. Aggregates for expanded clay concrete were gravel (up to 20 mm) and sand obtained as a result of crushing gravel.

The study of deformations was carried out on samples heated without formwork at 40, 60, 80, and 98 °C. The duration of heating was 15, 30, 60, and 180 min, and the intensity of the temperature rise varied from 7 to 320 °C per hour. At the same time, specimens with an open, non-decked surface and covered with a polyethylene film were warmed up in order to prevent moisture loss.

The research results showed that the nature and magnitude of deformation is influenced by the heating temperature, heating rate, material structure, as well as mass transfer with the environment. When concrete is heated in a covered state, an intensive increase in its size occurs during the period of temperature rise, and in an open state, it takes place only in the first period of heating. This is due to the fact that an environment with high humidity and temperature is formed in the space between the covering film and the concrete; therefore, moisture shrinkage is not observed in

the covered samples. At the same time, in open samples, such shrinkage takes place due to significant evaporation of moisture.

Moisture loss affects the increase in concrete resistivity. As a result, it is not possible to provide the required heating mode. Also, the specific resistance of concrete increases when it freezes, which is associated with a decrease in the amount of free liquid phase due to the transition of water into a solid state of aggregation. With an increase in the specific resistance of concrete, it becomes difficult to heat it up with an electric current. Therefore, the authors recommend starting electric heating in winter conditions no later than the moment when the temperature reaches 0 °C at the contact of concrete with the electrode.

It was found that with an increase in the heating rate, the deformations increase, and the strength decreases. Experimental data have shown that the rate of temperature rise should not exceed 20 °C.

B. D. Trinker et al. in their work “Features of the use of concrete from preheated mixtures in winter” note that by using mixtures heated to the temperature of isothermal holding, it is possible to improve the quality of reinforced concrete structures. In preheated concrete, physical and chemical reactions proceed more fully, strength increases, and there are no structural disturbances in the initial period of hardening, which are inevitable with conventional methods of heat treatment of concrete. The number of pores decreases, which is confirmed by a comparison of the values characterizing the rate of concrete saturation with water after contact heating at 50–70 °C, thermos curing of concrete obtained on the basis of mixtures preheated to a temperature of 50–70 °C, and concrete of normal hardening.

The authors note that the main characteristics of concrete with a working seam of concreting are water resistance in the direction of the surface of the working seam of concreting and the electrical conductivity of various sections of concrete saturated with an electrolyte solution.

The preheated electrically heated concrete mixture was placed up to half the height of a rectangular mold, heated to the same temperature, and kept in a thermostat. Then, a new layer of freshly heated mixture was laid on top, and the sample was kept in a thermostat for a specified time in a mode simulating the conditions for the formation of a working seam of concreting.

During the tests, the water pressure in the hydraulic system of the setup increased by 1 atm every hour up to 20 atm. The electrical conductivity of the concreting seam zone was determined with the passage of an AC with a frequency of 1000 Hz. The studies used sample beams with 40 cm long and a concreting seam in the middle, saturated before testing with a 10% sodium chloride solution.

Based on experimental data, the authors conclude that in the case of using preliminary electric heating of the concrete mixture to 50–70 °C, the water permeability of concrete with concreting joints differs little from the water permeability of normal hardened concrete. The greatest difference is observed with a break in concreting for more than 20 h. In this case, the water permeability of the heated concrete is slightly higher than the water permeability of normal hardened concrete.

The difference in the electrical conductivity of the concreting seam zone and monolithic concrete increases in proportion to the degree of completeness of the hardening of the previously laid concrete by the time the fresh concrete is laid.

Laying a mixture with a lower temperature on the hot surface of previously laid concrete leads to an increase in the permeability of the concreting seam zone by 4–7 times and an increase in the electrical conductivity of this zone by 3–6 times. Placing a heated concrete mixture on a colder surface of previously laid concrete does not affect the quality of concrete with a concreting seam. The authors note similar results when determining the adhesion strength of concrete layers.

The shortcomings of the preheating method include the relatively rapid loss of mobility of the concrete mixture. Experimental data have shown that the mobility decreases by about 30% and the water-to-cement ratio by 0.04–0.07. As a result, when electrically heating the mixture, it is recommended to add sulfite-yeast mash additives in an amount of 0.2–0.3% of the cement mass, which helps to slow down the loss of mobility of the mixture and also reduces cement consumption.

This method has been successfully used in the process of concreting special constructions. The strength of concrete from an electrically heated mixture at the time of cooling to 0 °C ranged from 30% to 67% of R_{28} , which also ensured the formation of the required structure by the time of freezing.

The authors conclude that it is advisable to use concrete from electrically heated mixtures for the building of high-rise, special, and other constructions operated in aggressive conditions.

The work of E. M. Buben and I. G. Mikhailov “Circular conveyor for the production of structures from hot concrete” notes that in the production of structures in horizontal forms, difficulties arise associated with the placement of specialized posts for electric heating of the concrete mix, heat retention during the molding process, and the provision of optimal modes of additional heat treatment of structures.

As an example of new technological equipment, taking into account the specifics of electric heating of the concrete mixture, a circular conveyor for the manufacture of stair flights, platforms, and balcony slabs, introduced at the reinforced concrete construction (RCC-21) plant of the Dniprozhelezobeton trust in Dnepropetrovsk (Ukraine), is presented. The use of this conveyor allows one to carry out (i) one-portion heating of the concrete mixture into two structures (directly above the place where the structures are molded), (ii) hot molding in vertical two-compartment thermoforms with double-sided heating, and (iii) quick laying of heated mixes within 1–2 min without significant loss of heat and mobility. Moreover, (i) the mixture is effectively compacted using repeated vibration; (ii) additional heating of products is carried out immediately after their molding in vertical thermoforms; and (iii) control is performed over the observance of temperature regimes of electric heating and heat treatment.

The authors of this work conclude that the circular conveyor allows the transition to continuous electric heating of the concrete mixture and the molding of concrete structures.

In the work of B. A. Krylov, A. F. Kravchenko, and S. Kh. Yarlushkin "On the issue of electroosmotic treatment of hardening concrete," it said about the phenomenon of electroosmosis (the movement of liquid in porous bodies under the influence of DC) and about its effect on the dehydration of the concrete mixture and on the physical and mechanical properties of concrete. The authors note that the amount of dehydration of a concrete mixture when processing it with a DC depends not only on the phenomenon of electroosmosis but also on other factors: the initial amount of water, the type of concrete and the method of its compaction, hydrostatic pressure, current parameters, electroosmotic action, hydrostatic pressure, temperature difference, and vibration.

The authors conclude that the electroosmotic dehydration (no more than 3%) of the concrete mixture is insignificant for almost all types of concrete, which is confirmed by theoretical and experimental studies. The greatest influence on the amount of concrete dehydration is exerted by vibration and mass transfer due to the presence of temperature gradients. It is also noted that the physical and mechanical properties of concrete that have undergone electroosmotic treatment practically do not change and do not differ from concrete that has not been treated.

The paper points the shortcomings of electroosmotic dehydration of concrete mixture:

- (i) Due to hydrolysis phenomenon, accompanying the treatment, the steel electrode is oxidized, and the polarity change leads to corrosion of both electrodes, which leads to a decrease in the durability of the equipment and a deterioration in the appearance of concrete structures.
- (ii) Special generators and areas for their installation and maintenance personnel are required, which leads to an increase in the cost of concrete structures and an increase in the complexity of manufacture.
- (iii) The inclusion in the operation chain, touching the preparation of concrete structures, and an additional technological redistribution require a significant amount of time (up to 60 min).
- (iv) There is a need for reliable and durable filters in production conditions, which must ensure strict geometric dimensions of concrete structures, to be one of the electrodes and filter water.

However, according to the authors, electroosmotic dehydration in combination with other methods of processing concrete mixture can give a certain effect.

V. Ya. Gendin and Yu. A. Ilyevsky in their work "A new method for determining the stackability of a concrete mixture heated by an electric current" note that the existing methods for controlling the stacking of a heated mixture have a number of shortcomings.

This paper describes a technique developed by the authors, which eliminates the shortcomings of existing methods for determining the stackability of an electrically heated concrete mixture. The tests are proposed to be carried out on a vibro-viscometer with heating the mixture, which is a box with internal dimensions of $200 \times 200 \times 200 \text{ mm}^3$. Its bottom and two opposite walls are made of textolite, and the other two walls are made of metal and are used as plate electrodes. The side

surfaces and the bottom of the box are insulated with wooden plates or foam. The voltage up to 250 V is supplied to the wall electrodes. For mixtures with very high resistivity, it is necessary to bring a mains voltage of 380 V to the electrodes.

A simultaneous determination of the specific electrical resistance is carried out by the “ammeter-voltmeter” method. The temperature of the mixture during heating and cooling is measured with a technical thermometer. After reaching the set temperature, the voltage is removed from the electrodes. The concrete mixture is kept in a viscometer until the determination of the stackability.

7.1.2 *Electromagnetic Activation of Concrete Mixture Components*

In addition to the pretreatment of concrete mixtures based on cement with the release of heat, which is electric heating, there are a number of methods for such processing without heat release. Many well-known electophysical methods (magnetic, electromagnetic, electrical) are accompanied by a high consumption of electric energy. In this regard, low-energy-intensive methods of exposure are promising.

These methods include electromagnetic activation of both mixtures as a whole and their individual components. Low-power activation treatment allows solving the urgent problem of increasing the efficiency of concrete and reinforced concrete structures at low energy costs.

An electromagnetic field is understood as a type of matter characterized by a set of mutually connected and mutually conditioning electric and magnetic fields [37].

A magnetic field is a force field acting on moving electric charges and on bodies with a magnetic moment.

Electric field arises around particles and bodies that have an electric charge and provides interaction between charges. The property of such a field is the action of a certain force on a charge placed in it, and its quantitative characteristic is intensity, namely, a vector physical quantity that characterizes the field at a given point and is numerically equal to the ratio of the force acting on a stationary test charge placed at this point to the value of a given charge.

The main quantity in the electric field of a conducting medium is the current density $\bar{\delta}$, a vector quantity directed along the field strength. It is numerically equal to the ratio of the current i flowing through an element of the surface s (perpendicular to the direction of the field strength at a given point) to the value s of this surface.

The efficiency of electrical activation of a concrete mixture or its components depends on the processing parameters. These parameters (voltage and current) oscillate in the range of 1–10 kV and 0.01–1 A during the electric pulse treatment of the cement-water suspension and 10–100 kV and 10–100 mA during the activation of cement and aggregates in a corona discharge [167].

Activation is such a treatment of a component or mixture of components, as a result of which their properties are used more fully. In studies on activation, the goal

is to increase the mechanical strength of the hardened cement stone, mortar, and concrete, to intensify their hardening or to reduce the consumption of cement without reducing the specified strength of the material [63].

Electromagnetic Activation of Mixing Water

One of the directions in the field of improving the technology for preparing concrete mixtures is the activation of mixing water. The existing methods of such activation practically do not require a change in the main technological process of preparing a concrete mixture; however, they significantly contribute to the improvement of its physical, mechanical, technological, and operational properties. By this they allow the control of hardening process and reduce the consumption of the binder. This, in turn, leads to a significant increase in production efficiency [302].

In the USSR, in the 1960s, the electromagnetic activation of mixing water began to be used at PermNIIUM (Perm). The result was an increase in the strength of concrete up to 26% [69].

The effect of the electromagnetic treatment of mixing water for the manufacture of concrete products in the studies of Yuzhgiprocerement (Kharkov) was expressed in an increase in strength up to 10–25% [115, 118]. This technology was used, in particular, at the Novocherkassk Reinforced Concrete Structures Plant, which made it possible to increase the strength up to 30% [2, 99, 193].

A generalized classification of water electroactivation methods is shown in Table 7.3.

In [92], the effect of a high-frequency electric field on water was studied. The analysis showed that the greatest increase in the strength of a cement stone prepared from a mixture of cement with water, activated by the above method, was obtained as a result of pulsed high-frequency treatment of water for 4 min. However, it is noted that for effective application of this method, it is necessary to create powerful high-frequency equipment with a wide range of intensity.

When water is treated with DC, water acquires pronounced acidic and alkaline properties at the anode and cathode, respectively. By this, the following water parameters are changed: temperature, density, dielectric constant, redox potential, surface tension, etc.

Table 7.3 Methods of electrical impact on mixing water and their brief description

Electrical impact method	Characteristic method
Homogeneous DC field	It is associated with the phenomena of electrophoresis, polarization interaction, and electrocoagulation
Homogeneous AC field	It is associated with the phenomenon of polarizing coagulation
Homogeneous DC and inhomogeneous AC fields	It is based on the effect of dielectrophoresis and dipolophoresis
Electric discharge	It is characterized by the following physicochemical stages: pre-breakdown, electrical breakdown, and post-discharge phenomena

The current strength, activation time, and the degree of water mineralization are important. For example, with an increase in the degree of mineralization, the acidic and alkaline properties of water sharply increase. When using such water, an increase in concrete strength by 20–25% was observed.

In [167], the results of studies of water treatment with a uniform external DC field of duration from 1 to 15 min and a strength of 10–35 V/cm are given.

The samples were manufactured with a water-to-cement ratio of 0.32. As a result, the increase in the strength of the samples made with the treated mixing water was 33% in comparison with the strength of the control samples. It was found that when using mixing water, pretreated with an electric field, hardening is accelerated in the early stages. Also, there is an increased plasticity of concrete mixtures on such water. The structure of the samples molded from mixtures on mixing water treated with an electric field was denser and more homogeneous.

In [168], it was found that the discharge-pulse activation of the mixing water leads to an increase in the strength of the cement stone. When cement is mixed with water activated by discharges, hydration proceeds more intensively, which leads to an increase in early and brand strength.

Electromagnetic activation of mixing water is widely used in Russia and abroad. It should be noted that the most important aspect is the correct choice of the activation mode. Otherwise, the effect of processing will be absent or lead to a decrease in the quality parameters of the material [167].

In [242], the effect of impulse activation of the sealer on the strength and durability of concretes at high-voltage liquid breakdown (electrohydraulic effect) was investigated. As a result of studying the microstructure of concrete, it was revealed that activated water significantly deepens the process of dissolving minerals and improves structure formation.

Electrophysical Impact on Concrete Aggregates

In scientific research works to find a solution to the problem of improving the quality of concrete, there are also proposals of methods for activating aggregates.

The authors of [92] argue that the activation of pieces of rocks in various liquid media under conditions of pulsed electrical breakdown leads to an improvement in the properties of conglomerates. The use of a filler activated in this way makes it possible to significantly increase the mechanical strength.

In this case, the surface is activated by a pulsed discharge, and the specific granulometric composition of the aggregate is provided. The contact layers of the aggregate crushed in this way are strengthened. This is due to the penetration of cement hydration products into numerous pores and microcracks on the highly developed surface of the aggregate. An increased bond strength between the surface of the activated aggregate and water is also noted.

In [167], it is pointed that the activation of sand in an electrostatic field of negative polarity leads to an increase in the workability of mortar mixtures. The combination of surface-active substances and sand activation in a field of positive polarity leads to

an even greater increase in the diameter of the spread. The author experimentally established that the effect of plasticization depends on such parameters of electrical processing as the electric potential of the contact electrode and the moisture content of the activated sand and additives.

The activation of dispersed fillers by electric voltage slows down structure formation at the initial time and leads to an intensification of the growth of plastic strength at the stage of formation of the condensation-crystallization structure.

Upon electrical activation of the surface-active centers of the fillers, the porosity and the contact density change.

Electrophysical Effect on Cement

Optimal parameters of cement electric activation depend on the mineralogical composition of clinker and cement additives [32, 67, 70, 80]. The most effective addition to cement for activation was ground quartz.

The activation of cement by electric voltage at optimal parameters can increase the strength of concrete by 25–30%; when concrete hardens in normal humidity conditions, the activation of cement affects the period of 14–21 days. The concrete of increased strength on activated cement is characterized by an increased degree of cement hydration (including alite), an increase in the degree of condensation of a hydrosilicate gel, a redistribution of the differential porosity, and a decrease in the total porosity of concrete [167]. In this case, the parameters of electrical processing are characterized by a combination of low-voltage high-density current or high-voltage corona discharge [92].

The use of high-voltage corona-activated cement in mortar mixtures improves rheological characteristics [92]. When cement is activated by a high-voltage corona discharge, an increase in the strength of artificial building conglomerates is also provided, especially at a later time of hardening. This effect also leads to an increase in the strength of cement-based materials.

In [296], it was found that cement activated by high-voltage current has a higher rate of dissolution and hydrate formation processes, and when activated, an increase in the energy of its interaction with water and the strength of the cement stone are ensured.

The author of [167] came to the conclusion that activation of the surface of dispersed particles of binding systems using high-voltage unipolar electric polarization increases the reactivity of the surface, which improves the physical and mechanical properties of concretes.

The study of the influence of electric fields, including in discharges on the hardening and properties of binders, is devoted in the works of A. D. Bulat, S. A. Eremina, G. N. Gavrilova, N. P. Gorlenko, V. A. Matvienko, Yu. S. Sarkisov, V. I. Vereshchagin, etc. [41, 68, 75, 76].

Electophysical Impact on Cement Slurries and Concrete Mixtures

Cement suspensions and concrete mixtures from the standpoint of their electrical activation differ in the dynamics of surface properties and the ratio between solid and liquid phases. To achieve the maximum effect from electric activation, it is necessary that the polarity of the contacting electrode coincides with the sign of the integral charge of the surface of the dispersed phase.

In this case, it is necessary to take into account the possible overcharging of the surface of the solid phase when using additives or during the hardening process. The positive potential is in combination with the addition of alkaline salts, and the negative potential is in combination with the compounds containing aluminum or calcium ions.

It was found in [167] that the efficiency of electrical activation of concrete mixtures increases with an increase in current density to 0.4 mA/m^2 , and at higher values it stabilizes.

The dependence of the increase in strength of the cement stone and concrete activated by polarization on the strength of the electrostatic field at values of more than 10^5 V/m obeys a logarithmic law.

In the process of electrical activation of cement suspensions, intensive evaporation of moisture is observed at an electric field strength of $3 \times 10^4 \text{ V/m}$. This leads to an increase in the density of the dispersed system and the formation of migration channels in the stone structure.

The author [167] studied two methods of activating a concrete mixture by electric polarization: (i) in a concrete mixer during mixing and (ii) in a holding bin before placing into molds.

The efficiency of electrical activation of concrete mixtures depends on parameters such as the magnitude of the electrical potential and the processing time.

Moreover, an economical way is described for affecting the concrete mix with low-power electrical impulses. In this case, the important factors are the electric field strength at the time of discharge and the number of pulses. It is concluded that when a concrete mixture is exposed to discharges of high-voltage electrical impulses of low power, electrophoretic concentration and electrocoagulation of dispersed components are achieved [167].

The concrete mixture is a dispersed system of the type “dielectric in an electrolyte solution.” The processes occurring in mixtures under the action of an electric field and their brief characteristics are presented in Table 7.4.

The influence of an external electric field on the process of structure formation of concrete mixtures was considered in the works of [82, 200]. It was noted that the electric field changes surface states in heterogeneous systems. Due to this, the kinetics of adsorption and dissolution, sedimentation processes, the properties and structure of water, and the conditions for the formation and growth of crystals change. The following changes were also revealed in the phase composition of cement hardening products under the influence of an electric field: (i) an increase in the degree of alite conversion, (ii) a finely dispersed nature and stability of Ca

Table 7.4 Classification of processes and phenomena in concrete mixtures under the impact of electric field

Type of processes or phenomena	Brief characteristic
Electrochemical	Redox reactions at the “electrode-dispersed system” interface
Polarizing	Surface phenomena: electrode; dispersion medium molecules; electrolyte solution; double electric layer around dispersed particles
Electrodiffusiophoresis and electrocoagulation of polarized particles	Displacement and precipitation of dispersed phase particles
Dispersed system electrization	Accumulation of charge at interphase boundary

(OH)₂ crystalline hydrates and ettringite, and (iii) an increase in the degree of condensation of gel-like calcium hydrosilicates.

In the works of [74, 75, 167], it was found that an AC field at different frequencies causes a different relationship between hydrated neoplasms in cement stone. The effect of fields with a frequency from 175 to 1575 Hz was considered.

At 175 Hz, the dissolution of aluminate phases and an increase in the content of calcium hydroaluminates and portlandite Ca(OH)₂ were observed. The frequency of 650 Hz affects the dissolution of the belite phases. The range of 1100–1575 Hz is the range of frequencies influencing the dissolution of alite components. There is an increase in the amount of hydrosilicates of calcium and portlandite and a decrease in the amount of hydroaluminate phases.

As a result, it is concluded that a selective change in the rate of dissolution of various mineral components can cause, in turn, changes in hydration neoplasms, which will optimize their ratio in cement stone.

In [167], attention is paid to the removal of moisture from the surface of the cement dough under the influence of an electric field on the hardening of cement. We are talking about the compaction of the package of particles in the test under the action of electrophoresis and the appearance of free moisture on the surface of the sample. Under the action of the field, water evaporates, but after some time it becomes structured, and its removal from the surface is difficult.

With increasing field strength, the structuring is enhanced. The moisture on the surface and its subsequent evaporation ultimately leads to the formation of migratory capillaries in the cement dough. As a result, the physical and mechanical properties of the cement stone deteriorate and a destructive rather than constructive nature of polarization is noted.

Intense and long-term (up to 30 min) exposure of the high-frequency field to the cement slurry leads to its strong heating, as well as vaporization and drying of the solution, which leads to a loss of strength [167].

In [92], it is noted that the effect of a high-frequency electric field with a frequency of up to 68 MHz and a power of up to 4 kW, regulated by changing the strength of the anode current of the generator within 0.5–1 A for a time from 1 to 45 min on a cement slurry, does not lead to a significant increase in the final strength

of the samples, although the rate of hardening and an accelerated increase in the strength of the samples are observed.

In [167], an increasing strength and improving structure of the cement stone when exposed to a high-frequency electric field are pointed out. The author associates the effect of the field on the processes of cement hydration with a change in the thickness of the electric double layer on the surface of the particles of the initial substance and the products of its hydration, with the deformation of the electric double layer, which has a pulsating character and with the appearance of diffuse flows within the electric double layer and outside it. As a result, the kinetics of the hardening process changes and there is an intensive removal of cement hydration products from the surface of its grains.

In [82], the influence of external electric fields on the kinetics of structure formation of cement stone is considered. The ability of the mixture to produce its own electric field is noted. The stage of the kinetics of the process of hardening of mortar mixtures is taken into account, and significant changes in the parameters of the mixture are monitored.

It is proposed to place the solution mixture as one of the two layers of a two-layer capacitor (the second will be a dielectric with a low dielectric constant) and apply a voltage. In such a capacitor, a charge also appears at the interface between the two media, gradually increasing after the voltage is turned on and decreasing when the capacitor is discharged.

Next, the field in the capacitor is examined, and the field strength in both layers is determined. It is noted that at the initial moment of time, the field strength is determined by the dielectric properties, and over time, it is determined by the conductivities. The beginning of the process is taken as the moment of the beginning of the redistribution of charges in the substance. The conclusion is made about the essential role of the law of voltage change on the electrodes.

The performed analysis reveals that as the kinetics develops, the structure formation of the solution mixture changes exponentially. Thus, we can talk about a change in the electric field strength along a steeply falling exponent. As a consequence, it is concluded that the electric field in the solution mixture exists for a longer time when treated with an electric field of constant voltage than when processing with a sinusoidal voltage.

The work of [167] is devoted to the consideration of coagulation under the influence of external electric fields. The authors note that in polar media between particles in an electric field, attraction arises, and, as a result, linear aggregates-chains are formed, oriented along the force lines of field. The removal of the same field leads to the disintegration of such aggregates.

The electrokinetic properties of cement stone determine a number of processes such as adsorption, coagulation, and so on. It has been established that repulsive forces act between the approaching particles during coagulation, and the particles must have sufficient kinetic energy to overcome them. Based on the data obtained, the authors claim that the particle charge has a beneficial effect on colloidal stability. It is concluded that the origin of the repulsive forces should be sought in the interaction of diffuse electrical layers. The interaction between complexes consisting

of colloidal particles and diffuse layers is associated with the deformation of their ionic atmospheres. It is necessary to quantitatively interpret this interaction from the viewpoint of the electric field during the hydration of cements in mortar mixtures.

In [92], emphasis is placed on the fact that the electric field has the strongest effect on the structure of the double electric layer (DEL). It is noted that the polarization of DEL in an electric field causes a change in the thickness of the shell of structured water. This affects the interaction energy between the particles, which ultimately affects the packing density and the conditions for the formation of the hardening structure.

However, according to the theory of DEL polarization, the appearance in the external electric field at the poles of a particle of regions with drops in electrolyte concentrations is accompanied by tangential flows of ions. The concentration of ions along the outer boundary of the DEL changes, the layer deforms, and the surface potential changes. As a result, a dipole moment and a long-range electric field arise outside the DEL.

In [92], the formula for the total interaction energy of particles in an electric field is given as

$$U = U_1 + U_2 + U_3 + U_4 \quad (7.2)$$

where U_1 is the interaction energy of van der Waals-London, U_2 is the energy of electrostatic repulsion due to the coupled charges on the particle surface, U_3 is the interaction energy of particles due to the polarization of the double layer, and U_4 is the energy of interaction of particles caused by the polarization of the material of the particle and the medium.

It is noted in [167] that the kinetics of particle aggregation depends on the strength of the electric field: with an increase in the strength, it increases, and with an increase in frequency, it decreases.

The polarization and electrization of concrete mixtures in an external high-voltage electric field in the process of vibration compaction change its rheological properties and create an activated nonequilibrium state of the system, which contributes to the formation of a more ordered structure of concrete with increased physical and mechanical properties.

The structuring ability of the solid phase of cement-water systems polarizable in an electric field depends on the ratio of the polarity of the surface charge of the filler additives and the polarity of the external electric field, as well as the concentration and valence of the additive-electrolyte cation [312].

Another way to improve the physicochemical characteristics of a cement stone due to the activation of the surface, the liquid phase, and the effect on the morphology of the structure is a discharge-pulse effect. As a result of such activation in pastes of clinker minerals, the time of the induction period is sharply reduced, which indicates an intensive acceleration of the hardening process [168].

In [242], a high-voltage impulse compaction of a concrete mixture is considered. The essence of high-voltage impulse activation is to use the electrohydraulic effect. The medium for obtaining such an effect can be cement dough, cement-sand mortar,

and cast concrete mixture. Studies in the field of high-voltage impulse activation were carried out by S. N. Bershtein, T. N. Mayboroda, B. G. Ryasny, A. I. Savenkov, Yu. M. Strakhov, etc. [234, 282].

7.2 Conclusions

1. In this chapter, the classification of electrophysical methods regulating the properties of cement concretes was performed on the basis of known scientific results. The existing methods of electrophysical impact in cement concrete technology were discussed in necessary details. In particular, the various methods of electrical heat treatment of concrete and application areas were considered.
2. Besides the pretreatment of concrete mixtures based on cement with the release of heat, there are a number of methods for such processing without heat release. Well-known electrophysical methods (magnetic, electromagnetic, electrical) are accompanied by a high consumption of electric energy. Therefore, the low-energy-intensive methods of exposure were studied. Electrothermal impact on concretes and concrete mixtures was treated.
3. A detailed consideration was devoted to electromagnetic activation of concrete mixture components. The electromagnetic activation of mixing water being one of the directions in the field of improving the technology for preparing concrete mixtures was discussed and experimental results were presented.
4. The electrophysical impact on concrete aggregates was treated, too. In this case, the surface was activated by a pulsed discharge, and the specific granulometric composition of the aggregate was provided. The electrophysical effect on cement was also a very important factor, and it was shown that the activation of cement by electric voltage at optimal parameters can increase the strength of concrete by 25–30%.
5. The polarization and electrization of concrete mixtures in an external high-voltage electric field in the process of vibration compaction change its rheological properties and create an activated nonequilibrium state of the system improving physical and mechanical properties of final concrete structure. The electrophysical impact on cement slurries and concrete mixtures was studied with classification of corresponding processes and phenomena.

Chapter 8

Electrophysical Effect on Concrete Mixtures and Their Components



Abstract In this chapter, the mechanism of interaction between the magnetic field and mixing water and its influence on concrete strength is studied. The changes in such parameters as surface tension, dielectric constant, temperature, redox potential, hydrogen ion content, and density in the process of water activation are found in dependence on the strength of the electric current, the activation time, and the degree of water mineralization. A tendency is established to harden the contact layers of concrete aggregates on electric pulse crushing during hardening, regardless of their mineralogical composition. The processing of cement for the preparation of concretes and mortars is considered using mortar mixtures of cement, activated by high-voltage corona discharge. Moreover, the processing of cement dough in concrete is studied and the mechanism of the influence of the electric field on the hardening of cements is explained in addition to the effects at the molecular and ionic levels. Finally, the ultrasonic and acoustic activation of concrete mixtures is reviewed and estimated.

Keywords Mixing water · Concrete strength · Hardening · Concrete aggregates · Mortar · Cement dough

8.1 Treatment of Mixing Water for Concrete

At present, numerous developments are known for the activation of the raw components of the concrete mixture [103–106, 110, 114, 245, 254–260, 268, 270, 272]. Under certain conditions, the combined effect of physical and chemical factors gives a resultant effect, which is by no means the sum of the effects obtained from each exposure separately. The activation of the constituents of the concrete mixture, namely, the aggregate, water, and cement, allows, under certain conditions, one to increase the strength of the concrete.

Of particular interest is the study of the modified state of water, achieved under various physical effects on it [205, 209, 210, 215, 221, 224, 225]. At the end of the last century, the study of the effect of the action of a magnetic field on water and water systems began. The first studies on the use of water modified in a magnetic

field for mixing cement dough and concrete appeared in the mid-1960s. They showed that the use of magnetic water increased the strength of cement samples up to 10.5% and increased the strength of concrete samples up to 33% under plant conditions [1]. The increase in strength depends on the mineralogical composition of the cement. The greatest strength is for cements with a large amount of tricalcium silicate C_3S and tetracalcium aluminoferrite C_4AF (16–17%). Moreover, the increase depends on the strength of the magnetic field and the rate of water flow in the magnetic field. The increase in strength also persists after 7 and 28 days, which indicates a more complete manifestation of the binding properties and not only about the acceleration of hydration processes.

However, the mechanism of interaction between the magnetic field and water is still not clear. There are hypotheses that it seems convenient to divide it into the following three main groups [2]:

- (i) Explaining the observed effect by the action of a magnetic field on impurities in water.
- (ii) Suggesting changes in the structure of water as a result of interaction with a magnetic field.
- (iii) Substantiating the effect by a combination of the action of a magnetic field on the structure of water and its impurities.

The first group includes the works of V. B. Evdokimov, L. D. Kislovsky, S. I. Rempel, T. Vermeiern, etc. They believe that the magnetic field mainly affects the properties of salt ions without changing the structure of water. In this case, “deformation” and coagulation of the salt ions contained in the water occur, which causes a change in the magnetic moment and the charge of the ion. This leads to a change in the crystal lattice of the precipitated solid phase [64].

In the works of [5, 18], electrochemical activation of mixing water is considered. It is shown that in the presence of impurities in water, solvated structures can form, and the pH of water in the near-electrode zones changes. The active state of water is metastable and keeps for a certain time, namely, a relaxation period (from 30 min to several hours). Electrochemically treated water accelerates the process of hydration and structure formation of the cement stone and accelerates the setting process from the hardening of cement in the initial period. The amount of water is reduced by 35%, and the strength of the concrete is increased by more than 50%.

Impurities in water, activated by physical influences, affect the processes of cement hydration and structure formation of cement stone [4, 16, 17]. They play the role of crystallization centers; create an alkaline environment ($pH > 9$); accelerate the dissolution of calcium silicates in cement; reduce the surface tension of water, thereby reducing the water demand of cement dough; and finally, interacting with cement minerals, accelerate chemical processes.

Many researchers are of the opinion that the magnetic field affects the structure of water. Assumptions are made about the possibility of changing the structure of water without impurities. As a result of the polarization of electron clouds in water molecules, the latter acquire an induced magnetic moment directed opposite to the external magnetic field [2]. The energy of hydrogen bonds changes; they bend and break, and this leads to a change in the mutual arrangement of molecules and, thus, in the structure of water.

In [34, 170, 292], the effect of a magnetic field on the mixing water was investigated. Changes in the structure, physicochemical properties of water, and the nature of the interaction of water molecules with each other were observed. The effect of magnetization was determined by the change in the mobility of the concrete mixture and the strength of the concrete samples. The plasticizing effect of the magnetization of the mixing water was established, too. The mobility of the concrete mixture increases by 6–7 cm of the cone displacement, or by 14–15%. The complex effect of the plasticizing effect and the reorientation of water molecules accelerate the process of hydration and hardening of concrete. With the same mobility of the concrete mixture and the same cement consumption, the excess of the concrete strength on magnetized water in comparison with the control concrete made on tap water is 10–12%. An increase in the strength of concrete when using magnetized water leads to a decrease in cement consumption by up to 8%.

The result of the positive effect of magnetic water is presented, which allows one to completely abandon the liquid plasticizer C-3 and obtain a significant economic effect depending on the cost of the additive.

The structure of water can be characterized by an openwork structure with a large number of hydrogen couples. This predetermines its low density and insufficient chemical activity.

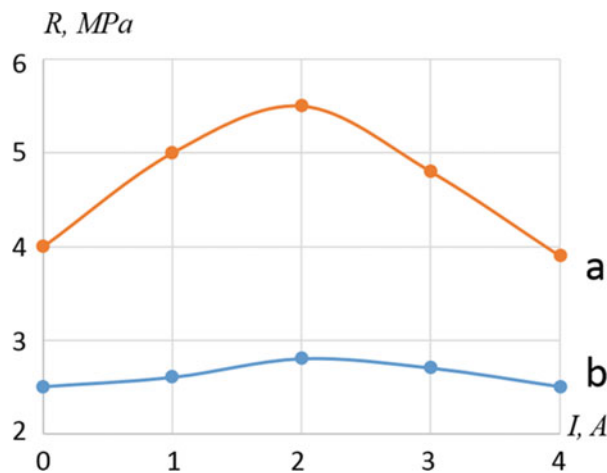
The authors of works [29, 33, 314] propose to destroy such a structure by applying magnetic fields. The effect is judged by the change in the density and viscosity of water after magnetic treatment. The destruction or distortion of the structure of water leads to an increase in the concentration of its contacts with the surface of the solid phase due to broken hydrogen couples, which should increase the adhesive properties of the system. The authors applied the results obtained in the study of the structure formation of the $\text{CaSO}_4 \cdot 0.5\text{H}_2\text{O-H}_2\text{O}$ system. A DC electromagnet was used to magnetize the water with a water flow rate of 1 m/s.

The magnetized water altered the hardening kinetics of the stucco. By selecting the optimal induction of the magnetic field, it is possible to reduce the time of the beginning and end of setting by 20%. The normal density of gypsum decreases, the ultimate strength in compression and bending increases (Fig. 8.1), and the density of neoplasms increases.

From above, it can be concluded that at present there is no unified viewpoint on the nature of the effect of changing the properties of water as a result of the interaction with a magnetic field. This is largely due to the variability of the chemical composition and metastability of the structure of the treated water, the lack of a unified processing technique, and indication of its degree. The reliability of the effect can be even doubted. However, the experimental results obtained on the treatment of mixing water in electric and magnetic fields by most authors give positive results [10, 20, 21, 29, 31, 33, 34]. It can be considered objective evidence that:

- (i) The use of magnetically activated water allows one to obtain concrete structures, the strength of which can increase by up to 50% or more in comparison with concretes mixed with ordinary water.

Fig. 8.1 Dependence of the strength of gypsum samples on the magnitude of the magnetizing current: (a) compressive strength and (b) flexural strength



- (ii) The mobility of concrete mixtures, mixed with magnetized water, increases by 60–120%. Consequently, for mixing mixtures, it is necessary to take 15–25% less magnetized water than ordinary water.
- (iii) The use of activated water accelerates the process of concrete hardening, which will reduce the heat treatment time by 15–20%.
- (iv) Microscopic studies show the formation of a more homogeneous structure and smaller particles of neoplasms.
- (v) Water activation can reduce cement consumption by up to 20%.

Other methods of water treatment appear to be different in the mechanism of action, but close in the final result. Thus, in [10, 20, 21], it was shown that when water is treated with DC, the potential energy of substances dissolved in water deviates from thermal equilibrium. At the anode, water acquires pronounced acidic properties and it shows alkaline properties at the cathode.

In the process of water activation, changes in such parameters as surface tension, dielectric constant, temperature, redox potential, hydrogen ion content, density, and others occur. A quantitative change in the listed parameters depends on the strength of the electric current, the activation time, and the degree of water mineralization.

Experiments have shown that the activation parameters depend on the amount of salts in the water. With an increase in the degree of mineralization, the acidic and alkaline properties of water sharply increase. The use of such water allows one to increase the strength of concrete by 20–25%. The greatest increase in strength was observed when first acidic and then alkaline water were used as mixing water.

If during the treatment with an electric field, soluble electrodes [20] containing aluminum are used, the water will have an increased content of multivalent ions of aluminum hydroxide, which has a high adsorption capacity, has a high dispersion and activity, is evenly distributed in the volume of water, and is a weak acid. When cement is mixed with such water, an active reaction occurs between calcium oxide hydrate, being a strong base, and aluminum hydroxide, being a weak acid.

As a result of the reactions, calcium hydroaluminates are formed, and they are evenly distributed in the system, forming an openwork structure reinforced with chain aggregates. These aggregates serve as ready-made crystallization centers. At these centers, neoplasms crystallize more easily and faster, falling out of supersaturated solutions when the binder interacts with water. The consequence of this process is the acceleration of the hardening processes. Due to its hydroxyl groups, aluminum hydroxide is more easily adsorbed on the binder grains and hydration products, and this leads to plasticization of the cement paste when it is mixed with water, previously treated with the electric field of soluble electrodes.

Also, due to an increase in the concentration of multivalent ions, the diffuse part of the electric double layer is compressed, and the thickness of the ionic spheres decreases. Similar results were obtained when treating water with a high-voltage electric discharge [32, 131, 288, 289].

Experimental studies were carried out on the treatment of water with a uniform external DC field [69, 308–312]. As a result, its stable positive effect on the physical, mechanical, and technological properties of the concrete mixture was revealed. The water was processed for 1–15 min at an electric field strength from 10 to 35 V/cm. The strength values of cement concrete samples with ratio $W/C = 0.32$ on activated water showed an increase in some cases of up to 33%, and the change in strength values at different times of hardening decreased over time, that is, mixing water treated in constant electric and mixing treated in a constant electric field accelerate early hardening.

The results of experimental data on concrete mixtures showed that the mixture prepared with treated water had a cone displacement of 12–14 cm, that is, increased plasticity, and the mixture with ratio $W/C = 0.5$, prepared with ordinary water, had 6–7 cm. Samples prepared with treated water have a denser and more uniform structure.

All of the above gives grounds to draw conclusions about the prospects of studying the electrophysical treatment of mixing water.

8.2 Processing of Aggregates for Concrete

It is not only the mixing water that can be subjected to electrophysical processing. A number of works are known on the electrical activation of the components of the concrete mixture. The activation of mineral components under conditions of pulsed electrical breakdown of pieces of rocks in various liquid media predetermines the improvement of the properties of artificial conglomerates [35–37]. Low-temperature plasma, formed as a result of a high-voltage spark discharge [35] and the rapid release of electrical energy, appears in the electro-pulse technology of destruction and treatment of solids with a working solid.

It was found that the use of a filler obtained by the electric pulse technology leads to a noticeable increase in mechanical strength (up to 26.5%). The main reason for increasing the strength of concrete, according to the authors, is the activation of the

aggregate surface by a pulsed discharge. Moreover, the electric pulse technology provides a predetermined particle size distribution of the aggregate. The state of the surface is determined by physicochemical processes at the boundary between the aggregate and the cement stone and ultimately affects the composition and properties of the contact zone.

As a result of the studies carried out on the development of the physical foundations and technology of electric pulse destruction, a number of features of the crushing solids that are fundamentally different from mechanical destruction have been established [35, 314]. The most important of them, in relation to the subsequent use of the solid after electric pulse crushing for the preparation of concrete mixtures, include:

- (i) More developed roughness and reactivity of the crushing product surface.
- (ii) A newly formed surface enriched in purity.
- (iii) Directional receipt of a modified surface.
- (iv) Less defectiveness of the crushing solid due to the selective nature of the trajectory of the electric discharge channel and the process of destruction along various inclusions and cleavage planes that make up the rock of minerals.

A tendency has been established to harden the contact layers of aggregates on electric pulse crushing during hardening, regardless of their mineralogical composition [37]. This is due to the penetration of cement hydration products into numerous pores and microcracks located on the material surface activated in the process of electric pulse grinding, followed by coalescence of this surface with the cement stone.

This is confirmed by the presence of a more developed contact zone with diffuse contours in samples with a filler on electric pulse crushing.

The bond strength of water with the surface of the electric pulse activated material is higher. The mobility of a concrete mixture made on the product of electric impulse crushing is much lower than on aggregates of mechanical crushing.

8.3 Processing of Cement for the Preparation of Concretes and Mortars

Particular attention is paid to the activation of cements. The surface of Portland cement grains has an electrical “relief” due to active centers of different polarity [40]. These centers affect the basic properties of cement (water demand, setting time, hardening rate) and determine the intensity of interfacial interaction processes: adsorption, dissolution, and hydration. By regulating the concentration and activity of surface centers, it is possible to directionally change the hydration capacity of the cement.

This regulation can be carried out quite effectively with the help of electrical and electromagnetic influences [41, 42, 312, 316, 317]. In this case, the parameters of

electrical processing are characterized by a combination of low-voltage (30–220 V) high-density current (0.1 A/cm^2) [20] or high voltage (40–100 kV) in a corona discharge [42].

The use of mortar mixtures of cement, activated by high-voltage corona discharge [300], leads to noticeable changes in rheological characteristics. In a wide range of changes in the water-to-cement ratio (0.4–0.7), mortar mixtures on activated cement have better rheological characteristics in comparison with the control samples.

The technology of activation of cement by high-voltage corona discharge provides, along with an improvement in rheological properties, a significant increase in the strength of artificial building conglomerates, especially at later periods of hardening. It has been established that the impact on the binder with a high-voltage corona discharge leads to an increase in the strength of materials based on cement stone by 30–40% and fine-grained and heavy concrete up to 28% [295].

The treatment of clinker minerals with a high-voltage corona discharge has a significant effect on the electronic-ionic structure of the dispersed phase and, consequently, on the colloidal-chemical properties of hydration products. The effect of corona discharge on C_3S and $\beta\text{-C}_2\text{S}$ increases the hydraulic activity of clinker and changes the conditions of crystallization of hydrated formations, increases the content of calcium hydrosilicates, and also contributes to a decrease in the content of Ca(OH)_2 , which in turn leads to an increase in the activity of Portland cement and materials based on it.

A study of the activation of the initial cement by electric polarization by microcurrents ($1\text{--}5 \text{ mA/cm}^2$) of high voltage (50–30 kV) in a breakdown-free mode [296] showed that with optimal parameters of the field strength and the time of its application, an increase in the strength of the cement stone by 12–15 MPa and an increase in concrete strength by 5–8 MPa are provided. It was found that cement activated by high-voltage current has a higher rate of dissolution and hydrate formation. The activation of cement by a high-voltage current provides an increase in the energy of its interaction with water and the strength of the cement stone. The highest efficiency of cement electric activation remains in the first 2 hours after treatment and decreases within 30–36 hours.

It was shown in [297] that activation of the surface of dispersed particles of binding systems using high-voltage unipolar electric polarization increases the reactivity of the surface, especially at the site of the functional groups $\equiv \text{Si} - \text{OH}$ and $= \text{Si} = (\text{OH})_2$, which improves the physical and mechanical properties of concrete, including silicate. The dependence of the adsorption capacity of quartz dispersions in a potassium chloride solution on the parameters of the electric polarization of ground quartz sand with a specific surface area of $300 \text{ m}^2/\text{kg}$ was studied using pH-metry. It was found that the electric polarization of ground quartz leads to a change in its adsorption capacity at the site of active surface centers. The optimal values of stress and polarization time of the silicate component of the binder silicate concrete provide an increase in the strength of concrete by one grade.

8.4 Processing of Cement Dough for Concrete

Of great practical importance is the experimentally established fact that the activation of aqueous dispersions of binders in a magnetic field leads to a greater and stable increase in strength than the treatment of mixing water in a magnetic field [2]. Treatment of dispersions in a magnetic field with a strength of 6000 Oe in the first period of structure formation [2] gives an increase in strength after 28 days of hardening by 43% (an increase in the strength of cement samples when processing mixing water under the same conditions is only 26%).

Treatment of the same dispersion in a magnetic field at a magnetic field strength of 1000 Oe leads to a decrease in the strength of 28-day-old specimens of normal hardening, although in this case a slight increase in strength is observed after 3 and 7 days. The magnetic field increases the number of crystallization centers and shortens the induction period [2, 67].

In a magnetic field, the work of formation of a nucleus decreases, an orienting effect on the growth of crystals is manifested, and the activation energy decreases. In this case, a large number of particles appear per unit volume, and the dispersion of neoplasms increases. Magnetic action leads to mechanical destruction of the created framework and to the orientation of particles in a magnetic field. As a result of this, bonds in contacts are strengthened due to dipole-dipole and dipole-ion interactions, as well as due to the approach of particles caused by orientation. This promotes an increase in the number of contacts per unit volume and directed growth of crystals, which leads to a large contact area.

Experimental data show that magnetized water has the greatest effect on the process of structure formation of tricalcium silicate dispersions [2]. In dispersions of tricalcium aluminate, this effect at the first stages of structure formation is insignificant, and during the formation of the spatial framework of the crystallization structure due to large destructive phenomena, the samples obtained in unusual water give large discrepancies in the strength values. The greatest influence of magnetized water on the process of structure formation of tricalcium silicate dispersions can be explained based on the concept of the effect of a magnetic field on the mixing water. This effect consists in an increase in the number of crystallization centers as a result of the orienting effect of the magnetic field on the ions of substances dissolved in water.

In tricalcium silicate dispersions, where a significant part of the gel-like mass exists for a long time, the crystallization pressure is negligible, the spatial structure has elasticity and a certain plasticity, and therefore, additional crystallization centers favorably affect the strength of the hardened material. In addition, calcium salts in industrial water contribute to an increase in the dispersion of neoplasms in the process of hydration of tricalcium silicate.

It was shown in [68] that the effect of an AC magnetic field on a binder dispersion leads to positive results only when the dispersion is processed in a pasty state. The effect of an AC magnetic field is associated with the difficulty in the development of the coagulation structure. The result is a denser initial stone structure. The use of a

DC magnetic field is effective after the start of setting. DC magnetic field orientation acts on the dipoles of molecules of the liquid phase and hinders thermal diffusion. It contributes to an increase in the concentration of interparticle contacts (an increase in daily strength up to 30–40%).

The combination of magnetic treatment of cement-water dispersions with mechanical activation [2], including vibration, can be of great practical importance. By the end of the first stage of the structure formation process, a loose spatial framework of coagulation structure is formed, on the basis of which a condensation-crystallization structure arises. At this moment, vibration destroys the defective coagulation structure. It leads to the formation of a stronger and more perfect coagulation structure as a result of the convergence of particles and an increase in the number of coagulation contacts caused by dispersing the grains of the original binder and imparting additional energy to colloidal particles to overcome the energy barrier. The formation of a condensation-crystallization framework of a hardened material based on a stronger and more perfect structure leads to high mechanical performance.

An external electric field has an effect similar to the magnetic field on the process of structure formation [67, 70]. In heterogeneous systems, the electric field changes the surface states and, due to this, the kinetics of adsorption and dissolution, sedimentation processes, the structure and properties of water, and the conditions for the formation and growth of crystals. The influence of external electric fields on such phenomena as electrophoresis and electroosmosis in dispersed systems and removal of moisture from the surface are also possible. Studies have established [70] that, in addition to structural changes, the electric field introduces features into the phase composition of cement hardening products: an increase in the degree of alite conversion, finely dispersed nature and stability of $\text{Ca}(\text{OH})_2$ crystalline hydrates and ettringite, and an increase in the degree of condensation of gel-like calcium hydrosilicates.

At different frequencies, AC field causes a different ratio between hydrated neoplasms in the cement stone [71, 74]. So, at a frequency of 175 Hz, the aluminate phases dissolve: the content of calcium hydroaluminates and portlandite $\text{Ca}(\text{OH})_2$ increases. The frequency of the electric field equal to 650 Hz is the range of frequencies influencing the dissolution of the belite phases. The frequency range influencing the dissolution of alite components is 1100–1575 Hz; the amount of hydrosilicates of calcium and portlandite increases, and the amount of hydroaluminate phases decreases. A selective increase in the rate of dissolution of certain mineral components can cause corresponding changes in hydration neoplasms, which will optimize their ratio in cement stone [74].

In explaining the mechanism of the influence of the electric field on the hardening of cements, in addition to the effects at the molecular and ionic levels, one should take into account such a phenomenon as the removal of moisture from the surface of the cement dough [70]. In the initial period after turning on the electric field, the packing of particles in the cement dough is compacted under the action of electrophoresis, and free moisture appears on the surface of the sample. This moisture is evaporated by the field. After a while, the water is structured and its removal from

the surface is difficult. This structuring is enhanced with increasing electric field strength. The supply of moisture to the surface and its evaporation lead at the setting stage after the end of the induction period to the formation of migration capillaries in the test. The latter should cause a deterioration in the physical and mechanical properties of the cement stone.

Therefore, to obtain the maximum effect of stimulating the hardening of cement by an electric field, it is necessary to take into account both the constructive and destructive nature of polarization. Prolonged, intense exposure (15–30 min) of a high-frequency electric field [75] to the cement slurry also leads to its strong heating, vaporization, and drying of the slurry, which can cause a loss of final strength.

A high-frequency electric field is a common method of influencing a material. However, it was shown in [75] that the effect of a high-frequency electric field (a frequency of 40 and 68 MHz and a power of 2–4 kW, regulated by changing the strength of the anode current of the generator within 0.5–1 A) for 1–45 min on the cement mortar does not lead to a significant increase in the final strength of the samples. It only contributes to an increase in the rate of hydration hardening and a faster growth in the strength of the samples.

At the same time, in the work of [76], an increase in the strength and improvement of the structure of a cement stone as a result of exposure to a high-frequency electric field are established. Moreover, its effect on the processes of cement hydration is associated with a possible change in the thickness of the double electric layer on the surface of the particles of both the initial substance and the products of its hydration, with the deformation of the double electric layer, which has a pulsating character, as well as with the appearance of diffusion fluxes within the double electric layer and beyond. All this, according to the authors, leads to a change in the kinetics of the hardening process and intensive removal of the products of hydration of the binder from the surface of its grains.

In the initial period of activation, the influence of electric and magnetic fields on water-cement mixtures is manifested. The simultaneous imposition of magnetic and electric fields on the system does not lead to their neutralization, since the spheres of their influence are separated [77].

The magnetic field mainly acts on ions dissociating from dissolved salts. Ionic action causes the appearance of an induced magnetic moment in water molecules and, accordingly, a change in a number of its properties. The DC field of high intensity leads to the phenomena of water electrolysis and electroosmosis. With further processing of the cement slurry with electric discharges, the specific energy increases, and with each subsequent pulse, the action of the shock wave, which causes cavitation phenomena in air inclusions, increases. The action of the electromagnetic field decreases, which leads to mechanical dispersion of the cement and uniformity of morphology.

It is believed that at the stage of “ionization,” the minimum energy value is in the range from 0.1 to 0.6 kJ/dm³, and at the stage of dispersion, it is in the range from 4.8 to 6 kJ/dm³ [78]. Practical results show (i) the concrete mixture treated with high-voltage and spark discharges has an increased number of new formations, which are evenly distributed and practically have no pores; (ii) mortar and concrete mixtures

reduce their mobility; and (iii) the increase in the strength of the samples ranges from 10% to 30%.

8.5 Concrete Mixture Treatment

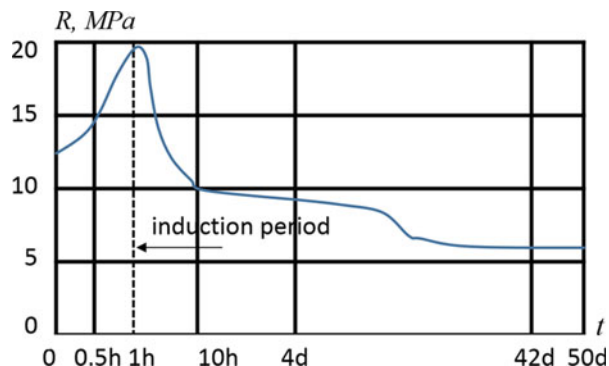
Technological methods aimed at improving the quality of concretes and mortars are associated, first of all, with the impact on the formation of the structure of the cement stone. Its properties after the completion of the hardening processes depend not only on the characteristics and state of the binder but also to a large extent on the time of physicochemical and physicomechanical effects on the process of formation of the structure. So, the high quality of the material is ensured when technological influences are produced at certain periods of the development of a dispersed structure.

In the early stages of structure formation, the electrostatic force has a positive effect and is useful, destroying the adsorption layer or the shielding shell of hydrates [298]. In the later stages of hardening, when the interface changes, the electrostatic force has a negative effect, leading to the destruction of the forming crystallization structure, which leads to a decrease in the strength of the concrete. Therefore, the electrophysical treatment of cement-water dispersions with electric and magnetic fields is advisable to be carried out at the first stage of structure formation, that is, during the formation of a coagulation structure, when the cement particles are covered with films of hydrated neoplasms that impede the access of water to the clinker grains.

Based on the data of numerous experiments, the dependence of the strength of concrete on the time of the beginning of treatment with an electric and magnetic field has been established, which is a curve of the relative strength of concrete that has experienced the effect of fields at the early and later stages of hardening (see Fig. 8.2).

The actual strength of untreated concrete, hardening under normal conditions, is taken as one hundred percent strength.

Fig. 8.2 Dependence of concrete strength on the time of beginning the treatment with electric field



One of the types of electrophysical impact on concrete mix is discharge-pulse activation. The main factors affecting the suspension processed by discharge pulses are a shock wave, a powerful flow of liquid diverging and converging in the discharge zone, acoustic fields of wide spectra, electromagnetic radiation, and heat and light fluxes.

High-voltage electrical discharges [53, 61, 78, 80, 82] and spark discharges [61] can be used as discharge pulses. The current density in the main stage of the discharge can reach 10 A/cm^2 [61], with the formation of electromagnetic fields in a wide frequency range. The energy density released in the discharge channel is more than $5\text{--}10 \text{ J/cm}^3$. The plasma temperature of the discharge channel can reach several thousand degrees. Due to the low compressibility of the liquid and its inertia, at a high expansion rate of the discharge channel, a shock wave arises, the pressure amplitude of which can reach several thousand MPa. This wave propagates in the medium being treated in the form of a compression wave with a steep leading edge. Propagating in all directions of the discharge channel, the wave acts on the liquid and the particles located in it [61].

The impact on the concrete mixture with a high-voltage electric discharge [77, 78] was carried out using electric discharge devices at an operating voltage of up to 100 kV and a number of discharges from 50 to 300. The energy consumption was $1.6\text{--}10 \text{ kJ/dm}^3$. Improvement of methods of influence has ensured a decrease in energy consumption. The fundamental effect of high-voltage electric and spark discharge on the mixture is the observance of the conditions:

$$E_s \geq i; \quad (8.1)$$

$$E_s \geq d, \quad (8.2)$$

where E_s is the specific electrical energy introduced into the volume, e_i is the energy providing the ionization of the mixture, and e_d is the energy providing dispersion of cement particles with destruction of their crystal lattice.

Our review of the electrophysical effects on the concrete mixture and its components would be incomplete without considering the ultrasonic and acoustic activation of concrete mixtures, where processes similar to electrophysical effects are possible. A number of researches and monographs on ultrasonic and acoustic activation are known [53, 62, 63].

The possibility of using ultrasound as a mean of influencing a cement gel is largely associated with the formation of cavitation bubbles in a liquid medium [53, 62]. There are two processes going on here. Ultrasonic action accelerates the process of dissolution of solid particles, since when standing waves occur, the adsorption and diffuse layers are disturbed, and cavitation phenomena cause the formation of many microcracks in crystals, facilitating the destruction and dissolution of the substance. As a result, the active surface and the rate of dissolution of the solid phase increase. Moreover, the gas phase is displaced from the surface of the cement particles, which leads to more complete hydration [62].

During sonication of aqueous dispersions of clay minerals [53], structural bonds between the dispersed phase and the dispersion medium are broken and primary aggregates are destroyed; some dispersion of the particles begins. Subsequently, ultrasonic influence as a result of dispersion, the release of a large amount of free surface energy, and the distribution of particles and hydration films promote the gradual formation of a new, more compact, and durable structure. Ultrasonic action on clay minerals was carried out at an oscillation frequency of 19.5 kHz, the amplitude of the alternating ultrasonic pressure was 0.6 MPa·s, the vibration amplitude of the dispersed phase particles was 2.42 μm , and the particle acceleration amplitude was $8.6 \times 10^4 \text{ m/s}^2$.

It has been shown that under the simultaneous action of ultrasonic vibrations and compression pressure [62], the adsorbed water dipoles of the diffuse layer are reformed, air is displaced from the surface of the cement particles, and their almost complete hydration occurs. On the surface of the particles, water shells of minimum thickness remain.

It was shown in [63] that the acoustic activation of the concrete mixture itself is more effective in comparison with the activation of its mortar part and, moreover, of the cement paste. It is assumed that not only the cement grains but also the aggregate is subjected to acoustic action. Carbonate film and dust-like particles are removed from its surface, and adsorbed and trapped gases are removed from microcracks. All this ultimately leads to a significant increase in the adhesion of the aggregate to the cement stone. Activation was applied to concrete mixtures on cements with a specific surface area of $5000 \text{ cm}^2/\text{g}$, for which an increase in compression strength of 20–30% for moderately plastic, 30–35% for plastic, and 35–55% for cast mixtures were obtained.

8.6 Systematization of Ideas About the Mechanisms of Electrophysical Effects on the Concrete Mixture and Its Components

Due to the variety of proposed mechanisms, we present them for all methods in comparison (Table 8.1), which allow us to perform certain generalizations.

Thus, of the whole variety of mechanisms, the most frequent references are (i) ionization of a mixture by means of electrophysical action on impurities in water, (ii) changes in the structure and properties of water, (iii) modification of the solid phase surface, and (iv) dispersion of cement particles. In this case, the most promising methods providing such results, in our opinion, are the electric-discharge treatment of the components of the concrete mixture and the impact on the concrete mixture with magnetic fields.

At the same time, the contradictory opinions of various authors on a number of issues are obvious, for example, in the mechanism of the effect of mixing on water. Also, many authors believe that electrophysical effects contribute to a decrease in the

Table 8.1 Mechanisms of action of various electrophysical methods on concrete components and concrete mixture

Electrophysical methods	Supposed mechanisms of influence
Magnetic water treatment	(i) Changes in the properties of salt ions included in the composition of water [4, 5, 16–18] (ii) the structure of water remains unchanged [4, 5, 16–18] (iii) changes in the structure and properties of water [2, 29, 31, 33, 34] (iv) changes in the properties of salt ions and the properties of water [10, 20, 21]
Water treatment with DC	(i) the effect on the salt of substances dissolved in water [20] (ii) change in the properties of water [20, 69] (iii) increase in the adsorption capacity of the solid phase [10] (iv) compression of the diffuse part of the double electric layer [10]
High-voltage electric discharge water treatment	(i) Influence on the structure of hydrogen bonds in water [32] (ii) changes in the properties of salt ions and the properties of water [32]
High-voltage spark discharge treatment of aggregates: Electro-pulse technology	(i) Obtaining a modified surface [35–37] (ii) less defectiveness of the crushing product [35–37] (iii) increase in the roughness and reactivity of the surface of the crushing product [35–37] (iv) enrichment according to the purity of newly formed surfaces [35–37]
Electric polarization of cement by microcurrents	(i) Activation of the surface of cement grains [296]
High-voltage unipolar electrical polarization of silicate components	(i) Enrichment according to the cleanliness of the grain surfaces [297] (ii) increasing the reactivity of surfaces at the site of the functional groups $\equiv \text{Si} - \text{OH}$ and $= \text{Si} = (\text{OH})_2$ [298]
Combination of high- and low-voltage corona activation of cement	(i) Influence on the electronic-ionic structure of the dispersed phase [42, 295, 300] (ii) dispersion of cement grains [42, 295, 300]
Processing of cement dough in magnetic field	(i) Changes in the properties of salt ions included in the composition of water [195] (ii) orientation of particles in magnetic field [195] (iii) increase in the number of crystallization centers [161, 195] (iv) destruction of the emerging framework of the coagulation structure [195, 239]

(continued)

Table 8.1 (continued)

Electrophysical methods	Supposed mechanisms of influence
Processing of cement dough in electric field	<ul style="list-style-type: none"> (i) Acceleration of the diffusion of water to the solid phase and hydrates into the solution [29, 160, 201, 239] (ii) acceleration of the processes of dissolution and hydration [17, 160] (iii) increase in the number of crystallization centers and the rate of their nucleation; reduction in the induction period [100, 160, 201, 239] (iv) acceleration of reactions on the C₃S surface [74, 160, 239]
Combination of magnetic treatment of cement dough with mechanical activation	<ul style="list-style-type: none"> (i) Destruction of the coagulation structure by vibration [2] (ii) dispersion of cement grains [2] (iii) changes in the structure and properties of water [2] (iv) change in the kinetics of adsorption and dissolution [2]
Concrete processing in AC and DC magnetic fields	<ul style="list-style-type: none"> (i) Changes in the properties of salt ions included in the composition of water [296] (ii) orientation of particles in magnetic field [195] (iii) increase in the number of crystallization centers [161, 195] (iv) destruction of the coagulation structure being created [195, 296] (v) Destruction of the shielding shell of hydrate formations [1] (vi) destruction of the crystallization structure at the late stages of hardening [1]
Concrete processing by electric field	<ul style="list-style-type: none"> (i) Changes in the kinetics of adsorption and dissolution [159, 161] (ii) changes in the structure and properties of water [31, 34]
Simultaneous exposure of the concrete mixture to electric and magnetic field	<ul style="list-style-type: none"> (i) Changing the properties of water [208] (ii) changes in the properties of salt ions included in the composition of water [296] (iii) observed such phenomena as water electrolysis, electroosmosis, and low-frequency dielectric dispersion [296]
High-frequency electric field application	<ul style="list-style-type: none"> (i) Reducing the thickness of the electric double layer [33]
Discharge-pulse activation	<ul style="list-style-type: none"> (i) Ionization of the mixture [208, 296] (ii) change in the thickness of the electric double layer [33, 77] (iii) dispersion of cement particles with destruction of their crystal lattice [208, 296]

(continued)

Table 8.1 (continued)

Electrophysical methods	Supposed mechanisms of influence
	(iv) activation of the liquid phase and an increase in the number of active centers on the surface of the binder and their additional excitation [286]
Ultrasonic activation	(i) Destruction of the solid phase [18, 128] (ii) acceleration of the process of dissolution of solid particles [18, 128] (iii) displacement of the gas phase from the surface of cement particles [18]
Combination of ultrasonic activation with compression pressure	(i) Reducing the thickness of the double electric layer [62] (ii) displacement of the gas phase from the surface of cement particles [62]
Acoustic activation	(i) Removal of carbonate film and dust particles from the surface of cement and filler [168] (ii) displacement of the gas phase from the surface of solid particles [168]

electrical double layer around the solid phase. However, there is an opinion that electric pulse activation enhances the electrostatic interaction of particles, which increases the thickness of the adsorption film and, accordingly, decreases the packing density. There are many contradictions in the characteristics of the resulting concrete.

In most cases, there is no correct provability of the proposed mechanisms of the processes, which confirms the need for their further studies.

8.7 Conclusions

1. In this chapter, the electrophysical effects on concrete mixtures and their components were considered in necessary details. First, treatment of mixing water for concrete was performed. The mechanism of interaction between the magnetic field and mixing water and its influence on concrete strength was studied on known experimental results. The changes in such parameters as surface tension, dielectric constant, temperature, redox potential, hydrogen ion content, and density in the process of water activation were found and the quantitative changes in the above parameters depend on the strength of the electric current, the activation time, and the degree of water mineralization.
2. The processing of aggregates for concrete was discussed. A tendency was established to harden the contact layers of aggregates on electric pulse crushing during hardening, regardless of their mineralogical composition.
3. The features of the processing of cement for the preparation of concretes and mortars were considered. The use of mortar mixtures of cement, activated by

high-voltage corona discharge, leads to noticeable changes in rheological characteristics.

4. The processing of cement dough in concrete was studied and the mechanism of the influence of the electric field on the hardening of cements was explained in addition to the effects at the molecular and ionic levels. Moreover, the removal of moisture from the surface of the cement dough due to this effect was considered, too.
5. The electrophysical effects on the concrete mixture and its components were reviewed and the ultrasonic and acoustic activation of concrete mixtures considered, where processes similar to electrophysical effects are possible. Finally, a systematization of ideas on the mechanisms of the electrophysical effects on the concrete mixture and its components was performed.

Chapter 9

Features of Electrophysical Impact on Mortar and Concrete Mixtures



Abstract In Chap. 8, a method for activation of concrete mixtures in a high-voltage AC field at the stage of mixing is developed, allowing one to obtain concretes with increased physical, mechanical, and operational properties. With this, the degree of hydration of cement clinker minerals and Portland cement is increased together with the content of neoplasms compared to non-activated binding systems. The influence of the position and the presence of varnish coating of electrodes on the efficiency of electric activation of foam and fiber-foam concretes are investigated. The possibility of regulating and controlling the physical and mechanical properties and structure formation of these concretes with activation by low-energy AC impact and its influence on porosity and compaction of interporous partitions are proved. Experimentally, the optimal modes of low-energy processing of foam and fiber-foam concrete mixtures with AC field are revealed.

Keywords Concrete mixture · High-voltage AC field · Foam · Fiber-foam concretes · Low-energy AC impact

9.1 Optimization of the Parameters of Electric Treatment of Concrete Mixtures According to the Criterion of Concrete Strength

To create conditions under which the beneficial effect of electric impact at the mixing stage can be manifested to the greatest extent, it is necessary to establish the optimal parameters of electrical processing. These include the following: the value of the potential, the specific area of the electrodes (the ratio of the area of the electrodes to the volume of the processed mixture), and the duration of the electric impact during mixing [242, 244, 274–276, 278].

The electrical activation of the concrete mixture during the mixing process was carried out in a laboratory mixer. The magnitude of the potential applied to the electrodes was monitored with a kilovoltmeter, and the current with a microammeter.

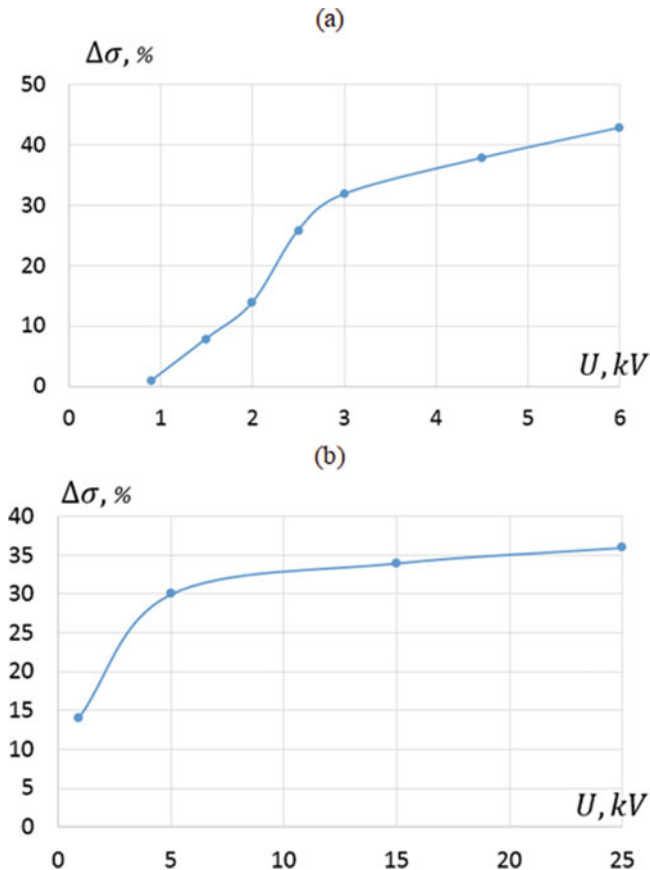


Fig. 9.1 Dependence of the increase in the strength of concrete, electrically activated in the AC (a) and DC (b) fields, on the magnitude of the electric voltage

During the research, the basic composition of fine-grained concrete mixture was used: $S = 1266$ kg, $C = 633$ kg, and $W = 323$ l per 1 m^3 (where S is the sand, C is the cement, and W is the water).

At the first stage of research, the dependence of the strength of fine-grained concrete, activated in AC and DC field with mixing, on the value of the potential applied to the electrodes was studied. The duration of the electrical treatment is taken equal to 180 s, which corresponds to the technological duration of mixing, and the specific area of the electrodes is $3.4 \text{ m}^2/\text{m}^3$.

The dependence of the increase in strength on the magnitude of the electric voltage in Fig. 9.1 shows that a significant increase in strength occurs when an AC voltage of 3–6 kV and a DC voltage of 5–25 kV are applied.

Violation of the equilibrium state of DEL around the cement particles under the influence of AC field and the appearance of ionic flows inside and outside the DEL in

this connection lead to an acceleration of the processes of dissolution and hydration and coagulation structure formation.

This will help to improve the structure and strength properties of the hardened cement stone. This can be manifested to the greatest extent with a combination of external electrical action and mechanical movement of particles of a dispersed system during mixing.

This assumption is confirmed by the results of a study of the influence of an electric field (AC, DC, rectified half-wave), when it is applied to a concrete mixture during mixing and an immobile mixture immediately after preparation.

The research results show that the effect of a DC field on a stationary concrete mixture has a negative effect on strength and to the greatest extent when a negative potential is applied to both electrodes (up to 20–25%). This is probably due to the fact that, due to the effect of electric orientation at a negatively charged surface, the structuring of the hydration layer is enhanced [69], and the diffusion movement of ions, mass transfer, and, accordingly, dissolution are hampered. This is consistent with the opinion of the authors of [297] on the “freezing” effect of the electrostatic field on the dissolution process. The slowdown in hydration activity at an early stage affects the decrease in the concrete strength.

When mixing the concrete mixture, dispersed particles continuously change their position in space and orientation relative to the vector of lines of force of the electric field. In this case, accordingly, the double electric layer of particles, polarized under the influence of the electric field, is deformed and the orientation of the dipoles of liquid phase changes. Periodic deformation of the DEL, as well as the movement of the liquid relative to the interface, which occurs during mixing, leads to the appearance of tangential flows of ions and an increase in mass transfer near the interface. At the same time, the dissolution process is activated, and the number of mutual contacts increases, which is reflected in an increase in the strength of concrete up to 30–35% in comparison with the control sample.

When an AC field of low frequency is applied to a stationary mixture, pulsating deformation of the DEL and continuous tangential ion fluxes occur, which, according to A. I. Biryukov and A. N. Plugin et al. [33–36, 208–211], promotes the acceleration of the removal of hydration products into the volume and, accordingly, the acceleration of dissolution.

However, the manifestation of these processes is limited, since they occur only in the direction of the vector of the force lines of field. This also limits the number of possible additional contacts in the system: interaction of dispersed particles with each other and dissolved ions with dipoles of the liquid phase. In this case, the increase in concrete strength is 20–25%.

The most effective is the effect of AC field on the concrete mixture in the mixing mode. The total influence of the AC high-voltage field and mechanical action causes the strongest violation of the DEL equilibrium and creates a new nonequilibrium state in the dispersed binder system, which leads to the activation of the processes of dissolution and hydrate formation. This is confirmed by the largest increase in concrete strength up to 40–45%. Strength changes upon application of a rectified

(half-wave) field are insignificant; therefore, further studies were carried out upon activation in AC and DC high-voltage fields.

The influence of the factor taking into account the geometric parameters of the electrodes and their location on the housing was studied in two stages. Initially, the influence of the placement of electrodes along the height of the housing wall was studied. On the basis of a study of the compressive strength of cube specimens with an edge of 2×10^{-2} m, made of cement stone ($W/C = 0.3$), it was found that the most advantageous is the placement of electrodes along the entire height of the wall of the concrete mixer housing. This is, apparently, due to the fact that with such an arrangement the maximum probability of uniform hit of the entire volume of concrete mixture into the active zone of action of a high-voltage electric field is achieved.

9.2 Influence of the Composition of the Concrete Mixture on the Efficiency of Electrical Activation

The efficiency of electrical treatment also depends on technological factors, such as the composition of concrete, water-to-cement ratio, the type of additives introduced, and others [115, 118, 121, 124–127, 135, 137].

The study of the influence of technological factors was carried out with optimal parameters of electrical processing: voltage is 6 kV (AC field), 25 kV (DC field); specific area of electrodes is $3.4 \text{ m}^2/\text{m}^3$; and the duration of electric impact is 180 s.

The mobility of fine-grained mixtures was estimated by the value of the immersion of the StroyTsNIIL cone, and the workability of conventional mixtures was estimated by the displacement of a standard cone.

The results of studies of the effect of the water-to-cement ratio on the strength of fine-grained concrete and concrete with a coarse-grained aggregate are shown in Tables 9.1 and 9.2 and in Figs. 9.2 and 9.3.

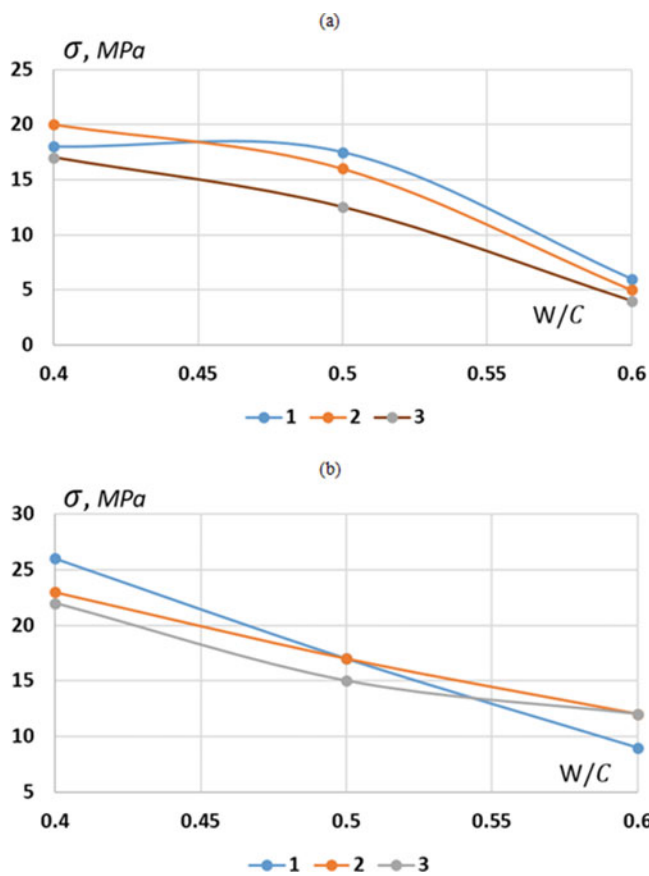
The presented data show that for fine-grained concrete, the relative change in strength with an increase in the water-to-cement ratio increases. This is due to the fact that the electric field promotes a more intense interaction of the liquid phase with binder particles and accelerates the removal of hydration products to the region of

Table 9.1 Influence of water-to-cement ratio on the strength of fine-grained concrete, electric activated at the preparation stage

Activation type	Concrete strength σ , MPa, strength gain $\Delta\sigma$, %, cone displacement (CD) at W/C ratio								
	0.4			0.5			0.6		
	σ	$\Delta\sigma$	CD	σ	$\Delta\sigma$	CD	σ	$\Delta\sigma$	CD
In AC field	18.9	3	0.9	17.4	39	2.8	6.6	50	5.8
In DC field	19.7	7	1	16.1	29	3.3	5.4	35	5.7
Without activation	18.3	–	0.9	12.5	–	2.3	4	–	5

Table 9.2 Influence of the water-cement ratio on the strength of heavy concrete, electroactivated at the preparation stage

Activation type	Concrete strength σ , MPa, strength gain $\Delta\sigma$, %, cone displacement (CD) at W/C ratio								
	0.4			0.5			0.6		
	σ	$\Delta\sigma$	CD	σ	$\Delta\sigma$	CD	σ	$\Delta\sigma$	CD
In AC field	26.4	18	3.6	17.6	17	4.5	11.4	-3	6.8
In DC field	23.4	5	3.3	17.3	15	4.7	9.4	-20	6.6
Without activation	22.2	-	3.0	15.0	-	4.3	11.7	-	6.6

**Fig. 9.2** Dependence of the strength of concrete, electrically activated during mixing: (a) fine-grained; (b) with coarse-grained aggregate vs. the water-to-cement ratio. The figures correspond to (1) activation in AC field, (2) activation in DC field, and (3) without activation

lower concentrations and the formation of crystallization centers. Apparently, the increased water activity under the influence of the field contributes to the disaggregation of cement floccules (formed during cement caking), their watering, and an

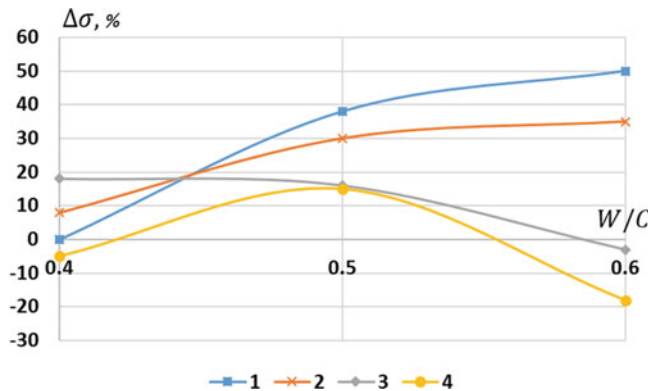


Fig. 9.3 Relative change in the strength of electrically activated concrete at different W/C ratio: 1 and 3 are activation in AC field; 2 and 4 are activation in DC field; 1 and 2 are the fine-grained concrete; and 3 and 4 are the concrete with coarse-grained aggregate

increase in the number of coagulation contacts between cement particles. As a result, the water-holding capacity of the cement paste increases, and an increase in the number of mutual contacts contributes to a decrease in the intergranular space.

The development of crystalline hydrate structure is transferred from the near-surface zone to the intergranular space at an early stage. In the case of a high water-to-cement ratio ($W/C = 0.6$), the excess of the liquid phase is more actively bound to hydrates at the initial stage, the liquid phase is redistributed between new neoplasms, and a more homogeneous structure of the concrete matrix is formed. During the subsequent heat and moisture treatment, a less porous, and, therefore, more durable structure is formed.

An increase in the strength of concrete in comparison with control samples at the same W/C may indicate, according to A. E. Sheikin et al. [251], an increase in the degree of cement hydration in electrically activated concrete.

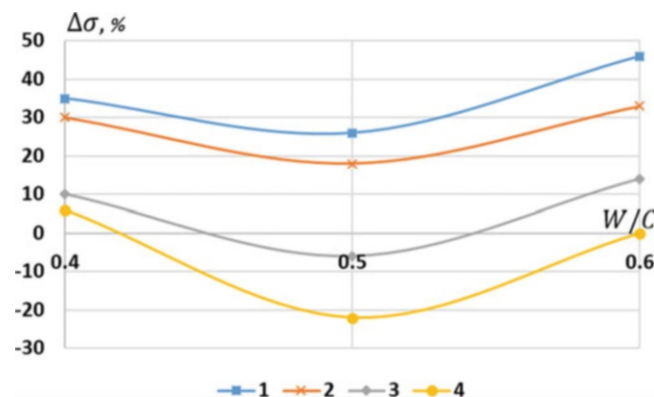
For concretes with a coarse-grained aggregate, the relationship is somewhat different. The nature of the curves indicates that a change in the strength of the cement matrix at a high W/C ratio has an insignificant effect on the overall strength of heavy concrete in the case of processing in AC field, and when processing in DC field, a negative result is observed.

The effect of plasticizing Dofen and PFS additives on the efficiency of electric activation was studied at different water-to-cement ratio on samples of fine-grained concrete [161, 163–166]. The results of studies of the effect of a high-voltage electric field on a concrete mixture at the stage of mixing with the use of surface-active substances (see Table 9.3 and Fig. 9.4) showed the highest efficiency of electrical treatment in AC field in combination with the addition of the superplasticizer Dofen.

A feature of the dependencies shown in Fig. 9.4 is the identical nature of the curves for all cases, having a minimum value of the increase in concrete strength at $W/C = 0.5$. Moreover, for the PFS addition, a negative value is observed at this point, which is much lower for DC field.

Table 9.3 Influence of Dofen and PFS additives on the efficiency of electrical activation of fine-grained concrete

Activation type	Additive type	Strength of fine-grained concrete σ , MPa, and strength gain $\Delta\sigma$, %, at W/C ratio					
		0.4		0.5		0.6	
		σ	$\Delta\sigma$	σ	$\Delta\sigma$	σ	$\Delta\sigma$
In AC field	Dofen	22.4	36	11.54	24	5.7	65
	PFS	10.1	10	7.0	-6	8.2	23
In DC field	Dofen	21.2	29	11.0	19	5.5	60
	PFS	9.66	6	5.8	-23	6.6	0
Without activation	Dofen	16.4	-	9.2	-	3.4	-
	PFS	9.1	-	7.5	-	6.6	-

**Fig. 9.4** Influence of Dofen and PFS additives at different W/C ratio on the efficiency of electrical activation of fine-grained concrete: 1 and 3 are the activation in AC field; 2 and 4 are the activation in DC field; 1, 2—with the use of the Dofen additive; and 3, 4—with the use of the PFS additive

This is consistent with the data of V. A. Matvienko [158–160, 162, 167], who showed that the effect of AC field under stationary conditions on cement dough in the presence of surface-active substances at $W/C = 0.3$ is the least effective. Apparently, this is due to the fact that the effect of an electric field on surface processes in a dissolving cement system is complicated by the presence of the shell of surface-active substances on a dispersed particle. The electric double layer is separated from the medium by the film of surface-active substances, and with the most compact arrangement of particles in the system (for concrete at $W/C = 0.5$), the effect of electric field on the dissolution processes is neutralized. At the same time, in the interparticle space, due to the polarizing action of the field, the effect of “freezing” of dissolution takes place, which negatively affects the strength of the concrete.

The above experimental results indicate that electric activation in combination with the PFS addition is ineffective. For fine-grained concrete with Dofen addition at

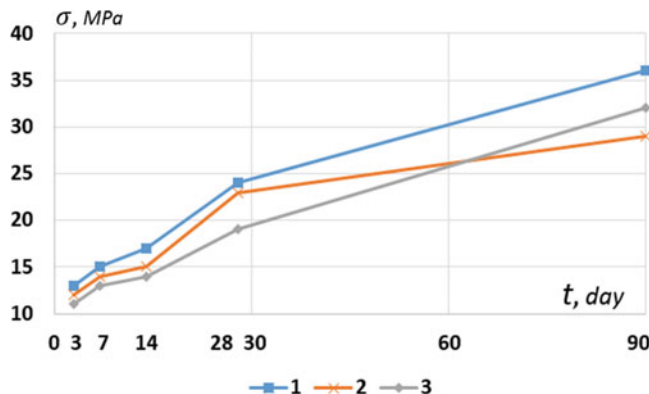


Fig. 9.5 Growth of concrete strength under normal moisture conditions of concrete hardening ($C/S = 0.5$, $W/C = 0.5$): (1) activation in AC field, (2) activation in DC field, and (3) control sample

values of water-to-cement ratio lower and higher than 0.5, electric activation during mixing is effective and to a greater extent in AC field.

Studies of changes in the strength of concrete over time were carried out using the example of fine-grained concrete. The parameters of the electrical treatment were taken based on the results of tests for the strength in compression of concrete specimens subjected to heat and moisture treatment according to the standard mode. The results are shown in Fig. 9.5. An increase in the strength of electrically activated concrete is noted already on the third day and retains a linear relationship for 28 days of hardening. At the same time, the increase in strength upon activation in AC field is higher than in DC field and keeps up to 90 days, whereas samples activated in DC field by this time have a strength lower than the control samples.

According to I. M. Grushko and V. A. Biryukov et al. [80, 82], during the combined electromagnetic and ultrasonic treatment of cement suspensions, substances similar to hydrated neoplasms characteristic of cement stone subjected to heat and moisture treatment are formed in them. During heat treatment, they act as crystal-chemical hardening intensifiers, and during hardening in normal humidity conditions, the same substances aggravate destructive processes, which leads to a decrease in the strength of the material. Apparently, similar phenomena take place under the combined mechanical and high-voltage electrical impact on the mixed mixture, which is confirmed by the increase in the strength of concrete. For concretes electrically activated in AC field, hardened during heat and moisture treatment, the increase in strength is significantly higher (40%) than during hardening under normal conditions (20% at 28 days of age).

9.3 Influence of High-Voltage Electric Field of Corona Discharge on Mineral Components of Concrete

Corona discharge is the most efficient way to generate electrical charges of the required polarity. According to [302], approximately 10^{14} – 10^{15} ions per cubic meter of space are formed in the electrostatic precipitator in less than 0.1 s. The development of the design of the setup for the activation of composite cements, containing in their composition the mineral additives similar in granulometric composition to Portland cement (diluent additives) (Fig. 9.6), is based on the principles of operation of vertical tubular electrostatic precipitators [99, 100, 102].

The design of the setup for the surface modification of dispersed mineral components of concrete is based on the principles of operation of vertical tubular electrostatic precipitators [99, 100, 102]. The surface modification process can be carried out according to the following scheme. First, the initial dispersed mineral components are charged in the high-voltage field of the corona discharge, while a sample of a finely dispersed component (“guest particles”) is poured through an electrization chamber—(1) with a negative corona electrode—and a sample of coarse components (“carrier particles”) through a charging chamber and (2) with a positive corona electrode (see Fig. 9.7). The electrization chamber assembly consists of a corona electrode located in the center of the tube, which is made of copper wire

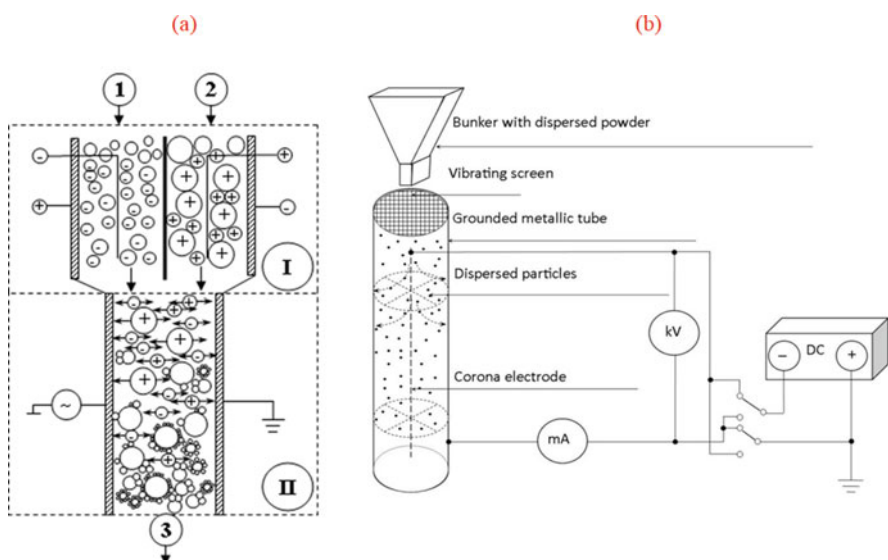
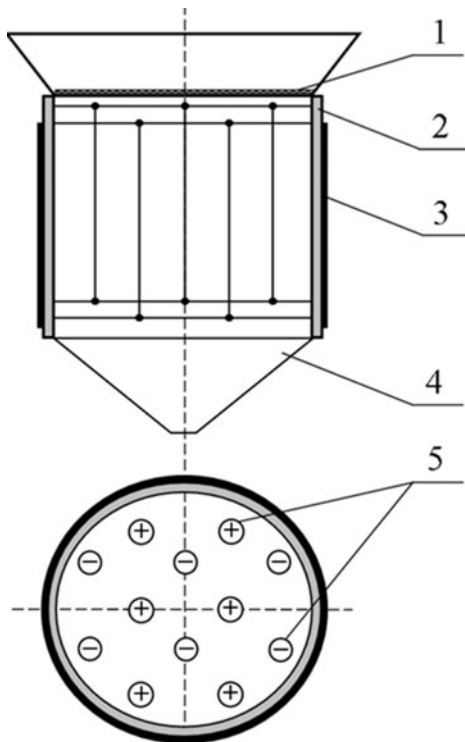


Fig. 9.6 Schemes of setup for activating the components of composite cement in corona discharge field: (a) scheme of plant for surface modification of dispersed mineral constituents of concrete: I—chamber of particle electrization (bipolar charging) in the corona discharge field; II—agglomerator; (b) scheme of device for activation of dispersed mineral constituents of concrete in the corona discharge field with one corona electrode

Fig. 9.7 Scheme of electrization chamber: (1) spraying chamber with vibrating sieve, (2) electrization chamber, (3) outer metallic grounded coating, (4) outlet channel, and (5) matrix of corona discharge wires



with a diameter of 0.6 mm. The volt-ampere characteristics of the electrization chamber are as follows: electric field strength $E = 18\text{--}20 \text{ kV/cm}$, current $I = 30\text{--}50 \mu\text{A}$.

As a result of the action of the electric field, which is created between the corona and external electrodes, the initial mineral components adsorb ions from the interelectrode space and acquire a negative (positive) charge.

Bipolarly charged mineral dispersed components then enter in the agglomerator, where, under the action of a high-voltage alternating electric field, oscillations with different amplitudes and frequencies are carried out. Large particles oscillate with greater amplitude and frequency than small particles, and the frequency and amplitude gradient of the oscillations cause an increase in the frequency of particle collisions, which leads to the formation of spheroidal agglomerates. Such processing of dispersed mineral components has an effect on reducing the water-to-cement ratio when developing compositions of high-tech self-compacting concretes without loss of workability. It should also be noted that with such a treatment, an increase in the hydraulic and pozzolanic activity is achieved, respectively. In turn, the activation of the surface of the particles of dispersed mineral components of concrete should provide an increase in the strength of adhesive contacts and the strength of the composite material as a whole.

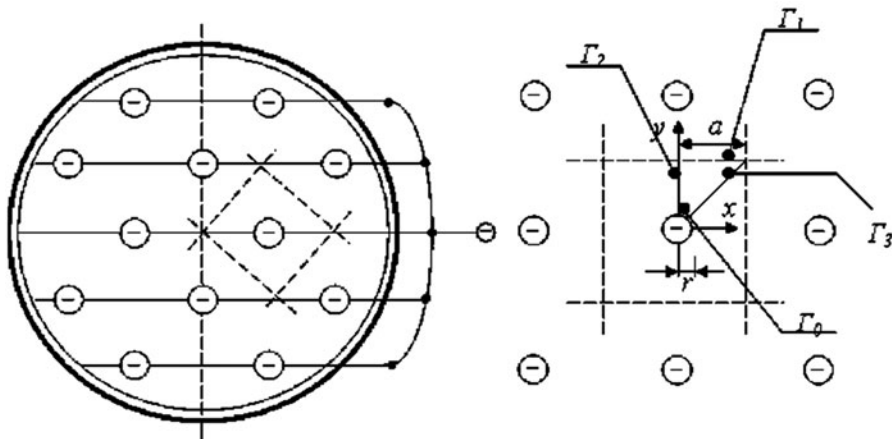


Fig. 9.8 Scheme of connection and arrangement of the electrode matrix in the setup for electrical treatment of composite cement with unipolar charging of particles

Computer simulation of the electrostatic field of a corona discharge shows that the electric field strength at the corona electrode is much higher than in the interelectrode space. Therefore, with an increase in the diameter of the charging chamber, the efficiency of electrical processing decreases. To increase the productivity of the setup and the efficiency of activation by removing restrictions on the diameter of the tubular electrification chamber, a device for the electrostatic activation of cement was developed. Its principal difference is the equipment of the electrification chamber with several corona electrodes built into the matrix (see Fig. 9.7).

To determine the concentration of mobile ions in the corona region, created by a matrix of vertical electrodes, a mathematical calculation was performed. It is necessary to solve the problem for an isosceles right-angled triangle in one of the lateral vertices of which an electrode is placed (Fig. 9.8).

The coordinates of the grid nodes: $x = m\xi$; $y = n\xi$ and the spatial step ξ of the coordinates are determined by the formula:

$$\xi = \frac{a}{K}$$

where K is the number of steps, a is the distance from the center of the electrode to the grid, and m, n are the coordinates on the electrode surface.

At the node, corresponding to the electrode surface: $m = 0, n = 0$ (boundary Γ_0). On the segment: $y = a, n = K$ (boundary Γ_1), the potential is equal to zero. The segment adjacent to the electrode $x = 0, m = 0$ (boundary Γ_2) and the segment $y = x, n = m$ (boundary Γ_3) are perpendicular to the equipotential surface. The electrostatic region of a straight wire (r is the radius of the cross-section) of a coaxial grounded tubular metallic cylinder (a is the radius) is described by the following formulae [160]:

$$\int_S \bar{E} d\bar{S} = 2\pi\zeta h E = \frac{\lambda h}{\epsilon_0}.$$

or $E = \frac{\lambda}{2\pi\zeta\epsilon_0}$.

Then

$$U = \int_r^a E dr = \frac{\lambda h}{\epsilon_0} \ln \left(\frac{a}{r} \right)$$

and

$$V = \int_\zeta^a E d\zeta = \frac{\lambda h}{\epsilon_0} \ln \left(\frac{a}{\zeta} \right) = \frac{\lambda h}{\epsilon_0} \ln \left(\frac{a}{r} \right) \frac{\ln \left(\frac{a}{\zeta} \right)}{\ln \left(\frac{a}{r} \right)} = \frac{U \ln \left(\frac{a}{\zeta} \right)}{\ln \left(\frac{a}{r} \right)}.$$

Then

$$\bar{E} = -\nabla V = -\frac{dV}{d\zeta} = \frac{U}{\zeta \ln \left(\frac{a}{r} \right)}.$$

Here E is the potential of the electrostatic field at the electrode surface S , λ is the linear density of the electric charge, h is the length of the electrode, $\epsilon_0 = 8.85 \times 10^{12}$ F/m is the electric constant, ζ is the distance between the electrodes, U is the potential of the electrode, and V is the potential of the electrostatic field at a distance a from the axis of the cylinder.

The field strength of the corona discharge initiation at the surface of the wire electrode in air and atmospheric pressure is found in accordance with Peak's law (the Kaptsov's assumption [160]).

Various mathematical models of electrostatic field of the corona discharge have been presented in [38, 160, 203, 284, 312, 316] and obtained on the basis of the following assumptions [45]:

- (i) The thickness of the ionization zone is negligible.
- (ii) The drift zone of the corona discharge contains only unipolar ions.
- (iii) Thermal diffusion and ion recombination can be neglected.
- (iv) Ion mobility is a constant value.
- (v) Ion recombination takes place in a thin boundary layer.

Current density in a gas atmosphere is defined as

$$j = qnbE = \rho bE,$$

where q is the ion charge, n is the concentration of ions, and E is the intensity of the electrostatic field of the corona discharge; charge density and ion mobility are defined respectively as

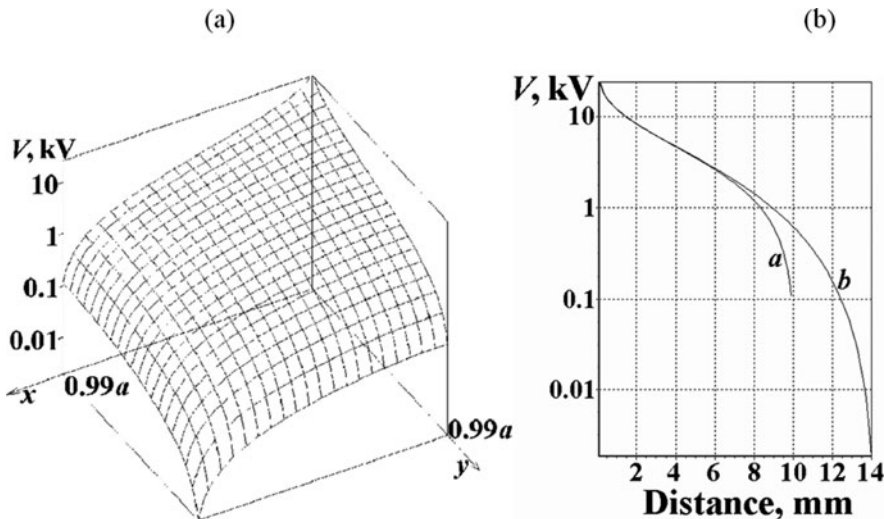


Fig. 9.9 Change in the potential of the electrostatic field of corona discharge at electrode surface: (a) along the x -axis and y -axis and (b) along straight line $x = y$

$$b_+ = 1.4 \frac{\times 10^{-4} \text{ m}^2 \text{s}}{\text{V}}; \quad b_- = 1.9 \frac{\times 10^{-4} \text{ m}^2 \text{s}}{\text{V}};$$

and bulk charge density at the electrode surface is: $\rho_r = \frac{I}{2\pi r b E_r}$, where I is the value of the electric current of the corona discharge at the electrode surface [173].

Computer simulation results show (see Figs. 9.9, 9.10 and 9.11) that the corona electrostatic field is established in less than 4 milliseconds. With the cross-section diameter of the electrode $d = 0.6$ mm, the distance between the electrodes $2a = 20$ mm, and the potential $U = 25$ kV, the corona current at the electrode surface is equal to $I = 0.5$ mA/m, and the bulk charge density at the electrode surface is $170 \mu\text{C}/\text{m}^3$ (10^6 charged ions in 1 mm^3). There are no ions at the dead center ($x = a$, $y = a$).

At the same time, already at a distance of $0.01a$ from the dead center, the bulk charge density remains quite high and equals to $85 \mu\text{C}/\text{m}^3$. The corona discharge is unstable, so the position of the dead center ($x = a \pm \delta$; $y = a \pm \delta$) will change along the height of the tubular cylinder. Thus, any dispersed particle cannot pass through the cylinder without collision with a flow of ions on its way. This ensures that the particles of the dispersed mineral components of concrete move along the entire cylindrical tube of the electrification chamber in the corona discharge field. In the outer region of the corona discharge, only negative ions are present, which create a unipolar space charge in the interelectrode space. Particles of dispersed mineral components of concrete, being in the outer region of the corona discharge, adsorb ions and acquire an excess electric charge.

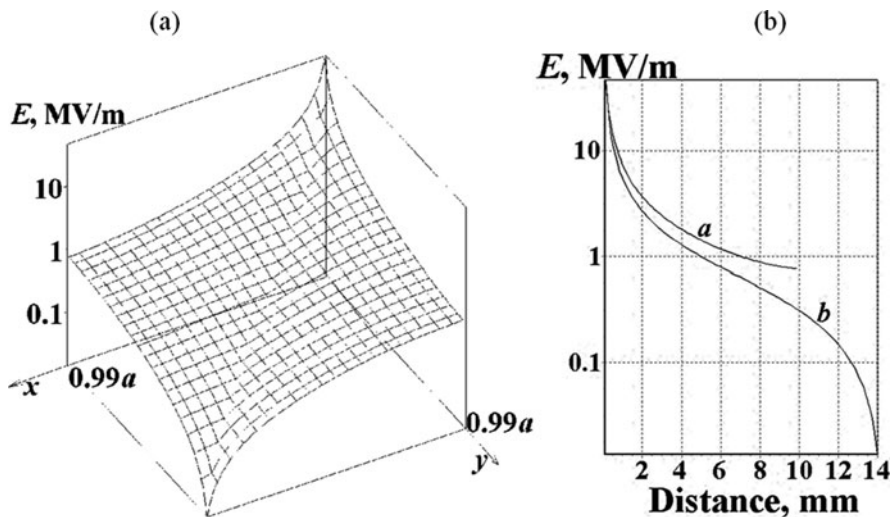


Fig. 9.10 Change in the intensity of the electrostatic field of the corona discharge at the electrode surface: (a) along the x -axis and y -axis and (b) along straight line $x = y$

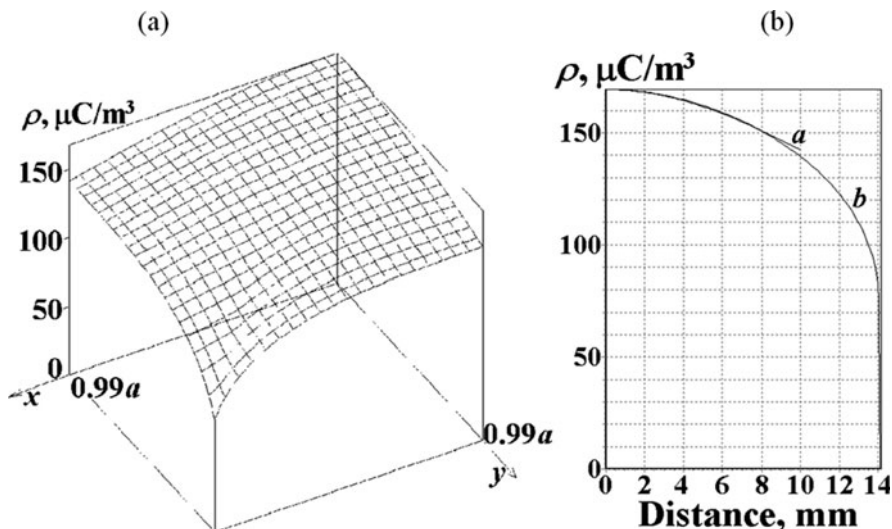


Fig. 9.11 Change in the bulk charge density of the corona discharge at the electrode surface: (a) along the x -axis and y -axis and (b) along straight line $x = y$

Based on computer simulation of an electrostatic corona discharge, the concentration of mobile ions in the corona region, created by a matrix of vertical corona electrodes, has been calculated, which makes it possible to determine the main design characteristics of devices for activating mineral dispersed concrete components.

9.4 Influence of High-Voltage Electrostatic Field on the Rheological Properties of Mineral Powders

To assess the autohesion of raw materials, a number of indirect characteristics are used, in particular, the angle of repose, which is determined by measuring the contours of a cone formed by filling material from a funnel from a certain height (Fig. 9.12a) or when removing a spatula from a layer of bulk material (Fig. 9.12b). This angle reflects the total effect of autohesion and internal friction of the bulk material [237–239].

The nature of the change in the autohesion of particles of various mineral dispersions before and after treatment in a high-voltage electric field was also evaluated by the value of the bulk density of the dispersions. To determine autohesion, the following powder materials were used: microsilica of dry gas cleaning, chamotte-kaolin powder, fly ash of thermal power station (TPS), and ground limestone, and they were sifted through a sieve No. 008, TPS slag, and Portland cement clinker.

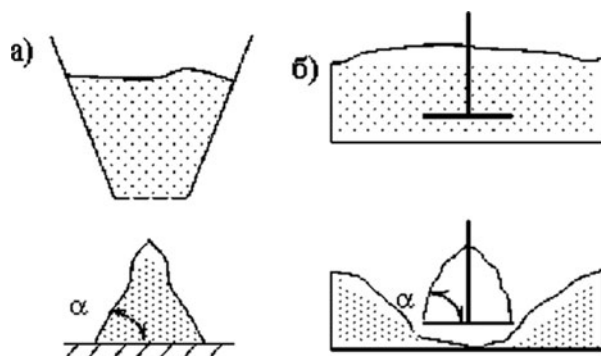
Before determining the value of the angle of repose and bulk density, dispersed materials were dried at $T = 105\text{--}110\text{ }^{\circ}\text{C}$ to constant weight.

The polarity of the corona electrode during processing of mineral dispersions corresponded to the integral sign of their surface charge [251].

It was found that the maximum absolute value of autohesion by the angle of repose is observed for dispersions from microsilica and ground limestone, and the minimum value corresponds to fly ash. This is primarily due to the fact that, according to the classification of bulk materials by autohesion [195], ground limestone belongs to the group of strongly sticking powders with a breaking strength of more than 600 Pa, and fly ash belongs to the group of weakly sticking dusty materials (60–300 Pa).

A characteristic feature of dispersions treated in an electric field of a corona discharge in comparison with the control samples is the lower values of the bulk density and the angle of repose. This is due to a change in the balance of forces that arise during mutual contact of particles (molecular, electrical, mechanical, and

Fig. 9.12 Scheme for determining the angle of repose for dispersed mineral additives



Coulomb). With a certain balance of these forces, autohesion will promote or prevent dense packing of particles.

Electric forces arise as a result of the contact of particles with each other, when donor-acceptor processes occur and an electric double layer (DEL) is formed, which is associated with the electrical inhomogeneity of the surface of the contacting particles.

In this case, the charge distribution on the surface of particles consisting of a dielectric material is mosaic in nature. High-voltage processing of powders leads to polarization of particle charges. As a result, Coulomb repulsive forces appear between the individual areas with a unipolar charge, which reduce autohesion. Thus, the above effects are a consequence of a change in the balance of forces of autohesion interaction between particles as a result of modifying their electric surface properties. A change in the electric surface properties of powders should also affect interparticle interactions in the “solid-liquid” system.

9.5 The Idea and Essence of the Activation of Aerated Concrete Mixtures with Low-Power AC Electrophysical Impact

Management of the process of structure formation in a foam concrete mixture is one of the most important directions for improving the quality and, above all, the physical and mechanical properties of foam concrete. It is obvious that the strength characteristics of aerated concrete to a greater extent depend on the physical and mechanical properties of the material of the interporous partitions, including its density [4]. However, under real conditions, dense packing of solid particles in materials is an extremely rare and practically unattainable phenomenon due to the roughness and angularity of the filler grains.

In the technology of heavy concrete manufacture, the structure is usually compacted using mechanical vibration. As a result of the action of gravitational forces after thixotropic dilution of the cement slurry, an ordered arrangement of aggregate grains occurs. In such concretes, which have a coarse-grained aggregate in their composition, vibrations of low frequencies, equal to 50–100 Hz, are mainly used. However, in an aerated concrete and, in particular, in a foam concrete, the particles of inert components are less than 1 mm in size, requiring an increase in vibration frequency by a factor of 100 or more. Oscillations of such frequencies in viscous media quickly damp, and an increase in their power often leads to a negative change in the pore structure of foam concrete, which was recorded in a number of works.

In the technology of foam concrete, it turned out to be an effective method of compaction of the material of interporous partitions, eliminating capillary porosity in it and increasing the area of interparticle phase contacts by acting on the freshly laid foam concrete mixture of AC field.

It is known that the particles of cement and mineral filler have a surface electric charge. In the initial period of hydration of cement particles in the mixture and the appearance of coagulation interparticle contacts, solid charged particles in a liquid medium are in a “suspended” equilibrium state with fixation predominantly in the positions of a far energy minimum.

The action of the force of electrostatic repulsion prevents direct contact of the particles. At the same time, in some border areas they will continue to experience interparticle attraction. The forces of attraction and repulsion are balanced at a certain distance from the interface between neighboring particles when their potential energy is minimal. Thus, the displacements of unreacted cement and aggregate particles located in the gel-like medium of the hydrate phases will have an elastic-viscous character.

With an external periodic impact on such a structure (e.g., vibration), there will be a change in the spatial packing of solid particles. As a result of an increase in the proportion of phase contacts (of the “plane-plane” type) between the aggregate particles, their interaction after crystallization of the hydrate phases will increase, which will cause an increase in the strength of interporous partitions and, thus, the entire volume of aerated concrete.

Moreover, the relative movement of cement particles during vibration will contribute to an increase in the density of new formations in the places of contact of the particles and, thereby, to an increase in their binding capacity, to accelerate the process of cement hardening and, as a result, to maintain a stable pore structure of foam concrete. The effect of forced mechanical vibrations will be maximum, when their frequency coincides with the eigen-frequency of the vibrations of particles.

It is possible to excite vibrations of solid particles in the volume of interpore partitions by placing the foam concrete mixture in AC field. Then solid particles will vibrate under the influence of an electric force in accordance with the law of changes in the strength of the electric field.

As a result of the rising periodic mechanical impact created by AC field, charged particles, together with their solvation shells, are set in oscillatory motion [5]. Then, random fragile structural bonds in the mixture are destroyed, and, as a consequence, thixotropic liquefaction takes place in microvolumes. It contributes to a denser packing of particles of inert components in the material of the interporous partition.

The main advantage of this method is to supply the vibration energy directly to the aggregate grains without significantly affecting the macropores in the structure of the foam concrete mixture.

By considering the structure of fiber-foam concrete, it is necessary to take into account the influence and role of reinforcing fibers.

Synthetic fibers, like filler grains, have a certain surface electric charge, which forces them to perform forced vibrations in a high-frequency AC field. However, due to the difference in the shape of the fibers from the filler particles, their vibrations and displacements in the mixture under the influence of AC field will differ from each other.

In this case, it is necessary to take into account the direction of the force lines of electric field, which affects the final spatial arrangement of the fibers in the mixture after activation.

In fact, the fiber has a damping effect on solid sand particles during the vibrational motion of the entire system of concrete mixture, which is very important for eliminating the destruction of the structure at critical values of the parameters of electrical activation.

Thus, upon activation of a fiber-foam concrete mixture with AC field, reinforcement with synthetic fibers increases the efficiency of electrophysical processing and improves the physical and mechanical characteristics of fiber-foam concrete.

9.6 Theoretical Substantiation of the Expediency of Activation of Aerated Concrete Mixtures by Low-Power AC Electrophysical Impact

Let us consider the theoretical justification of the proposed technological method. Let the concrete mixture be located between electrodes disposed at a certain distance from each other, to which AC voltage is applied. The amount of charge of the filler grain is q .

In AC field, a force will act on the grain:

$$F(t) = F_0 \cos \omega t, \quad (9.1)$$

where $F_0 = qE_0$.

Since the grain is in a slightly viscous environment and surrounded by other grains, the following additional forces will be applied to it:

(i) Quasi-elastic force:

$$F_{qe} = kx, \quad (9.2)$$

where x is the displacement of the particle from the equilibrium position and k is the stiffness factor.

(ii) Resistance force:

$$F_r = r\nu \quad (9.3)$$

where ν is the particle velocity and r is the coefficient of the medium resistance.

In the steady state, the aggregate grain will perform forced harmonic oscillations with certain amplitude.

To maintain forced vibrations in a system with viscous friction, a certain power must be expended, absorbed by the concrete mixture during electrical vibration treatment (power losses), since it is spent on overcoming the resistance forces of the medium during the vibrations of the aggregate and, ultimately, turns into heat.

The absorption of energy by the mixture will be resonant. It is in this case that the electrical vibration treatment mode is most suitable for achieving the maximum efficiency of the technological method, namely, regulating the structure formation and properties of cellular concrete, activated by low-power AC impact.

9.7 Characteristics of the Optimal Activation Mode for Foam and Fiber-Foam Concrete by Low-Power Variable Electrophysical Impact

The effects of the geometric parameters of mixer on the mixing process of foam concrete mixture and its energy efficiency have been studied in [277].

The author of [67] carried out experimental studies of the physical and mechanical properties of foam and fiber-foam concretes, activated by low-power electrophysical exposure (see Table 9.4):

- (i) Compressive strength
- (ii) Average density
- (iii) Released moisture
- (iv) Sorption humidity at a relative air humidity of 75% and 97%
- (v) Thermal conductivity
- (vi) Vapor permeability (see Table 9.5)

For the research, 560 experimental cubes of foam and fiber-foam concretes of design class B1, design density D500, with dimensions of $7.07 \times 7.07 \times 7.07 \text{ cm}^3$, as well as 168 foam and fiber-foam concrete plates with dimensions of $25 \times 25 \times 4 \text{ cm}^3$ and 168 plates with dimensions of $10 \times 10 \times 3 \text{ cm}^3$ were manufactured and tested (Fig. 9.13).

First, the following parameters were investigated:

- (i) The position of the electrodes (inside, when the dielectric contacts with the mixture; outside, when the metal contacts with the mixture)
- (ii) The presence of coating of electrodes (zaponlack)

Moreover, the experiments varied:

- (i) Electric field strength (0; 2.5; 3; 3.5 V/cm)
- (ii) Frequency of AC (0; 40; 50; 60 kHz)
- (iii) Exposure duration (0; 0.5; 1; 1.5 min; see Table 9.4)

In the experiments, a concrete composition was used, including the following dosage of components: $C/S/W/FA = 1:0.3:0.64:0.015 = 350 \text{ kg/m}^3:105 \text{ kg/m}^3:223 \text{ l/m}^3:5.25 \text{ l/m}^3$ (where C is the cement, S is the sand, W is the water, and FA is the

Table 9.4 Schedule of additional experimental studies of the physical and mechanical properties of foam and fiber-foam concrete

Sample code		Variable parameters of electrophysical impact		
Foam concrete	Fiber-foam concrete	Field strength, V/cm	Frequency, kHz	Duration of processing, min
FC-0/0/0	FFC-0/0/0	0	0	0
FC-2.5/40/0.5	FFC-2.5/40/0.5	2.5	40	1
FC-2.5/40/1	FFC-2.5/40/1	2.5	40	2
FC-2.5/40/1.5	FFC-2.5/40/1.5	2.5	40	3
FC-2.5/50/0.5	FFC-2.5/50/0.5	2.5	50	5
FC-2.5/50/1	FFC-2.5/50/1	2.5	50	15
FC-2.5/50/1.5	FFC-2.5/50/1.5	2.5	50	1
FC-2.5/60/0.5	FFC-2.5/60/0.5	2.5	60	2
FC-2.5/60/1	FFC-2.5/60/1	2.5	60	3
FC-2.5/60/1.5	FFC-2.5/60/1.5	2.5	60	5
FC-3/40/0.5	FFC-3/40/0.5	3	40	15
FC-3/40/1	FFC-3/40/1	3	40	1
FC-3/40/1.5	FFC-3/40/1.5	3	40	2
FC-3/50/0.5	FFC-3/50/0.5	3	50	3
FC-3/50/1	FFC-3/50/1	3	50	5
FC-3/50/1.5	FFC-3/50/1.5	3	50	15
FC-3/60/0.5	FFC-3/60/0.5	3	60	1
FC-3/60/1	FFC-3/60/1	3	60	2
FC-3/60/1.5	FFC-3/60/1.5	3	60	3
FC-3.5/40/0.5	FFC-3.5/40/0.5	3.5	40	5
FC-3.5/40/1	FFC-3.5/40/1	3.5	40	15
FC-3.5/40/1.5	FFC-3.5/40/1.5	3.5	40	1
FC-3.5/50/0.5	FFC-3.5/50/0.5	3.5	50	2
FC-3.5/50/1	FFC-3.5/50/1	3.5	50	3
FC-3.5/50/1.5	FFC-3.5/50/1.5	3.5	50	5
FC-3.5/60/0.5	FFC-3.5/60/0.5	3.5	60	15
FC-3.5/60/1	FFC-3.5/60/1	3.5	60	1
FC-3.5/60/1.5	FFC-3.5/60/1.5	3.5	60	2

Note: FC—foam concrete; FFC—fiber-foam concrete

Table 9.5 Results of additional experiments, clarifying the optimal parameters of electrical activation of foam and fiber-foam concrete mixtures

Physical and mechanical characteristics of foam and fiber-foam concrete						
Sample code	Compressive strength, MPa	Density, kg/m ³	Sorption moisture, %		Thermal conductivity, W/(m · °C)	Water vapor permeability, mg/(m · h · Pa)
			At a relative humidity of 75%	At a relative humidity of 97%		
FC-0/0/0	1.11	516	18	8.1	0.124	0.22
FC-2.5/ 40/0.5	1.22	514	17	8.0	0.105	0.20
FC-2.5/ 40/1	1.25	513	20	8.1	0.115	0.21
FC-2.5/ 40/1.5	1.24	515	16	8.0	0.108	0.21
FC-2.5/ 50/0.5	1.25	511	17	7.9	0.112	0.19
FC-2.5/ 50/1	1.27	506	21	7.9	0.114	0.20
FC-2.5/ 50/1.5	1.26	508	18	8.0	0.098	0.22
FC-2.5/ 60/0.5	1.28	509	19	8.1	0.096	0.19
FC-2.5/ 60/1	1.29	511	18	8.0	0.098	0.20
FC-2.5/ 60/1.5	1.27	513	18	8.0	0.110	0.20
FC-3/40/ 0.5	1.22	511	19	8.1	0.10	0.19
FC-3/40/ 1	1.28	508	17	8.0	0.106	0.19

(continued)

Table 9.5 (continued)

Physical and mechanical characteristics of foam and fiber-foam concrete						
Sample code	Compressive strength, MPa	Density, kg/m ³	Vacation humidity, %	Sorption moisture, %	Thermal conductivity, W/(m · °C)	Water vapor permeability, mg/(m · h · Pa)
FC-3/40/ 1.5	1.24	511	20	8.0	0.098	0.21
FC-3/50/ 0.5	1.29	508	16	7.9	0.097	0.22
FC-3/50/ 1	1.32	506	17	7.5	0.093	0.24
FC-3/50/ 1.5	1.25	509	21	7.7	0.094	0.23
FC-3/60/ 0.5	1.28	510	19	7.8	0.096	0.22
FC-3/60/ 1	1.29	509	19	7.7	0.095	0.22
FC-3/60/ 1.5	1.27	512	17	7.7	0.098	0.21
FC-3.5/ 40/0.5	1.23	513	19	7.8	0.104	0.20
FC-3.5/ 40/1	1.28	512	20	7.8	0.103	0.21
FC-3.5/ 40/1.5	1.24	514	17	7.9	0.106	0.21
FC-3.5/ 50/0.5	1.26	512	18	7.9	0.108	0.20
FC-3.5/ 50/1	1.29	509	16	7.9	0.107	0.21

FC-3.5/ 50/1.5	1.27	514	20	8.0	11.7	0.110	0.20
FC-3.5/ 60/0.5	1.25	512	18	8.0	11.8	0.112	0.19
FC-3.5/ 60/1	1.28	510	21	8.1	11.8	0.116	0.19
FC-3.5/ 60/1.5	1.27	513	19	8.1	11.9	0.117	0.18
FFC-0/0/ 0	1.42	517	16	2.1	3.2	0.1	0.098
FFC-2.5/ 40/0.5	1.47	512	18	1.98	3.12	0.1	0.098
FFC-2.5/ 40/1	1.51	511	21	1.96	3.05	0.098	0.099
FFC-2.5/ 40/1.5	1.46	512	17	2.03	3.18	0.097	0.098
FFC-2.5/ 50/0.5	1.48	511	21	2.10	3.19	0.097	0.098
FFC-2.5/ 50/1	1.52	509	18	2.09	3.18	0.096	0.097
FFC-2.5/ 50/1.5	1.50	511	18	2.11	3.21	0.097	0.098
FFC-2.5/ 60/0.5	1.52	512	21	2.08	3.2	0.096	0.099
FFC-2.5/ 60/1	1.54	511	17	2.07	3.18	0.096	0.098
FFC-2.5/ 60/1.5	1.52	512	18	2.10	3.19	0.098	0.10
FFC-3/ 40/0.5	1.49	513	19	2.07	3.18	0.097	0.099

(continued)

Table 9.5 (continued)

Physical and mechanical characteristics of foam and fiber-foam concrete						
Sample code	Compressive strength, MPa	Density, kg/m ³	Vacation humidity, %	Sorption moisture, %	Thermal conductivity, W/(m · °C)	Water vapor permeability, mg/(m · h · Pa)
FFC-3/ 40/1	1.55	510	20	2.05	3.14	0.096
FFC-3/ 40/1.5	1.53	511	16	2.01	3.11	0.095
FFC-3/ 50/0.5	1.61	506	19	1.95	3.02	0.095
FFC-3/ 50/1	1.69	504	18	1.90	2.98	0.09
FFC-3/ 50/1.5	1.60	508	17	1.92	3.02	0.094
FFC-3/ 60/0.5	1.57	512	19	1.98	3.12	0.095
FFC-3/ 60/1	1.59	511	19	2.03	3.15	0.094
FFC-3/ 60/1.5	1.56	512	17	2.03	3.14	0.096
FFC-3.5/ 40/0.5	1.54	514	20	2.06	3.16	0.096
FFC-3.5/ 40/1	1.56	512	18	2.05	3.14	0.095
FFC-3.5/ 40/1.5	1.52	513	17	2.06	3.15	0.097
FFC-3.5/ 50/0.5	1.58	511	21	2.07	3.17	0.097

FFC-3.5/ 50/1	1.60	509	19	2.06	3.15	0.096	0.099
FFC-3.5/ 50/1.5	1.55	512	20	2.07	3.16	0.098	0.097
FFC-3.5/ 60/0.5	1.54	513	16	2.08	3.17	0.098	0.097
FFC-3.5/ 60/1	1.56	512	21	2.07	3.16	0.097	0.098
FFC-3.5/ 60/1.5	1.53	514	18	2.09	3.18	0.097	0.097

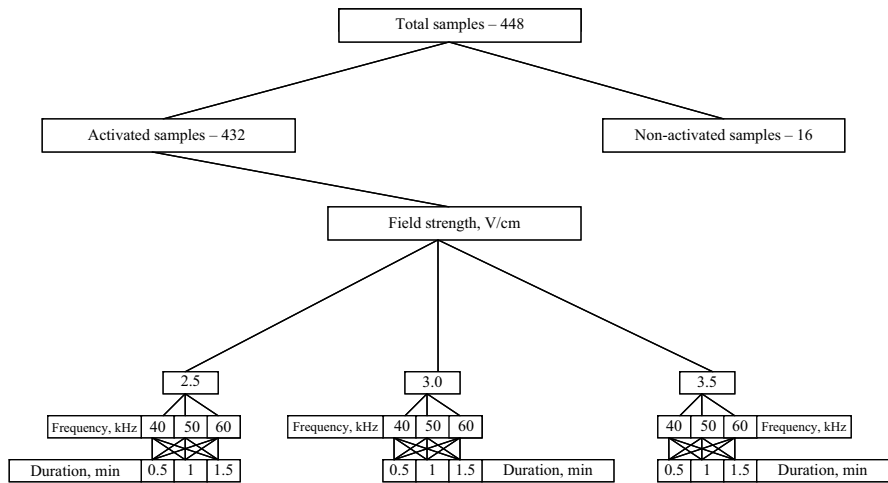


Fig. 9.13 Schedule of additional experimental research

foaming agent). The parameters of concrete mixtures, adopted in our experimental studies, were as follows:

- (i) The ratio of water to solid, $W/S = 0.49$
- (ii) The ratio of sand to cement, $S/C = 0.3$
- (iii) Content of foaming agent $FA = 5.25 \text{ kg/m}^3$
- (iv) Percentage of fiber reinforcement $\mu = 4\%$ (for fiber-foam concrete)

During the experiments, the viscosity of the cement-sand slips remained approximately constant and amounted to 320–330 mm.

9.8 Identifying Rational Modes of Low-Power Electrophysical Impact on Foam and Fiber-Foam Concrete Mixtures and Concretes

After carrying out all the planned (both basic and additional) experimental studies, we analyzed the results obtained in order to identify rational modes of low-power electrophysical impact on foam and fiber-foam concrete mixtures and concretes.

Figures 9.14, 9.15, 9.16, 9.17, 9.18, 9.19, 9.20, 9.21, 9.22 and 9.23 show the changes in the physical, mechanical, and structural properties of foam and fiber-foam concretes, depending on the values of the parameters of low-power AC impact.

We note from the results of the analysis as a whole that electrical activation provides the maximum positive effect on strength, average density, thermal conductivity, and vapor permeability. The influence of activation on the sorption moisture of materials was also revealed. Note, however, that it has been experimentally

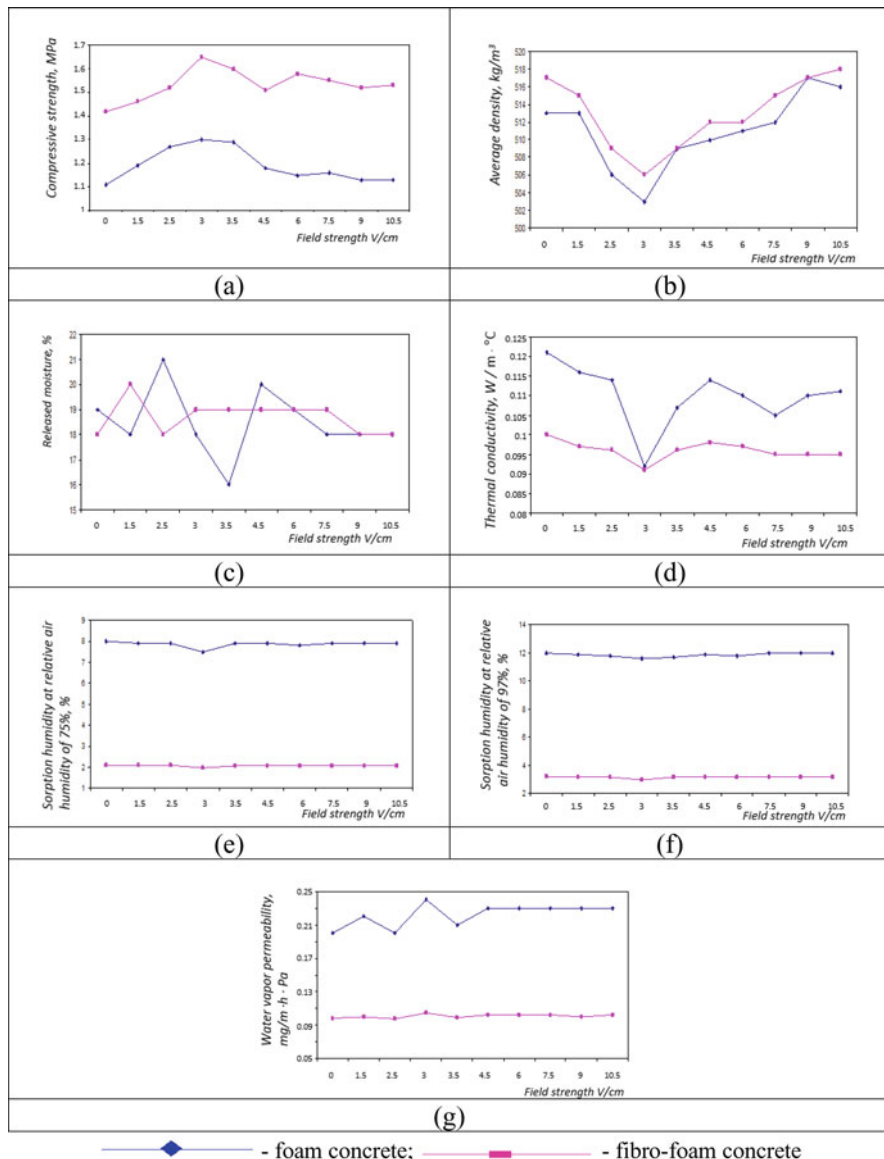


Fig. 9.14 Changes in the physical and mechanical properties of foam and fiber-foam concretes depending on the field strength during electrical activation: (a) compressive strength, (b) average density, (c) released moisture, (d) thermal conductivity, (e and f) sorption humidity at relative air humidity of 75% and 97%, and (g) water vapor permeability

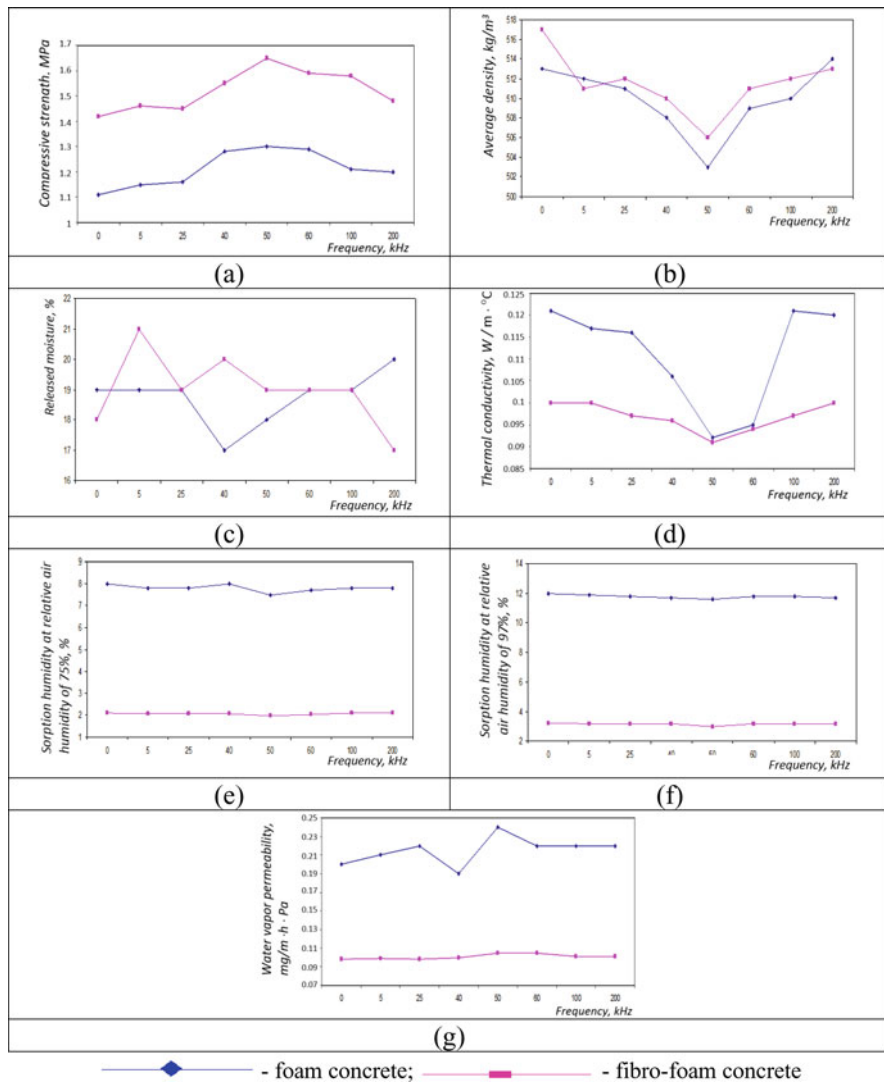


Fig. 9.15 Changes in the physical and mechanical properties of foam and fiber-foam concretes depending on the frequency of AC during electrical activation: (a) compressive strength, (b) average density, (c) released moisture, (d) thermal conductivity, (e) and (f) sorption humidity at relative air humidity of 75% and 97%, and (g) vapor permeability

established that the tempering humidity does not change as significantly in accordance with some pronounced regularity when activated by AC field.

After a comparative analysis of the properties of activated and non-activated foam and fiber-foam concretes, the optimal modes of electrical activation were established.

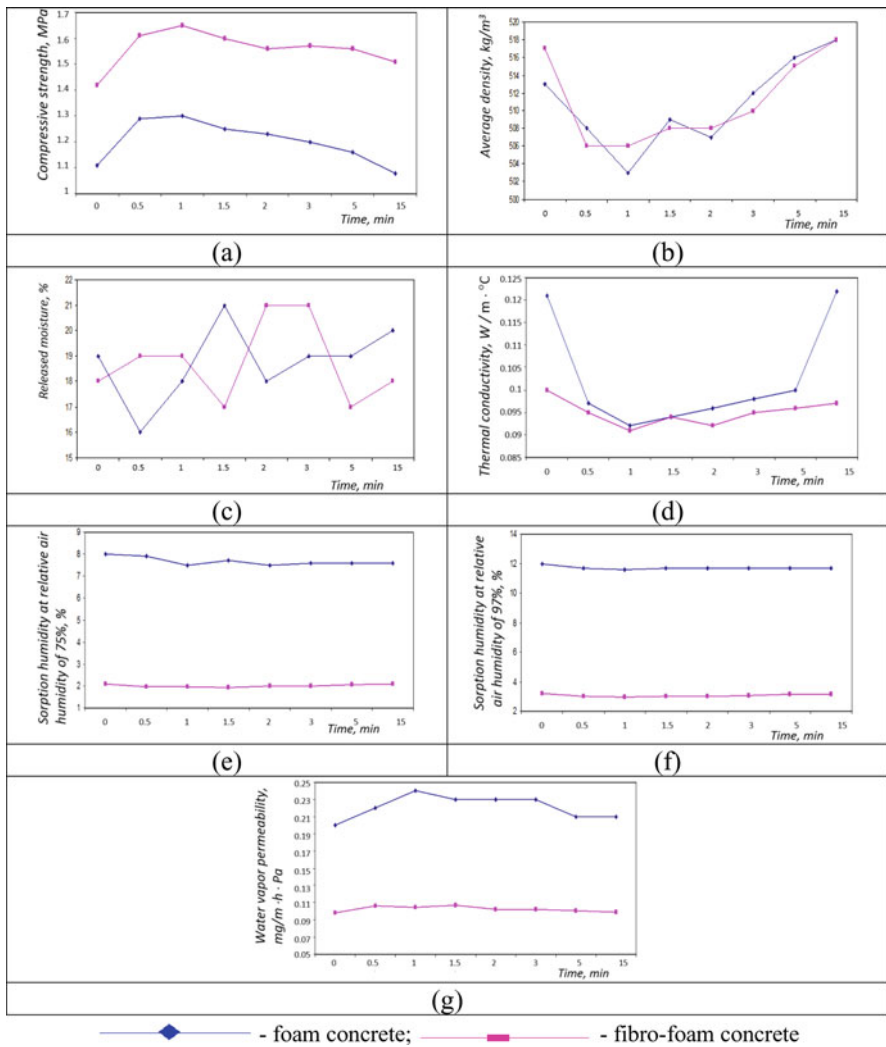


Fig. 9.16 Change in the physical and mechanical properties of foam and fiber-foam concretes depending on the time of electrical activation: (a) compressive strength, (b) average density, (c) released moisture, (d) thermal conductivity, (e and f) sorption humidity at relative air humidity of 75% and 97%, and (g) vapor permeability

The hypothesis about the possibility of controlling the properties of activated foam and fiber-foam concrete by changing the parameters of low-power variable electrophysical impact (intensity, frequency, and activation time) has been experimentally confirmed.

The analysis of the results obtained made it possible to clarify the optimal range of changes in the parameters of low-energy activation of foam and fiber-foam concrete mixtures by an electric field.

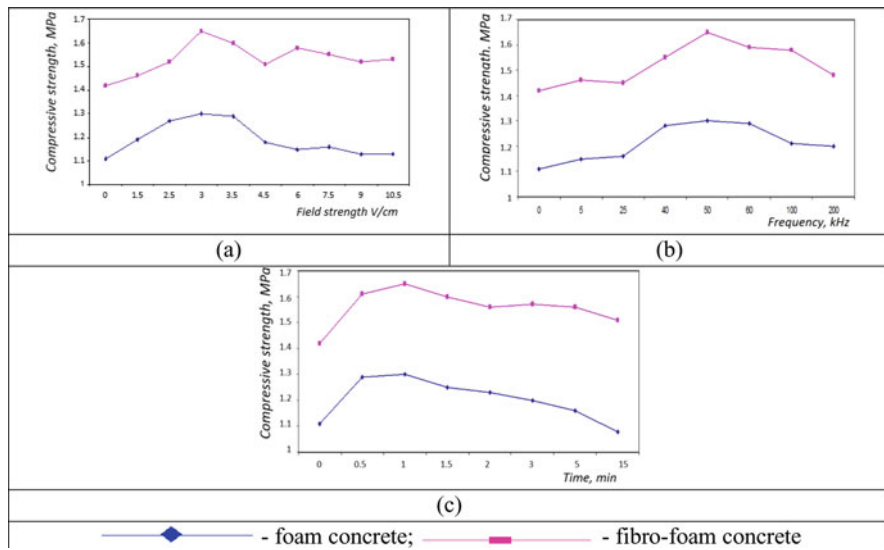


Fig. 9.17 Influence of changes in the parameters of electric field on the value of the strength of foam concrete in compression: (a) electric field strength, (b) AC frequency, and (c) processing time

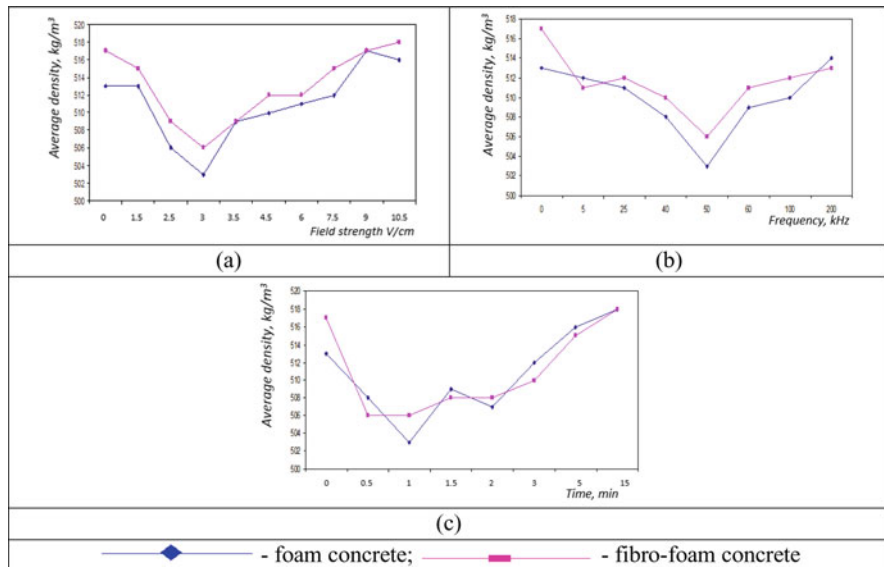


Fig. 9.18 Influence of changes in the parameters of the electric field on the value of the average density of foam concrete: (a) electric field strength, (b) AC frequency, and (c) processing time

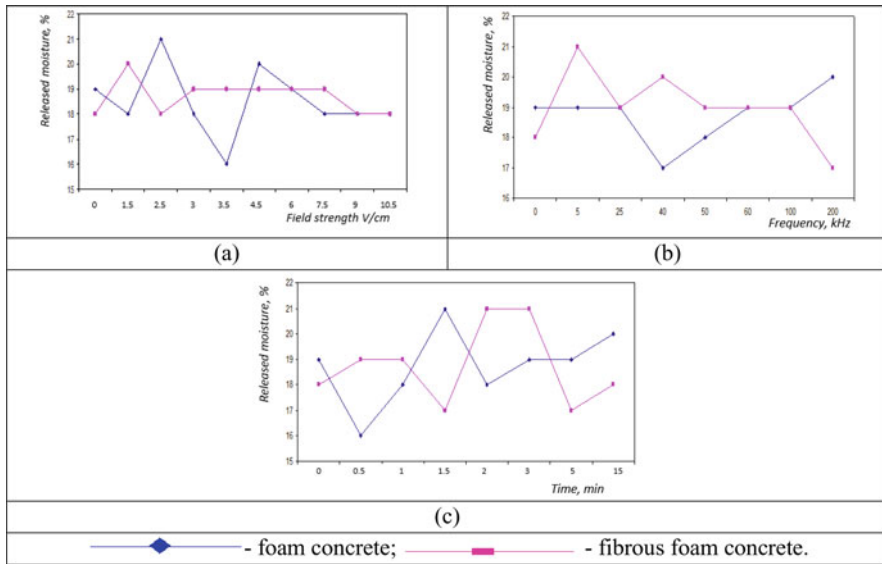


Fig. 9.19 Influence of changes in the parameters of the electric field on the value of the released moisture content of foam concrete: (a) electric field strength, (b) AC frequency, and (c) processing time

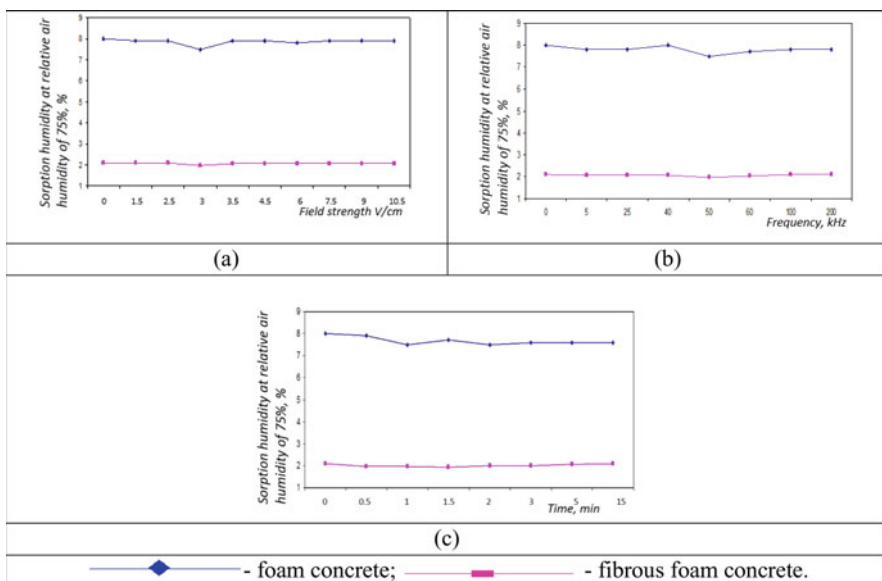


Fig. 9.20 Effect of changing the parameters of electric field on the value of the sorption moisture content of foam concrete at a relative humidity of 75%: (a) electric field strength, (b) AC frequency, and (c) processing time

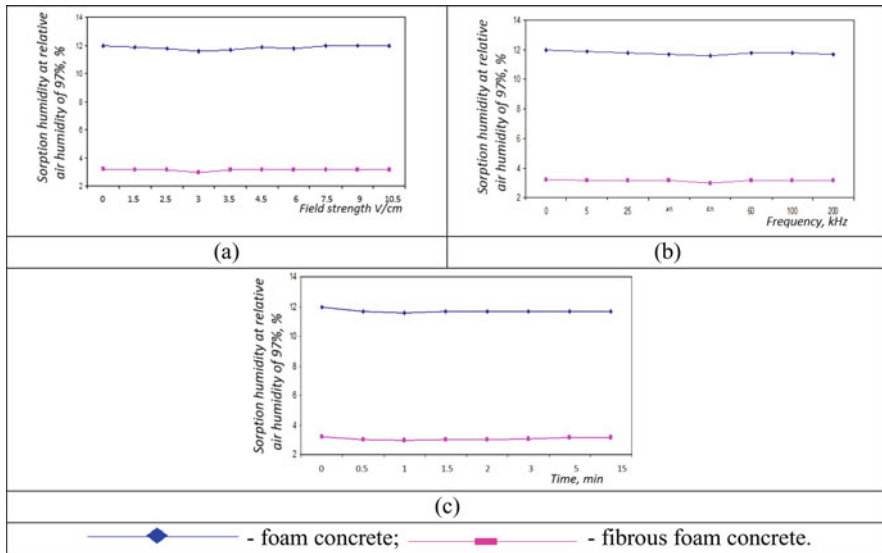


Fig. 9.21 Influence of changes in the parameters of the electric field on the value of the sorption moisture content of foam concrete at a relative air humidity of 97%: (a) electric field strength, (b) AC frequency, and (c) processing time

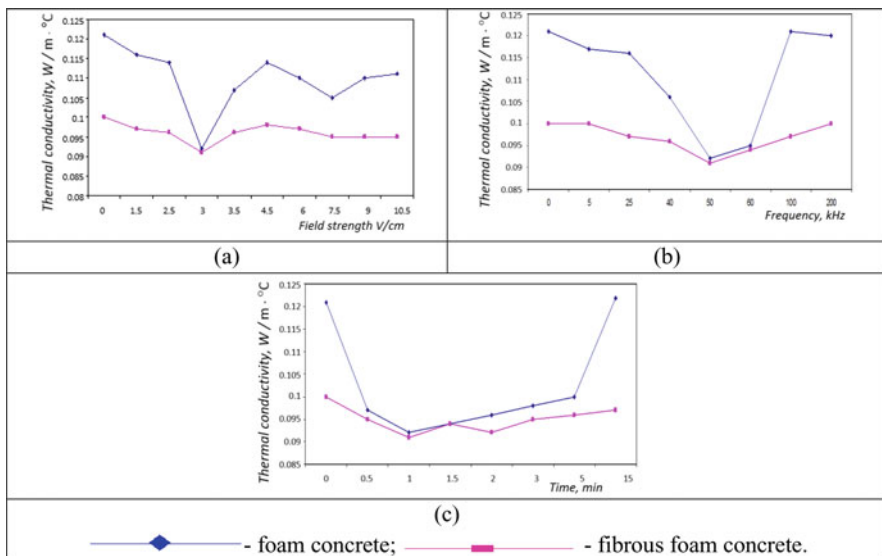


Fig. 9.22 Influence of changes in the parameters of electric field on the value of thermal conductivity of foam concrete: (a) electric field strength, (b) AC frequency, and (c) processing time

The field strength values at which the activation effect is maximum are in the region near the value 3 ± 0.5 V/cm.

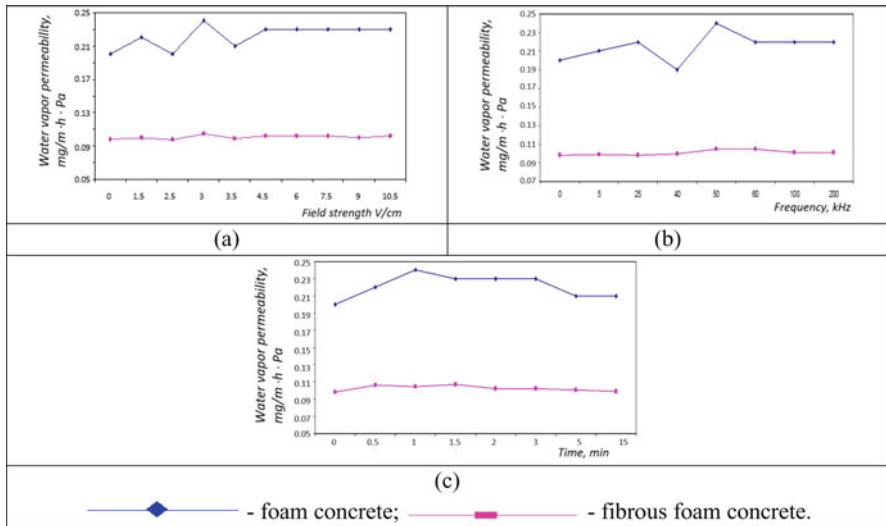


Fig. 9.23 Influence of changes in the parameters of electric field on the value of vapor permeability of foam concrete: (a) electric field strength, (b) AC frequency, and (c) processing time

The most effective frequency is 50 ± 10 kHz.

The optimal exposure time is in the range of 1 ± 0.5 min.

The given values of the intensity, frequency, and time of exposure, in connection with our additional research, with a smaller step in changing the varied parameters in comparison with the main studies can be considered final and do not need further clarification.

The analysis of our large-scale experimental studies also showed that when the activation by a low-power AC field was used with the identified most optimal values of its parameters, the physical and mechanical characteristics of foam and fiber-foam concrete changed, respectively:

- Compressive strength was increased by 19% and 21.6%.
- Average density was decreased by 1.9% and 2.5%.
- Released humidity had not changed significantly.
- Sorption humidity at a relative humidity of 75% and 97% was decreased by 7.4% and 9.5% and by 1.7% and 6.8%, respectively.
- Thermal conductivity was decreased by 25% and 12%.
- Vapor permeability was increased by 9% and 12%.

Thus, it is obvious that a comparison of the physical and mechanical characteristics of foam and fiber-foam concretes made using conventional technology and using the proposed activation method with low-energy AC impact showed the high efficiency of the latter.

9.9 Identification of the Optimal Mode of Activation of Foam and Fiber-Foam Concrete by Low-Energy-Consuming Electrophysical Impact

After carrying out all the planned experimental studies, we analyzed the results obtained in order to identify optimal modes of low-power electrophysical impact on foam and fiber-foam concrete mixtures and concretes.

According to the results of the analysis, in general, it can be noted that the low-energy activation has maximum positive effect on the compressive strength, average density, thermal conductivity, and vapor permeability.

The analysis [67] allowed one to clarify the optimal range of changes in the parameters of low-power electrical activation of foam and fiber-foam concrete mixtures.

In the case of coating the metal of the electrodes with zaponlack, the physical and mechanical characteristics deteriorated not only for activated foam and fiber-foam concretes, but also for those that were not subject to electrophysical effects.

An even more negative picture was observed when the position of the electrodes was changed to the metal inside, when the dielectric was in contact with the mixture. The effect of electric activation dropped sharply, which made it necessary to abandon the application of varnish and change the position of the electrodes.

The physical and mechanical characteristics changed as follows (first, the change in the quality index after applying the varnish is indicated, then after changing the position of the electrodes for foam and fiber-foam concrete, respectively): compressive strength decreased by 9%, 12%, and 8.9%; average density increased by 1.0%, 1.8%, and 1.4%; released humidity decreased by 5.9%; 23.5%, and 6.7%; sorption humidity at a relative air humidity of 75% and 97% did not change noticeably; thermal conductivity increased by 10.8%; 21.5%, and 5.4%; and vapor permeability decreased by 1.2%, 4.1%, and 0.6%.

Obviously, a comparison of the physical and mechanical characteristics of foam and fiber-foam concretes, made by conventional technology and with the use of the activation method with low-power variable electrical impact, showed the high efficiency of the latter.

9.10 Features of Changes in the Structure Formation and Properties of Foam and Fiber-Foam Concrete Mixtures and Concretes During Their Optimal Manufacture

Studies of changes in the nature of porosity and properties of foam and fiber-foam concretes, obtained with a rational and irrational combination of technological factors, using electrophysical activation with or without optimal parameters, made it possible to assess the total effect of the proposed technological modes.

Figures 9.24 and 9.25 show photos of the material microstructures obtained by using a microscope with a $200\times$ magnification.

When passing from technological modes (a) to modes (d), there is an increase in the uniformity of the distribution of pores in the structure of the material, a decrease in the coalescence of pores, and a decrease in the microporosity of the partitions. Also noticeable is the decrease in the thickness of the interporous partitions in concretes subjected to low-energy electrophysical activation due to the denser packing of solid particles. As a result, an increase in the volume of macropores is observed in the material, the shape of which is close to spherical.

After analyzing the photographs of the microstructures of foam and fiber-foam concretes obtained by using various technologies and different technological modes,

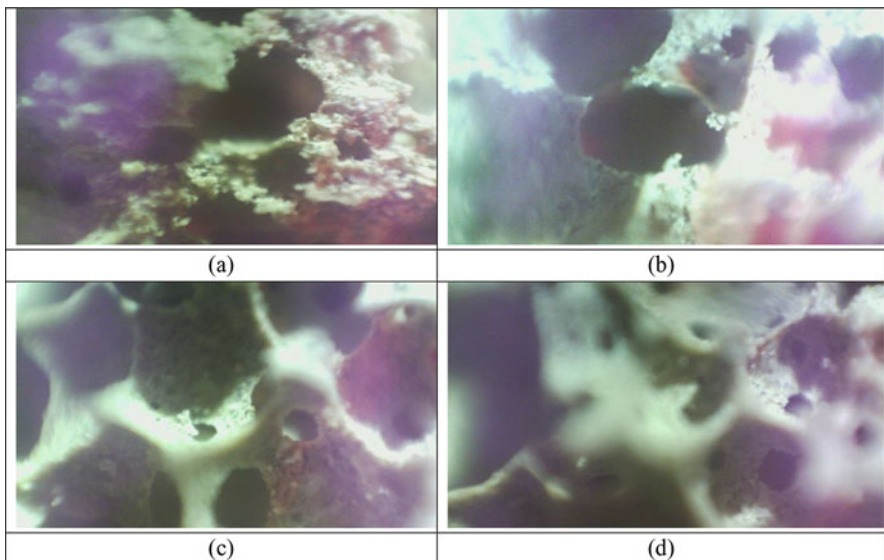


Fig. 9.24 Photos of the structure of foam concrete obtained: (a) without optimization of technological factors and without electrophysical activation, (b) without optimization of technological factors and activation with optimal parameters, (c) with optimization of technological factors and activation with nonoptimal parameters, and (d) with optimization of technological factors and activation with optimal parameters

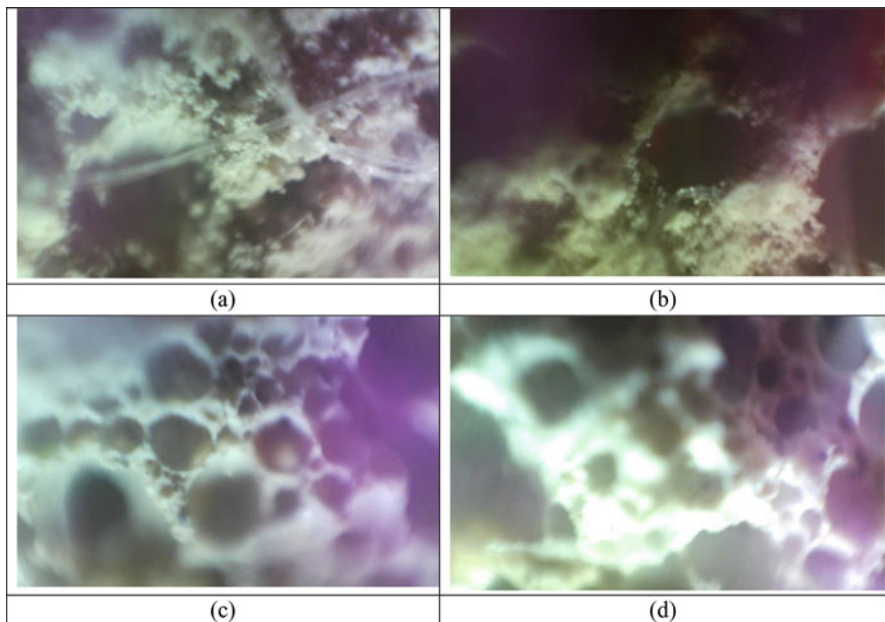


Fig. 9.25 Photos of the structure of fiber-foam concrete obtained: (a) without optimization of technological factors and without electrophysical activation, (b) without optimization of technological factors and activation with optimal parameters, (c) with optimization of technological factors and activation with nonoptimal parameters, and (d) with optimization of technological factors and activation with optimal parameters

it can be concluded that the nature of the porosity of these materials and, consequently, their basic properties can change due to the rationalization of technological factors and modes, as well as application in the manufacture technology of low-energy activation by AC field with optimal parameters.

Comparison of the structure formation of foam and fiber-foam concretes made using conventional technology with and without optimization of technological factors, as well as using the proposed method of activation with a low-energy AC field, unambiguously and convincingly showed the high efficiency of the latter, especially in combination with the optimal technological mode of preparation of cellular concrete, established by us.

Summing up, in general, the possibility of regulating and controlling the structure formation and physical and mechanical properties of foam and fiber-foam concrete by optimizing the technology of their manufacture in combination with the proposed activation method by the low-energy AC action can be considered proven.

9.11 Conclusions

1. A method has been developed for the activation of concrete mixtures in a high-voltage AC field at the stage of mixing, which, with low-energy consumption ($1.2\text{--}1.5 \text{ V} \cdot \text{A} \cdot \text{h/m}^3$), makes it possible to obtain concretes with increased physical, mechanical, and operational properties.
2. The optimal parameters of electrical activation of the concrete mixture in AC field (with current frequency of 50 Hz) during mixing have been determined, which provide the maximum effect of increasing the strength of concrete:
 - (i) Voltage at the electrodes, 3–6 kV
 - (ii) Specific area of electrodes, $2.8\text{--}3.4 \text{ m}^2/\text{m}^3$
 - (iii) Duration of electrical activation, 150–180 s
3. Electric treatment leads to a change in the nature of the structure formation of binding systems, namely, a decrease in destructive phenomena at an early stage of hardening, an acceleration of structure formation at the stage of formation of a condensation-crystallization structure, and a more intensive growth of plastic strength. The increase in the strength of concrete activated in AC field with optimal parameters of electrical treatment is equal to 20% at normal hardening and 30–40% with heat-and-humidity treatment (HHT).
4. It was found that activation in a high-voltage AC field increases the degree of hydration of cement clinker minerals (C_3S and C_3A) and Portland cement by 10–25% and leads to an increase in the content of neoplasms (ettringite, calcium hydroxide, low-basic calcium hydrosilicates) by 1.2–1.5 times compared to non-activated binding systems.
5. Electrical activation of the concrete mixture at the mixing stage leads to (i) a decrease in the integral porosity by 20% compared to the control samples and (ii) a change in the differential characteristics of the porous space, namely, a decrease in the number of large pores ($R = 10^{-3}\text{--}10^{-4.5} \text{ m}$) and an increase in the volume of small pores ($R = 10^{-5.5}\text{--}10^{-7} \text{ m}$). The change in the porous structure contributes to the improvement of the operational properties of concrete: (i) frost resistance increases by 20–30 cycles, and (ii) the shrinkage deformation during drying decreases by 30–35%.
6. Recommendations for high-voltage electrical activation of concrete mixture at the mixing stage have been developed. According to the results of pilot tests at JSC “RCP&C Plant” (Makeyevka, Ukraine), it was found that electrical treatment allows the saving up of up to 10% of cement, reducing the duration of isothermal heating by 2–2.5 h, and increasing the turnover of molds and the productivity of technological lines by 10–15%.
7. Electric activation of the concrete mixture allows one to reduce the cost of 1 m^3 of concrete mixture by 8% due to the saving of cement.
8. A method for regulating the structure formation and properties of foam and fiber-foam concretes activated by low-energy AC impact has been proposed. Its implementation in laboratory conditions has been developed, the practical

possibility of regulating the properties and structure formation at activation by low-energy AC impact has been proved, and its optimal modes have been experimentally revealed.

9. Extensive experimental studies have been carried out, which have proven that by using the most optimal technological modes and factors and activating a low-energy AC field with corresponding parameters, the physical and mechanical characteristics of foam and fiber-foam concrete are improved: (i) the compressive strength was increased by 19% and 21.6%, respectively; (ii) the average density was decreased by 1.9% and 2.5%, respectively; (iii) released moisture had not changed significantly; (iv) sorption humidity at a relative air humidity of 75% and 97% was decreased, respectively, by 7.4% and 4.8%, and by 2.5% and 5.3%; (v) thermal conductivity was decreased by 25% and 9%, respectively; and (vi) vapor permeability was increased by 11.4% and 5.2%, respectively.
10. The influence of the position and the presence of the varnish coating of the electrodes on the efficiency of electric activation of foam and fiber-foam concretes have been investigated, and the optimal combination of these factors has been determined.
11. Comparison of the physical and mechanical characteristics and structure formation of foam and fiber-foam concretes made according to the identified optimal technological modes and using the activation method with a low-energy AC field, in comparison with those made using conventional technology, showed the high efficiency of the recommendations developed.
12. The possibility of regulating and controlling the physical and mechanical properties and structure formation of foam and fiber-foam concretes by the proposed method of activation by low-energy AC impact and its influence on the nature of porosity and compaction of interporous partitions has been proved.
13. Experimentally, the optimal modes of low-energy processing of foam and fiber-foam concrete mixtures with AC field have been revealed.
14. The prescription parameters (type, dosage, particle size of the components of concrete mixtures) have been identified that have the greatest effect on the structure formation and properties of foam and fiber-foam concretes made according to optimal technological modes and using low-energy electrophysical activation with corresponding parameters.
15. Large-scale experimental studies have been carried out, which revealed the most significant prescription factors and the optimal ranges of their values change:
 - (i) Normal hardening Portland cement CEM I 42.5 N.
 - (ii) Sand with fraction of 0.16–0.315 mm.
 - (iii) Synthetic foaming agent “Centripor.”
 - (iv) The amount of additive-superplasticizer C-3 is equal to 0–0.2%.
 - (v) Sand-to-cement ratio, $S/C = 0.3 \pm 0.1$.
 - (vi) Water-to-solid ratio, $W/T = 0.49 \pm 0.03$.
 - (vii) Foaming agent content is equal to $1.5 \pm 0.3\%$.

- (viii) Fiber content is equal to 4%, contributing to the production of the most effective activated heat-insulating foam and fiber-foam concretes of class B1 with density D500.
- 16. Experimental studies of the operation of foam and fiber-foam concretes, manufactured according to the optimal recipe with corresponding technological parameters and activated by low-energy electrophysical impact with optimal parameters, at the age of 7, 28, 90, and 365 days with axial compression and tension, revealed an improvement in structural (strength and deformative) characteristics:
 - (i) Axial compression and tensile strength increased up to 11.9% and 12.7%, respectively.
 - (ii) Ultimate deformations during axial compression and tension were reduced to 14.0% and 15.8%, respectively.
 - (iii) The modulus of elasticity during axial compression and tension increased to 7.9% and 8.5%, respectively.
- 17. The influence of electrical activation on the change in the porosity of heat-insulating concrete was investigated, which revealed that the total porosity did not change significantly, and the open capillary porosity decreased to 6%.
- 18. It is proposed to introduce a new parameter, I_{ef} , being an indicator of the efficiency of electrical activation of the material and numerically equal to the ratio of the increment of the coefficient of structural quality of the material after activation to its value before activation.
- 19. A change in the diagrams “ $\sigma - \epsilon$ ” of foam and fiber-foam concrete was revealed, activated by low-energy AC impact, under axial compression and tension:
 - (i) The maximum shifts up and to the left.
 - (ii) The ascent angle at the origin increases.
 - (iii) The rise of the diagram in the ascending branch increases.
- 20. It was revealed that the change in the physical and mechanical characteristics of foam and fiber-foam concrete, activated by low-energy AC impact, is stabilized by the age of 365 days, but still continues to grow somewhat.

Common Conclusions to Part II

The concept of active centers and the electrical interpretation of cement hardening processes give grounds to determine the following directions for the development of concrete activation technology:

- (i) Modification of the electrical surface properties of dispersed concrete components by complex effects
- (ii) Post-molding use of surface-active substances to modify the porous structure of concrete
- (iii) Regulation of the rate of elementary processes of cement hardening
- (iv) Improving the technology of electrical activation of the concrete mixture
- (v) Electroosmotic impregnation of hardened concrete

Modification of the electric surface properties of dispersed concrete components using various surface-active substances, electrolytes, and their combinations, together with electrophysical effects, will increase the homogeneity and initial density of the concrete matrix, intensify the hydration of cement, and involve various industrial wastes in the production sphere. The implementation of this direction of the activation technology should be based on the electric surface balance (ESB) of the hardening system “filler—cement—hydration products—liquid phase,” which will change with the time of hardening. In this regard, special attention should be paid to ESB at the stage of loss of thixotropic properties by the concrete mixture, when interparticle interactions through interlayers of the liquid phase will be hampered by the forming rigid frame of the condensation-crystallization structure.

After molding (compaction of the concrete mixture), the main purpose of the surface-active substances actually ends. Subsequently, these substances, being adsorbed on the surface of dispersed particles, create a barrier for contact formation. In this regard, it is necessary to influence the freshly laid concrete, causing the desorption of surface-active substances by transferring them to the liquid phase. The development of desorption methods can be carried out on the basis of the principles of correspondence between the negative logarithm of the acid dissociation constant of surface centers and a solution of surface-active substances, both due to chemical additives and by electric effects. The surface-active substances desorbed in the initial period will subsequently remain in the pores and capillaries of concrete, modifying them.

Controlling the rate of elementary cement hardening processes is a difficult task, since their overlay takes place in time. Nevertheless, at certain stages of time, some of them are decisive. So, in the first minutes after mixing, dissociative adsorption and dissolution of clinker minerals are of paramount importance. In the first hours of

hydration, it is important to increase the number of crystallization centers. After the induction period and further, diffusion processes begin to control the hardening kinetics and so on. Taking into account the fact that these elementary processes are of an electrical nature, it is possible to change the speed of their passage by selecting the appropriate methods and parameters of electrical impact.

This scientific-technical direction is associated with the improvement of the technology of electrical activation of concrete mixture. The latter will be developed with the aim of increasing the efficiency of electrical effects (improving the physical and mechanical properties of concrete) and maximizing electrical safety using specialized pastes. In this case, special attention should be paid to the relationship between the parameters of electrical activation and the molding method, namely, casting, vibration, pressing, etc.

The technology of impregnation of hardened concrete using the phenomenon of electroosmosis has not yet been practically studied. This direction is effective, since it eliminates the need for drying products. Electroosmosis of high-molecular substances into the pores and capillaries of concrete should occur with simultaneous displacement of moisture and adsorptive fixation of molecules at the sites of active centers of internal surfaces. In this direction, various options and parameters of impregnation are possible, which opens up broad prospects for theory and practice.

References

1. V.A. Abalakin, A.D. Bulat, *Modern Problems of Building Materials Science* (Kazan, 1996), p. 45. (in Russian)
2. A. Abba, V.A. Matvienko, *Computer Materials Science and Quality Assurance* (Odessa, 1997), p. 105. (in Russian)
3. A. Abbud, *Experimental Studies and Methods of Calculation of Oblique Prestressed Reinforced Concrete Columns Taking into Account Complete Diagrams of Deformation of Materials*, PhD thesis (Technical Sciences), Rostov-on-Don, p. 197, 1987 (in Russian)
4. V.F. Afanasieva, Ind. Civil Constr. **8**, 25 (1993) (in Russian)
5. S.I. Agajanyan, *Modern Problems of Building Materials Science* (Kazan, 1996), p. 85. (in Russian)
6. B. Agathe, B. Laury, B. Laetitia, C. Florian, J. Aurélien, T.-r. Jean Michel, Cem. Concr. Compos. **103**, 233 (2019)
7. A.G. Aivazov, *Strength and Crack Resistance of Longitudinal Sections of Bending Ring Elements Under the Action of Transverse Forces*, PhD thesis (Technical Sciences). Moscow, p. 141, 1984 (in Russian)
8. I.N. Akhverdov, *Reinforced Concrete Centrifuged Pressure Pipes* (Stroyizdat, Moscow, 1969) (in Russian)
9. I.N. Akhverdov, *All-Russian Scientific and Technical Meeting: Technology of Forming Reinforced Concrete Products* (1979), p. 3. (in Russian)
10. I.N. Akhverdov, *Fundamentals of Concrete Physics* (Stroyizdat, Moscow, 1981) (in Russian)
11. V.A. Akopyan, E.V. Rozhkov, A.N. Soloviev, S.N. Shevtsov, A.V. Cherpakov, *Identification of Damages in Elastic Structures: Approaches, Methods, Analysis* (Southern Federal University Press, Rostov-on-Don, 2015) (in Russian)
12. V.A. Akopyan, A.N. Solov'ev, A.V. Cherpakov, S.N. Shevtsov, Rus. J. Nondestr. Test. **49**(10), 579 (2013)
13. G.A. Aksomitas, *Strength of Short Centrifuged Annular Columns with Longitudinal Reinforcement of Class At-U at Short-term Compression*, PhD thesis (Technical Sciences). Vilnius, p. 261, 1984 (in Russian)
14. H. Aktham, N.M. Alani, A. Bunnori, T. Noaman, T.A. Majid, Constr. Build. Mater. **209**, 395 (2019)
15. A.F.-K. Al-Khawaf, A.I. Nikulin, Bull. BSTU Named After V.G. Shukhov **5**, 66 (2019) (in Russian)
16. M.G. Altykis, R.Z. Rakhimov, Univ. News. Constr. **2**, 7 (1992) (in Russian)

17. A.S. Arbeniev, *Winter Concreting with Electric Heating of the Mixture* (Stroyizdat, Moscow, 1970) (in Russian)
18. R.D. Azelitskaya, *Acoustic and Magnetic Water Treatment* (Novocherkassk Polytechnical Institute, Novocherkassk, 1966), p. 37. (in Russian)
19. A.G. Azizov, *Reinforced Concrete Columns of Various Flexibility with Combined Prestressing of High-Strength Reinforcement*, PhD thesis (Technical Sciences), Rostov-on-Don, p. 217, 1983 (in Russian)
20. V.I. Babushkin, A.S. Koshmay, I.F. Ponomarev, A.G. Kholodny, *Cement* **9**, 8 (1986) (in Russian)
21. V.I. Babushkin, V.A. Matvienko, S.G. Vasyukevich, Y.A. Lagunov, *Univ. News. Constr.* **2**, 47 (1993) (in Russian)
22. A.N. Bambura, *Questions of Strength, Deformability and Crack Resistance of Reinforced Concrete* (Rostov-on-Don Engineering Building Institute Press, Rostov-on-Don, 1980), p. 19. (in Russian)
23. Y. Bamnios, E. Douka, A. Trochidis, *J. Sound Vib.* **256**(2), 287 (2002)
24. V.M. Batashev, *Proceedings of the Institute Energosetproekt*, vol 6 (Moscow, 1975), p. 70. (in Russian)
25. Y.M. Bazhenov, *Concr. Technol.* **1**, 6 (2005) (in Russian)
26. Y.M. Bazhenov, A.G. Komar, *Technology of Concrete and Reinforced Concrete Products: Textbook for Universities* (Stroyizdat, Moscow, 1984) (in Russian)
27. M.Y. Bekkiev, *The Influence of the Cross-Sectional Shape on the Strength, Deformability and Crack Resistance of Bent Elements of Heavy and Tuff Concrete*, PhD thesis (Technical Sciences), Rostov-on-Don, p. 225, 1985 (in Russian)
28. G.I. Berdichevsky, T.M. Pezold, V.G. Lastochnik, *Concr. Reinf. Concr.* **2**, 36 (1977) (in Russian)
29. G.I. Berdov, S.I. Linnik, *Univ. News. Constr. Archit.* **7**, 68 (1983) (in Russian)
30. O.Y. Berg, *Build. Archit.* **10**, 41 (1967) (in Russian)
31. A.F. Bernatsky, Y.V. Tselebrovsky, V.A. Chunchin, in *Electrical Properties of Concrete*, ed. by Y. N. Vershinin, (Energy, Moscow, 1980) (in Russian)
32. L.A. Bessonov, *Theoretical Foundations of Electrical Engineering. Electromagnetic Field: Textbook for Electric Technical, Energetical and Instrument Making Specialities of Universities*, 8th edn. (High School, Moscow, 1986) (in Russian)
33. A.I. Biryukov, A.N. Plugin, *Implementation of the Regional Integrated Scientific and Technical Target Program "Concrete"* (Kharkov, 1983), p. 56. (in Russian)
34. A.I. Biryukov, A.N. Plugin, I.A. Chulkov, *Improving the Durability of Concrete Transport Structures*, vol 714 (Moscow, 1982), p. 57. (in Russian)
35. A.I. Biryukov, A.N. Plugin, et al., *Physico-chemical Mechanics of Dispersed Systems and Materials* (Naukova Dumka, Kiev, 1980), p. 328. (in Russian)
36. A.I. Biryukov, A.N. Plugin, et al., *Physico-chemical Mechanics of Dispersed Systems and Materials* (Kiev, Naukova Dumka, 1980), p. 329. (in Russian)
37. A.I. Biryukov, Y.A. Spirin, L.P. Matskela, *Implementation of the Regional Integrated Scientific and Technical Target Program "Concrete"* (Kharkov, 1983), p. 62. (in Russian)
38. J. Bohm, *Electrostatic Precipitators* (Elsevier, Amsterdam, 1982)
39. M.I. Brusser, *Investigation of the Structural Porosity of Concrete and the Factors that Determine It*, PhD thesis (Technical Sciences), Moscow, 1971 (in Russian)
40. A.D. Bulat, *Electrophysical Activation of Cement Binders* (Russian Engineering Academy Press, Moscow, 2002) (in Russian)
41. A.D. Bulat, *Current State and Prospects of Development of Building Materials Science* (Samara, 2004), p. 91. (in Russian)
42. A.D. Bulat, Y.S. Danilova, *Current State and Prospects of Development of Building Materials Science* (Samara, 2004), p. 94. (in Russian)
43. N.P. Burmistrov, *Transp. Constr.* **9**, 47 (1967) (in Russian)
44. L. Butler, J.S. West, S.L. Tighe, *Cem. Concr. Res.* **41**(10), 1037 (2011)

45. A. Caron, L. Dascalescu, J. Electrostat. **61**(1), 43 (2004)
46. A.N. Chernov, *Building Materials Based on Industrial Waste* (UralNIIstromproekt, Chelyabinsk, 1982), p. 199. (in Russian)
47. A.N. Chernov, *Materials and Structures for Prefabricated Construction of Thermal Aggregates* (UralNIIstromproekt, Chelyabinsk, 1982), p. 119. (in Russian)
48. A. Cherpakov, I. Egorochkina, E. Shlyakhova, A. Kharitonov, A. Zarovny, S. Dobrohodskaya, MATEC Web Conf. **106**, 04009 (2017)
49. A.V. Cherpakov, E.A. Shlyakhova, I.O. Egorochkina, Y.A. Kokareva, Mater. Sci. Forum **931**, 373 (2018)
50. A.V. Cherpakov, A.N. Soloviev, V.V. Grinenko, O.U. Goncharov, Def. Sci. J. **66**(1), 44 (2016)
51. V.E. Chubarov, A.G. Umarov, V.D. Mayilyan, Eng. Bull. Don, 1 (2017) <http://www.ivdon.ru/ru/magazine/archive/n1y2017/3988> (in Russian)
52. M.H.F. Dado, O.A. Shpli, Int. J. Solids Struct. **40**, 5389 (2003)
53. Y.S. Danilova, *Activation of Cement Mortars Under the Influence of an Electric Field*, PhD thesis (Technical Sciences), Samara, 2002 (in Russian)
54. T. Darko, R. Miguel Fernández, M. Aurelio, J. Adv. Concr. Technol. **16**, 396 (2018)
55. A.D. Dimarogonas, Eng. Fract. Mech. **55**, 831 (1996)
56. S.A. Dmitriev, *Research of Strength, Stiffness and Crack Resistance of Reinforced Concrete Structures*. Issue 26 (Stroyizdat, Moscow, 1962), p. 5. (in Russian)
57. S.A. Dmitriev, V.M. Batashev, *Crack Resistance and Deformability of Conventional and Prestressed Reinforced Concrete Structures* (Stroyizdat, Moscow, 1965), p. 5. (in Russian)
58. S.A. Dmitriev, V.M. Batashev, *Features of Deformations of Concrete and Reinforced Concrete and the Use of Computers to Assess Their Influence on the Behavior of Structures* (Stroyizdat, Moscow, 1969), p. 157. (in Russian)
59. V.S. Dorofeev, V.N. Vyrovoy, V.I. Solomatov, *Ways to Reduce the Consumption of Building Materials and Structures: Textbook* (Kiev, 1989) (in Russian)
60. V.G. Dubinina, *Development of Optimal Parameters for Centrifugation of Reinforced Concrete Gravity Pipes*, PhD thesis (Technical Sciences), Nizhny Tagil, 2002 (in Russian)
61. S.S. Dukhin, N.A. Mischyuk, N.I. Rukobratsky, Colloid J. **1**, 17 (1988) (in Russian)
62. M.P. Dushenin, *Concrete Based on Electroactivated Cement Suspension and a Mixture of Aggregates with Low Voidness*, PhD thesis (Technical Sciences), Leningrad, 1990 (in Russian)
63. S.V. Dyakov, *The Effect of Electromagnetic Influence on the Properties of Concrete Mixture and Concrete*, PhD thesis (Technical Sciences), Vladimir, 1999 (in Russian)
64. V.A. Evdokimov, O.V. Smirnov, A.F. Yudina, *Technology of Construction of Buildings and Structures* (Leningrad Engineering Building Institute, Leningrad, 1984), p. 5. (in Russian)
65. A.V. Fedorov, V.N. Aksenov, Eng. Bull. Don **3** (2018) <http://www.ivdon.ru/ru/magazine/archive/n3y2018/5081> (in Russian)
66. M.F. Ferotto, O. Fischer, L. Cavalieri, Mater. Struct. **51**, 44 (2018)
67. N.I. Gamayunov, J. Appl. Chem. **5**, 456 (1983) (in Russian)
68. G.N. Gavrilov, B.V. Kadushkin, N.M. Romaschenko, *Proceedings IV All-Union Conference* (Nikolaev, 1988), p. 27. (in Russian)
69. G.N. Gavrilov, K.V. Petrov, Concr. Reinf. Concr., 6 (1995) (in Russian)
70. E.D. Gil'man, *Abstract Collection. General Construction Issues. Domestic Experience* (Moscow, 1973), p. 10. (in Russian)
71. E.D. Gil'man, Z.M. Larionova, A.I. Koketkina, *Issues of Strength, Deformability, Crack Resistance of Reinforced Concrete* (Rostov-on-Don, 1976), p. 23. (in Russian)
72. B.M. Gladyshev, *Mechanical Interaction of Structural Elements and Concrete Strength* (Vishcha School, Kharkov, 1987) (in Russian)
73. A.E. Golikov, Build. Archit. **6**, 5 (1983) (in Russian)
74. Y.I. Gol'tsov, S.A. Stel'makh, E.M. Scherban', H.S. Yavruyan, Sci. Stud. **4**(13) (2012) <https://naukovedenie.ru/PDF/11trgsu412.pdf> (in Russian)

75. N.P. Gorlenko, *Low-energy Activation of Cement and Oxide Binding Systems by Electric and Magnetic Fields*, DrSc thesis (Technical Sciences), Tomsk, 2007. (in Russian)
76. N.P. Gorlenko, G.E. Dunaevsky, Y.S. Sarkisov, Bull. Tomsk State Archit. Constr. Univ. **2**, 173 (2003) (in Russian)
77. F.K. Gorsky, *Mechanism and Kinetics of Crystallization* (Science and Technique, Minsk, 1969), p. 328. (in Russian)
78. I.G. Grankovsky, *Structure Formation in Mineral Binding Systems* (Naukova Dumka, Kiev, 1984) (in Russian)
79. M.N. Grigoryan, T.V. Polyakova, Y.A. Kokareva, I.A. Parinov, A.V. Cherpakov, IOP Conf. Ser. Mater. Sci. Eng. **1083**, 012016 (2021)
80. I.M. Grushko, V.A. Biryukov, I.I. Selivanov, I.F. Kiselev, Univ. News. Constr. Archit. **2**, 44 (1986) (in Russian)
81. I.M. Grushko, A.G. Ilyin, E.D. Chikhladze, *Improving the Strength and Endurance of Concrete* (Vishcha School, Kharkov, 1986) (in Russian)
82. I.M. Grushko, S.T. Rashevsky, A.D. Nosach, *Implementation of the Regional Integrated Scientific and Technical Target Program "Concrete"* (Kharkov, 1983), p. 49. (in Russian)
83. B.V. Gusev, *Proceedings of the II All-Russian Conference on Concrete and Reinforced Concrete*, vol 1 (Moscow, 2005), p. 17. (in Russian)
84. Y.P. Gushcha, *Influence of Inelastic Properties of Reinforced Concrete on Work and Distribution of Forces in Statically Indeterminate Structures*. Scientific Research Institute of Concrete and Reinforce Concrete (Stroyizdat, Moscow, 1975), p. 44. (in Russian)
85. Y.P. Gushcha, L.L. Lemysh, *Stress-Strain State of Concrete and Reinforced Concrete Structures*. Scientific Research Institute of Concrete and Reinforce Concrete (Stroyizdat, Moscow, 1986), p. 26. (in Russian)
86. D. Hilsenberg, I. Lehmann, J. Non-Cryst. Solids **1**, 257 (1986)
87. M. Ippei, L. Pietro, Cem. Concr. Res. **123**, 105770 (2019)
88. E.I. Ivaschenko, *Development of Methods for Calculating Reinforced Concrete Elements Based on Actual Deformation Diagrams of Materials, Taking into Account the Actual Change in the Area of their Cross-Sections*, PhD thesis (Technical Sciences), Voronezh, p. 230, 2006 (in Russian)
89. K. Jae-Jin, Y. Doo-Yeol, Cem. Concr. Compos. **103**, 213 (2019)
90. A.A. Kabanov, E.M. Zingel, Adv. Chem. **44**(7), 1194 (1975) (in Russian)
91. A.A. Kalninya, A.P. Klyavinya, I.Y. Laumanis, *Technological Mechanics of Concrete*, vol 6 (Riga, 1981), p. 101. (in Russian)
92. A.A. Kalninya, L.G. Skogoreva, et al., *Technological Mechanics of Concrete*, vol 5 (Riga, 1980), p. 119. (in Russian)
93. N.I. Karpenko, *General Models of Reinforced Concrete Mechanics* (Stroyizdat, Moscow, 1996) (in Russian)
94. I.V. Kaschuk, *Creation and Research of New Building Materials* (Tomsk, 1986), p. 53. (in Russian)
95. L. Kefei, L. Le, Cem. Concr. Res. **124**, 105811 (2019)
96. E.O. Kesli, V.Z. Buyal'skaya, *Cellular Concrete Constructions for Residential Buildings and Their Manufacturing Technology* (Leningrad, 1985), p. 53. (in Russian)
97. A.K. Khalyushev, M.G. Kholodnyak, K.V. Gubanov, *Construction and Architecture – 2015: International Scientific-practical Conference* (Rostov-on-Don, 2015), p. 400. (in Russian)
98. A.K. Khalyushev, M.G. Kholodnyak, M.P. Nazhuev, MATEC Web Conf. ICMTMTE **129**, 05012 (2017)
99. A.K. Khalyushev, A.L. Mailyan, S.A. Stelmakh, E.M. Shcherban, Mater. Sci. Forum **1011**, 23 (2020)
100. A.K. Khalyushev, S.A. Stel'makh, E.M. Shcherban, A.A. Chernil'nik, I.D. Padiev, D.Y. Sherement, Bull. Euro-Asian Sci. **11**(6), 81 (2019) <https://esj.today/PDF/47SAVN619.pdf> (in Russian)

101. A.K. Khalyushev, S.A. Stelmakh, E.M. Shcherban, M.G. Kholodnyak, *Heat Engineering Equipment for the Production of Building Materials, Products and Structures* (Don State Technical University Press, Rostov-on-Don, 2017) (in Russian)
102. A.K. Khalyushev, S.A. Stel'makh, E.M. Shcherban, A.K. Sysoev, AIP Conf. Proc. **2188**, 040015 (2019)
103. B.T. Khar'kovsky, V.P. Gulyakov, Y.G. Ushakov, *Questions of Theory and Practice of Magnetic Treatment of Water Systems* (Novocherkassk, 1975), p. 197. (in Russian)
104. M.G. Kholodnyak, E.V. Maltsev, *Construction-2013: International Scientific-Practical Conference* (Rostov-on-Don, 2013), p. 120. (in Russian)
105. M.G. Kholodnyak, E.V. Maltsev, *Construction-2013: International Scientific-Practical Conference* (Rostov-on-Don, 2013), p. 122. (in Russian)
106. M.G. Kholodnyak, M.P. Nazhuev, A.V. Zaretsky, Y.S. Fominykh, N.A. Dotsenko, Bull. Eurasian Sci., 3 (2019) <https://esj.today/PDF/38SAVN319.pdf> (in Russian)
107. M.G. Kholodnyak, S.A. Stelmakh, L.R. Mailyan, E.M. Shcherban, M.P. Nazhuev, Constr. Archit. **5**(4), 229 (2017) (in Russian)
108. M.G. Kholodnyak, S.A. Stelmakh, E.M. Shcherban, M.P. Nazhuev, A.V. Yanovskaya, S.A. Osadchenko, Eng. Bull. Don **3** (2018) <http://ivdon.ru/ru/magazine/archive/n3y2018/5047> (in Russian)
109. M.G. Kholodnyak, S.A. Stelmakh, E.M. Shcherban, D.A. Tretyakov, V.N. Dao, V.I. Zaikin, Bull. Eurasian Sci. **6** (2018) <https://esj.today/PDF/66SAVN618.pdf> (in Russian)
110. O.P. Kim, *Issues of Designing the Construction and Structures of Highways and Bridges in Siberia* (Tomsk, 1990), p. 76. (in Russian)
111. S.K. Kirthika, S.K. Singh, Constr. Build. Mater. **250**, 118850 (2020)
112. A.G. Klochkov, E.A. Chistyakov, Bull. Lvov Polytech. Inst. **3**(2), 15 (1966) (in Russian)
113. R. Klyukas, R. Vadluga, Bull. Ulyanovsk State Tech. Univ. **2**(46), 43 (2009) (in Russian)
114. L.K. Kolesnichenko, *Proceedings of Yuzhgiprorement*, vol 9 (Stroyizdat, Moscow, 1967), p. 131. (in Russian)
115. L.K. Kolesnichenko, T.Z. Gorfinkel', *Proceedings of Yuzhgiprorement* (Stroyizdat, Moscow, 1967), p. 143. (in Russian)
116. I.K. Kolodziy, *Production of Prefabricated Reinforced Concrete Products* (Vysshaya Shkola, Moscow, 1987) (in Russian)
117. P.G. Komokhov, Build. Mater. Equip. Technol. XXI Century **4**, 36 (2002) (in Russian)
118. S.F. Koren'kova, A.D. Bulat, Y.S. Danilova, *Modern Investment Processes and Construction Technologies*, vol 3, Pt. 2 (Russian Engineering Academy Press, Moscow, 2002), p. 20. (in Russian)
119. A.S. Korolev, A.A. Voroshilin, B.Y. Trofimov, Build. Mater. **5**, 8 (2005) (in Russian)
120. E.V. Korolev, Y.M. Bazhenov, V.A. Smirnov, *Construction Materials of a Variotropic-Frame Structure: Monograph* (Moscow State Building University Press, Moscow, 2011) (in Russian)
121. A.C. Koshmay, O.P. Mchedlov-Petrosyan, Cement **7**, 4 (1980) (in Russian)
122. A.V. Kosolapov, S.M. Sergeev, Univ. News. Build. Archit. **8**, 131 (1982) (in Russian)
123. A.A. Krasnoshchekov, B.V. Sobol, A.N. Solov'ev, A.V. Cherpakov, Rus. J. Nondestruct. Test. **47**(6), 412 (2011)
124. N.N. Kruglitsky, *Rheology of Concrete Mixture and Its Technological Tasks: IV All-Union Symposium* (Yurmala, 1982), p. 192. (in Russian)
125. N.N. Kruglitsky, *Physico-chemical Mechanics of Dispersed Systems in Strong Pulsed Fields* (Naukova Dumka, Kiev, 1982) (in Russian)
126. B.A. Krylov, *Methods of Electrical Treatment of Concrete and Their Theoretical Foundations* (Moscow, 1967) (in Russian)
127. A.A. Kryukov, A.E. Zhdanov, Bull. V.G. Shukhov Belgorod State Tech. Univ. **1**, 73 (2017) (in Russian)
128. A.I. Kudyakov, N.P. Dushenin, Univ. News. Constr. Archit. **10**, 63 (1987) (in Russian)

129. A.P. Kudzis, *Reinforced Concrete Structures of Annular Cross-Section* (Mintis, Vilnius, 1975) (in Russian)
130. A.I. Kurnosov, *Research of Work and Calculation of Reinforced Concrete Supports of Power Transmission Lines with Racks of Pipes Manufactured by Centrifugal Method*, PhD thesis (Technical Sciences), Moscow, 1970 (in Russian)
131. A.N. Kuznetsov, *Features of Hardening and Improvement of Concrete Properties by Discharge-Pulse Impact*, PhD thesis (Technical Sciences), Saint-Petersburg, 2007 (in Russian)
132. L.N. Lebedev, *Investigation of the Bearing Capacity and Crack Resistance of Flexible Prestressed Reinforced Concrete Elements of Annular Cross-Section*, PhD thesis (Technical Sciences), Dnepropetrovsk, p. 197, 1974 (in Russian)
133. A.A. Ledenev et al., Bull. V.G. Shukhov Belgorod State Tech. Univ. **4**, 16 (2016) (in Russian)
134. S.N. Leonovich, L.N. Zikeev, *Durability of Centrifuged Reinforced Concrete Racks. Survey Information* (Informenergo, Moscow, 1991) (in Russian)
135. E.L. Leus, *Rheology of Concrete Mixture and Its Technological Tasks: IV All-Union Symposium* (Yurmala, 1982), p. 145. (in Russian)
136. L.R. Mailyan, A.D. Gellerman, *Automation of Design Work in Rural Construction* (SevkavZNIIEPselstroy, Rostov-on-Don, 1985), p. 55. (in Russian)
137. R.L. Mailyan, E.D. Gil'man, *News of the North-Caucasus Scientific Center of High School*, vol 1 (1984), p. 6. (in Russian)
138. L.R. Mailyan, A.P. Korobkin, *Fundamental Research and New Technologies in Building Materials Science: All-Union Conference* (Belgorod Technological Institute of Building Materials, Belgorod, 1989), p. 23. (in Russian)
139. L.R. Mailyan, A.L. Mailyan, E.S. Ayvazyan, Eng. Bull. Don, 3 (2013) <http://www.ivdon.ru/ru/magazine/archive/n3y2013/1760> (in Russian)
140. L.R. Mailyan, S.A. Stelmakh, A.K. Khalyushev, M.G. Kholodnyak, E.M. Shcherban, M.P. Nazhuev, Eng. Bull. Don **2** (2018) <http://ivdon.ru/ru/magazine/archive/N2y2018/4832> (in Russian)
141. L.R. Mailyan, S.A. Stelmakh, A.K. Khalyushev, E.M. Shcherban, M.G. Kholodnyak, M.P. Nazhuev, Eng. Bull. Don **3** (2018) <http://ivdon.ru/ru/magazine/archive/n3y2018/5123> (in Russian)
142. L.R. Mailyan, S.A. Stelmakh, A.K. Khalyushev, E.M. Shcherban, M.G. Kholodnyak, M.P. Nazhuev, Build. Archit. **6**(1), 247 (2018) (in Russian)
143. L.R. Mailyan, S.A. Stelmakh, A.K. Khalyushev, E.M. Shcherban, M.G. Kholodnyak, M.P. Nazhuev, Bull. Eurasian Sci. **3** (2018) <https://esj.today/PDF/63SAVN318.pdf> (in Russian)
144. L.R. Mailyan, S.A. Stelmakh, M.G. Kholodnyak, A.K. Khalyushev, E.M. Shcherban, M.P. Nazhuev, Bull. Eurasian Sci. **4** (2018) <https://esj.today/PDF/07SAVN418.pdf> (in Russian)
145. L.R. Mailyan, S.A. Stelmakh, M.G. Kholodnyak, E.M. Shcherban, Sci. Stud., 4 (2017) <https://naukovedenie.ru/PDF/71TVN417.pdf> (in Russian)
146. L.R. Mailyan, S.A. Stelmakh, M.G. Kholodnyak, E.M. Shcherban, Bull. V.G. Shukhov Belgorod State Tech. Univ. **10**, 52 (2017) (in Russian)
147. L.R. Mailyan, S.A. Stelmakh, M.G. Kholodnyak, E.M. Shcherban, Bull. North-Caucasus State Tech. Inst. **3**(30), 134 (2017) (in Russian)
148. L.R. Mailyan, S.A. Stelmakh, M.G. Kholodnyak, E.M. Shcherban, A.K. Khalyushev, Buil. Archit. **5**(4), 224 (2017) (in Russian)
149. L.R. Mailyan, S.A. Stelmakh, E.M. Shcherban, N.A. Dotsenko, Bull. V.G. Shukhov Belgorod State Tech. Univ. **12**, 32 (2020) (in Russian)
150. L.R. Mailyan, S.A. Stelmakh, E.M. Shcherban, A.K. Khalyushev, A.S. Smolyanichenko, A.K. Sysoev, I.A. Parinov, A.V. Cherpakov, Appl. Sci. (Switzerland) **11**(8), 3591 (2021)
151. L.R. Mailyan, S.A. Stelmakh, E.M. Shcherban, M.G. Kholodnyak, Buil. Archit. **4**(56), 29 (2019) (in Russian)

152. L.R. Mailyan, S.A. Stelmakh, E.M. Shcherban, M.P. Nazhuev, Rus. J. Build. Constr. Archit. **4**(60), 22 (2020)
153. M.A.S. Hameed, B.H. Maula, Q.M. Bahnam, Int. Rev. Civil Eng. **10**(6) (2019). <https://doi.org/10.15866/irece.v10i6.17061>
154. A.A. Malodushev, *Electric Heating of Foam Concrete Mixture Immediately Before Laying in the Case*, PhD thesis (Technical Sciences), Saint-Petersburg, p. 151, 2000 (in Russian)
155. V.T. Mal'tsev, G.A. Tkachenko, N.V. Mal'tsev, Eng. Bull. Don **1** (2012) <http://ivdon.ru/magazine/archive/n1y2012/726> (in Russian)
156. V.T. Mal'tsev, G.A. Tkachenko, N.V. Mal'tsev, I.V. Vlasenko, Sci. Stud. **3** (2012) <http://naukovedenie.ru/sbornik12/12-48.pdf> (in Russian)
157. A. Mark, B. Hans, Cem. Concr. Res. **122**, 17 (2019)
158. V.A. Matvienko, J. Appl. Chem. **64**(9), 18571861 (1991) (in Russian)
159. V.A. Matvienko, J. Phys. Chem. **67**(7), 1536 (1993) (in Russian)
160. V.A. Matvienko, *Electrical Activation in the Technology of Concrete and Products*, DrSc thesis (Technical Sciences), Kharkov, 1993 (in Russian)
161. V.A. Matvienko, *Resource-Saving Technologies of Building Materials, Products and Constructions* (Belgorod Technological Institute of Building Materials, Belgorod, 1993), p. 90. (in Russian)
162. V.A. Matvienko, O.F. Cherezhnya, Cement **3**, 38 (1992) (in Russian)
163. V.A. Matvienko, V.N. Gubar', *The use of industrial waste for the production of building materials* (Kiev, 1990), p. 30. (in Russian)
164. V.A. Matvienko, V.N. Gubar', O.F. Cherezhnya, *New Technological Solutions for the Don-bass Construction Industry* (Kiev, 1989), p. 32. (in Russian)
165. V.A. Matvienko, V.N. Gubar', Y.A. Lagunov, *Resource-Saving Technologies of Building Materials, Products and Constructions* (Belgorod Technological Institute of Building Materials, Belgorod, 1993), p. 27. (in Russian)
166. V.A. Matvienko, M.M. Sychev, V.N. Gubar', Univ. News. Chem. Chem. Technol. **68** (1988) (in Russian)
167. V.A. Matvienko, S.M. Tolchin, *Electrical Phenomena and Activation Effects in Concrete Technology* (Makeevka, 1998) (in Russian)
168. G.V. Mazurenok, B.A. Plyusch, *Construction and Architecture Issues*, vol 12 (Minsk, 1982), p. 110. (in Russian)
169. R.G. Mette, M. Alexander, S. Henrik, D.L. Michel, Cem. Concr. Res. **122**, 189 (2019)
170. D.S. Mikhanovsky, Y.L. Aradovsky, E.L. Leus, *Plasticization of Concrete Mixture by Magnetic Treatment of Mixing Water at House-Building Plants* (Stroyizdat, Moscow, 1970) (in Russian)
171. E.E. Mikhelson, *Supports for Electric Overhead Lines Made of Centrifuged Reinforced Concrete* (Tsodna Publishing House, Tbilisi, 1949) (in Russian)
172. N. Mingjiang, W. Xihui, X. Gang, Q. Kunzan, C. Kefa, Powder Technol. **286**, 789 (2015)
173. M.S. Minkin, D.N. Kuimov, A.D. Lukyanov, Proc. Eng. **1353** (2016)
174. S.A. Mironov, *Theory and Methods of Winter Concreting*, 3rd edn. (Stroyizdat, Moscow, 1975) (in Russian)
175. O.P. Mchedlov-Petrosyan, *Chemistry of Inorganic Building Materials* (Stroyizdat, Moscow, 1977) (in Russian)
176. O.P. Mchedlov-Petrosyan, M.G. Stepanenko, Dokl. USSR Acad. Sci. **141**, 172 (1961) (in Russian)
177. O.P. Mchedlov-Petrosyan, A.V. Usherov-Marshak, A.M. Urzhenko, *Heat Release During Hardening of Binders and Concretes* (Stroyizdat, Moscow, 1984) (in Russian)
178. A.M. Mkrtchyan, V.N. Aksenen, Eng. Bull. Don **3** (2013) <http://www.ivdon.ru/ru/magazine/archive/n3y2013/1817> (in Russian)
179. A.M. Mkrtchyan, V.N. Aksenen, Eng. Bull. Don **3** (2013) <http://www.ivdon.ru/ru/magazine/archive/n3y2013/1818> (in Russian)

180. A.M. Mkrtchyan, D.R. Mailyan, Eng. Bull. Don **4** (2013) <http://www.ivdon.ru/ru/magazine/archive/n4y2013/2186> (in Russian)
181. A.K. Mohammed, C.B. Cheah, R. Mahyuddin, Constr. Build. Mater. **215**, 73 (2019)
182. A.G. Mukha, A.V. Klimenko, V.I. Vyrodov, *Implementation of the Regional Integrated Scientific and Technical Target Program "Concrete"* (Kharkov, 1983), p. 61. (in Russian)
183. S.A.Y. Murtazaev, M.S. Mintsaev, M.S. Saydumov, S.A. Aliev, Mod. Appl. Sci. **9**(4), 32 (2015)
184. S.A.Y. Murtazaev, M.S. Saidumov, V.S. Lesovik, N.V. Chernysheva, D.K.S. Bataev, Mod. Appl. Sci. **9**(4), 233 (2015)
185. T.F. Nagornaya, *Study of Strength and Crack Resistance of Eccentrically Compressed Reinforced Concrete Elements of Annular Cross-Section with Non-tensioned Reinforcement*, PhD thesis (Technical Sciences), Dnepropetrovsk, p. 163, 1970 (in Russian)
186. M.P. Nazhuev, E.A. Efimenko, R.A. Tsokalo, A.S. Nasevich, A.K. Khalyushev, Eng. Bull. Don **4** (2019) <http://www.ivdon.ru/ru/magazine/archive/n4y2019/5856> (in Russian)
187. M.P. Nazhuev, M.G. Kholodnyak, S.A. Stelmakh, *New Science: Strategies and Development Vector*, vol Pt. 2 (RITs AMI, Sterlitamak, 2015), p. 153. (in Russian)
188. M.P. Nazhuev, M.G. Kholodnyak, S.A. Stelmakh, *New Science: Modern State and Development Paths*, vol Pt. 2 (RITs AMI, Sterlitamak, 2016), p. 166. (in Russian)
189. M.P. Nazhuev, M.G. Kholodnyak, S.A. Stelmakh, *New Science: Modern State and Development Paths*, vol Pt. 2 (RITs AMI, Sterlitamak, 2016), p. 168. (in Russian)
190. M.P. Nazhuev, A.V. Yanovskaya, M.G. Kholodnyak, A.K. Khalyushev, E.M. Shcherban, S.A. Stelmakh, Eng. Bull. Don **3** (2017) <http://ivdon.ru/ru/magazine/archive/N3y2017/4313> (in Russian)
191. M.P. Nazhuev, A.V. Yanovskaya, M.G. Kholodnyak, S.A. Stelmakh, E.M. Shcherban, S.A. Osadchenko, Bull. Eurasian Sci. **3** (2018) <https://esj.today/PDF/58SAVN318.pdf> (in Russian)
192. N.I. Netes, *Concrete Mechanics and Technology* (Higher School, Kiev, 1987) (in Russian)
193. A. Nonat, X. Lecoq, S. Gauffinet, *The X Congress on the Chemistry of Cement*, vol 2 (Gothenburg, 1997), p. Zii055
194. D.V. Obernikhin, A.I. Nikulin, Bull. V.G. Shukhov Belgorod State Tech. Univ. **4**, 56 (2017) (in Russian)
195. K. Ogawa, H. Uchinava, K. Takemoto, Cem. Concr. Res. **10**, 17 (1980)
196. O.A. Sediek, T.-Y. Wu, M.C. Jason, E.-T. Sherif, J. Struct. Eng. **146**(6) (2020). [https://doi.org/10.1061/\(ASCE\)ST.1943-541X.0002637](https://doi.org/10.1061/(ASCE)ST.1943-541X.0002637)
197. V. Orlov, A. Chichurin, J. Phys. Conf. Ser. **1425**(1), 012129 (2020)
198. G.P. Pastushkov, *Multi-storey Frame Buildings with Load-Bearing Reinforced Concrete Centrifuged Elements*, DrSc thesis (Technical Sciences). Minsk, p. 487, 1994 (in Russian)
199. A.N. Pavlov, Y.I. Gol'tsov, L.R. Mailyan, E.M. Shcherban, S.A. Stel'makh, IOP Conf. Ser. Mater. Sci. Eng. **896**, 012124 (2020)
200. A.N. Pavlov, Y.I. Gol'tsov, L.R. Mailyan, S.A. Stel'makh, E.M. Shcherban, IOP Conf. Ser. Mater. Sci. Eng. **896**, 012123 (2020)
201. A.N. Pavlov, Y.I. Gol'tsov, S.A. Stel'makh, E.M. Scherban', Sci. Rev. **10**, 147 (2015) (in Russian)
202. G.A. Pavlova, A.N. Kuznetsov, *Current State and Prospects of Development of Building Materials Science* (Samara, 2004), p. 393. (in Russian)
203. V.T. Pertsev, D.Y. Zolotorubov, E.I. Shmit'ko, *Modeling in Materials Science* (Odessa, 1998), p. 22. (in Russian)
204. A.N. Petrov, *Deformation Model of Nonlinear Creep of Reinforced Concrete and Its Application to the Calculation of Plane-Stressed Elements and Systems Of Them*, PhD thesis (Technical Sciences), Moscow, p. 326, 2001 (in Russian)
205. K.V. Petrov, Univ. News. Constr. **11**, 53 (1996) (in Russian)

206. V.P. Petrov, *Technology and Properties of Centrifuged Concrete with a Combined Aggregate for the Supports of the Contact Network*, PhD thesis (Technical Sciences), Rostov-on-Don, p. 175, 1983 (in Russian)
207. G.N. Pisanko, E.N. Shcherbakov, P.G. Khubova, *Concr. Reinf. Concr.* **8**, 31 (1972) (in Russian)
208. A.A. Plugin, A.A. Dudin, A.A. Plugin, A.N. Plugin, *Scientific Bulletin of Construction*, vol 47 (Kharkov, 2008), p. 179. (in Ukrainian)
209. A.N. Plugin, A.A. Plugin, A.A. Dudin, et al., *Bull. Odessa State Acad. Constr. Archit.* **43**, 197 (2010) (in Ukrainian)
210. A.N. Plugin, A.A. Plugin, S.V. Miroshnichenko, D.A. Plugin, O.S. Borzyak, *Collection of Scientific Works of LNAU*, vol 71(94) (Lugansk National, Agricultural University Press, Lugansk, 2007), p. 189. (in Ukrainian)
211. A.N. Plugin, A.A. Scorik, A.A. Plugin, S.V. Miroshnichenko, O.A. Kalinin, I.V. Podtelezhnikova, O.S. Gerasimenko, *Railw. Transp. Ukr.* **1**, 11 (2004) (in Ukrainian)
212. V.I. Podolsky, Reinforced concrete overhead supports. Design, operation, diagnostics, in *Proceedings of VNIIZhT*, (Intekst, Moscow, 2007) (in Russian)
213. V.N. Pokrovskaya, I.A. Musatova, I.Y. Shporin, N.E. Martynyuk, *Problems of Creation and Application of Centrifuged Reinforced Concrete Structures in Construction* (Minsk, 1985), p. 65. (in Russian)
214. P.P. Polskoy, D.R. Mailyan, S.V. Georgiev, Eng. Bull. Don **4** (2014) <http://www.ivdon.ru/ru/magazine/archive/N4y2014/2734> (in Russian)
215. V.A. Pomazkin, A.A. Makaev, *Concr. Reinf. Concr.* **3**, 26 (1998) (in Russian)
216. F.C. Ponzo, A. Di Cesare, A. Telesca, A. Pavese, M. Furinghetti, *Appl. Sci. (Switzerland)* **11**, 1938 (2021)
217. A.N. Popov, *Production and Use of Reinforced Concrete and Concrete Pipes for Pressure and Non-pressure Pipelines* (Moscow, 1975) (in Russian)
218. A.N. Popov, P.A. Makarov, *Equipment for the Production of Concrete and Reinforced Concrete Pipes* (Stroyizdat, Moscow, 1965) (in Russian)
219. J.S. Popovics, J. Acoust. Soc. Am. **100**(5), 3451 (1996)
220. J.S. Popovics, J.L. Rose, *Int. J. Solids Struct.* **33**, 3925 (1996)
221. L.T. Prishepa, *Mechanism and Kinetics of Crystallization* (Nauka and Technika, Minsk, 1964), p. 282. (in Russian)
222. O.V. Radaykin, *Bull. V.G. Shukhov Belgorod State Tech. Univ.* **10**, 29 (2019) (in Russian)
223. S. Rajan, *Properties of Centrifuged Concrete and Improvement of the Design of Centrifuged Reinforced Concrete Supports for Power Transmission Lines*, PhD thesis (Technical Sciences), Rostov-on-Don, p. 267, 1997 (in Russian)
224. A.P. Ramachandran, M.W. Grutzeck, *Micro-structure Demonstration During Kydr. Cement Symposium* (Boston, 1990), p. 267
225. M. Regourd, I.H. Thomassin, P. Bailiff, I.C. Touray, *Cem. Concr. Res.* **10**(2), 223 (1980)
226. E.Y. Romanenko, *High-strength Concretes with Mineral Porous and Fibrous Additives for the Manufacture of Long Centrifuged Structures*, PhD thesis (Technical Sciences), Rostov-on-Don, p. 179, 1989 (in Russian)
227. E.Y. Romanenko, M.A. Trubitsin, Eng. Bull. Don, 1 (2018) <http://www.ivdon.ru/ru/magazine/archive/n1y2018/4680> (in Russian)
228. N.M. Romaschenko, G.N. Gavrilov, *Modern Problems of Building Materials Science* (Kazan, 1996), p. 43. (in Russian)
229. N.V. Rotych, V.V. Kononenko, R.V. Rotych, G.V. Ioshenko, *Univ. News. Chem. Chem. Technol.* **33**(1), 99 (1990) (in Russian)
230. G.K. Ruben, L.R. Mailyan, M.Y. Bekkiev, *Automatization of Design Work in Rural Construction* (SevKavZPIIEPselstroy, Rostov-on-Don, 1985), p. 25. (in Russian)
231. M.A. Ryazanov et al., *Bull. V.G. Shukhov Belgorod State Tech. Univ.* **12**, 58 (2016) (in Russian)

232. V.N. Safronov, *Electric Pulse Technology and Electromagnetic Processes in Loaded Solids* (Tomsk, 1982), p. 107. (in Russian)
233. M. Sargin, *Stress-Strain Relationships for Concrete and the Analysis of Structural Concrete Sections. SM Study* (Solid Mechanical Division, University of Waterloo, Ontario, 1970), p. 4
234. A.I. Savenkov, *Concretes Activated by High-voltage Pulse Treatment*, PhD thesis (Technical Sciences), Ulan-Ude, 2000 (in Russian)
235. I. Scalny, I.E. Ioung, *7th International Congress on the Chemistry of Cement*, vol II-1-3 (Paris, 1980), p. 343
236. E.M. Scherban', *Regulation of Structure Formation and Properties of Thermal Insulation Foam and Fiber-Foam Concrete Activated by Low-energy Variable Electrophysical Effects, Technological and Prescription Factors*, PhD thesis (Technical Sciences), Rostov-on-Don, p. 216, 2014 (in Russian)
237. E.M. Scherban', Y.I. Gol'tsov, G.A. Tkachenko, S.A. Stel'makh, Eng. Bull. Don, 3 (2012) www.ivdon.ru/magazine/archive/n3y2012/899 (in Russian)
238. E.M. Scherban', S.A. Stel'makh, Y.I. Gol'tsov, H.S. Yavruyan, Eng. Bull. Don 4 (2013) <http://www.ivdon.ru/magazine/archive/n4y2013/2193> (in Russian)
239. E.M. Scherban', G.A. Tkachenko, Y.I. Gol'tsov, S.A. Stel'makh, Mod. Probl. Sci. Educ. 1 (2012) www.science-education.ru/101-5445 (in Russian)
240. V.P. Seagull, Concr. Reinf. Concr. 4, 42 (1987) (in Russian)
241. K.P. Shalalas, A.P. Kuzis, *Reinforced Concrete Constructions* (Vilnius, 1970), p. 129. (in Russian)
242. G.V. Shamrina, *Cement Concretes Activated in an Electric Field at the Mixing Stage*, PhD thesis (Technical Sciences), Makeevka, 2001 (in Russian)
243. K.P. Shapalas, A.P. Kuzis, *Proceedings VII All-Union Conference* (Vilnius, 1972), p. 62. (in Russian)
244. E.M. Shcherban, S.A. Stelmakh, A.K. Khalyushev, M.G. Kholodnyak, *Technology of Building Reinforced Concrete Products and Structures for Industrial and Civil Buildings and Structures for Energy and Infrastructure Construction* (Don State Technical University Press, Rostov-on-Don, 2019) (in Russian)
245. E.M. Shcherban, S.A. Stelmakh, M.G. Kholodnyak, M.P. Nazhuev, E.M. Rymova, R.A. Live, Bull. Eurasian Sci. 5 (2018) <https://esj.today/PDF/51SAVN518.pdf> (in Russian)
246. V.V. Shchugaev, A.M. Lyudkovsky, A.V. Shapiro, Concr. Reinf. Concr. 1, 20 (1984) (in Russian)
247. V.L. Shchutsky, M.Y. Gritsenko, D.A. Dedukh, Eng. Bull. Don, 4 (2015) <http://www.ivdon.ru/ru/magazine/archive/n2p2y2015/3000> (in Russian)
248. V.L. Shchutsky, A.S. Nasevich, K.V. Kurgin, S.S. Slabukha, Bull. Eurasian Sci. 1 (2020) <https://esj.today/PDF/08SAVN120.pdf> (in Russian)
249. V.L. Shchutsky, A.V. Shilov, T.D. Talipova, Sci. Stud. 8(2) (2016) <http://naukovedenie.ru/PDF/29TVN216.pdf> (in Russian)
250. S.N. Shevtsov, A.N. Soloviev, I.A. Parinov, A.V. Cherpakov, V.A. Chebanenko, *Piezoelectric Actuators and Generators for Energy Harvesting. Innovation and Discovery in Russian Science and Engineering* (Springer, Cham, 2018)
251. A.E. Sheykin, Y.V. Chekhovsky, M.I. Brusser, *Structure and Properties of Cement Concretes* (Stroyizdat, Moscow, 1979) (in Russian)
252. V.N. Shivanov, V.K. Yagodin, Concr. Reinf. Concr. 1, 37 (1968) (in Russian)
253. I.M. Shubert, *Investigation of the Stress-Strain State of Centrifuged Ring Racks of Overpasses During Compression with Torsion*, PhD thesis (Technical Sciences), Minsk, p. 227, 1983 (in Russian)
254. A.I. Shuisky, A.K. Khalyushev, S.A. Stelmakh, E.M. Shcherban, M.G. Kholodnyak, Eng. Bull. Don, 3 (2017) <http://www.ivdon.ru/ru/magazine/archive/N3y2017/4309> (in Russian)
255. A.I. Shuisky, S.A. Stelmakh, M.G. Kholodnyak, E.M. Shcherban, *Construction and Architecture – 2015: International Scientific-Practical Conference* (Rostov-on-Don, 2015), p. 386. (in Russian)

256. A.I. Shuisky, S.A. Stelmakh, M.G. Kholodnyak, E.A. Torlina, *Construction and Architecture – 2015: International Scientific-Practical Conference* (Rostov-on-Don, 2015), p. 383. (in Russian)
257. A.I. Shuisky, S.A. Stelmakh, M.G. Kholodnyak, K.S. Yavruyan, E.M. Shcherban, *Construction and Architecture – 2015: International Scientific-Practical Conference* (Rostov-on-Don, 2015), p. 388. (in Russian)
258. A.I. Shuisky, S.A. Stelmakh, E.M. Shcherban, A.K. Khalyushev, M.G. Kholodnyak, M.P. Nazhuev, Eng. Bull. Don **4** (2017) <http://ivdon.ru/ru/magazine/archive/n4y2017/4373> (in Russian)
259. A.I. Shuisky, S.A. Stelmakh, E.M. Shcherban, A.K. Khalyushev, M.G. Kholodnyak, M.P. Nazhuev, Eng. Bull. Don **4** (2017) <http://ivdon.ru/ru/magazine/archive/n4y2017/4374> (in Russian)
260. A.I. Shuisky, S.A. Stelmakh, E.M. Shcherban, A.K. Khalyushev, M.G. Kholodnyak, A.V. Shatalov, Eng. Bull. Don **2** (2017) <http://ivdon.ru/ru/magazine/archive/N2y2017/4126> (in Russian)
261. A.I. Shuyskiy, S.A. Stel'makh, E.M. Shcherban, M.G. Kholodnyak, Mater. Sci. Forum **931**, 508 (2018)
262. V.I. Solomatov, M.K. Takhirov, M.D. Takher Shah, *Intensive Concrete Technology: Joint Edition of USSR – Bangladesh* (Stroyizdat, Moscow, 1989) (in Russian)
263. A.N. Soloviev, A.V. Cherpakov, P.V. Vasiliev, I.A. Parinov, E.V. Kirillova, Adv. Eng. Res. **20**(3), 205 (2020)
264. A.N. Soloviev, I.A. Parinov, A.V. Cherpakov, *Proceedings of the 2nd Annual International Conference on Material, Machines and Methods for Sustainable Development (MMMS2020)*, Lecture Notes in Mechanical Engineering, Banh Tien Long, Yun-Hae Kim, Kozo Ishizaki, Nguyen Duc Toan, Ivan A. Parinov, Ngoc Pi Vu (Springer, Cham, 2021), p. 233
265. A.N. Soloviev, I.A. Parinov, A.V. Cherpakov, Y.A. Chaika, E.V. Rozhkov, Mater. Phys. Mech. **37**(2), 192 (2018)
266. A.N. Soloviev, I.A. Parinov, A.V. Cherpakov, Y.V. Esipov, *Proceedings of the 2nd Annual International Conference on Material, Machines and Methods for Sustainable Development (MMMS2020)*, Lecture Notes in Mechanical Engineering, Banh Tien Long, Yun-Hae Kim, Kozo Ishizaki, Nguyen Duc Toan, Ivan A. Parinov, Ngoc Pi Vu (Springer, Cham, 2021), p. 255
267. V.I. Soroker, M.F. Kozyuk, *Energy Construction*, vol 9 (1968), p. 57. (in Russian)
268. S.A. Stel'makh, *Influence of the Parameters of Low-energy Variable Electric Fields on the Properties of Activated Thermal Insulation Foam and Fiber-Foam Concrete*, PhD thesis (Technical Sciences), Rostov-on-Don, p. 185, 2014 (in Russian)
269. S.A. Stelmakh, M.G. Kholodnyak, E.M. Shcherban, A.S. Nasevich, A.V. Yanovskaya, Russian Application for Utility Model No. 2020103753/09, 01.29.2020 (in Russian)
270. S.A. Stelmakh, E.M. Shcherban, A.K. Khalyushev, M.G. Kholodnyak, M.P. Nazhuev, Y.V. Galkin, Eng. Bull. Don **2** (2017) <http://ivdon.ru/ru/magazine/archive/N2y2017/4125> (in Russian)
271. S.A. Stel'makh, E.M. Shcherban, M.G. Kholodnyak, IOP Conf. Ser. Mater. Sci. Eng. **687**, 022008 (2019)
272. S.A. Stelmakh, E.M. Shcherban, M.G. Kholodnyak, M.P. Nazhuev, in *Current State and Prospects for the Development of Construction, Heat and Gas Supply and Power Supply: Proceedings of VI All-Russian Conference*, ed. by F. K. Abdrazakova, (Amirit, Saratov, 2017), p. 266. (in Russian)
273. S.A. Stelmakh, E.M. Shcherban, M.G. Kholodnyak, M.P. Nazhuev, A.A. Chernilnik, Russian Application for Utility Model No. 192492, 09.18.2019 (in Russian)
274. S.A. Stelmakh, E.M. Shcherban, M.G. Kholodnyak, M.P. Nazhuev, A.G. Taroyan, S.V. Cheburakov, Eng. Bull. Don **4** (2018) <http://ivdon.ru/ru/magazine/archive/n4y2018/5212> (in Russian)

275. S.A. Stelmakh, E.M. Shcherban, M.G. Kholodnyak, M.P. Nazhuev, A.G. Taroyan, A.V. Yanovskaya, Eng. Bull. Don **4** (2018) <http://ivdon.ru/ru/magazine/archive/n4y2018/5213> (in Russian)
276. S.A. Stelmakh, E.M. Shcherban, M.P. Nazhuev, M.G. Kholodnyak, *Problems and Prospects for the Development of Construction, Heat and Gas Supply and Energy Supply: Proceedings of VIII All-Russian Conference* (Science, Saratov, 2018), p. 347. (in Russian)
277. S.A. Stel'makh, E.M. Shcherban, A.Y. Prokopov, A.I. Shuiskii, S.M. Madatyam, I.A. Parinov, A.V. Cherpakov, Appl. Sci. (Switzerland) **10**(22), 8055 (2020)
278. S.A. Stel'makh, E.M. Scherban', I.A. Serebryanova, Y.I. Gol'tsov, H.S. Yavruyan, Eng. Bull. Don **4** (2013) <http://ivdon.ru/magazine/archive/n4y2013/2198> (in Russian)
279. S.A. Stel'makh, E.M. Shcherban, A.L. Zholobov, IOP Conf. Ser. Mater. Sci. Eng. **463**, 022034 (2018)
280. B.V. Stefanov, N.G. Rusanova, A.A. Volyansky, *Technology of Concrete and Reinforced Concrete Products* (Vishcha School, Kiev, 1982) (in Russian)
281. Y.Y. Steyerman, *Centrifuged Concrete* (Tekhnika da Shroma, Tiflis, 1933) (in Russian)
282. Y.M. Strakhov, T.I. Mayboroda, B.G. Ryasny, Concr. Reinf. Concr. **3**, 9 (1993) (in Russian)
283. L.A. Suleimanova, Bull. V.G. Shukhov Belgorod State Tech. Univ. **1**, 9 (2017) (in Russian)
284. M. Suleman Tahir, M. Saleem, M. Siebenhofer, J. Electrostat. **70**, 144 (2012)
285. M.M. Sychev, J. Appl. Chem. **63**, 1303 (1985) (in Russian)
286. M.M. Sychev, P.G. Komokhov, et al., *Physico-chemical Mechanics of Dispersed Systems and Materials* (Naukova Dumka, Kiev, 1980), p. 303. (in Russian)
287. M.M. Sychev, V.A. Matvienko, V.N. Gubar', Proc GosNII Cem. Ind. **97**, 145 (1988) (in Russian)
288. H.F.W. Taylor, *8th International Congress on the Chemistry of Cement* (Rio-de-Janeiro, 1986), p. 72
289. H.F.B. Taylor, 11th International Congress on Chemistry of Cement. Moscow **2**(3), 17 (1989) (in Russian)
290. Y.A. Tevelev, *Reinforced Concrete Pipes* (ASV, Moscow, 2004) (in Russian)
291. T. Tomasz, Constr. Build. Mater. **61**, 97 (2014)
292. V.A. Ulazovsky, V.I. Kuznetsov, *Questions of Theory and Practice of Magnetic Treatment of Water Systems* (Novocherkassk, 1975), p. 209. (in Russian)
293. V.I. Ural et al., Bull. V.G. Shukhov Belgorod State Tech. Univ. **4**, 129 (2016) (in Russian)
294. Y.I. Vasilievsky, *Investigation of the Strength and Crack Resistance of Circular Reinforced Concrete Sections (Pile Supports of Marine Hydro-Technical Structures*, PhD thesis (Technical Sciences), Odessa, 1964 (in Russian)
295. V.I. Vereschagin, V.N. Safronov, et al., Univ. News. Constr. Archit. **8**, 56 (1988) (in Russian)
296. V.I. Vereschagin, V.N. Safronov, O.V. Silkina, *VIII All-Union Scientific and Technical Meeting on Cement Chemistry and Technology* (Moscow, 1991), p. 245. (in Russian)
297. V.I. Vereschagin, V.N. Safronov, O.V. Silkina, *Investigation of Rheological Characteristics of Cement Pastes and Mortar Mixtures During Cement Activation by High-Voltage Corona Discharge* (Tomsk, 1998) (in Russian)
298. V.I. Vereschagin, O.V. Silkina, Cement **1**, 4 (1992) (in Russian)
299. L.A. Volkov, *Design, Research and Determination of the Parameters of Equipment for the Manufacture of Reinforced Concrete Pipes by Centrifugation Method*, PhD thesis (Technical Sciences), Moscow, p. 173, 1999 (in Russian)
300. V.A. Voznesensky, *Statistical Methods of Experiment Planning in Technical and Economic Research* (Finances & Statistics, Moscow, 1981) (in Russian)
301. P.P. Wadluga, A.P. Kuzis, *Research on Reinforced Concrete Structures*, vol 1 (Vilnius, 1966), p. 3. (in Russian)
302. H. Wagh, Hunningty Concr. **5**, 40 (1994)
303. Z. Wang, X.T.C. Man, R.D. Finch, B.H. Jansen, J. Test. Eval. **26**, 405 (1998)
304. L. Wen-Yao, C. Chia-Hung, Mag. Concr. Res. **71**(4), 184 (2019)
305. W. Xiaohui, L. Xila, Cem. Concr. Res. **33**(10), 1669 (2003)

306. G.J. Xiong, X.Y. Wu, F.F. Li, Z. Yan, *Constr. Build. Mater.* **25**(5), 2263 (2011)
307. K.S. Yavruyan, M.G. Kholodnyak, A.I. Shuisky, S.A. Stelmakh, E.M. Shcherban, *Eng. Bull. Don* **4** (2015) <http://ivdon.ru/ru/magazine/archive/n4y2015/3431> (in Russian)
308. A.F. Yudina, *Technology and Economics of Construction* (Novosibirsk, 1977), p. 80. (in Russian)
309. A.F. Yudina, *Modern Technology of Construction of Buildings and Structures* (Leningrad, 1985), p. 35. (in Russian)
310. A.F. Yudina, *Technology and Economics of Construction. Problems and Ways to Solve Them* (Siberian State Academy of the Way of Communication, Novosibirsk, 1997), p. 80. (in Russian)
311. A.F. Yudina, *Resource-Saving Technology of Concrete Works Based on the Use of Electrotreated Mixing Water*, DrSc thesis (Technical Sciences), Saint-Petersburg, 2000 (in Russian)
312. N.M. Zaychenko, *Concretes Electroactivated at the Vibration Compaction Stage*, PhD thesis (Technical Sciences), Makeevka, 1995 (in Russian)
313. N.M. Zaichenko, A.K. Khalyushev, S.A. Stelmakh, E.M. Shcherban, M.G. Kholodnyak, A.A. Chernilnik, Russian Patent for Invention No. 2716285, 03.11.2020 (in Russian)
314. D.Y. Zolototrubov, *Regularities of Formation of Densely Packed Structure of Dispersed-Granular Building Materials Under Electrophysical Influence*, PhD thesis (Technical Sciences), Voronezh, 2006 (in Russian)
315. *Technology of Concrete and Reinforced Concrete Products. Textbook for Engineering-Building Universities*, ed. by V. N. Sizov, (Higher School, Moscow, 1972) (in Russian)
316. *Manual for Electrotherm Treatment of Concrete* (Stroyizdat, Moscow, 1974) (in Russian)
317. *Physico-chemical Mechanics of Dispersed Structures in Magnetic Fields*, ed. by N. N. Kruglitsky, (Naukova Dumka, Kiev, 1976) (in Russian)
318. *Handbook of Precast Concrete Technology*, ed. by B. V. Stefanov, (Vishcha School, Kiev, 1978) (in Russian)
319. *Guidelines for the Design, Manufacture and Use of Reinforced Concrete Centrifuged Structures of Annular Section*, vol 47 (NIIZhB, Moscow, 1979), p. 64. (in Russian)
320. *European Committee for Concrete. Code – Sample EKB – FIP for Standards in Reinforced Concrete Structures* (Research Institute of Reinforced Concrete, Moscow, 1984), p. 284. (in Russian)
321. *Production of Concrete and Reinforced Concrete Structures: Reference Book*, ed. by B. V. Gusev, A. I. Zvezdova, K. M. Korolev, (New Age, Moscow, 1998) (in Russian)
322. *Pipes Made of Concrete, Reinforced Concrete and Stressed Concrete. CPI – International Concrete Production*, vol 45 (ad-Media, Tver, 2005) (in Russian)
323. *Concrete Materials. Technologies Equipment* (Stroyinform, Rostov-on-Don, 2006) (in Russian)

Index

A

- Acid dissociation constant, 217
AC magnetic field, 140, 166
Acoustic activation, 139, 142, 170, 171, 174, 175
Adhesion, 142, 148, 171
Adhesive contact, 186
Adsorption, 140, 141, 154, 156, 162, 164, 165, 167, 169, 170, 172–174, 217
Aerated concrete mixture, 192–195
Age, 7, 14, 38, 42, 45, 47, 48, 50, 55, 56, 62–64, 69–74, 90, 96, 105, 133, 134, 184, 215
Aggregate, 6, 7, 14, 18–20, 23, 31, 32, 36–65, 67–93, 95–121, 123, 133–135, 142, 143, 146, 150, 152, 156, 158, 159, 163, 164, 171, 172, 174, 180–182, 192–195
Alite, 141, 153–155, 167
Angle of repose, 191
Angular velocity, 15–17, 74–77, 81–90, 134
Annular cross-section, 4, 5, 7, 8, 11, 14, 18, 20, 22, 23, 26, 30, 36, 37, 40–43, 51, 105, 132, 133
Ascending branch, 64, 104, 120, 133, 134, 215
Ascent angle, 64, 133, 215
Autohesion, 191, 192
Axial compression, 9, 11, 38, 39, 42, 44–46, 48, 50, 55, 56, 64, 68, 71, 76–79, 91, 92, 127, 133, 215
Axial tension, 38, 39, 42, 44, 45, 47, 48, 50, 55, 56, 64, 68, 71, 77–79, 91, 92

B

- Basic regression equation, 77
Bearing capacity, 9, 10, 75, 93, 95–97, 99–112, 114, 116, 117, 120, 124, 127, 131, 132, 134, 135
Bending moment, 12
Bernoulli beam theory, 33
Binder, 32, 140–142, 146, 151, 153, 163, 165–169, 174, 179, 180

C

- Calcium hydroxilicate, 141, 155, 165, 167, 213
Capacity, 4, 32, 59, 95–121, 146, 162, 164, 165, 172, 182, 193
Cavitation, 141, 168, 170
Cellular concrete, 195, 212
Cement caking, 181
Cement concrete, 139–158, 163
Cement consumption, 6, 23, 148, 161, 162
Cement dough, 6, 19, 140–142, 155, 157, 160, 167, 172, 173, 175, 183
Cement floccule, 181
Cement stone, 19, 47, 140–142, 151–157, 160, 164, 165, 167–169, 171, 179, 180, 184
Cement suspension, 154, 184
Cement-to-water ratio, 5, 23, 148, 152, 163, 165, 180–184, 186
Cement-water dispersion, 141, 167, 169

- Centrifugal force, 4, 16, 19, 20, 23, 27, 51, 75, 76
- Centrifugation, 3–7, 13, 15, 18, 19, 22–24, 26, 28–30, 33, 34, 36–38, 45, 50–53, 55, 58, 64, 65, 74–76, 90, 93, 105, 106, 120, 123, 131–135
- Centrifuged (CF) concrete, 79
- Centripetal forces, 50, 74, 90, 134
- Chamotte-kaolin powder, 191
- Clinker, 153, 157, 165, 169, 191, 213, 217
- Coagulation, 140, 141, 151, 156, 160, 166, 167, 169, 172, 173, 179, 182, 193
- Coalescence, 164, 211
- Compaction, 3–6, 17, 19, 22, 23, 25, 26, 28–31, 76, 149, 155, 157, 158, 192, 214, 217
- Compressed zone, 8, 11, 128, 130
- Compressibility, 7, 9, 10, 170
- Compression diagram, 10
- Compression pressure, 6, 28–30, 140, 142, 171, 174
- Compressive strength, 9, 12, 21, 47, 50, 54–57, 68, 71, 77–79, 81, 83, 84, 86, 87, 89, 91, 92, 96, 127, 162, 180, 200, 203–205, 210, 214
- Concrete mixture, 3–6, 16–18, 20–33, 75, 76, 140, 142–152, 154, 155, 157–175, 177–215, 217, 218
- Concrete structure, 3–12, 19, 20, 22, 26, 27, 29, 33, 35, 36, 51, 61, 75, 76, 144, 145, 147–151, 158, 161
- Cone displacement, 161, 163, 180, 181
- Convection heating, 143
- Coulomb repulsive force, 192
- Creep shrinkage, 7
- Critical Euler force, 128, 130
- Crushed granite, 32
- Crystallization center, 140, 160, 163, 166, 172, 173, 181, 218
- D**
- Damping decrement, 33, 36
- Damping effect, 194
- DC magnetic field, 139, 140, 167, 173
- Dead center, 189
- Deformation diagram, 39, 42, 44, 59, 61, 62, 64, 65, 70, 72–74, 97, 100–102, 120, 133
- Deformative properties, 7
- Dehydration, 6, 149
- Descending branch, 44, 97, 99, 101, 102, 104, 105, 109, 120, 134
- Diagram approach, 97, 99, 105, 111–121, 134, 135
- Differential characteristic, 58, 96, 213
- Dipole-dipole interaction, 140, 166
- Dipole-ion interaction, 140, 166
- Discharge-pulse activation, 139, 152, 170, 173
- Dissolution, 140, 141, 153–155, 160, 164, 165, 167, 170, 173, 174, 179, 183, 217
- Dofen additive, 183
- Donor-acceptor processes, 192
- Drift zone, 188
- Drying, 8, 155, 168, 213, 218
- Dust, 142, 174
- E**
- EKB-FIP, 70, 72
- Elastic-plastic properties, 9, 10
- Electric activation, 153, 154, 165, 182–184, 210, 213, 214
- Electric double layer (DEL), 141, 156, 157, 163, 173, 178, 179, 183, 192
- Electric heat treatment, 143
- Electric polarization, 140, 153, 154, 165, 172
- Electric surface balance (ESB), 217
- Electrization, 155, 157, 158, 185–187, 189
- Electrochemical activation, 160
- Electroosmosis, 149, 167, 168, 173, 218
- Electroosmotic dehydration, 149
- Electrophoresis, 141, 151, 155, 167
- Electrostatic field, 152, 154, 179, 187–190
- Equipotential surface, 187
- Ettringite, 141, 155, 167, 213
- External electric field, 139, 140, 154, 156, 157, 167
- F**
- Fiber-foam concrete (FFC), 193–197, 202, 205, 209, 210, 212, 214, 215
- Filler, 33, 142, 152, 153, 157, 163, 164, 174, 192–194, 217
- Filling process, 5
- Filtration, 4, 23, 142
- Filtration channel, 6, 22
- Fisher's criterion, 77
- Flexural tensile strength, 38, 47
- Fly ash, 191
- Foam concrete (FC), 142, 192, 193, 195, 196, 200, 206–209, 211
- Foaming agent (FA), 195, 202, 214
- Fourier transform, 33
- Freezing, 8, 148, 179, 183
- Freshly laid concrete, 145, 217
- Frost resistance, 146, 213
- Full factorial experiment (FFE), 32, 76, 77

G

Graph-analytical method, 35

H

Hardening, 49, 105, 139–143, 145–149, 151–157, 160–169, 173–175, 184, 193, 213, 214, 217, 218
 Harmonic oscillation, 3, 194
 Heat-and-humidity treatment (HHT), 213
 Heavy concrete, 67, 68, 146, 165, 181, 182, 192
 High-frequency electric field, 139–141, 151, 155, 156, 168, 173
 High-voltage corona activation, 140
 High-voltage electrostatic field, 191–192
 High-voltage spark discharge, 140, 163, 172
 Hooke's law, 103
 Humidity, 7, 146, 153, 184, 195, 200, 203–205, 207–210, 214
 Hydration product, 141, 152, 156, 163–165, 179, 180, 217
 Hydraulic activity, 165
 Hydrodynamic pressure, 6
 Hydrolysis, 149

I

Induction heating, 143
 Integral characteristic, 38, 50, 64, 98
 Internal friction, 191
 Interporous partition, 142, 192, 193, 211, 214
 Inverse method, 33
 Ion mobility, 188
 Ion recombination, 188
 Ionization zone, 188
 Iterative calculation, 97, 99, 100

J

Joule-Lenz law, 144

L

Least squares method, 77
 Lightweight contaminant, 22
 Limestone ground, 191
 Limiting state, 68, 90, 120, 133
 Limiting strain, 38
 Liquid phase, 6, 23, 140, 147, 154, 157, 167, 174, 179, 180, 182, 217
 Loading speed, 26, 27
 Longitudinal reinforcement, 8, 11, 12, 124–127

M

Magnetic water, 160, 161, 172
 Manufacturing technology, 13, 37, 38, 45–51, 55, 69, 90, 106–108, 112
 Mathematical planning of experiment, 76
 Mechanical activation, 140, 167, 173
 Microcracking, 7
 Mineral powder, 191–192
 Mixing water, 151, 152, 158, 160–163, 166, 174
 Modulus of elasticity, 7–10, 34, 35, 49, 50, 53, 58–60, 64, 65, 69, 127, 130, 133, 134, 215
 Moisture, 5, 7, 141, 144–147, 153–155, 167, 168, 175, 182, 184, 195, 200, 202–205, 207, 208, 214, 218
 Moisture evaporation, 141
 Molding process, 4, 148
 Mold rotation, 6, 26, 29, 76
 Mortar, 142, 151–153, 156, 157, 165, 168, 169, 171, 174, 177–215

N

Neoplasm, 155, 161–163, 166, 167, 169, 182, 184, 213
 Number of revolutions, 17–19, 25–31

P

Pasty dispersion, 140
 Peak's law, 188
 Perforated wall, 4
 PFS additive, 182, 183
 Plasticization, 153, 163
 Porosity, 6, 29, 34, 35, 153, 192, 211–215
 Pozzolanic activity, 186
 Pressing head, 5
 Pulsed electrical breakdown, 152, 163

R

Rectified (half-wave) field, 179
 Redox potential, 151, 162, 174
 Reinforced concrete, 3–5, 7–14, 28, 72, 96–99, 101, 103–105, 108–110, 112, 120, 124, 129, 131, 132, 134, 135, 145–148, 150, 151
 Reinforcing frame, 5, 126, 127, 130
 Resonance method, 33–34, 36
 Response function, 76
 Rheological properties, 157, 158, 165
 Roll pressing, 3, 4

S

- Salt ion, 160, 172, 173
 Scale factor, 7, 42
 Seam zone, 147, 148
 Sedimentation, 4, 140, 154, 167
 Setting time, 33, 164
 Shear modulus, 9, 33
 Shielding shell, 141, 169, 173
 Shock wave, 168, 170
 Short centrifuged columns, 8
 Shrinkage, 6–8, 146, 147, 213
 Sludge drainage, 5, 23
 Slurry, 6, 141, 155, 158, 168, 192
 Spatula, 191
 Spectral characteristics, 33, 36
 Stackability, 149, 150
 Standing wave, 141, 170
 Steady state, 194
 Strength properties, 7, 179
 Stress-strain state, 8, 45
 Student's *t*-test, 77
 Supercritical stage, 99, 109
 Surface-active substance, 152, 182, 183, 217
 Surface modification, 185
 Surface tension, 151, 160, 162, 174

T

- Tangent modulus, 9
 Tensile strength, 11, 47, 50, 54–58, 62, 64, 68, 71, 76–79, 81, 83, 84, 86, 87, 89, 91, 92, 127, 133, 215
 Tension in bending, 38, 42, 44
 Thawing, 8, 145
 Thermal diffusion, 140, 167
 Thermos curing, 144, 147
 Thixotropic dilution, 192
 Torsional stress, 4
 Transverse vibration, 34

U

- Ultimate compressibility, 68
 Ultimate tensile strength, 44, 68
 Ultrasonic activation, 139, 140, 174
 Ultrasonic method, vi, 51–54
 Ultrasonic sounding, 51
 Unevenness, 6
 Unipolar ion, 188

V

- Variotropic structure, 36
 Varnish, 210, 214
 Vertical tubular electrostatic precipitator, 185
 Vertical vibroforming, 5
 Vibrating table, 4
 Vibration, 3–5, 8, 19, 22–25, 28, 33, 34, 36–38, 45, 51, 64, 105, 106, 131–133, 141, 142, 144, 148, 149, 157, 158, 167, 171, 173, 192, 193, 195, 218
 Vibration hydraulic pressing, 3, 4
 Vibro-centrifugation, 13, 18, 23, 30, 33, 34, 36–38, 43, 45, 50–52, 55, 58, 64, 65, 74, 88, 105, 106, 120, 123, 132–134
 Vibro-centrifuged (VCF) concrete, 13, 15–65, 67–93

W

- Water mineralization, 152, 162, 174
 Water permeability, 5, 147
 Wind load, 125, 127
 Workability, 23, 152, 180, 186

Y

- Yield area, 100

Z

- Zaponlack, 195, 210